The Role of Angiopoietin-2 in Vascular Calcification

By Alexandra Frances Todd

A Thesis submitted to UCL in fulfilment of the requirement for the degree of Doctor of Philosophy

February 2018

Developmental Biology and Birth Defects
Developmental Biology and Cancer Programme
Institute of Child Health

University College London

Declaration

I, Alexandra Frances Todd, confirm that the work presented in this thesis is my own. Where information has been derived from other sources, I can confirm that this has been indicated in the thesis.

Abstract

Cardiovascular disease (CVD) is a leading cause of mortality in paediatric patients with chronic kidney disease (CKD), particularly in those undergoing dialysis. One of the earliest events in CVD is endothelial damage, which may result from changes in levels of vascular growth factors that control blood vessel function and stability. Markers of endothelial dysfunction and vascular calcification are observed during CKD, and are documented as early as the first decade of life. Previous research indicates that growth factors controlling blood vessel function and stability are altered in CKD patients; circulating levels of the pro-inflammatory/anti-angiogenic molecule angiopoietin-2 (Angpt2) are notably increased in children on dialysis and correlate with surrogate markers of vascular calcification. I therefore hypothesise that Angpt2 may promote medial calcification in CKD.

Through *in vitro* studies using intact vessel rings and explanted vascular smooth muscle cells (VSMCs) from paediatric pre-dialysis and dialysis patients, I have shown that addition of exogenous Angpt2 in a pro-calcaemic environment (medium supplemented with 2.7 mM calcium, and 2.0 mM phosphate) increases calcium deposition within vessels from dialysis patients, but has no effect on control or pre-dialysis vessels. In endothelial cells, Angpt2 acts through the receptor tyrosine kinase with immunoglobulin-like and EGF-like domains-2 (Tie2); this receptor was detected through immunofluorescence in the media layer of the intact vessels and by protein and RNA analyses of explanted VSMCs. The calcifying effect of Angpt2 in VSMCs could be blocked by downregulating Tie2 expression by small interfering ribonucleic acid (siRNA), but was not prevented by addition of the Angpt2 antagonist, vascular stabiliser and anti-inflammatory molecule, Angpt1. Vascular calcification is driven through several pathophysiological mechanisms including osteogenic gene expression, apoptosis and vesicle release; these have been investigated in both vascular rings and explanted VSMCs. While the full mechanism has yet to be elucidated, this thesis provides evidence to suggest that manipulation of Tie2 and angiopoietin pathways may have potential to decrease the rate of vascular calcification in patients with CKD.

Acknowledgements

To my supervisors Dr David Long, Dr Rukshana Shroff, and Professor Lesley Rees
Thank you for your guidance over the past several years. Your incredible patience with a floundering young scientist has been most appreciated, and I have gained an insight into the medical world through your mentorship. Working with you in this environment has internalised my love of translational research, and I have the utmost respect for the scientific process and the relationship with the clinical world.

Professor Paul Winyard and Dr Jenny Papakrivopoulou
Thank you for your teatime advice on science, life and growing up.

Dr Maria Kolatsi-Joannou and Dr Karen Price
Thank you for taking me under your wings when I first arrived, young and fresh-faced, and guiding me through the worlds of histology and tissue culture. Thank you for always listening, and the pep talks and life tips along the way.

Dr Elisavet Vasiloupoulou, Dr Sara Benedetti,
Dr Jennifer Huang, and Miss Chiara Mari
Thank you for becoming a little family – I could not have asked for a better group of girls to look up to, laugh with, and cry with.

Miss Hortensja Brzóska
My adopted sister – I could not have dreamt of a better one. Thank you for the KimWipes when I've cried, the reagents when I've run out of mine, and the coffee when I've been shattered.

Simon
Thank you for all the late night coffee runs and keeping me sane in this crazy city.

My parents, Barbara and Ray
Thank you for allowing me to go thousands of miles away for the best education possible. You've given me everything I need to succeed, and I hope someday to repay you for it.

Table of Contents

Abbreviations

Abbreviation	Full name
ABIN2	A20 binding inhibitor of NF-KB activation-2
ADMA	asymmetric dimethylarginine
AHSG	α2-HS-glycoprotein (fetuin-A)
AKT	protein kinase B
Angpt	angiopoietin
ANOVA	analysis of variance
BCA	bicinchoninic acid
BLAST	basic alignment search tool
BMP2	bone morphogenic protein 2
bp	base pair
CD	cluster of differentiation
cDNA	complementary deoxyribonucleic acid
CEC	circulating endothelial cell
cIMT	carotid intima media thickness
CKD	chronic kidney disease
CNN1	calponin
CO_2	carbon dioxide
CRP	C-reactive protein
CT	computed tomography
CVD	cardiovascular disease
DAB	3,3'-diaminobenzidine
DDAH1	dimethylarginine dimenthyaminohydrolase-1
DMEM	Dulbecco's-modified Eagle’s medium
DNA	deoxyribonucleic acid
dNTP	deoxynucleotide triphosphate
DoK	downstream of kinase
DOKR	downstream of kinase (DoK)-related protein
DPBS	Dulbecco's phosphate-buffered saline
EBM	endothelial basal medium

EBSS	Earle's basic salt solution
ECM	extracellular matrix
EDTA	ethylenediaminetetraacetic acid
EMP	endothelial microparticle
eNOS	endothelial nitric oxide synthase
EPC	endothelial progenitor cell
ERK	extracellular regulated kinases
ESRD	end-stage renal disease
FAK	focal adhesion kinase
FBS	foetal bovine serum
Flt-1	FMS-related tyrosine kinase
FOXO	forkhead box O
FSP1	fibroblast specific protein-1
GFR	glomerular filtration rate
GOSH	Great Ormond Street Hospital
GRB	growth factor receptor-bound protein
H&E	haematoxylin and eosin
HCl	hydrochloric acid
HD	haemodialysis
HDL	high-density lipoprotein
HIF	hypoxia-inducible factor
HPRT	hypoxanthine-guanine phosphoribosyltransferase
HRP	horseradish peroxidase
hsCRP	high sensitivity C-reactive protein
HuAoFib	human aortic fibroblast
HuAoVSMC	human aortic vascular smooth muscle cell
HUVEC	human umbilical vein endothelial cell
ICAM-1	intercellular adhesion molecule-1
Ig	immunoglobulin
IHC	immunohistochemistry
IKK	IκB kinase
IL	interleukin

IMT	intima media thickness
kDa	kilodalton
KDIGO	Kidney Disease: Improving Global Outcomes
KDOQI	Kidney Disease Outcomes Quality Initiative
LDL	low density lipoprotein
LVH	left ventricular hypertrophy
M199	Medium 199
mg	milligram
MGP	matrix gla protein
miRNA	microRNA
mL	millilitre
mm	millimetre
mRNA	messenger ribonucleic acid
NaOH	sodium hydroxide
NCBI	National Centre for Biotechnology Information
ng	nanogram
NHS	National Health Service
NO	nitric oxide
O.C.T	optimal cutting temperature
OPN	osteopontin
PFA	paraformaldehyde
PBS	phosphate-buffered saline
PCR	polymerase chain reaction
PD	peritoneal dialysis
PFP	platelet-free plasma
PI3K	phosphatidylinositol 3-kinase
PWV	pulse wave velocity
qRT-PCR	quantitative reverse transcription polymerase chain reaction
RIPA	radioimmunoprecipitative assay
RNA	ribonucleic acid
RRT	renal replacement therapy
RUNX2	runt-related transcription factor 2

SDMA	symmetric dimethylarginine
SDS	sodium dodecyl sulphate
sFLT	soluble FMS-related tyrosine kinase-1
siRNA	small interfering ribonucleic acid
SM22α	smooth muscle protein 22-alpha (transgelin)
SP7	osterix
sTie2	soluble tyrosine kinase with immunoglobulin-like and EGF-like domains
sVCAM-1	soluble vascular cell adhesion molecule
TAE	tris-acetate-ethylenediaminetetraacetic acid
Tie	tyrosine kinase with immunoglobulin-like and EGF-like domains
TNF-α	tumour necrosis factor alpha
TUNEL	terminal deoxynucleotidyltransferase dUTP nick end labelling
UK	United Kingdom
USRDS	United States renal data system
VCAM	vascular cell adhesion molecule
VEGF	vascular endothelial growth factor
VSMC	vascular smooth muscle cell
VWF	Von Willebrand factor
WPB	Weibel-Palade bodies
αSMA	alpha smooth muscle actin
µg	microgram
µL	microlitre
µm	micrometre
µM	micromolar

List of Figures

List of Tables

Chapter 1: Introduction

1.1 Chronic Kidney Disease

1.1.1 Chronic Kidney Disease in the UK

In England alone, approximately two million individuals are diagnosed with moderate to severe chronic kidney disease (CKD), making it one of the most prevalent diseases in the population at a cost to the National Health Service (NHS) of almost £1.45 billion each year (Kerr *et al* 2012). Two percent of individuals diagnosed with CKD progress to end-stage renal disease (ESRD, CKD Stage 5); this equates to almost 55000 adults and 900 children who require renal replacement therapy (RRT) within the United Kingdom (UK) (Pruthi *et al* 2014).

CKD also significantly increases the risk of an individual developing cardiovascular disease (CVD), which is a leading cause of early mortality amongst CKD patients (Steenkamp *et al* 2014). Cardiovascular events such as myocardial infarction and stroke in CKD patients cost the NHS almost £175 million per year, indicating that CKD and subsequent CVD is not only a strain on patients and their families, but also on the resources of the health system (NICE 2014).

This thesis focuses on the paediatric CKD population as these young patients, despite their age, also remain at high risk of developing CVD. Initially, I will outline the pathology and diagnosis of CKD, the risk factors that predispose these patients to develop CVD, and the basic pathology of CVD in these patients.

1.1.2 Structure and Function of the Kidney

The human kidneys are paired, bean-shaped organs which are situated in the upper posterior of the abdominal cavity (Kurts *et al* 2013). A single kidney is composed of two distinct regions – the outer renal cortex, and the inner medulla – which can be further broken down into segments formed of multiple conical masses known as the renal, or Malpighian, pyramids (Kurts *et al* 2013). The broad base of the renal pyramid

is situated within the cortex, while the apex of the pyramid is located in the medulla (Figure 1.1).

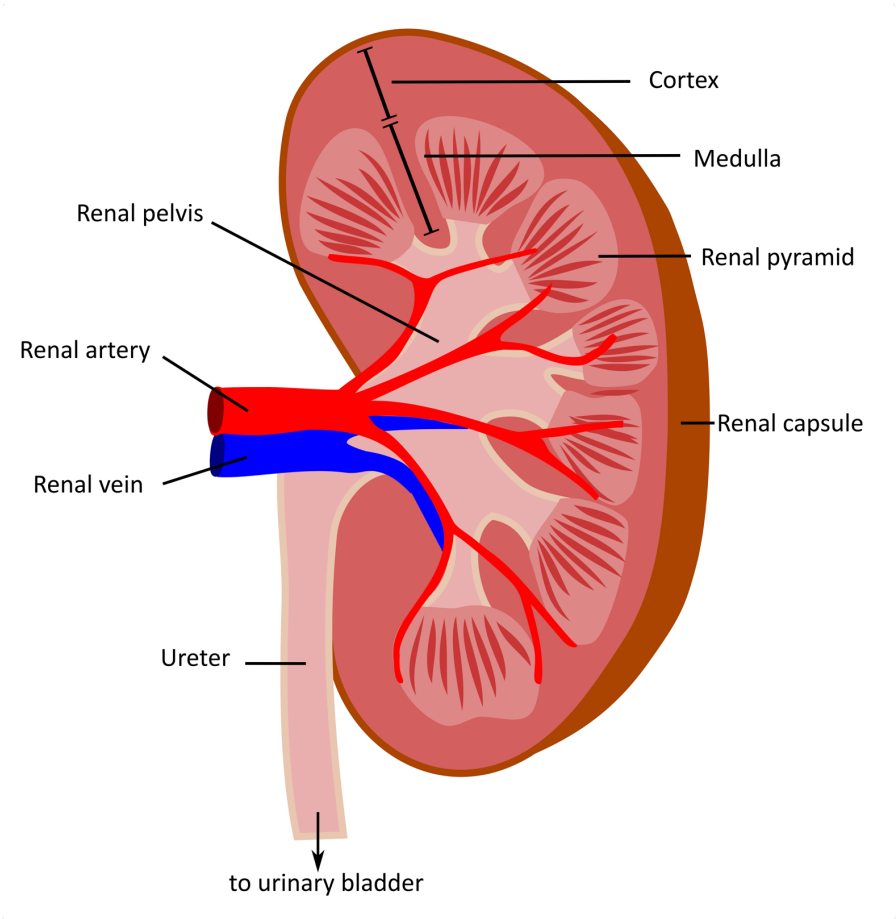

Figure 1.1: Basic structure of the kidney

The human kidney is divided into two primary regions: the outer renal cortex, and the inner renal medulla (Kurts *et al* 2013). Within the kidney, the renal (Malpighian) pyramids are composed of thousands of parallel nephrons with the aligned tubules and collecting ducts converging towards the inner cortex (Kurts *et al* 2013). The collecting ducts merge to the papillary ducts, which divert urine towards a single ureter (Kurts *et al* 2013). Each individual kidney is vascularised by a single renal artery, from which subsequent branching of the vasculature allows for perfusion of the entire kidney.

Each renal pyramid consists of many parallel nephrons, with each healthy kidney containing between 700000 to 1.5 million (Keller *et al* 2003). The nephron (Figure 1.2) is the functional unit of the kidney, acting as a tiny blood filtration unit, and is composed of the renal corpuscle which consists of the glomerulus, in conjunction with

the Bowman's capsule, as well as a single highly specialised tubule leading to the collecting duct (Keller *et al* 2003). The tubule consists of three regions – the proximal tubule, the loop of Henle and the distal tubule – each of which is specialised for different aspects of reabsorption (Kurts *et al* 2013).

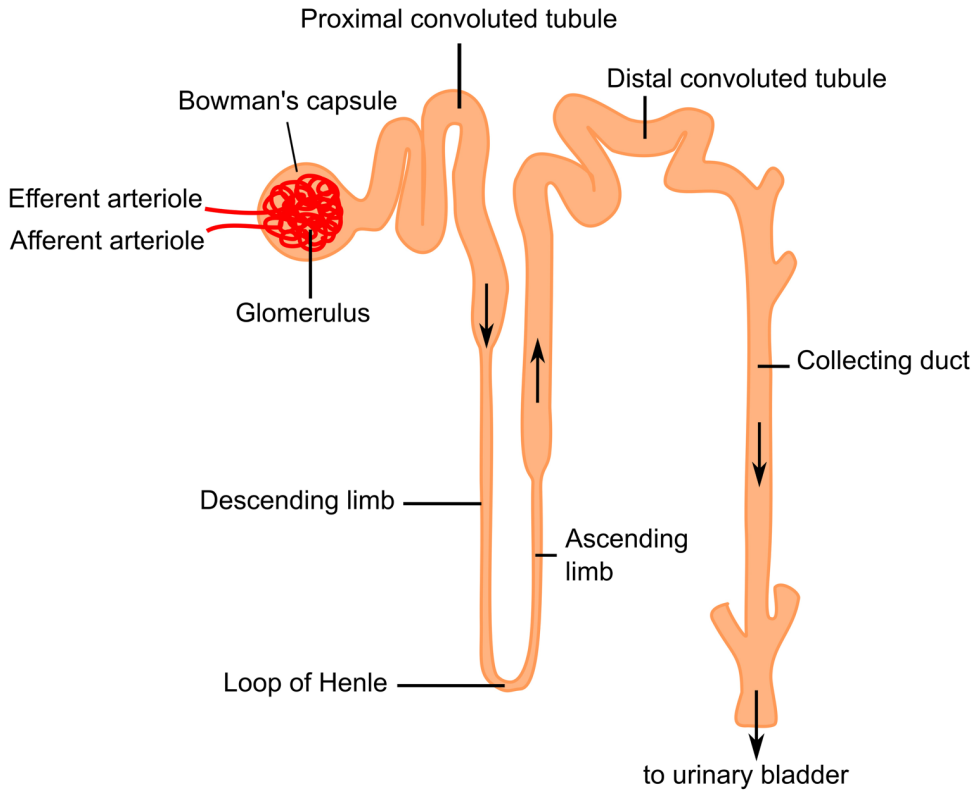

Figure 1.2: Basic structure of a nephron

The structure of a single nephron, the functional unit of the kidney, is composed of a glomerulus, surrounded by the Bowman's capsule, and a highly specialised tubule consisting of several distinct segments (the proximal convoluted tubule, the Loop of Henle, and the distal convoluted tubule) (Kurts *et al* 2013).

In a healthy individual, the kidney is essential for the maintenance of blood homeostasis (Kurts *et al* 2013, Wadei and Textor 2012). To do so, it takes on several roles including filtration of metabolic waste products such as creatinine and urea, electrolyte balance, and production of the hormones renin and erythropoietin, which regulate blood pressure and red blood cell production respectively (Kurts *et al* 2013, Wadei and Textor 2012).

The kidney is an extensively vascularised organ and receives 10% of the cardiac output (Long *et al* 2012). An individual renal artery supplies each kidney, which subsequently branches to perfuse the anterior and posterior of the kidney before joining an expansive capillary network. These rich vascular networks are formed through a combination of angiogenesis and vasculogenesis; new arteries branch from the renal artery alongside the invasion of the developing ureteric bud into the metanephric mesenchyme, whilst the expansive capillary network is mainly formed from endothelial progenitor cells (EPCs) that reside in the renal cortex (Adams and Alitalo 2007, Stolz and Sims-Lucas 2015). The capillaries of the glomeruli are lined with highly fenestrated endothelial cells, in which the fenestrations range from 70–100 nm in diameter, and act as the first filtration barrier through which fluid (yet no blood cells) can pass (Grahammer *et al* 2013, Stolz and Sims-Lucas 2015). The vasa recta and peritubular capillaries surround the tubules of the nephrons, which facilitate reabsorption and secretion between the blood and inner lumen of the nephron (Pallone *et al* 2012).

The kidney also hosts an expansive renal lymphatic network that, although less well characterised, is crucial for the removal of excess proteins and fluid (Seeger *et al* 2012). When the integrity of this lymphatic network is disrupted, as it is in polycystic kidney disease, it may potentiate inflammation and oedema thus contributing to the pathogenicity of the disease (Huang *et al* 2016).

1.1.3 Definition of CKD

Renal damage can impair the ability of the kidney to adequately filter the blood, leading to impaired kidney function and CKD. CKD is defined according to the National Kidney Foundation Disease Outcomes Quality Initiative (KDOQI) Guidelines (2012) which state that, for at least three months:

1) The glomerular filtration rate (GFR), which is defined as the amount of blood that passes through the glomeruli per minute, must be maintained at or below 60 mL per minute per 1.73 m^2 of body mass.

OR

2) There must be kidney damage as indicated by albuminuria or histological abnormalities.

The severity of CKD is then divided into stages, depending on the patient's GFR, where Stage 1 is early renal disease and Stage 5 is ESRD (Table 1.1).

Stage	Description	GFR (mL/min/1.73m^2)
1	Kidney damage with normal or increased GFR	>90
2	Kidney damage with mildly decreased GFR	60–89
3a	Mild to moderate decrease in GFR	44–59
3b	Moderate to severe decrease in GFR	30–44
4	Severe decrease in GFR	15–29
5	Kidney failure	<15 (or dialysis)

Table 1.1: Stages of CKD as defined by GFR

The table was derived from the Kidney Disease Improving Global Outcomes (KDIGO) guidelines (2012), which include the segmentation of Stage 3 CKD into two stages (mild to moderate [3a], and moderate to severe [3b]).

There are currently only two treatment options for patients with CKD Stage 5, which are dialysis or transplantation (Pruthi *et al* 2014). Transplantation, without a period of dialysis, is the ideal course of action; however, the availability of compatible organs limits the frequency of transplantation. In a given year, approximately 7100 people in the UK require single or multiple organ transplants (NHS Blood and Organ Donation Figures 2014–2015). Eighty percent of these people require a kidney, making it the most needed organ (NHS Blood and Organ Donation Figures 2014–2015). Comparatively, only 2925 transplants were actually conducted in the UK in 2014 (NHS Blood and Organ Donation Figures 2014–2015). Dialysis, either peritoneal dialysis (PD) or haemodialysis (HD), is the second-best option for patients with CKD Stage 5; however, thrice weekly visits to a HD unit or nightly cycles on a home PD machine do not represent a good quality of life for CKD patients. Furthermore, dialysis has been linked to a significantly increased risk of developing CVD in both adult and paediatric populations (Parekh *et al* 2002, Johnson *et al* 2009), and the overall survival time following the initiation of dialysis remains low (Stokes 2011).

1.1.4 Prevalence of CVD in CKD

The significance of CVD as a leading cause of mortality in CKD patients came to light in the mid-1990s following a paper by Foley *et al* (1998), which highlighted the discrepancy in cardiovascular mortality rates between the general population and adult CKD patients on dialysis, as well as the relationship between mortality in these groups and both age and ethnicity (Figure 1.3A). CVD mortality encompasses death due to arrhythmias, atherosclerosis, cardiac arrest, cardiomyopathy, myocardial infarction and pulmonary oedema (Foley *et al* 1998). Particularly striking is the difference in risk to young adults (25–34 years), as patients with CKD in this age-range exhibit CVD mortality rates comparable to that of 80-year olds in the general population (Foley *et al* 1998). Data from the United Kingdom Renal Registry also indicates that CVD was responsible for 23–28% of deaths in patients with CKD on RRT across a 10-year period (January 2003–December 2012) and is thereby a leading cause of death in these individuals (Figure 1.3B; Steenkamp *et al* 2014).

Over the last decade, it has also been shown that paediatric CKD patients have the same propensity to develop CVD as their adult counterparts. A review of the United States Renal Data System (USRDS 2011) highlighted the number of cardiac-related deaths in children with CKD (Mitsnefes 2012). In these data, CVD is defined as deaths from cardiac arrest, arrhythmia, cardiomyopathy, cerebrovascular disease and myocardial infarction. In patients receiving dialysis, CVD was the leading cause of death in patients on both HD and PD (32% HD, 28% PD; Figure 1.4).

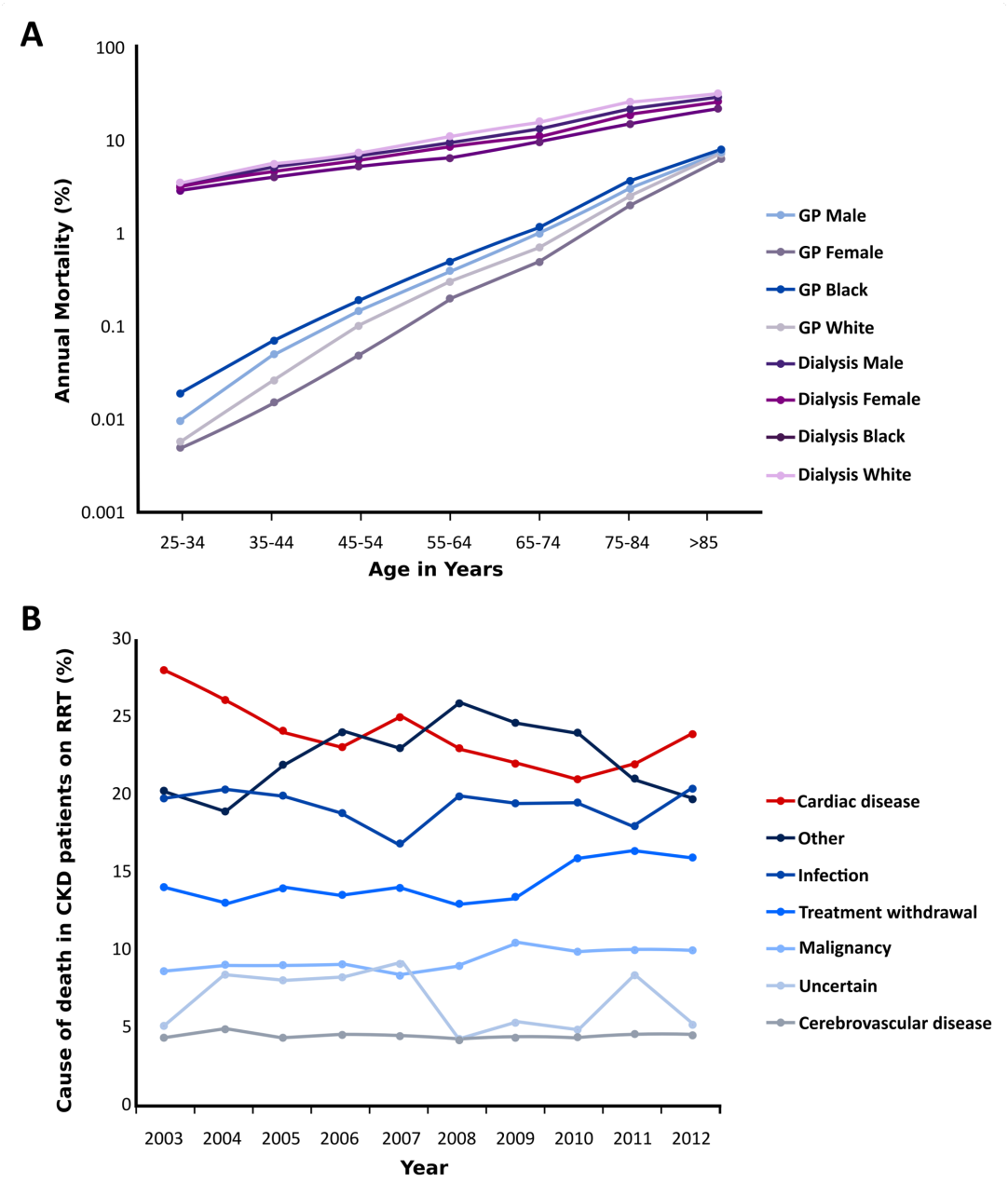

Figure 1.3: Cardiovascular mortalities by age and ethnicity

A: Cardiovascular mortality is shown per decade of age as segregated by gender, ethnicity and whether an individual is part of the general population (GP) or receiving dialysis. This figure is redrawn from Foley *et al* (1998) and is based on data from the United States. **B:** Data from the UK Renal Registry (Steenkamp *et al* 2014) indicates that CVD was one of the key causes of death in patients with CKD on RRT between 2003–2012. This figure is redrawn from Steenkamp *et al* (2014).

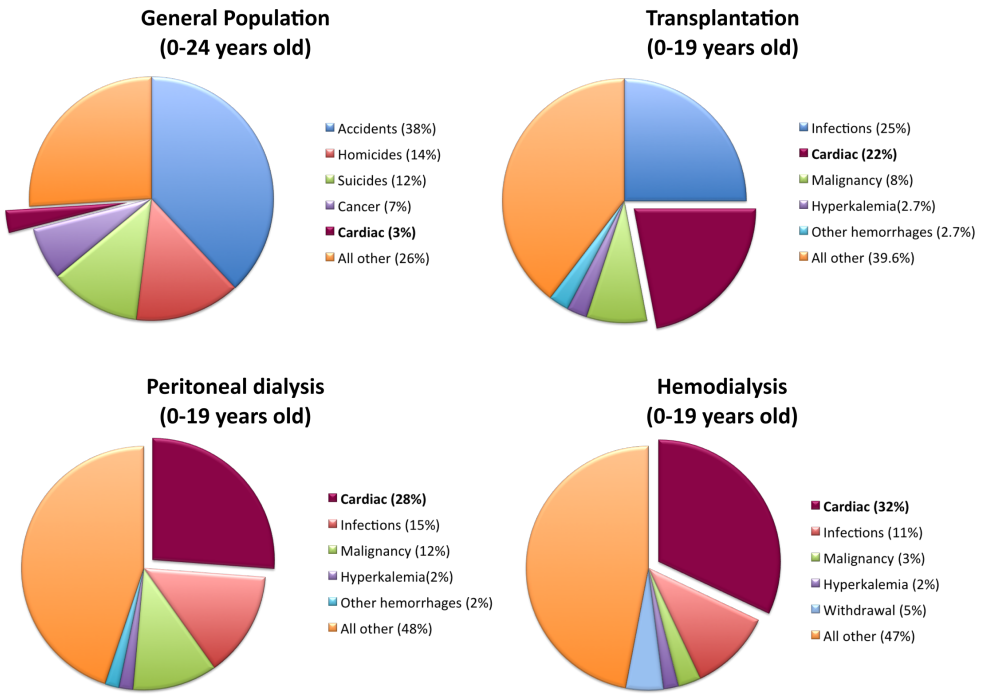

Figure 1.4: Causes of mortality in paediatric patients in the United States
These charts highlight the leading causes of child mortality in the US, both for the general population and paediatric patients on RRT. CVD is highlighted as a key cause of mortality in patients on RRT, while only responsible for 3% of deaths in the general paediatric population. Figures are redrawn from Mitsnefes (2012).

Comparatively, CVD was the second highest cause of death (22%) in patients having received renal transplants following infections, which were the primary cause of death (25%). Mitsnefes (2012) also emphasised the changes in CVD mortality over the past 30 years; while the mortality rate for patients undergoing dialysis has remained steady, the mortality rate for individuals that have received transplants has dramatically decreased. This reduction in deaths can be attributed to improved drug therapies, earlier transplantation, and reduced rejection rates as well as, potentially, an altered cardiovascular risk profile following transplantation. However, despite these developments in drug therapy and transplantation, patients with CKD continue to exhibit a significantly increased rate of CVD-associated mortality.

These data were more recently corroborated by a retrospective study by Chavers *et al* (2015), in which USRDS data from 1995–2010 were examined to determine the one-year mortality rate for paediatric CKD patients undergoing RRT. Again, CVD was the

leading cause of death in paediatric CKD patients undergoing dialysis (33%), whilst infection was the leading cause of death in patients who had undergone transplantation (26%; Chavers *et al* 2006).

A similar study was conducted in Canada to generate the Canadian Paediatric End-Stage Renal Database (Samuel *et al* 2011). This database utilised patient information from the Canadian Organ Replacement Registry and the Canadian Institute for Health Information Discharge Abstract Database and contained 843 patients from 9 of 10 provinces (excluding Quebec, as patient information could not be released) that began RRT between 1992 and 2007; all patients began RRT before 18 years of age (Samuel *et al* 2011). Of the 107 patients that died during the following years, 23 deaths (21%) were due to cardiac failure, which was the leading single cause of death (Samuel *et al* 2011).

Within Europe, the Cardiovascular Comorbidity in Children with CKD (4C) study is a large observational study currently examining the development of CVD and morbidity in paediatric (aged 6–17 years) patients with CKD Stage 3b–5 (Querfeld *et al* 2010). The project currently spans 12 countries, with patients from over 55 nephrology units including Great Ormond Street Hospital NHS Foundation Trust (GOSH). The study aims to follow patients from diagnosis through to RRT and adulthood whilst systematically collecting measurements of cardiovascular function and health (Querfeld *et al* 2010). Although in its infancy, this longitudinal study is one of the largest paediatric studies to date and may provide important insights into disease development and CVD morbidity in these patients. In particular, this study benefits from a routine and standardised examination of the patients rather than relying on retrospective analysis of existing databases as done in previous studies.

Collectively, these studies indicate that CVD is a serious problem for paediatric patients with CKD. Therefore, there is an essential need to further examine the mechanisms by which CVD begins and progresses in these children. If this is done, it has potential to lead to the development of new interventions to improve mortality from CVD in CKD patients.

1.1.5 Risk Factors for CVD

Many risk factors predispose an individual towards developing CVD; in adults, these risk factors can be divided into 'traditional' (or Framingham) and 'CKD-related' risk factors (Table 1.2). Traditional risk factors are those that predispose a given individual in the general population towards developing CVD, such as old age, obesity, and diabetes (Foster *et al* 2015, Fruchart *et al* 2004); these risk factors have been studied since the late 1940s through the Framingham Heart Study.

Traditional CVD Risk Factors	CKD-Associated Risk Factors
Increased age	Decreased GFR
Caucasian	Proteinuria
Male	High circulating calcium
Hypertensive	High circulating phosphate
Increased low-density lipoprotein (LDL) cholesterol	Dyslipidaemia
Decreased high-density lipoprotein (HDL) cholesterol	Low albumin
Diabetes mellitus	Haemodynamic overload
Tobacco use	Anaemia
Physical inactivity	Increased clotting factors
Stress	High circulating homocysteine
Family history of CVD	Oxidative stress
Left ventricular hypertrophy	Infection
Increased body mass	Chronic inflammation

Table 1.2: Traditional and CKD-related risk factors for CVD

Traditional cardiovascular risk factors are most prevalent in adults whilst CKD-related risk factors are specialised to the disease state and place the patient at a much greater risk of developing CVD. Many patients with CKD can present with a combination of both traditional and non-traditional risk factors, as several of the traditional risk factors contribute to one's risk of developing CKD. Table was derived from Fruchart *et al* (2004).

The Framingham Heart Study utilises the town of Framingham, Massachusetts as the site of an epidemiological study spanning several generations. In this town, detailed biological measurements (such as blood pressure and serum creatinine) have been systematically recorded and the correlation to CVD development has led to the identification of numerous CVD risk factors (Mahmood *et al* 2014). In this cohort, mild renal insufficiency (as defined by serum creatinine levels of 136–265 μmol/L in men, and 120–265 μmol/L in women) was shown to pose as a risk factor for CVD (defined as a diagnosis of coronary heart disease, congestive heart failure, or ischaemic stroke) (Culleton *et al* 1999).

Given that many of the traditional risk factors also predispose one to develop kidney disease, many adult CKD patients already possess these risk factors prior to CKD diagnosis (Levin *et al* 2001, Locatelli *et al* 2003). However, CKD patients have their risk compounded by their altered vascular environment such as hypercalcaemic and hyperphosphataemic serum, haemodynamic overload and an increase in oxidative stress (Block *et al* 1998). These 'CKD-associated' risk factors significantly amplify the likelihood of developing CVD (Gansevoort *et al* 2013). In contrast, most children do not possess the traditional Framingham risk factors for CVD development (namely diabetes mellitus, increased age, and tobacco use).

1.1.6 Effects of Dialysis on the Development of CVD

Although dialysis is clearly a necessity in ESRD barring pre-emptive transplantation, it significantly increases the risk of a CKD patient developing CVD. Indeed, a proportional relationship has been established between CVD development and the length of time that a patient is on dialysis (Figure 1.5A, Goodman *et al* 2000). A study by Goodman and colleagues (2000) in a young CKD population (n = 39, aged 7–30 years) highlighted the relationship between coronary artery calcification, which is a critical contributor to CVD, and the length of time spent on dialysis. To examine this, vascular calcification was measured using electron-beam computed tomography (CT) and patients were given an Agatston score based on the size and density of the calcified region (Goodman *et al* 2000). Overt calcifications were observed in 88% of patients over 20 years of age (n = 16), and patients who had spent longer on dialysis were more likely to exhibit calcification (Goodman *et al* 2000).

None of the CKD patients under 20 years of age (n = 23) exhibited signs of vascular calcification (Goodman *et al* 2000). Comparatively, calcification was noted in only 5% of control subjects (n = 60, aged 20–30) (Goodman *et al* 2000).

This study not only indicated a correlation between vascular calcification and the length of time on dialysis, but was also one of the first studies to suggest that 'calcium begets calcium'; that is, after calcium deposition begins, subsequent depositions occur readily and rapidly. Two years after their first CT vascular scan, 22 of the dialysis patients were re-examined (Goodman *et al* 2000). Of these 22 patients, 12 patients initially exhibited no signs of vascular calcification. Two years later, two of these 12 patients now exhibited signs of calcification (Goodman *et al* 2000). Of the 10 remaining patients that exhibited calcification on the initial scan, 90% exhibited an increase in their calcification score of almost two-fold (Figure 1.5B; Goodman *et al* 2000). Using intact arterial rings, Shroff and colleagues (2010) have similarly observed that arterial rings containing high calcium depositions at baseline (particularly arterial rings that stain positive for Von Kossa, indicating visible calcium depositions) calcify more readily than arterial rings with no or low calcium levels and maintain their Von Kossa positivity.

In another study, Oh *et al* (2002) utilised cardiac CT and high-resolution ultrasound to measure vascular calcification and carotid intima-media thickness (cIMT) in 39 young adults (mean age: 27.3±5.9 years) with ESRD (13 receiving dialysis, 26 post-transplantation). Of these patients, 92% exhibited significant vascular calcification; however, patients that were receiving dialysis exhibited more marked calcium deposition than patients that had received transplants (Oh *et al* 2002). Both dialysis and transplanted patients exhibited similarly increased cIMT measurements when compared with age-matched controls (Oh *et al* 2002). Interestingly, whilst smoking correlated with increased cIMT in age-matched controls, it did not correlate with increased cIMT in the patients with ESRD (Oh *et al* 2002). Instead, it was associated with increased time on dialysis, and elevated serum calcium and serum phosphate levels (Oh *et al* 2002). This suggests that whilst these traditional risk factors may be present in patients, they are of less importance to the development of CVD when renal risk factors are present.

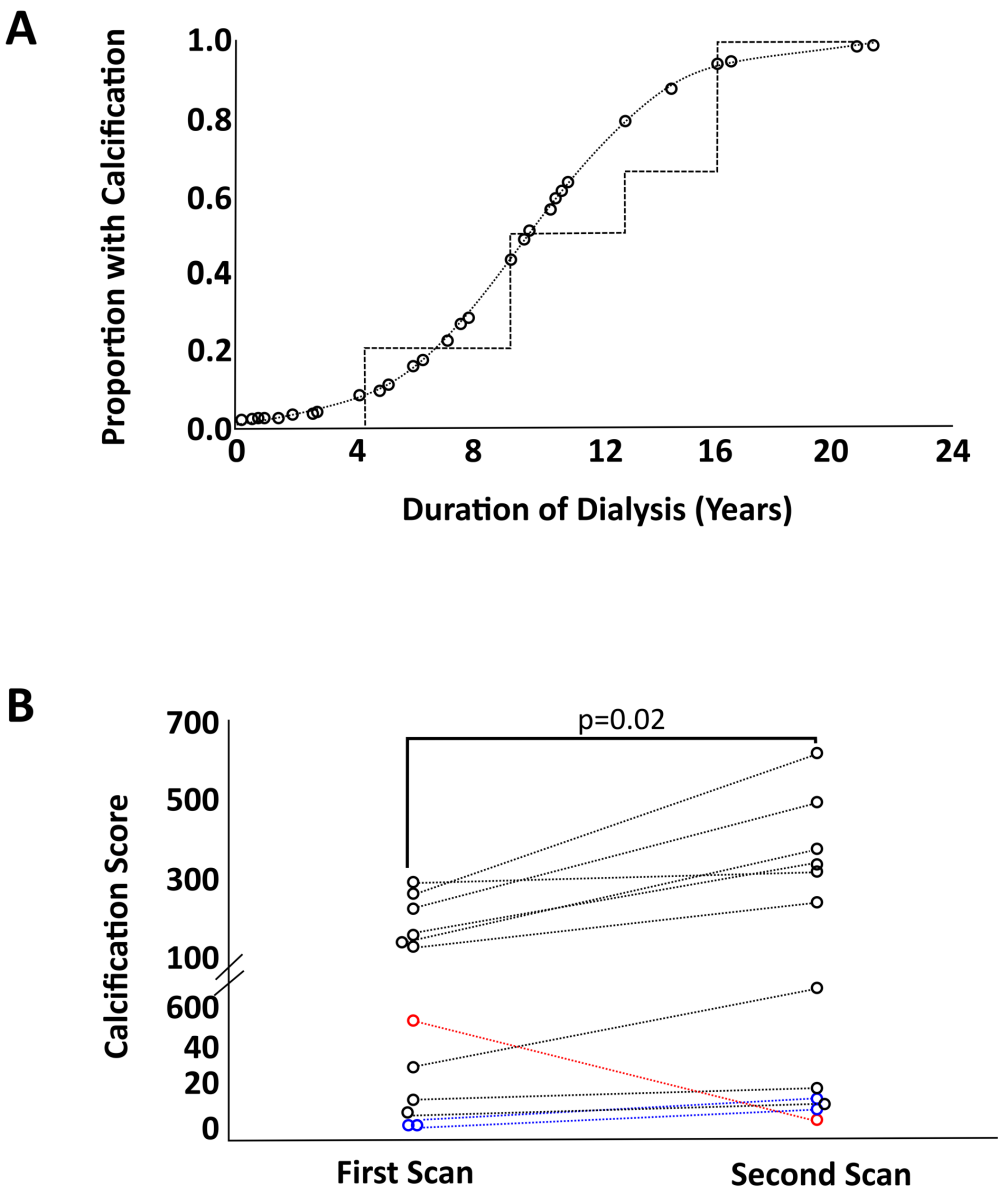

Figure 1.5: CVD risk increases with dialysis

A: Coronary artery vascular calcification in young adult (age 20–30) CKD patients (n=39) exhibit increased prevalence with increased time on dialysis, as determined by electron-beam CT and quantification using Agatston scoring of calcium depositions. The length of time on dialysis excludes periods of transplantation-induced healthy renal function. **B:** In 9 of 10 patients who exhibited calcium deposition at initial investigation, the calcium score was increased at a second scan taken two years later. One patient (in red) exhibited an unexplained decrease in calcification at the second scan. Two patients (in blue) did not exhibit calcification on the initial scan but exhibited low levels of calcification at the second scan. Figures have been redrawn with modification from Goodman *et al* (2000).

1.2 Molecular and Pathological Mechanisms of Vascular Calcification

1.2.1 Vascular Calcification in this Thesis

Throughout this thesis, I have focused on vascular calcification as a manifestation of CVD. Therefore, this section describes the histology and pathology of vascular calcification, the molecular mechanisms that drive the pathology and the methodologies that can be used to model calcification in a laboratory environment. Although the work in this thesis focuses on vascular calcification in children, this section will also explore calcification in the adult population and animal models, as limited research has been conducted to date in the paediatric CKD population.

1.2.2 Vascular Structure and Function

CVD is caused by damage to the vasculature, which begins at the cellular level. Therefore, understanding the structure of the blood vessel is key to investigating the pathology of both vascular calcification and its relationship with endothelial dysfunction (see Section 1.3).

Blood vessels are composed of three primary layers of cells (Figure 1.6). The first layer is the tunica intima; this is composed of vascular endothelial cells that form a single cell layer lining the blood vessel, separating the tunica media from the lumen (Adams and Alitalo 2007). The second layer of cells is the tunica media, which is composed of a tight arrangement of uniformly aligned smooth muscle cells (SMCs) embedded in an extracellular matrix (ECM) (Adams and Alitalo 2007). Finally, the outer layer, the adventitia, is composed of fibroblasts and collagen fibres.

The tunica intima and the tunica media are separated by an elastin sheet, labelled the internal elastic lamina (Adams and Alitalo 2007). Similarly, the tunica media and the adventitia are separated by the external elastic lamina (Adams and Alitalo 2007). The endothelial layer is exceedingly thin, and this quality remains consistent across vessel types whilst the other cellular layers (SMCs and fibroblasts) may vary in width depending on the function of the vessel and the contractility strength required (Alberts *et al* 2002).

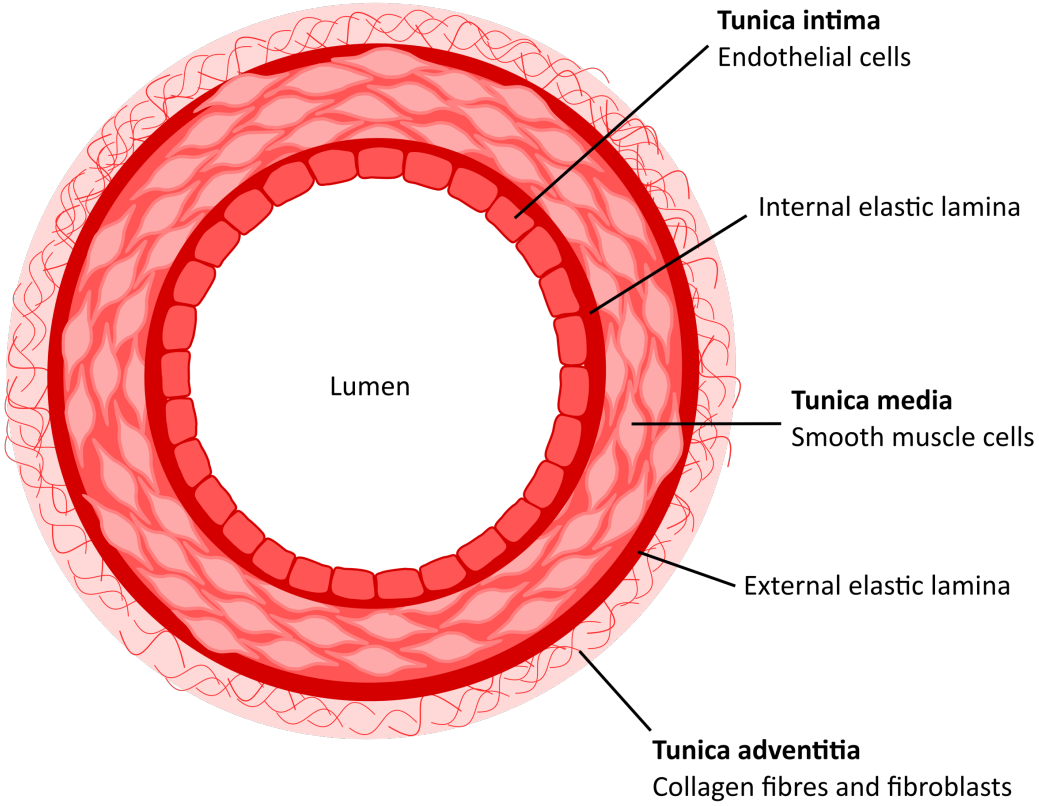

Figure 1.6: Structure of a blood vessel

Blood vessels are composed of three layers of cells: the tunica intima (composed of endothelial cells), the tunica media (composed of vascular smooth muscle cells (VSMCs), embedded in the ECM) and the tunica adventitia (composed of fibroblasts and collagen fibres) (Adams and Alitalo 2007). An elastin sheet separates each layer. Circulating blood fills the luminal space.

1.2.3 Forms of Vascular Calcification

Vascular calcification can be broadly divided into two forms – intimal calcification, and medial calcification – which occur in the tunica intima and the tunica media, respectively (Amann 2008; Figure 1.7).

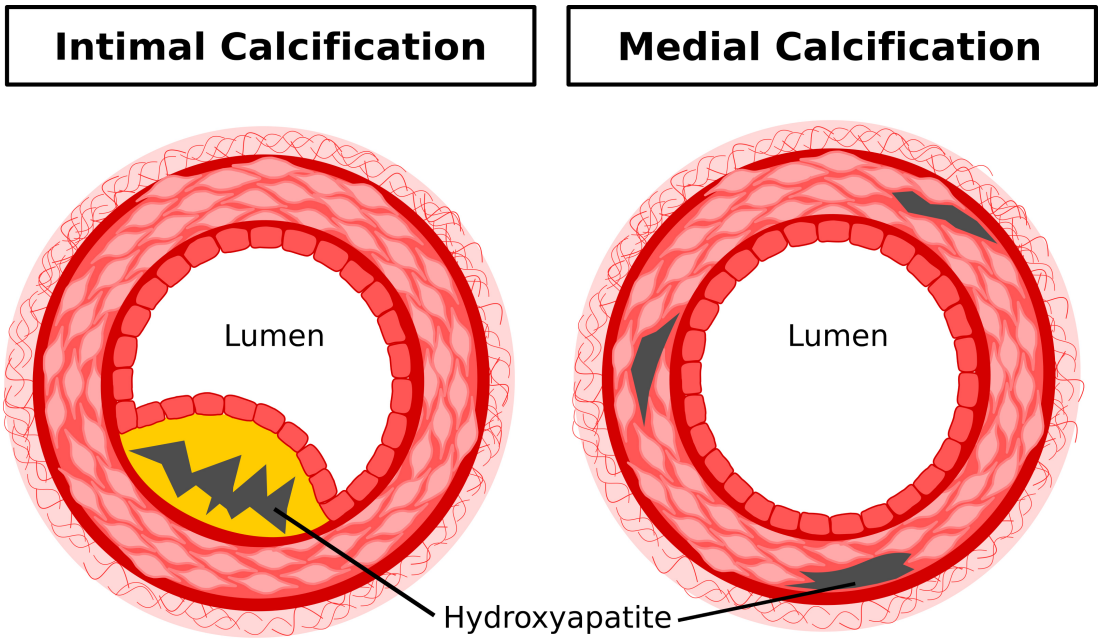

Figure 1.7: Intimal and medial calcification

Intimal calcification and medial calcification develop in the tunica intima and tunica media, respectively. Both intimal and medial calcification are characterised by vascular thickening and stiffening due to hydroxyapatite deposition (Sage *et al* 2010). However, in intimal calcification, deposition occurs between the intima and medial layers, whilst in medial calcification, deposition occurs within the tunica media (Sage *et al* 2010).

Intimal calcification is found predominantly in the adult vasculature (Amann 2008). It is characterised by the formation of plaque within the endothelial layer of the blood vessel; these plaques grow to occlude the artery and are composed of accumulated lipids, SMCs and inflammatory cells (Brunet *et al* 2011, Ross 1999, Sanz and Fayad 2008, Weber and Noels 2011). The restriction of flow increases blood pressure, which leads to vascular stenosis and eventually ischaemia. Development of atherosclerosis is strongly linked to the presence of traditional Framingham risk factors, such as increased age, lipid dysregulation, obesity, hypertension, diabetes and tobacco use (Sage *et al* 2010).

Medial calcification, also known as Mönckeberg's sclerosis, occurs in the tunica media of the vasculature and is characterised by SMC loss and an increase in osteogenic gene

expression (Shroff *et al* 2012). Medial calcification is the primary form of calcification observed in paediatric CKD patients, although it can be observed in conjunction with intimal calcification in adults (Drüeke and Massy 2010). Whilst intimal calcification occurs due to an accumulation of lipids and foam-like cells, infiltration of inflammatory cells, oxidative stress, and apoptosis, medial calcification is driven by endothelial dysfunction, osteogenic differentiation of VSMCs, loss of calcification inhibitors, and an imbalance in calcium and phosphate levels (Shroff *et al* 2012).

During medial calcification, cumulative deposition of hydroxyapatite within the tunica media leads to concentric thickening and stiffening of the vessel wall. Hydroxyapatite is a crystalline structure formed of inorganic calcium (Ca) and phosphate (P), and this lack of contractility drives an increase in systolic blood pressure and increased ventricular afterload (Covic *et al* 2006). This subsequently manifests in left ventricular hypertrophy (LVH), a prominent clinical sign of progressive CVD that is characterised by an increased thickening of the ventricular myocardium (Murphy *et al* 1998). LVH is a biological adaptation to account for increased ventricular afterload and altered coronary perfusion; these result from altered systolic/diastolic pressure and/or aortic stenosis (Lorell *et al* 2000). At a cellular level, the cardiomyocytes become hypertrophic which in turn increases the muscular capacity of the myocardium (Lorell *et al* 2000). LVH is a key indicator of CVD in paediatric patients and precedes cardiac ischaemia and myocardial infarction (Mitsnefes *et al* 2006).

1.2.4 Modelling Vascular Calcification In Vitro and In Vivo

There are two primary ways in which vascular calcification is currently modelled *in vitro*:

1) Primary VSMC cultures and established cell lines
2) Intact vessel rings.

Monolayer cell culture is the more common method of modelling calcification of SMCs, as it provides a relatively simple means by which gene expression levels can be compared and quantified for a given set of media conditions.

VSMC culture has been used extensively to show dose-dependent effects of ionic calcium and phosphate on calcium deposition and vesicle release (Juno *et al* 2000,

Kapustin *et al* 2015, Reynolds *et al* 2004, Wada *et al* 1999). However, utilising a cell model, whether primary cells or a cell line, poses significant challenges as to whether this truly reflects the *in vivo* situation and the interactions between the cell types that occur in a blood vessel. Moreover, culture conditions may cause the cells to differentiate, altering their phenotype (Rzucido *et al* 2007). To overcome some of these issues, low passage primary cells can be utilised; however, this requires a supply of fresh tissue from which to isolate the cells. Moreover, *in vitro* conditions can cause all VSMCs, at any passage, to change to a pan-mesenchymal phenotype and develop osteochondrocytic characteristics (Campbell and Campbell 2012).

Intact vessel rings provide an alternative method to model vascular calcification in culture, particularly when utilising human samples. In this model, intact blood vessels are cut into rings; this maintains the defined layers in the vascular structure, which provides a more realistic and representative model of the physiological interaction between the tunica intima, tunica media and the adventitia (Shroff *et al* 2013). One key benefit of this model is that one can study blood vessels directly obtained from patients with the disease of interest, such as CKD (Shroff *et al* 2013). Because diseased vessels are exposed to a different circulating environment than healthy vessels – for example, high levels of calcium and phosphate in uremic serum, or dialysis-induced haemodynamic stress – these diseased vessels may respond differently to *in vitro* stimulation than healthy vessels (Shroff *et al* 2013).

Intact arterial rings obtained from adult CKD Stage 5 patients provided insights into the disorganised SMC arrangement within vessels from dialysis patients. In healthy vessel rings, the SMCs are aligned and run parallel to the elastic lamina; the elongated nuclei reflect this parallel formatting (Moe *et al* 2002). Comparatively, the nuclei of VSMCs in dialysis vessel rings are of smaller size and take a haphazard non-linear arrangement (Moe *et al* 2002). In the adult vascular rings examined by Moe and colleagues (2002), the disorganised arrangement was observed even in vessel rings that were not yet Von Kossa positive (denoting hydroxyapatite deposition in the vessel). Additionally, Moe and colleagues (2002) were unable to detect infiltrating macrophages within the calcified tunica media, implying that inflammation is not required for the progression of calcification of VSMCs. Instead, the authors proposed that calcification was associated with an increase in expression of bone matrix

proteins, namely bone morphogenic protein (BMP2) and runt-related factor (RUNX2). This work on intact vessel rings helped to formulate new insights into the mechanisms underlying medial calcification.

Intact arterial rings were also used in two papers by Shroff *et al* (2008; 2010) examining medial calcification in paediatric CKD patients. Arterial rings from paediatric controls contained low calcium levels (9.4±2.3 μg/μl, as detected by the quantitative *o*-cresolphthalein colorimetric assay), whilst calcium levels were significantly higher in pre-dialysis CKD patients (20.4±6.5 μg/μL) (Shroff *et al* 2008). Comparatively, paediatric CKD patients on dialysis exhibited the greatest levels of calcium, measuring 39.2±6.0 μg/μL (Shroff *et al* 2008). By utilising this unique resource of intact arterial rings from a paediatric CKD population, Shroff *et al* (2008) were able to demonstrate that that dialysis vessels contained higher baseline levels of calcium, compared to both vessels from paediatric controls and vessels from paediatric pre-dialysis CKD patients.

Additionally, vessel rings from paediatric controls, pre-dialysis CKD, and dialysis CKD patients were shown to respond differently to stimulation by exogenous calcium (2.7 mM Ca) and phosphate (2.0 mM P) (Shroff *et al* 2010). Vessel rings from control patients showed no increase in calcium load following exposure to high levels of calcium and phosphate; in contrast, vessel rings from pre-dialysis CKD patients exhibited a significant increase in calcium load (19.7±1.1 μg/μL versus 115.1±49.0 μg/μL, in 1.8 mM Ca and 1.0 mM P compared with 2.7mM Ca and 2.0 mM P respectively, $p = 0.03$) (Shroff *et al* 2010). The vessel rings from paediatric CKD patients undergoing dialysis also exhibited a significant increase in calcium deposition when cultured with elevated exogenous calcium and phosphate (129.0±53.0 μg/μL versus 711.0±206.0 μg/μL in 1.0 mM P and 1.8 mM Ca compared with 2.0 mM P and 2.7 mM Ca respectively, $p<0.0001$) (Shroff *et al* 2010).

The primary disadvantage of this model is that human tissue is a limited resource; the blood vessels, for either isolation of cells or intact ring culture, can only be obtained at a single time-point when the patient undergoes abdominal surgery. The samples are difficult to obtain, and rely on ethical approval, patient consent and surgical cooperation.

1.2.5 In Vivo Modelling – Human Models of Calcification

Vascular calcification can also be measured in both adult and paediatric patients using non-invasive techniques. The blood vessels can be visualised by radiography, electron-beam and multi-slice CT, and high-resolution ultrasound (Owen *et al* 2011, Sanz and Fayad 2008). These techniques can facilitate the measurement of cIMT, which is "the distance between the lumen-intima interface and the media-adventitia interface of the far wall" (Litwin *et al* 2005).

High-resolution ultrasound has shown that the cIMT increases markedly in children on dialysis (n = 37) with small rises also detected early in CKD development (Litwin *et al* 2005). Transplanted patients (n = 34), despite previously being on dialysis, had cIMT measurements similar to pre-dialysis CKD patients (n = 55) suggesting that the increase in vascular thickness may partly be reversed following transplantation (Litwin *et al* 2005). The authors propose that this 'reversal' of phenotype may be due to the removal of the uremic milieu following transplantation, as well as the restoration of normal serum calcium and serum phosphate concentrations (Litwin *et al* 2005). Other studies have also shown an increase in cIMT with increased duration on dialysis (Mitsnefes *et al* 2004, Saygili *et al* 2002). A later study by Litwin and colleagues (2008) followed paediatric CKD patients over the course of a year through dialysis and transplantation, and showed that prolonged CKD was associated with an increase in cIMT, most notably in children on dialysis. The authors showed that these responses correlated with increased LDL cholesterol, uric acid, blood pressure and serum phosphate. Conversely, they showed that whilst prolonged CKD was associated with an increase in cIMT, transplantation following dialysis was associated with decreasing cIMT (Litwin *et al* 2008).

Another parameter that can be measured is pulse wave velocity (PWV): the speed at which a pulse wave travels between two set points of a vessel. PWV indicates the elasticity and contractility of a vessel, and these properties are reduced by calcification (Haydar *et al* 2004). Again, this technique is non-invasive and is measured using high-resolution ultrasound (Karohl *et al* 2011). While PWV can be altered in response to nitric oxide (NO) bioavailability, it is primarily indicative of fibrosis and calcification (Fitch *et al* 2001). When major arteries experience reduced contractility, particularly

in the aortic arch, the cardiac workload required for blood circulation increases significantly. This subsequently drives up the systolic blood pressure and leads to LVH and reduced coronary perfusion (Duncker *et al* 1993).

1.2.6 In Vivo Modelling – Murine Models of Calcification

Murine models are beneficial for studying physiological and disease processes *in vivo*. Both cells and aortic rings can be obtained from animals to extend the experimental system further, while the physiological measurements observed with CKD and/or calcification can also be measured (i.e. blood pressure and renal function, as well as kidney and vascular histology). Transgenic animals can be utilised to examine the effect of overexpression or deletion of a gene of interest.

There are three common methods used to model vascular calcification during CKD in rodents: the remnant kidney model, provision of high dietary adenine, and electrocauterisation of the kidney (Neven and D'Haese 2011, Shobeiri *et al* 2010). However, an important limitation is that there is currently no true mouse model available to replicate the effects of dialysis in patients. In addition, there are differences in the progression and severity of CKD in mouse models due to the specific genetic background of a mouse, which alters their susceptibility to renal damage (Laouari *et al* 2012, Long *et al* 2013).

The remnant kidney model utilises a 5/6 nephrectomy to simulate progressive nephron loss, which leads to CKD (as determined by an increase in serum creatinine) (Neven and D'Haese 2011). This injury, when supplemented with a high phosphate diet, results in hyperphosphataemia (Neven and D'Haese 2011). However, vascular calcification is constrained primarily to the aortic arch unless the injury is combined with a high phosphate, high lactose diet (1.2% phosphate, 1% calcium, and 20% lactose) or with 1,25(OH) vitamin D_3 supplementation (Henley *et al* 2005). The high lactose diet increases intestinal reabsorption of dietary calcium and phosphate and induces medial calcification, whilst supplementation with Vitamin D_3 induces widespread calcification of the aortic wall (Henley *et al* 2005). There are currently few studies utilising the lactose diet, whilst the latter method utilising vitamin D_3 has been

more widely used in the literature (Haffner *et al* 2005, Henley *et al* 2005, Kawata *et al* 2008).

The electrocautery model of CKD induces renal failure through cauterised ablation of the renal cortex, after which the second kidney is removed (Shobieri *et al* 2010). The severity of CKD in this model can be variable, and the mice do not always exhibit hyperphosphataemia (Shobieri *et al* 2010). This model is generally used in either low-density lipoprotein receptor knockout (*LDLR*$^{-/-}$) mice, or apolipoprotein E-deficient (*apoE*$^{-/-}$) mice. These two transgenic strains develop extensive calcification whilst wild-type mice do not exhibit calcification. The *LDLR*$^{-/-}$ mice are obese, hypertensive and diabetic, all of which are 'traditional' risk factors for CKD (Shobieri *et al* 2010). *ApoE*$^{-/-}$ mice lack apolipoprotein and exhibit increased cholesterol and rapid development of atherosclerotic lesions, which are in turn augmented by CKD (Zhang *et al* 1992). However, as both of these transgenic mice raise more risk factors that are 'traditional' for CVD, they pose more similarities to the CKD phenotype found in adults rather than the phenotype observed in children.

Finally, vascular calcification during CKD can also be induced by an adenine-rich diet, as excess adenine undergoes oxidation to produce 2,8-dihydroxyadenine that precipitates in the kidney. These precipitates damage the renal tubules, triggering inflammation and subsequent fibrosis (Neven and D'Haese 2011). Rodents exposed to an adenine-rich (0.75%) diet exhibit calcification of the aortic media within 4 weeks of undergoing a high phosphate diet (1.03% P, 1.06% Ca), and exhibit hyperphosphataemia (Katsumata *et al* 2003). However, almost 50% of rats are resistant to calcification despite exhibiting severe CKD, although the cause for this is unclear (Neven and D'Haese 2011). However, Price *et al* (2006) have shown that the proportion of rats that exhibit medial calcification using this adenine model of CKD can be improved (100% penetrance of calcification versus 30% in controls) if they are fed a low-protein (2.5%) diet without added calcium or phosphate. By altering dietary protein, rather than dietary calcium or phosphate, these mice do not exhibit high serum calcium or phosphate levels unless induced by renal damage (Price *et al* 2006).

1.2.7 Mechanisms of Vascular Calcification

Vascular calcification was once believed to be a passively occurring process, progressing as an individual aged (Leopold 2013, Schinke and Karsenty 2000). However, increasing evidence from studies utilising the *in vitro* and *in vivo* models described in Sections 1.2.3 through 1.2.5 has shown that calcification is actually a highly regulated process similar to bone formation (Leopold 2015). It is driven by a combination of mineral dysregulation, the release of matrix vesicles, osteogenic gene expression and apoptosis (Shroff *et al* 2012). Given the correct conditions, these processes can occur independently of age, as is indicated by the prevalence of calcification in paediatric CKD patients. However, due to the multifactorial pathology, it is difficult to define a clear preventative strategy. Within this section, I will outline the different mechanisms that contribute to vascular calcification in CKD patients (Figure 1.8).

1.2.7.1 Mineral Dysregulation

During CKD, patients typically exhibit both elevated calcium (hypercalcaemia) and elevated phosphate (hyperphosphataemia); this creates the ideal environment to promote hydroxyapatite formation (Shroff 2011). Hydroxyapatite is the main type of external calcium deposition and is a crystalline structure formed of inorganic calcium and phosphate ions. In CKD, dietary phosphate cannot be excreted as rapidly as it is ingested, whether this is through the damaged kidney or through dialysis (Kestenbaum 2007). Therefore, ionic phosphate levels build up within the serum over the course of time. While this can be limited by the use of phosphate binders or regulated restriction of dietary phosphate, there is currently no clear strategy to prevent hydroxyapatite formation (Kestenbaum 2007).

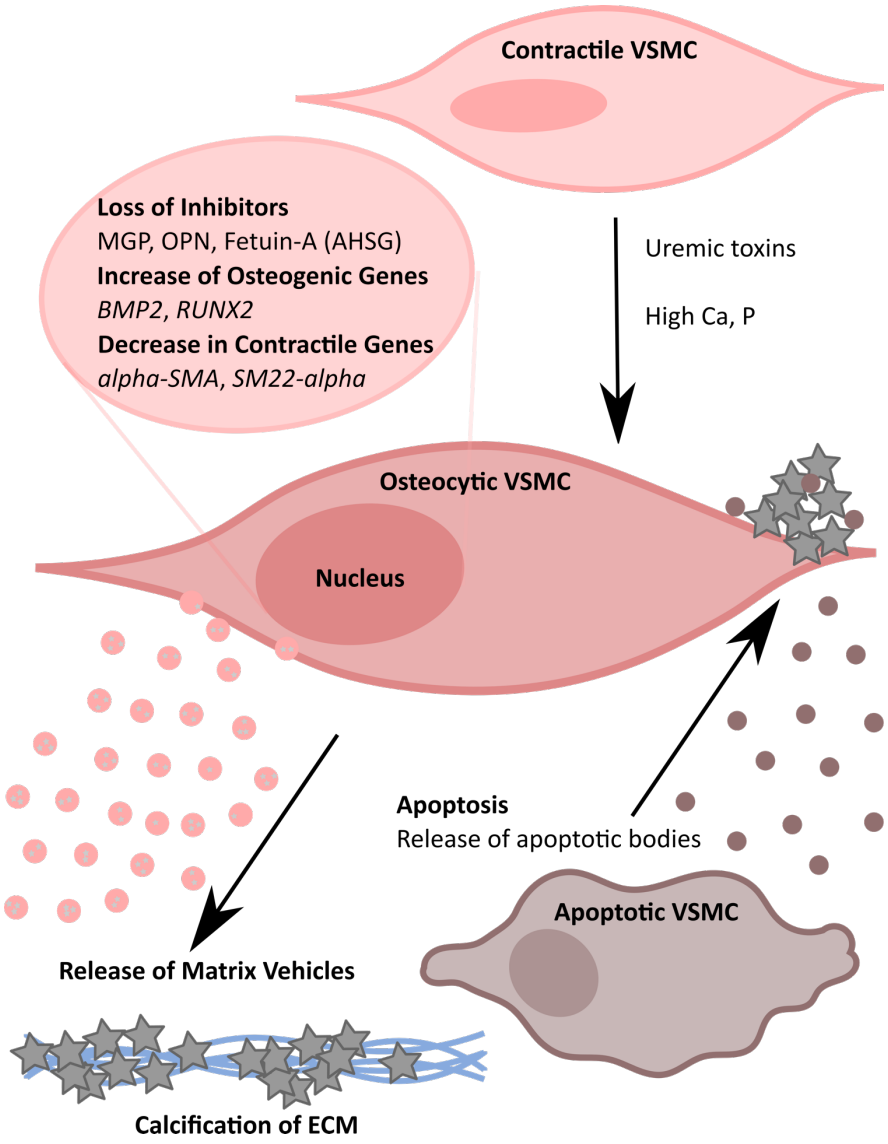

Figure 1.8: Modulators of vascular calcification

In the presence of elevated calcium (Ca) and phosphate (P), contractile VSMCs take up the excess calcium. This increase in calcium triggers upregulation of osteogenic genes, such as bone morphogenic protein-2 (*BMP2*) and runt-related transcription factor 2 (*RUNX2*). This is accompanied by a loss of osteogenic inhibitors like matrix-Gla protein (*MGP*), osteopontin (*OPN*) and fetuin-A, as well as a decrease in contractile smooth muscle genes like alpha smooth muscle actin (*αSMA*). These changes induce an osteocyte-like phenotype. The intracellular calcium is packaged up into matrix vesicles that are released from the cell. These matrix vesicles are a source of ionic calcium, which then allows the ECM to calcify. Apoptotic bodies are released from dead or dying cells and act as nidi from which calcification can perpetuate.

1.2.7.2 Matrix Vesicle Formation

One means through which calcification is regulated is through the release of matrix vesicles: spherical extracellular particles, 50–200 nm in diameter, which are bound by biologically active membranes (Anderson 1995). Matrix vesicles were originally detected in the bone growth plate; however, they are also released by quiescent VSMCs and infiltrating macrophages during atherosclerotic development (Anderson 1969, New *et al* 2013).

Under normal physiological conditions, VSMCs continually release matrix vesicles from the plasma membrane (Reynolds *et al* 2004). However, in the presence of elevated phosphate, 2.4 mM calcium is enough to trigger doubling ($9.89\pm0.26\times10^8$ particles/mL versus controls $4.92\pm0.46\times10^8$ particles/mL) of the release rate of vesicles (Reynolds *et al* 2004). Under serum-free conditions, this increased rate of vesicle release was also accompanied by an increase in apoptotic bodies (Reynolds *et al* 2004). However, this increase in apoptotic bodies did not occur if the culture medium was supplemented with 5% foetal bovine serum (FBS), likely due to the presence of calcification inhibitors within the serum (Reynolds *et al* 2004).

Matrix vesicles adapt to exposure to high calcium and phosphate environments through altering their internal composition. Using electron microscopy, Reynolds and colleagues (2004) were able to observe calcium phosphate crystals within the released vesicles; these vesicles appear to form the nidi for subsequent calcification. Comparatively, the matrix vesicles released under quiescent conditions did not contain calcium phosphate crystals but were instead loaded with inhibitors of calcification such as MGP, osteopontin, and fetuin-A (Reynolds *et al* 2004). Following treatment with high calcium and phosphate, these matrix vesicles exhibited a significant loss of the calcification inhibitor MGP (Kapustin *et al* 2011). Fluorescent tracking of AlexaFluor488-bound fetuin-A uptake in monolayer VSMC cultures has indicated that, although VSMCs do not produce fetuin-A, they are able to actively take up fetuin-A from their environment (Kapustin *et al* 2015).

1.2.7.3 Apoptosis

When VSMCs (derived from cardiac donor aorta) reach confluence, they exhibit a 'hill-and-valley' phenotype (Proudfoot *et al* 1998). However, when the monolayer of VSMCs becomes overly confluent, some cells retract and subsequently pull in the surrounding cells; in doing so, multicellular nodules are formed (Proudfoot *et al* 1998). Proudfoot and colleagues (1998) described these nodules as containing "concentric layers of cells arranged around the outer part of the nodule, with many small cells in the middle of the nodule." These nodules, which stain positive with Alizarin red stain and Von Kossa (both indicating calcium deposition), contain live cells (Proudfoot *et al* 1998; 2000). These cells can continue to proliferate following an elongated lag phase; however, if these nodules are left to develop in culture, there is a loss of cells from the nodule centre over time due to an increase in apoptosis (Proudfoot *et al* 1998; 2000).

Interestingly, optical sectioning of these nodules using confocal microscopy and quantification of nuclear morphology indicated that apoptosis was initiated prior to the overt onset of calcification (Proudfoot *et al* 2000). Proudfoot and colleagues (2000) went on to demonstrate that apoptotic bodies were released prior to the onset of calcification, and formed foci from which mineralisation could occur. Note that these apoptotic bodies are not nodules themselves but instead appear to be initiators of nodule calcification, as they possess the ability to take up and accumulate extracellular calcium (Proudfoot *et al* 2000). Interestingly, these nodules have been shown to express high levels of MGP, despite their large hydroxyapatite depositions; it has therefore been postulated that MGP is potentially trapped within the hydroxyapatite accumulation, thus preventing calcium-binding activity and promoting further calcification (Proudfoot *et al* 1998; 2000).

1.2.7.4 Osteogenic Differentiation

Vascular calcification can occur due to VSMCs in the tunica media differentiating to an osteoblast-like phenotype (Shroff *et al* 2012). In a healthy arterial vessel wall, VSMCs adopt a 'mature' contractile phenotype and express a combination of contractile proteins and inhibitors of calcification (Shroff *et al* 2012). During

atherosclerosis and arteriosclerosis, these cells exhibit a loss of the anti-osteogenic genes in favour of pro-osteogenic genes, leading to the development of an osteocytic phenotype rather than the phenotype of a SMC (Shroff *et al* 2012). Transdifferentiation between these phenotypes can alter the contractility of the vessel wall without inducing apoptosis (Shroff *et al* 2012). Importantly, cultured VSMCs are known to spontaneously convert to an osteoblast-like phenotype, particularly if overly confluent; this is one weakness of the *in vitro* models of vascular calcification (Chamleu *et al* 1974, Shanahan *et al* 1999).

1.2.8 Osteogenic Genes

Contractile VSMCs are associated with the expression of anti-osteogenic genes and calcification inhibitors, whilst an osteogenic phenotype is accompanied by the expression of pro-osteogenic genes. There are many anti- or pro-osteogenic genes; however, in this thesis, I will focus on the main ones studied to date in published studies of vascular calcification (Table 1.3).

Role	Gene	Gene Name	Function
Pro-osteogenic	*RUNX2*	Runt-related transcription factor 2	Transcription factor
	SP7	Osterix	Transcription factor
	BMP2	Bone morphogenic protein 2	Osteogenic growth factor
Anti-osteogenic	*MGP*	Matrix-Gla Protein	Calcium-binding protein
	AHSG	Alpha2-HS-glycoprotein (Fetuin-A)	Calcium-binding protein
	OPN	Osteopontin	Calcium-binding protein

Table 1.3: Examples of pro- and anti-osteogenic genes

1.2.8.1 Matrix-Gla Protein

MGP is a 14 kDa calcium-binding ECM protein that acts as an anti-osteogenic agent. MGP is synthesised by both chondrocytes and VSMCs and prevents calcification of the ECM through interaction with the pro-osteogenic factor BMP2 (Wallin *et al* 1999,

Zebboudj *et al* 2002). MGP can assume one of two forms: an inactive, dephosphorylated uncarboxylated (GLU) form or an active, phosphorylated carboxylated (GLA) form (Schurgers *et al* 2010). The enzymatic conversion between the two forms relies on vitamin K (Murshed *et al* 2004). Both MGP and vitamin K are necessary to maintain a functional contractile vasculature. Whole-body deletion of *Mgp* does not affect the embryonic development of the vasculature in mice (Luo *et al* 1997). Instead, their arteries become extensively calcified after birth, leading to death within two months (Luo *et al* 1997). These mice are also growth-retarded, as calcification of the cartilage causes fusion of the growth plates (Luo *et al* 1997).

Warfarin, a vitamin K antagonist, acts as an anticoagulant and is often prescribed to reduce the risk of stroke, blood clots and heart attacks in patients with atrial fibrillation. However, warfarin has also been shown to increase medial calcification in mice, likely through inhibiting vitamin K activity and the formation of the active (GLA) form of MGP (Price *et al* 1998, Tantisattamo *et al* 2015). With increased vascular calcification as a potential side effect, the use of warfarin in CKD patients is therefore controversial. Administration of warfarin to patients with compromised renal function has been associated with an increased risk of haemorrhage and ischaemic stroke, particularly in patients undergoing dialysis (Limdi *et al* 2009, Shah *et al* 2014). When exogenous Vitamin K was given to warfarin-treated rats with calcified vessels, there was a therapeutic effect on the vascular contractility; therefore, it has been proposed that the reabsorption of calcium may also be an active process mediated by the carboxylated form of MGP (Schurgers *et al* 2007).

In humans, *MGP* deficiency occurs in Keutal syndrome – a rare autosomal recessive disease that occurs due to a loss-of-function mutation in *MGP* (Munroe *et al* 1999). The disease manifests as abnormal calcification of the cartilage, leading to dysmorphic features and hearing loss, as well as extensive calcification of the vasculature (Munroe *et al* 1999). The severity of the disease is variable, though pathogenicity is linked primarily to the extent and localisation of vascular calcification (Munroe *et al* 1999). There has been one known attempt at vitamin K supplementation in Keutal syndrome, as it was proposed that additional vitamin K would support conversion of remaining (though low) levels of uncarboxylated (inactive) MGP to the carboxylated (active)

form; however, the patient exhibited no improvement in circulating levels of carboxylated MGP (Cranenburg *et al* 2011).

1.2.8.2 Fetuin-A

Fetuin-A, also known as alpha-2-Heremans-Schmid-glycoprotein (AHSG), is a 62 kDa circulating inhibitor of calcification that prevents the mineralisation of calcium and phosphate but does not alter existing hydroxyapatite deposition (Heiss *et al* 2003, Reynolds *et al* 2005). The mechanism by which fetuin-A prevents mineralisation is unique; the protein forms temporary spheres in conjunction with calcium, phosphate and albumin – termed 'calciprotein particles' by Heiss and colleagues (2003). These 30–150 nm particles can be detected by electron microscopy, and prevent pathological mineralisation and aggregation of the calcium phosphate crystals (Heiss *et al* 2003, Reynolds *et al* 2005).

In healthy non-calcified arterial rings, fetuin-A was not detected by immunohistochemical staining; however, when arterial rings had either intimal or medial calcification, the calcium-rich regions of the tunica media exhibited positive intracellular staining for fetuin-A (Reynolds *et al* 2005). When the fetuin-A composition of calcified monolayer cultures of human VSMCs was compared with the fetuin-A composition of normal (uncalcified) human VSMCs, neither population was shown to express human fetuin-A (Reynolds *et al* 2005). However, the calcified human VSMCs were shown to contain high levels of bovine fetuin-A, suggesting that fetuin-A was actively taken up from the FBS in the culture medium rather than being produced by the VSMCs themselves (Reynolds *et al* 2005). Under high calcium and phosphate environments, calcification was inhibited in VSMCs by treating them with a physiological dose of fetuin-A (Reynolds *et al* 2005). Fetuin-A was shown to concentrate in matrix vesicles that did not subsequently act as a nidus for calcification, whereas matrix vesicles low in fetuin-A were able to propagate calcium depositions (Reynolds *et al* 2005, Kapustin *et al* 2015).

Global deletion of fetuin-A in C57/BL6 mice results in mild ectopic calcification, although this phenotype is enhanced to widespread calcification, particularly in smaller blood vessels, in mice on a DBA/2 background (Schafer *et al* 2003). On the

DBA/2 background, the increase in vascular calcification is associated with high blood pressure, renal failure and hyperthyroidism (Schafer *et al* 2003). However, such phenotypes are not observed in C57/BL6 mice, even when fed a high fat-high mineral diet, as these mice are resistant to developing CKD (Schafer *et al* 2003, Laouari *et al* 2012). In mice exhibiting fetuin-A deficiency, the primary site of hydroxyapatite deposition is the tunica intima rather than the tunica media, suggesting that the inhibitory capacity of fetuin-A has greater effects on atherosclerosis rather than arteriosclerosis (Westenfield *et al* 2009). If this holds true for patients, decreased fetuin-A levels are potentially more problematic for adults with CKD than for children. Again, this difference in disease pathology supports the necessity to conduct studies examining the mechanisms of vascular calcification in paediatric patients as well as in adults.

Serum fetuin-A levels are significantly lower in adults receiving HD than in healthy controls, a reduction that is associated with increased cardiovascular and mortality risk (Ketteler *et al* 2003). In contrast, an American study examined adult pre-dialysis (Stage 3–4) CKD patients and found no correlation between circulating fetuin-A levels and patient mortality (Ix *et al* 2007). At the 10-year follow-up point, 25% of the patients had died, 49% due to CVD, but this did not correlate with their earlier fetuin-A levels (Ix *et al* 2007). Van Summeren and colleagues (2008) noted that, in a cohort of paediatric renal transplant patients (n = 29), circulating fetuin-A was significantly lower ($p<0.005$) than in healthy paediatric controls (n = 54) whilst the carotid intima-media thickness was significantly increased ($p<0.001$) in the renal patients compared to the healthy controls. However, despite these comparative differences, there were no detectable correlations between calcification, vascular parameters and serum fetuin-A levels (van Summeren *et al* 2008).

An interesting study in rats has recently been published questioning the use of dietary restriction as a means to control phosphate levels, as this may lead to malnutrition which in turn decreases fetuin-A levels (Yamada *et al* 2015). However, when these authors compared the lifespan of Sprague-Dawley rats with adenine-induced uraemia on either a high- or low-protein diet, there were no significant differences between dietary groups (Yamada *et al* 2015). However, whilst the diet had no effect on

calcification, it did enhance inflammation that also decreased fetuin-A (Yamada *et al* 2015).

1.2.8.3 Bone Morphogenic Protein-2

BMP2 is a pro-osteogenic growth factor that can promote calcification (Li *et al* 2008). Mice lacking both copies of *Bmp2* are embryonic lethal, although heterozygous mice are phenotypically normal (Zhang and Bradley 1996). Thirty percent of deaths result from failure of the pro-amniotic canal to close, whilst the remaining 70% have cardiac defects (Zhang and Bradley 1996).

Circulating BMP2, as measured using an enzyme-linked immunosorbent assay (ELISA), is increased in uremic serum from adult patients undergoing dialysis; however, there is wide variation in expression levels between patients (Chen *et al* 2006). When cultured in the presence of human uremic serum, bovine VSMCs increase BMP2 production, which is released from the cells into the surrounding medium (Chen *et al* 2006). *BMP2* messenger RNA (mRNA) expression was detected in adult atherosclerotic plaques by *in situ* hybridisation, at the sites of calcification rather than throughout the vessel (Boström *et al* 1993). Similarly, the calcifying nodules of over confluent cells express *BMP2* mRNA whilst *BMP2* mRNA is not expressed by the surrounding VSMCs in monolayer culture (Boström *et al* 1993).

BMP2 does not induce calcification in human VSMCs under normal phosphate conditions; however, in the presence of elevated phosphate, BMP2 enhances calcification of human VSMCs (Li *et al* 2008). In human VSMCs, BMP2 stimulation induces upregulation of the sodium-dependent phosphate co-transporter, Pit-1, and competitive inhibition of the Pit-1 transporter can attenuate BMP-induced calcification (Li *et al* 2008). BMP2-driven calcification is accompanied by an increase in *RUNX2* (a calcification transcription factor) mRNA expression levels; this is coupled with a decrease in mRNA expression levels of the contractile protein, smooth muscle 22-alpha (*SM22α*, transgelin), as detected in cultured human VSMCs (Li *et al* 2008).

1.2.8.4 Osteopontin

Osteopontin (OPN) is a 33 kDa secreted calcium-binding protein, although the size of this protein increases to approximately 41 kDa following post-translational glycosylation and/or phosphorylation (Christensen *et al* 2007). Numerous cell types produce OPN, including osteoblasts, endothelial cells, and VSMCs (Christensen *et al* 2007). OPN facilitates cellular adhesion and migration, and production in the VSMCs is increased in response to low circulating levels of calcium and phosphate (Giachelli 2004).

Interestingly, VSMCs isolated from the aortas of $Opn^{-/-}$ mice showed no morphological differences to VSMCs isolated from the aortas of $Opn^{+/+}$ mice (Speer MY *et al* 2005). Despite the deletion of *Opn*, these VSMCs did not calcify (as quantified using the *o*-cresolphthalein assay and Alizarin red staining) under normal culture conditions across a 7-week period (Speer *et al* 2005). However, when stimulated with 2.4 mM phosphate, the $Opn^{-/-}$ VSMCs calcified twice as much as the $Opn^{+/+}$ VSMCs (Speer *et al* 2005). This relationship remained consistent across different phosphate concentrations, and the calcification phenotype could be rescued with transduction of the *Opn* cDNA into the $Opn^{-/-}$ cells (Speer *et al* 2005).

A separate study in wild-type mice indicated that uninjured, healthy arteries expressed very low levels of Opn (Giachelli *et al* 1993). However, following vascular injury, expression levels of Opn were significantly increased in neointimal VSMCs; occasional VSMCs at the media-adventitial interface also expressed Opn (Giachelli *et al* 1993; Speer and Giachelli 2004). This pattern of expression following vascular injury is similarly observed in human vessels where OPN expression increases with the degree of vascular calcification in the vessel, with particular localisation near plaque deposits (Giachelli *et al* 1993, Hirota *et al* 1993, Ikeda *et al* 1993). Supported by this evidence, OPN is therefore believed to be a crucial protein released in response to calcification-inducing environments, although the mechanism by which this occurs is still under investigation.

1.3 Endothelium and Angiogenic Growth Factors

1.3.1 Vascular Growth Factors in this Thesis

The overarching aim of this thesis is to understand the potential role of vascular growth factors on calcification. The primary role of these growth factors is to modulate the endothelium, and thus I will briefly introduce the concept of endothelial dysfunction and altered vascular growth factors in the context of renal disease. In particular, I will describe one family of vascular growth factors called the angiopoietins that have been studied in this thesis.

1.3.2 Endothelial Dysfunction

The endothelium, a monolayer of endothelial cells separating the circulating blood from the contractile VSMCs, plays a key role in maintaining vascular homeostasis through the regulation of vasoconstrictors and vasodilators in response to damaging physical and circulating factors which may initiate inflammation, induce cellular apoptosis, and modulate vascular tone and contractility (Deanfield *et al* 2007).

Endothelial dysfunction can be defined as the loss of this ability to self-regulate and maintain vascular homeostasis. It is one of the earliest manifestations of CVD and can begin several months to years prior to overt manifestations of CVD. This physiological disturbance can be characterised by cellular disruptions to the endothelium without adequate repair mechanisms (Moody *et al* 2012).

1.3.2.1 NO and Asymmetric Dimethylarginine

NO is one of the key components for maintaining endothelial health (Cannon 1998). This vasodilator is derived from L-arginine and synthesised by endothelial NO synthase (eNOS) (Wang *et al* 2010). Under healthy conditions, endothelial cells remain in a quiescent state. However, alterations in shear stress, such as those induced by high blood pressure, drive atherosclerotic development and neointimal hyperplasia, mediated in part by a decrease in NO production (Coppolino *et al* 2008, Fitts *et al* 2014).

eNOS activity can be compromised by the increased presence of a metabolic waste product and L-arginine analogue, asymmetric dimethylarginine (ADMA). ADMA is a strong predictive risk factor for CVD, as it competitively binds eNOS over L-arginine and thus reduces the synthesis of NO (Fliser 2010). Elevated ADMA is associated with high levels of LDL cholesterol, and is thus seen in many conditions giving rise to CVD including diabetes and CKD (Böger *et al* 2000). Indeed, patients with CKD have been shown to have significantly increased levels of circulating ADMA compared to healthy individuals and these elevated levels are not cleared through dialysis (Xiao *et al* 2001). Interestingly, ADMA levels are almost six times higher in patients on HD than in patients on PD potentially due to altered vascular dynamics induced by HD (Kielstein *et al* 1999).

A recent *in vivo* study has utilised a proximal tubule-specific knockout for an ADMA-metabolising enzyme, dimethylarginine dimenthyaminohydrolase-1 (DDAH1), to determine if kidney-specific elevated ADMA is a response to prevent renal injury (Tomlinson *et al* 2015). Following folate-induced acute tubular injury, the $Ddah1^{PT-/-}$ mice exhibited a significant reduction in renal injury when compared with wild-type mice ($Ddah1^{fl-/fl}$) treated with folic acid. Furthermore, the $Ddah1^{PT-/-}$ mice showed significantly lower levels of collagen deposition, an attenuated kidney: bodyweight ratio, lower levels of cytokines and no change in blood pressure (Tomlinson *et al* 2015). These data suggest that, although a systemic increase in ADMA may be detrimental to the endothelium and instigate vascular damage, it may also act locally as a protective mechanism to delay damage to the kidneys.

1.3.2.2 Endothelial activation and repair

Another crucial element in endothelial dysfunction is the ability of the endothelium to repair itself. Although it remains controversial, a hypothesis is that there are two endothelial cell subtypes, designated ‘endothelial progenitor cells’ (EPCs) and detached ‘circulating endothelial cells’ (CECs), and that the balance of these two cell subtypes is integral to endothelial repair (Figure 1.9; Mohandas and Segel 2010). EPCs are defined as undifferentiated endothelial cells that originate from haematopoietic stem cells in the bone marrow; these cells are believed to possess regenerative potential, in that they can attach and repopulate damaged regions of the endothelium

as well as engage in the formation of new blood vessels (Coppolini *et al* 2008, Urbich *et al* 2003).

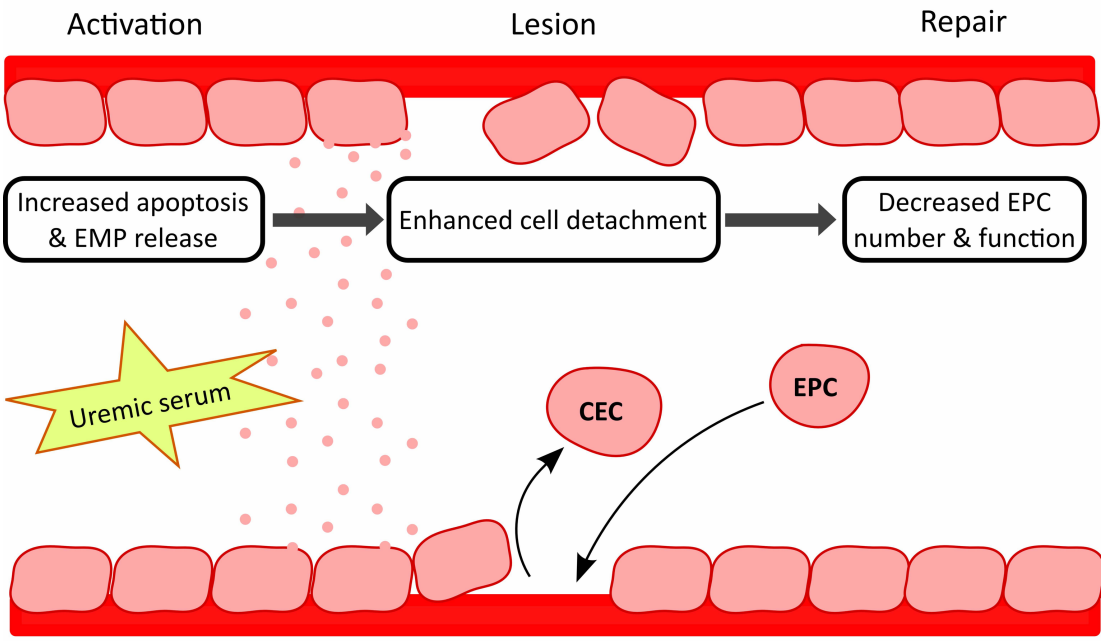

Figure 1.9: Endothelial dysfunction and protective cell populations

Endothelial dysfunction can be divided into three phases: endothelial activation, the formation of a lesion, and repair of the damaged endothelium. Endothelial activation is triggered by physical or chemical changes in the circulatory environment, such as alterations in shear stress or factors in uremic serum. Apoptosis of endothelial cells triggers budding of the endothelial cell membrane, which results in the release of endothelial microparticles (EMPs) containing chemokines, which attract repair mechanisms to the site of injury. Damaged endothelial cells (circulating endothelial cells; CECs), although mature and intact, detach from the endothelial lining and enter the circulatory system, leaving a gap in the endothelium. In healthy individuals, the presence of endothelial progenitor cells (EPCs) in the circulation should attach and repair these damaged regions; however, in disease states, the reduced presence of EPCs prevents adequate repair. The diagram is redrawn with modification from Jourde-Chiche *et al* (2011).

Comparatively, CECs are defined to be mature detached endothelial cells that enter the circulation following a loss of adhesive signalling (Figure 1.9). While both EPCs

and CECs are in the circulation, EPCs possess positive regeneration potential whilst increased CECs indicate a loss of cells from the intact endothelium. As such, the respective levels of these two populations are proposed to be indicative of the endothelium's repair capability, as the rate of endothelial loss (number of CECs) cannot exceed the rate of repair (number of EPCs) whilst still maintaining a functional endothelial layer.

Another indication of endothelial dysfunction is the release of endothelial microparticles (EMPs; Figure 1.9). The term 'EMP' is used to describe vesicles, between 100 nm–1 μm in size, that are released from activated endothelial cells. These microparticles are believed to contain signalling factors, which can trigger an inflammatory cascade and attract repair mechanisms to the site of injury (Dignat-George and Boulanger 2011).

1.3.2.3 Endothelial dysfunction in CKD

One of the most common measurements of endothelial dysfunction is flow-mediated dilatation (FMD), which examines the contractility and distensibility of the blood vessel in response to altered flow (Charakida *et al* 2010). FMD is typically measured in the brachial artery, although in smaller patients (such as small paediatric patients) the femoral artery may be used; this allows for greater reproducibility of the measurements, as well as preventing large percentage changes due to small diameter changes when compared with the baseline (Charakida *et al* 2010). To increase blood flow to the brachial artery, a sphygmomanometer cuff is placed on the distal forearm, 1–2 cm below the crease of the elbow, and inflated to 50 mm Hg for approximately 5 minutes (Charakida *et al* 2010). Following release of the cuff, the vessel reaches maximal dilation within 45–60 seconds and this measurement is then compared with the baseline diameter of the vessel (Charakida *et al* 2010). Both diameters (baseline and dilated) are measured using high-resolution ultrasound, with the exact location along the brachial artery noted so as to allow for subsequent measurements of diameter at a later point in time (Charakida *et al* 2010).

As a measurement of vascular tone, FMD allows the effects of endothelial dysfunction on the vessel's ability to contract and dilate in response to signalling factors to be quantitatively observed. During endothelial dysfunction, one of the vascular responses

is a reduction in NO (discussed in Section 1.3.2.1); by inducing reactive hyperaemia, in which the blood is rapidly restored following a short ischaemic episode, FMD examines the efficiency of NO release and the relative health of the endothelium (Flammer *et al* 2012).

FMD has been shown to decrease as the severity of CKD increases. In a study of adult patients (n = 159) with CKD (but without diabetes or CVD), FMD was shown to correlate with the stage of CKD with a reduction in FMD as the severity of CKD increased (Yilmaz *et al* 2006). Similarly, this study also indicated that decreased FMD correlated with an increase in markers of oxidative stress and ADMA (Yilmaz *et al* 2006).

Although there are limited studies examining endothelial dysfunction in paediatric CKD patients, Kari *et al* (1997) showed that, in a paediatric CKD population (n = 23) without confounding risk factors (i.e. no smoking, hypertension, hypercholesterolaemia, or obesity), patients already exhibited signs of endothelial dysfunction as determined by a significant decrease in FMD (Figure 1.10). Due to their young age (mean = 12 years old), these results were unexpected and this study was the first to show the early age at which paediatric CKD patients develop the first signs of CVD.

However, Wilson *et al* (2008) found that, although there was more variation between peak FMD measurements in children with CKD (n = 42), there was no overall difference between patients and controls. The authors attributed this to a lesser degree of disease severity than the Kari study, and noted that it took 30 seconds longer to reach peak FMD in children with CKD than controls; this suggested that there is a less rapid endothelial response to increased flow in children with CKD (Wilson *et al* 2008).

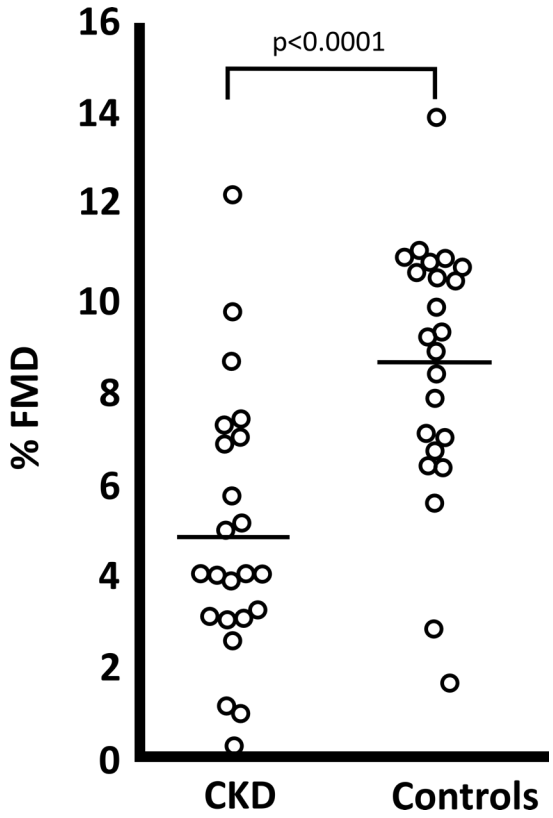

Figure 1.10: Endothelial dysfunction in paediatric patients

FMD is significantly reduced in paediatric patients with CKD, despite these individuals not showing any other signs of CVD. This figure has been redrawn from Kari *et al* (1997).

Decreased EPCs, increased CECs and an increase in EMPs have all been observed in patients with CKD (Dursun *et al* 2009, Jie *et al* 2010, Krenning *et al* 2009, Rodríguez-Ayala *et al* 2000). Collectively, these studies have shown that the critical balance between EPCs and CECs is compromised in CKD. In an adult CKD population, patients exhibit significantly lower numbers of EPCs ($CD34^+$) and, although these patients still maintain an EPC population, the remaining cells exhibit reduced mobility and adhesion (Krenning *et al* 2009). Motility assays indicate that EPCs are compromised as early as Stage 1 of CKD, indicating just how early in renal disease endothelial dysfunction occurs (Krenning *et al* 2009). EPCs ($CD34^+$, KDR^+) in paediatric CKD patients are shown to decrease by 50% during HD when compared to healthy paediatric controls (no data given for PD dialysis; Jie *et al* 2010). Again, the remaining EPC population from the paediatric CKD patients exhibited reduced mobility and adhesion capabilities (Jie *et al* 2010).

While patients with CKD exhibit reduced EPCs, they also have an increase in CECs that correlates with disease severity. Uremic serum is believed to be one trigger of endothelial detachment and anti-angiogenesis, as factors harmful to the endothelium within the circulatory system are not cleared by dialysis (Rodríguez-Ayala *et al* 2006). An antibody specific to myosin heavy chain class-I-related chain A, a marker of endothelial cell inflammation, was used to separate inflammatory CECs in venous blood samples of 19 CKD patients (55±3 years old) and 20 healthy controls (49±2 years old) using fluorescence-activated cell sorting (Rodríguez-Ayala *et al* 2006). Using this sample, there was a significant increase in CECs in CKD patients (7.6±2.7%) when compared to the controls (1.6±0.3%), whilst there was a significant decrease in EPCs in the CKD patients when compared to the controls (Rodríguez-Ayala *et al* 2006).

Although both PD and HD carry a high risk of developing CVD, it has been suggested that HD is more damaging to the endothelium than PD dialysis, potentially due to alterations in shear stress (Boulanger *et al* 2007). Indeed, patients undergoing treatment with HD exhibit higher levels of CECs than either control individuals or CKD patients on PD (Jourde-Chiche *et al* 2009, Merino *et al* 2010). One suggestion is that the choice of dialysis membrane may play a role, as certain dialysis membranes have been associated with an increase in the release of cytokines (Hoffman *et al* 2003).

EMPs have also been recently investigated in patients with CKD. In a detailed paediatric study by Dursun *et al* (2009) using 70 CKD patients (12 HD, 25 PD, 33 pre-dialysis and 18 healthy controls), the number of EMPs ($CD144^+$) were measured in each population and correlated with PWV and cIMT. Paediatric patients with CKD exhibited higher levels of EMPs compared with healthy controls, and patients on dialysis demonstrated significantly higher EMP levels when compared with pre-dialysis CKD individuals ($p<0.05$) (Dursun *et al* 2009). Furthermore, patients on HD had significantly more $CD144^+$ EMPs than patients on PD (Dursun *et al* 2009). Platelet-free plasma (PFP) from these patients was then used to stimulate cultured human umbilical vein endothelial cells (HUVECs) to determine if the uremic toxins present in CKD plasma could potentiate EMP release (Dursun *et al* 2009). Using an antibody for s-Endo 1-associated antigen (CD146), the investigators utilised flow cytometry to determine EMP number (Dursun *et al* 2009). PFP from children with

CKD induced greater $CD146^+$ EMP release than PFP from control patients (Dursun *et al* 2009). $CD146^+$ EMP release from HUVECs was also significantly greater when the cells were exposed to PFP from HD patients compared with PD ($p<0.05$). Patients with the greater EMP levels also exhibited increased markers of vascular stiffness (Dursun *et al* 2009).

Although EMPs are endothelial-derived, they contain crucial signalling molecules involved in vascular calcification, including the pro-calcification factor osteocalcin, and have the ability to induce osteocalcin expression in SMCs (Soriano *et al* 2014). EMPs have also been described as mediators of calcification as elevated extracellular phosphate has been shown to increase EMP production; these EMPS possessed pro-thrombotic tendencies (Abbasian *et al* 2015). Although no firm mechanism is defined as yet, these studies provide evidence for a potential endothelial-SMC relationship in vascular calcification.

One proposed treatment to target endothelial dysfunction in patients with renal disease is supplementation of L-arginine to improve NO bioavailability. The addition of L-arginine in an animal model of CKD has been shown to attenuate renal disease progression (Dupont *et al* 2011). However, this has not worked in paediatric patients; a study in which young CKD patients were supplemented with L-arginine showed no significant improvements in endothelial function (Bennett-Richards *et al* 2002). This suggests that endothelial dysfunction is triggered and sustained by factors in addition to NO bioavailability in patients with CKD. One possibility is that endothelial dysfunction is triggered by an alteration of factors within the uremic milieu, particularly vascular growth factors or inflammatory cytokines.

One potential trigger could be cholesterol, a traditional risk factor for CVD (Fruchart *et al* 2004). Recent studies have shown that high-density lipoprotein (HDL) which is usually a protective factor for the endothelium can become atherogenic in some disease states (Speer *et al* 2013). In CKD, HDL has been shown to induce endothelial dysfunction due to the production of another arginine derivative, symmetric-dimethylarginine (SDMA) and suppression of NO activity (Speer *et al* 2013).

Another possibility, which will be explored in this thesis, is that endothelial dysfunction is triggered by changes in vascular growth factors that control blood vessel function and stability. In particular, I will focus on a growth factor family called the angiopoietins (Woolf *et al* 2009). Recent experiments from our laboratory have shown that the angiopoietins may contribute to CVD in CKD patients (Shroff *et al* 2013).

1.3.3 Angiopoietins and the Receptor Tyrosine Kinases

1.3.3.1 Angiopoietins

The angiopoietins are a family of secreted vascular growth factors that are best known for their roles in angiogenesis and the maintenance of vascular stability. There are currently 4 known angiopoietins – angiopoietin-1 (Angpt1), angiopoietin-2 (Angpt2), mouse angiopoietin-3 (Angpt3) and human angiopoietin-4 (Angpt4) (Davis *et al* 1996, Maisonpierre *et al* 1997, Valenzuela *et al* 1999). For this thesis, the primary focus is on Angpt1 and Angpt2, which bind to the receptor tyrosine kinase Tie2 (tyrosine kinase that contains immunoglobulin-like loops and epidermal growth factor-similar domains).

1.3.3.2 Molecular structure of the angiopoietins

Angpt1 was first discovered in 1996 as a ligand for the Tie2 receptor, using secretion-trap expression cloning (Davis *et al* 1996). By utilising a probe consisting of the Tie2 ectodomain fused to human IgG and coupled to a BIAcore sensor chip, Davis and colleagues (1996) screened conditioned media from a variety of cell lines to detect if Tie2 binding activity could occur. Of these cell lines, two (a human neuroepithelioma cell line, SHEP1-1, and a mouse myoblast cell line, C2C12ras) exhibited positive binding activity that could be inhibited by the addition of soluble Tie2 (Davis *et al* 1996). Tie2 phosphorylation was also induced in cultured endothelial cells when treated with conditioned media from these two cell lines; soluble Tie2 could inhibit this phosphorylation, and it was proposed that this Tie2-binding molecule was a secreted factor (Davis *et al* 1996). To isolate this secreted factor, Davis and colleagues (1996) constructed cDNA libraries from both of these cell lines, and these were then screened for ligand expression by staining with Tie2-Fc fusion proteins. Positive

staining indicated that the ligand of interest (in this case, Angpt1) was expressed, and the plasmid DNA was extracted and electroporated into bacterial cells for rapid amplification (Davis *et al* 1996). Following transfection of the amplified plasmid, the transfected cells were again stained with Tie2-Fc for the Tie2 ligand; these cells exhibited a significant increase in positive staining, and thus their plasmids were determined to contain the ligand deemed 'angiopoietin-1' (Davis *et al* 1996). The human and mouse Angpt1 cDNA sequence was subsequently obtained from the isolated plasmid, and the amino acid sequence of the protein was then determined and the protein structure characterised (Davis *et al* 1996).

The structure of Angpt1 consists of two distinct domains: a N-terminus coiled-coil domain, rich in alpha helices and a C-terminus fibrinogen-like domain (Figure 1.11). Angpt1 is a highly glycosylated protein, containing five consensus sequences for N-glycosylation. By treating Angpt1 with PNGase-F, an amidase, Davis and colleagues (1996) highlighted the degree of glycosylation, as the glycosylated protein had a molecular weight of ~70 kDa compared with the native unglycosylated structure with a molecular weight of ~55 kDa. The N-terminus of the protein contains a hydrophobic amino acid sequence, characteristic of secretory molecules to allow the protein to easily cross the lipid-based plasma membrane (Davis *et al* 1996).

The 498 amino acid sequence is highly conserved between species, with mouse and human transcripts sharing 97.6% identity (Davis *et al* 1996). However, Huang *et al* (2000) have identified three other splice variants of Angpt1 of 367 (Angpt1-367), 285 (Angpt1-285) and 154 (Angpt1-154) amino acids in length (Figure 1.12). Each of these isoforms appears to possess unique binding characteristics in regard to their capacity to bind and phosphorylate the Tie2 receptor. Whilst the full-length Angpt1 and isoform Angpt1-285 can bind to Tie2 due to the presence of the C-terminal fibrinogen domain, only the full-length Angpt1 can induce tyrosine phosphorylation of the receptor (Huang *et al* 2000). Interestingly, the secretory consensus sequence is conserved between each of these isoforms, indicating that they are destined for secretion and thus likely all have a biologically active role.

Angpt1 and Angpt2 both have the propensity to form dimers and multimers under non-reducing conditions, due to the presence of cysteine residues near the N-terminus of

the peptide chain that form disulphide bonds between chains (Kim *et al* 2000). These cysteine residues are crucial for Tie2 binding, as binding cannot occur if cysteine is substituted with another amino acid. Angpt1 preferentially forms large multimers, whereas Angpt2 preferentially forms dimers (Kim *et al* 2000). Additionally, only Angpt1-367 can form multimers with full-length Angpt1, due to the presence of the full coiled-coil domain in this isoform (Huang *et al* 2000). The binding affinities of Angpt1 are closely linked to the oligomerisation state, as Angpt1 activates and phosphorylates Tie2 when in tetra or pentameric form. In dimeric or trimeric form, Angpt1 can bind Tie2 but does not induce phosphorylation, and in monomeric form, Angpt1 does not engage with Tie2 but rather preferentially binds to the α5β1 integrin (Weber *et al* 2005).

Angpt2 was discovered shortly after Angpt1 using low stringency hybridisation screening (Maisonpierre *et al* 1997). Angpt2 shares 60% homology with Angpt1; the N-terminus coiled-coil domain and the C-terminus fibrinogen-like domain are conserved between both proteins (Maisonpierre *et al* 1997). Unlike Angpt1, Angpt2 exhibits a greater variation between species, as mouse and human transcripts share only 85% homology (Maisonpierre *et al* 1997). A secondary human transcript for Angpt2, containing 443 amino acids ($Angpt2_{443}$), has also been isolated; however, this isoform lacks part of the coiled-coil domain due to the site of alternative splicing (Figure 1.12, Kim *et al* 2000). $Angpt2_{443}$ can bind but not phosphorylate Tie2 (Kim *et al* 2000). Both Angpt2 and $Angpt2_{443}$ are highly glycosylated proteins, likely due to their roles as secretory signalling molecules, with molecular weights of ~68 kDa and ~61 kDa respectively, when in glycosylated form (Kim *et al* 2000). Interestingly, $Angpt2_{443}$ is expressed at high levels in both primary carcinoma cells and in macrophages and is thus believed to have a potential role in inflammatory actions (Kim *et al* 2000).

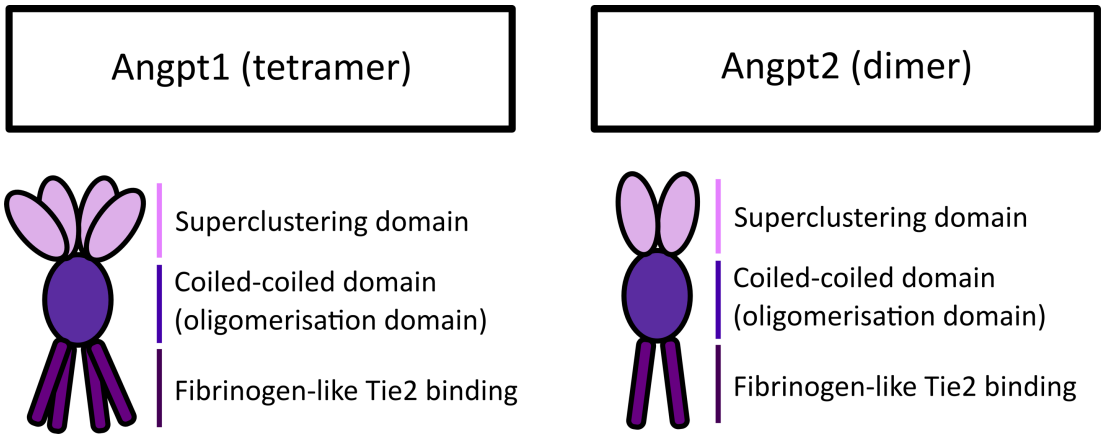

Figure 1.11: Structure of Angpt1 and Angpt2

Angpt1 and Angpt2 are structurally similar, consisting of a superclustering domain, a coiled-coil domain and a fibrinogen-like domain. However, Angpt1 preferentially forms tetramers whilst Angpt2 preferentially forms dimers. This figure is redrawn with modification from Augustin *et al* (2009).

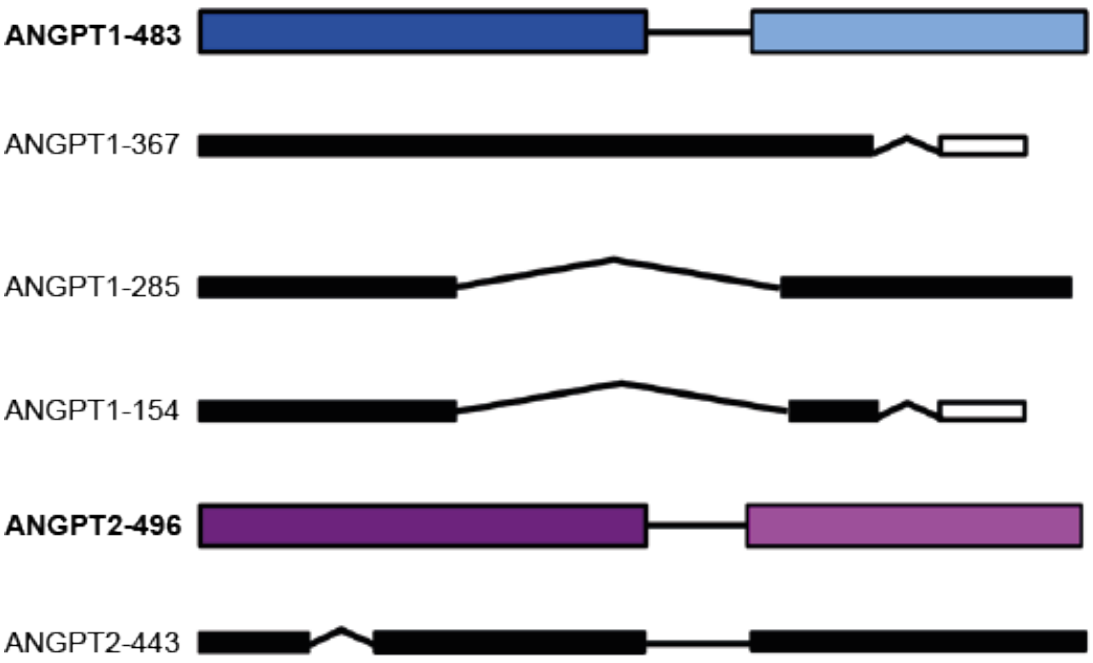

Figure 1.12: Alternative splicing isoforms of *ANGPT1* and *ANGPT2*

Alternative splicing of *ANGPT1* can lead to the formation of several isoforms, contributing to different multimerisation states: ANGPT1 (full length; 483 amino acids), ANGPT1-367 (367 amino acids), ANGPT1-285 (285 amino acids) and ANGPT1-154 (154 amino acids). In this diagram, the dark blue box is the Angpt1

coiled-coil domain and the light blue box is the Angpt1 fibrinogen-like domain; the black and white versions underneath indicate the splice isoforms. Alternative splicing of *ANGPT2* leads to two described isoforms: ANGPT2 (full length; 496 amino acids), and ANGPT2-443 (443 amino acids). In this diagram, the dark purple box is the Angpt2 coiled-coil domain, and the light purple box is the Angpt2 fibrinogen-like domain; the black version underneath indicates the splice variant. Thin black lines indicate the region of the gene that is spliced out in the variant. Figure redrawn with modifications from Jones *et al* (2001).

1.3.3.3 Angiopoietin binding and receptor phosphorylation

Both Angpt1 and Angpt2 bind with similar affinity to the receptor tyrosine kinase Tie2 (Davis *et al* 1996, Maisonpierre *et al* 1997). Binding of Angpt1 to Tie2 is responsible for tyrosine phosphorylation of the receptor in cultured endothelial cells. In contrast, Angpt2-Tie2 binding does not induce phosphorylation of the receptor (Davis *et al* 1996, Maisonpierre *et al* 1997). Maisonpierre *et al* (1997) then showed that Angpt2, in an excess of Angpt1, could competitively bind to Tie2 and thus block receptor phosphorylation thus suggesting that Angpt2 was a natural antagonist of Angpt1. It was subsequently postulated that phosphorylation of the Tie2 receptor is based on the balance between the angiopoietin ligands and their agonist-antagonist relationship (Maisonpierre *et al* 1997).

Although the central dogma is that Angpt1 is a Tie2 agonist whilst Angpt2 is an antagonist, there is some evidence to support Angpt2 acting as a Tie2 agonist under certain conditions. In particular, the role of Angpt2 as an agonist appears to occur during tumorigenesis when there is a surplus of vascular endothelial growth factor A (VEGFA, another vascular growth factor that binds to receptor tyrosine kinases) in the surrounding environment (Daly *et al* 2013).

Lobov and colleagues (2002) investigated the relationship between VEGFA and Angpt2 by injecting these growth factors into 5-day old Sprague-Dawley rats. Following a 24-hour period, these pups were culled, fixed, and their vasculature was examined. Under these conditions, the combination of Angpt2 and VEGFA supported the sprouting and migration of endothelial cells. Additionally, Yuan *et al* (2009)

stimulated HUVECs *in vitro* with exogenous Angpt2 (200 or 400 ng/mL). In this situation, they observed phosphorylation of the Tie2 receptor though to a lesser degree than when HUVECs were stimulated with the same concentration of Angpt1 (Yuan *et al* 2009). This suggested that although both angiopoietins can act as Tie2 agonists, Angpt2 is a weaker agonist of the receptor (Yuan *et al* 2009). Finally, Maisonpierre *et al* (1997) showed that Angpt2 could induce phosphorylation for ectopically expressed Tie2 in NIH 3T3 fibroblasts. Collectively, these experiments indicated that the ability of Angpt2 to phosphorylate Tie2 is context-dependent and may be altered in different cell types and biological environments.

1.3.3.4 Molecular Structure of the Tie Receptors

Tie2 is a receptor tyrosine kinase that consists of two primary domains: an extracellular domain (composed of three epidermal growth factor (EGF) repeats, two immunoglobulin (Ig)-like loops, and three fibronectin type III repeats), and an intracellular tyrosine kinase domain (Figure 1.13). The first Ig-like region and three EGF modules are essential for angiopoietin binding (Fiedler *et al* 2002). Tie2 possesses two tyrosine residues at sites 1102 and 1108 in humans (1100 and 1106 in mouse), which can undergo phosphorylation to stimulate the downstream pathways. Bogdanovic *et al* (2006) demonstrated that, following receptor activation by either Angpt1 or Angpt2, Tie2 is internalised. The rate of internalisation is dependent on whether Angpt1 or Angpt2 activates the receptor, with Angpt1 initiating a significantly more rapid response. When Tie2 is internalised, the ligand is released and remains biologically active for subsequent binding, thus indicating that release does not occur due to external cleavage of Tie2 (Bogdanovic *et al* 2006).

Tie1 shares a high degree of homology to Tie2 (Macdonald *et al* 2006). However, the biological role of Tie1 is not as well characterised, as it has been seen as an orphan receptor (Korhonen *et al* 2016). Though no ligand has been found for Tie1, the receptor has been shown to play a role in regulating Tie2 availability and subsequent phosphorylation (Savant *et al* 2015, Korhonen *et al* 2016). Under quiescent conditions in endothelial cells, Angpt1 is constitutively expressed and binds to Tie2; this maintains endothelial cell stability (Thurston *et al* 1999, Thurston *et al* 2000). Not all Tie2 receptors are required to be active to maintain this balance, and it is suggested

that Tie1: Tie2 dimerisation occurs to prevent either angiopoietin from binding (Singh *et al* 2011). In the setting of inflammation and endothelial leakage (Dunne *et al* 2013), Tie1 is cleaved from Tie2; this allows for increased Angpt1 binding to Tie2, which drives an anti-inflammatory response and helps to maintain vascular stability (Korhonen *et al* 2016).

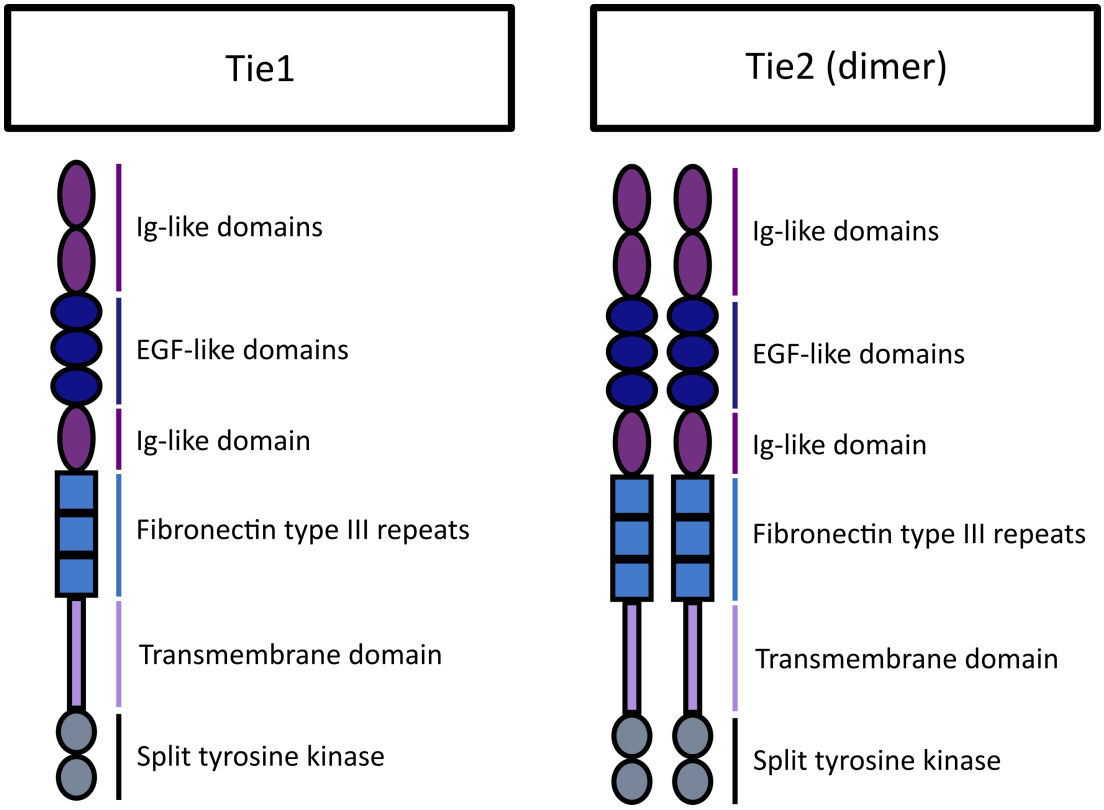

Figure 1.13: Structure of Tie1 and Tie2

Tie1 and Tie2 share the same domains, whilst Tie1 is a monomer and Tie2 dimerises. Figure redrawn with modification from Augustin *et al* (2009).

1.3.3.5 Expression and storage of the angiopoietins

Under quiescent conditions, Angpt1 is constitutively produced by pericytes, which are perivascular cells that surround the endothelial layer of the blood vessels and stabilise the vasculature (Saharinen and Alitalo 2011). In comparison, Angpt2 is primarily stored within the Weibel-Palade bodies (WPB) of the endothelial cells (Rondaij *et al* 2006). WPBs are column-shaped secretory organelles between 1–6μm in length that are unique to the endothelium (Rondaij *et al* 2006). The WPBs store and rapidly release

proteins in response to external stimuli such as hypoxia, inflammatory agents such as thrombin and histamine, and shear stress (Rondaij *et al* 2006). WPBs are composed of densely packed parallel rod-like structures, surrounded by a matrix and a lipid bilayer. These take on a more aligned arrangement, increase in electron density, and compact further as the WPBs mature (Valentijn *et al* 2011). This allows these bundles to be more flexible in their immature state which may allow them to manoeuvre more readily within the cytoplasm (Valentijn *et al* 2011). The most notable component of the WPB is the pro-thrombotic multimeric protein Von Willebrand Factor (VWF), which is stored in the compact rods (Rondaij *et al* 2006). VWF is essential to the formation of WPB; VWF-deficient dogs have no WPB in their endothelial cells, while conversely, ectopic VWF expression in other cell types initiates WPB formation in these cells (Haberichter *et al* 2005). The WPBs also store inflammatory and adhesion proteins, including the cellular adhesion molecule P-selectin (Fiedler *et al* 2004). Following stimulation with cytokines, such as histamine and thrombin, P-selectin is released from the WPB and expressed on the surface of activated endothelial cells where it promotes leukocyte recruitment (Fiedler *et al* 2004; 2006). Though both Angpt2 and P-selectin can be co-expressed and co-regulated by VWF, the storage of Angpt2 and P-selectin are mutually exclusive (Fiedler *et al* 2004). This exclusivity can be specific to individual cells, or to individual WPBs within a single cell; the reasons behind this are not yet known (Fiedler *et al* 2004).

1.3.3.6 Angiopoietins in angiogenesis

During blood vessel formation, Angpt1 promotes vascular stabilisation through promoting cell-cell interactions between endothelial cells and the surrounding pericytes (Carmeliet and Jain 2011). The biological effects of Angpt2 on blood vessels are dependent on the environmental concentrations of VEGFA. Crucially, Angpt2 acts to promote vascular regression when upregulated in a low-VEGFA environment, whilst vascular destabilisation is followed by angiogenesis under a VEGFA rich milieu (Figure 1.14) (Maisonpierre *et al* 1997). Additionally, Koblizek *et al* (1998) provided some of the first *in vitro* evidence to implicate the interaction between Angpt1 and Tie2 in sprouting angiogenesis. Endothelial cell-coated microbeads, embedded and cultured in a 3-dimensional fibrin gel, were treated with either control or Angpt1-containing conditioned media; those treated with Angpt1 exhibited endothelial sprout

formation. However, when endothelial cells were derived from *Tie2*-deficient mice, Angpt1 did not induce sprouting, suggesting that Tie2 was necessary for Angpt1 signalling (Koblizek *et al* 1998). Koblizek and colleagues (1998) used this same culture system to test the effects of VEGFA, in which they observed that VEGFA could promote sprouting but that this sprouting was not Tie2-dependent.

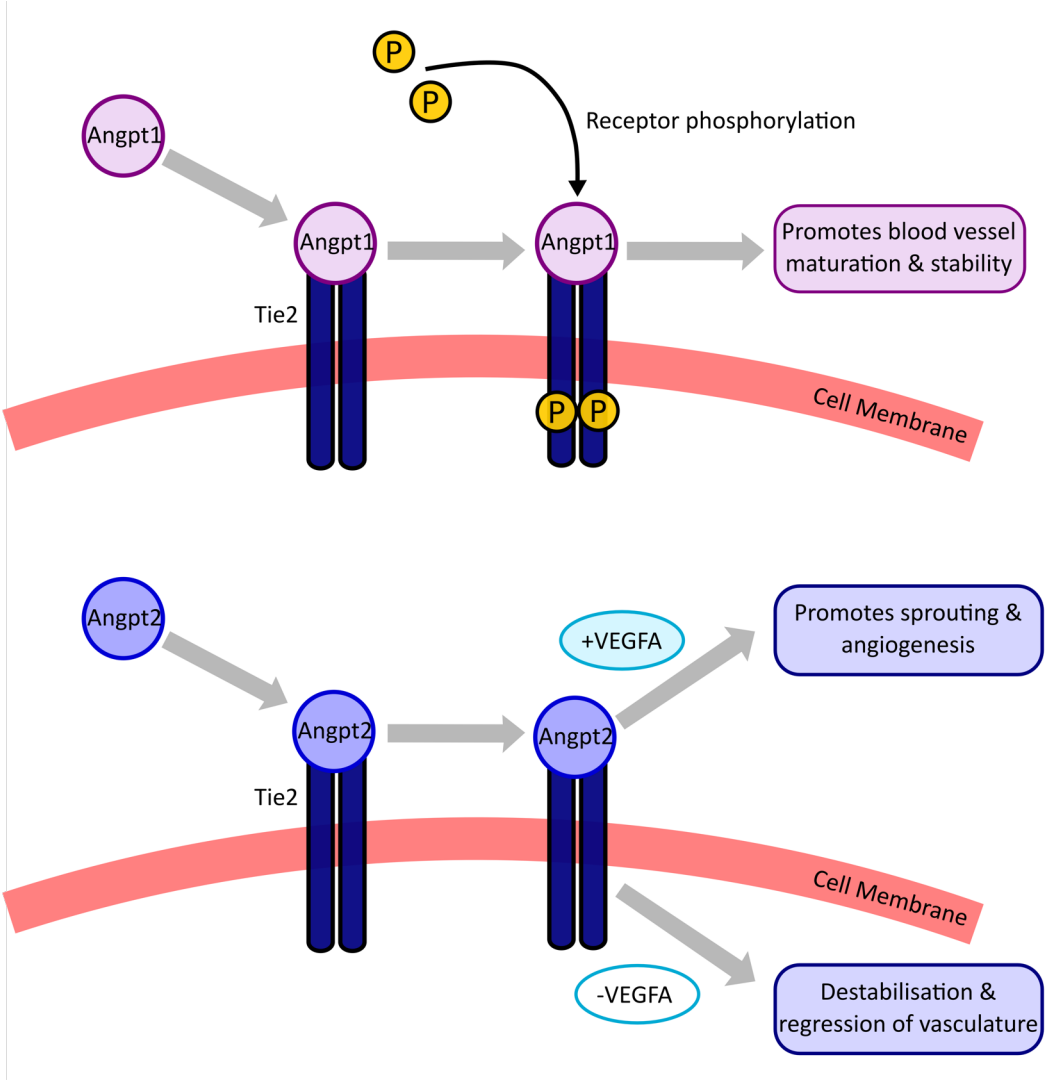

Figure 1.14: Functional roles of Angpt1 and Angpt2 in vascular stabilisation
Angiopoietin-1 (Angpt1) binding to Tie2 phosphorylates the receptor, which promotes blood vessel maturation and stability. Conversely, Angiopoietin-2 (Angpt2) can also bind without activating Tie2. The effects of Angpt2 can lead to vascular regression in the absence of vascular endothelial growth factor-A (VEGFA), whilst it promotes sprouting and angiogenesis in a VEGFA-rich environment.

1.3.3.7 Downstream effects of angiopoietin binding

The binding, or lack thereof, of the angiopoietins can activate several downstream pathways supporting inflammation, endothelial survival and endothelial migration (Figure 1.15, Huang *et al* 2010). The binding of Angpt1 to Tie2 activates one of these key pathways, leading to endothelial destabilisation (as outlined in Figure 1.14). Upon binding, the tyrosine kinase residues on the receptor undergo phosphorylation. The phosphatidylinositol 3-kinase (PI3K)/protein kinase B (PKB, also known as AKT) pathway is activated under these quiescent conditions (Thurston and Daly 2012; Potente *et al* 2005). This blocks the function of the Angpt2-promoting transcription factor forkhead box O (FOXO1); *in vitro* silencing of FOXO1 in endothelial cells has been shown to significantly reduce Angpt2 expression, as well as increase the expression of both eNOS and the apoptosis inhibitor *survivin* (Thurston and Daly 2012; Potente *et al* 2005). Conversely, low levels of Angpt1 result in a subsequent decrease of binding and phosphorylation of Tie2; this thereby increases the expression of Angpt2 and decreases the expression of eNOS (Thurston and Daly 2012; Potente *et al* 2005).

Tie2 also inhibits the inflammatory regulator, A20 binding inhibitor of NF-κB activation-2 (ABIN2), which regulates the activation of both IκB kinase (IKK) and NF-κB, and therefore helps to attenuate the inflammatory response induced by cytokines such as TNF-α and interleukin (IL)-1 (Hughes *et al* 2003; Lawrence 2009). Through interaction with ABIN2, Tie2 can act in an anti-inflammatory capacity, which may help to stabilise the endothelium (Hughes *et al* 2003).

Tie2 also plays a regulatory role in endothelial proliferation and migration through two known pathways. When stimulated by Angpt1, Tie2 can tyrosine phosphorylate 'downstream of kinase (DoK)-related protein' (DOKR), leading to the recruitment of the cytoskeletal factor Nck and p21-activating kinase (PAK)(Master *et al* 2001). This activity is crucial for vascular remodelling, and complete endothelial deletion of Nck has been shown to lead to defective angiogenesis and embryonic lethality (Clouthier *et al* 2015).

Tie2 can also alter proliferation and migration through phosphorylation of growth factor receptor-bound protein (GRB)-2, leading to the conversion of Ras to its active state and the eventual activation of extracellular signal-regulated kinases (ERK)-1 and 2 (Walker *et al* 1998). Similarly to the DOKR pathway, *in vitro* deletion of pathway components (in this case, specific deletion of *Erk2* in *Erk1*$^{-/-}$ mice) resulted in reduced angiogenesis, when compared with wild-type mice, and embryonic lethality (Srinivasan *et al* 2009).

1.3.3.8 Integrin binding to the angiopoietins

Another mechanism by which Angpt2 can act upon cells is through integrin binding (Figure 1.15). These large, heterodimeric transmembrane proteins consist of multiple subunits and play a significant role in regulating adhesion to the ECM and cytoskeletal organisation (Aplin *et al* 2001). Integrin binding can activate ERKs, similarly to Tie2; however, it can also regulate the phosphorylation and activity of focal adhesion kinase (FAK), a critical enzyme that helps to promote stability of the endothelium (Belvitch and Dudek 2012).

The Angpt2-integrin pathway has been increasingly investigated in diabetic retinopathy, as the disease manifests – in response to hyperglycaemia – as leakage in the microvasculature alongside an upregulation in Angpt2 (Patel *et al* 2004). However, a dose-dependent relationship between Angpt2 and pericyte apoptosis was observed following injection of exogenous Angpt2 into the eyes of wild-type mice (Hammes *et al* 2004).

In another study, astrocytes were also shown to undergo apoptosis when treated with Angpt2 in a high-glucose environment (Yun *et al* 2016). However, these astrocytes did not express Tie2 and instead, Angpt2 was shown to bind to the αvβ5 integrin (Yun *et al* 2016). Angpt2 has likewise been shown to bind to the α3β1 integrin in pericytes (Felcht *et al* 2012). Hakanpaa and colleagues (2015) have recently shown that Angpt2, but not Angpt1, can bind and activate β1-integrin to induce endothelial destabilisation. From their results, the authors propose that Tie2 downregulation in endothelial cells initiates Angpt2- β1-integrin signalling.

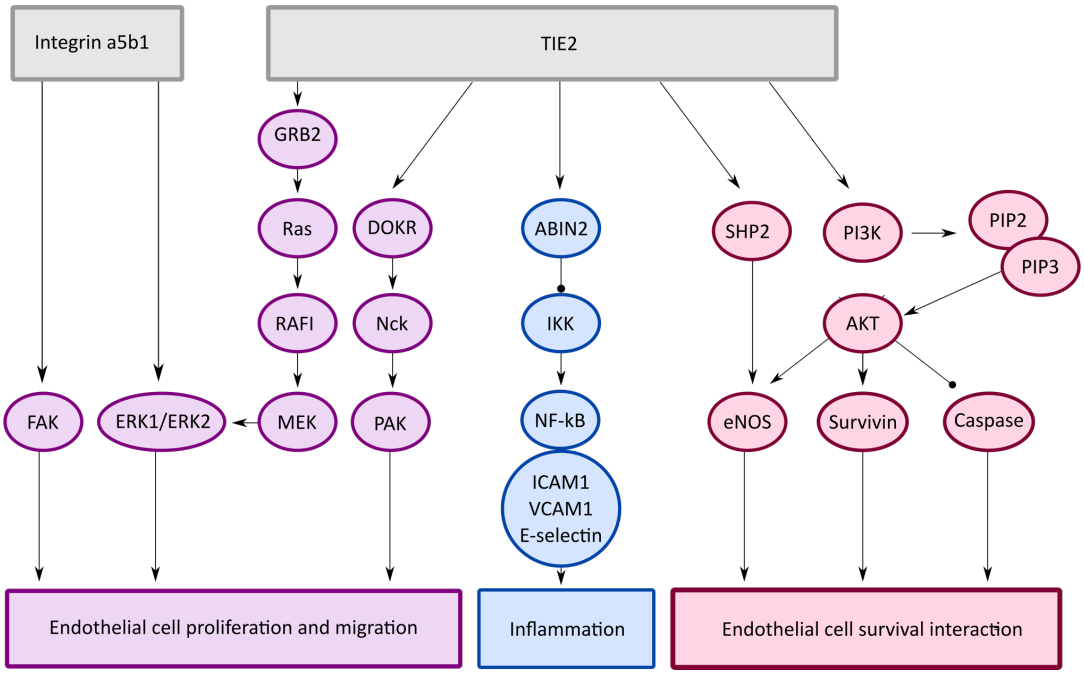

Figure 1.15: Downstream cascades initiated by Tie2 and integrin binding
Binding of the angiopoietins to Tie1 and integrins (shown here, α5β1) may activate numerous downstream components leading to endothelial cell proliferation and migration, inflammation, and endothelial cell survival interaction. Diagram redrawn with modification from Huang *et al* 2010.

The abbreviations for components in the above pathways are as follows (note that many of these are not in the abbreviations list on page 10 as they are not recurring abbreviations): ABIN2, A20-binding inhibitor of NFκB; AKT, protein kinase B; DOKR, Dok-related protein; eNOS, endothelial nitric oxide synthase; ERK, extracellular signal-regulated kinase; FAK, focal adhesion kinase; GRB2, growth factor receptor-bound protein 2; ICAM1, intercellular adhesion molecule 1; IKK, IκB kinase; MEK, mitogen-activated protein kinase kinase; Nck, non-catalytic region of tyrosine kinase adaptor protein 1; NFκB, nuclear factor kappa-light-chain-enhancer of activated B cells; PAK, p21-activated protein kinases; PIP, phosphatidylinositol; P13K, phosphoinositide 3-kinase; RAFi, RAF-inhibitor; SHP2, Src homology-2 domain containing protein tyrosine phosphatase-2; VCAM1, vascular cell adhesion molecule 1.

1.3.4 Angiopoietins in Disease

1.3.4.1 Angiopoietins in inflammation

Angpt2 is implicated in short-term inflammatory responses, helping to recruit neutrophils to the site of infection. Fiedler *et al* (2006) challenged wild-type and *Angpt2*$^{-/-}$ C57BL/6 mice with thioglycollate-induced peritonitis to induce an inflammatory response; while wild-type mice responded with an influx of neutrophils to the peritoneal cavity, this was significantly dampened in *Angpt2*$^{-/-}$ mice. Subsequent peritoneal infection with *Staphylococcus aureus* induced the same differential response; additionally, though wild-type mice exhibited a phenotype indicative of an active immune response within 2-4 hours of infection, *Angpt2*$^{-/-}$` mice showed no signs of inflammation.

Fiedler *et al* (2006) also modelled long-term infection in both wild-type and *Angpt2*$^{-/-}$ mice using *Streptococcus pneumonia*; however, there were no significant differences in the immune response between wild-type and *Angpt2*$^{-/-}$, suggesting that Angpt2 is only a short-term inflammatory trigger for which there is overall redundancy in the long-term situation. Fiedler *et al* (2006) initially examined Tie2 expression on their murine neutrophil population (as this would be a means for which Angpt2 could directly act upon the neutrophils for recruitment) using fluorescence-activated cell sorting (FACS); however, they did not see expression of Tie2 on their cells. However, other studies utilising neutrophils isolated from human blood samples have suggested that Tie2 is indeed present on these cells, as determined through FACS (Lemieux *et al* 2005, Brkovic *et al* 2007).

Patients admitted to intensive care with septicaemia presented with high levels of circulating Angpt2 (9.8±3.2 ng/mL), which corresponded with low survival rates over a 28-day hospitalisation period, with Angpt2 levels increasing during the time-period (Kümpers *et al* 2009). Comparatively, healthy adult controls exhibited Angpt2 levels of 0.57±0.20 ng/mL (Kümpers *et al* 2009). It should be noted that the pathologically high levels of Angpt2 are substantially lower than the levels of Angpt2 utilised in many *in vitro* studies (Yuan *et al* 2009). The authors of this study postulated that the elevated circulating Angpt2 levels are not due to septicaemia itself but rather a side- effect of

the inflammatory endothelial state. Collectively, these studies show that Angpt2 may be elevated in inflammatory conditions and be involved in the rapid recruitment of neutrophils to the site of infection.

1.3.4.2 Angiopoietins in cancer

Tissue-specific alterations of the angiopoietin balance have been identified in cancers, specifically during tumorigenesis (Saaristo *et al* 2000, Takahama *et al* 1999). A key characteristic of tumour growth is the extensive neovascularisation of the malignant tissue, which allows for increased perfusion and nutrient dispersion within the rapidly expanding tissue. Apart from driving cell proliferation and tissue expansion, this expansive vascularisation increases the risk of tumour rupture and spontaneous intraperitoneal bleeds (Saaristo *et al* 2000, Takahama *et al* 1999).

Tanaka *et al* (1999) examined angiopoietin expression in both healthy and malignant liver samples from patients diagnosed with hepatocellular carcinoma, as well as healthy controls. The tumour samples were histologically classified into two groups – hypervascular and hypovascular – based on their vascular staining patterns; these were then matched against healthy liver tissue from the same patient (Tanaka *et al* 1999). *ANGPT1* mRNA levels remained consistent across both tumour and healthy tissue samples (Tanaka *et al* 1999). In comparison, *ANGPT2* mRNA was detected in 83.3% of the hypervascular tumour tissue while only 18.2% of the hypovascular tumour tissue expressed Angpt2 (Tanaka *et al* 1999). No detectable *ANGPT2* mRNA was found in the healthy tissue (Tanaka *et al* 1999). Transfecting human hepatic cells with Angpt2 *in vitro* did not drive cellular proliferation; however, injecting the transfected hepatic cells near the liver bed of nude mice (n = 20) led to the growth of haemorrhagic tumours in 100% of the mice (Tanaka *et al* 1999). Injection of mock-transfected cells induced no tumorigenic changes (n = 20). Increased *ANGPT2* mRNA has also been correlated with decreased patient survival rates across cancer types, such as gastric cancer (Etoh *et al* 2001) and breast cancer (Sfliligoi *et al* 2003).

These studies indicate that raised Angpt2 levels occur in several cancer types and are associated with adverse clinical outcomes (Etoh *et al* 2001, Sfliligoi *et al* 2003, Tanaka *et al* 1999). Increased Angpt2 may promote tumour growth in these conditions and be

a therapeutic target in cancer. Specific targeting of endogenous Angpt2 using Angpt2-selective peptide-FC fusion proteins and antibodies was shown to reduce tumour growth and, in some cases, completely ablate tumours, in mouse xenograft models of tumorigenesis (Oliner *et al* 2004). However, constant dosing was required to maintain tumour regression as clearance of the anti-Angpt2 protein or antibody corresponded with an increase in tumour regrowth (Oliner *et al* 2004). Because of these promising results, one of the angiopoietin-specific recombinant peptide-FC fusion proteins, AMG 386 (Trebananib, Amgen) progressed to Phase I human trials where it was well tolerated in a small sample size (Mita *et al* 2010). AMG 386 is currently undergoing Phase III clinical trials in women with ovarian cancer, primary peritoneal cancer and fallopian tube cancer (Amgen NCT01493505).

1.3.4.3 Angiopoietins in CKD

The angiopoietins are of key interest in the study of CKD and CVD, as many nephropathies are characterised by endothelial damage. Davis *et al* (2007) showed that targeted podocyte overexpression of Angpt2 in the glomerulus of mice increased glomerular endothelial cell apoptosis, and this was accompanied by decreased environmental VEGFA whilst circulating Angpt1 levels remained unchanged. Under these conditions, the vasculature is primed for destabilisation and regression, and the unstable glomerular endothelium led to increased albuminuria, though this did not reach the nephrotic range (Davis *et al* 2007).

Numerous studies in both adult and paediatric populations have now shown an imbalance in circulating levels of the angiopoietins in CKD patients. Chang *et al* (2013) recently examined the association between albuminuria and circulating Angpt2 using plasma samples from 416 adult patients with pre-dialysis CKD stages 3-5. Circulatory growth factors Angpt1, Angpt2, VEGFA and soluble Tie2 (sTie2, the angiopoietin receptor) were measured; however, only Angpt2 showed a positive correlation with albuminuria. Angpt2 also correlated with markers of inflammation, namely IL-6 and TNF-α, and high-sensitivity C-reactive protein (hsCRP); however, there was no correlation between hsCRP and albuminuria (Chang *et al* 2013).

Several studies by David *et al* (2009, 2010, 2012) have investigated the relationship between Angpt2 and CKD in the adult population. The first study from this group displayed a positive linear relationship between increasing Angpt2 levels and CKD severity, the length of disease, and the length of time spent on dialysis (David *et al* 2009). Additionally, this work suggested a correlation between increased vascular calcification and increased Angpt2 levels (David *et al* 2009).

A further study by David *et al* (2012) examined Angpt1 and Angpt2 levels in 128 adult CKD patients across CKD Stage 4 and 5 on both HD and PD, and both vascular plaque and arterial stiffness were quantified and compared to 20 healthy controls. Their data indicated that, at baseline, CKD patients had increased levels of circulating Angpt1 and Angpt2 compared with controls; however, whilst levels of Angpt1 did not vary between CKD groups, Angpt2 levels were increased in patients on dialysis compared with CKD Stage 4 patients (David *et al* 2012). Dialysis modality did not alter Angpt2 levels. Additionally, sTie2 increased across controls, CKD Stage 4 patients and dialysis CKD patients respectively (David *et al* 2012). This demonstrated that Angpt2 was an independent predictor of mortality in CKD patients and correlated with markers of CVD (cholesterol, hsCRP, and osteoprotegerin) but not vascular calcification or arterial stiffness.

Interestingly, previous work from the same group did not find any association between Angpt1 or Angpt2 and vascular calcification; however, sTie2 levels were shown to significantly correlate with arterial stiffness (David *et al* 2010). The authors suggested that the discrepancy between these two studies with regard to the relationship between calcification and Angpt2 might have been due to differing disease severity in the CKD cohorts examined; whilst the 2010 study was based on CKD Stage 5 patients, the 2012 study included less severe CKD Stage 4 patients.

1.3.4.4 Angiopoietins in paediatric CKD patients

Few studies to date have examined the expression of angiopoietins in the paediatric population. However, a recent study from Shroff *et al* (2013) confirmed that paediatric patients exhibit the same angiopoietin imbalance as is seen in adults with CKD; this study set the groundwork (and subsequent funding) for the current project. Utilising a

cohort of 75 children (25 healthy controls, 20 pre-dialysis CKD patients, 16 CKD patients undergoing PD, and 14 CKD patients undergoing HD) from GOSH, Shroff *et al* (2013) investigated circulatory levels of Angpt1 and Angpt2 in paediatric CKD patients and their correlation with markers of cardiovascular health. Given the young age of this cohort (mean age in years: pre-dialysis = 10.7±4.1, dialysis = 14.2±3.9, healthy control = 13.1±2.8), many of the traditional cardiovascular risk factors were minimised thereby reducing external factors with potential to influence the development of CVD.

Blood samples and measurements of vascular parameters were done during routine clinical visits. Serum was utilised to measure circulating levels of Angpt1, Angpt2, VEGFA, Flt-1, E-selectin, P-selectin, intracellular adhesion molecule-1 (ICAM-1), and vascular cell adhesion molecule-1 (VCAM-1); vascular scans were conducted to measure the cIMT and PWV (Shroff *et al* 2013).

Circulating Angpt1 was decreased in pre-dialysis CKD patients compared with healthy controls ($p = 0.02$), whilst dialysis patients exhibited levels of Angpt1 similar to healthy controls (Figure 1.16A) (Shroff *et al* 2013). However, circulating Angpt2 was significantly increased in patients receiving dialysis compared with both healthy controls and pre-dialysis CKD patients ($p<0.0005$, Figure 1.16B) (Shroff *et al* 2013). Given that the effects of the angiopoietins are driven by the ratio between the two factors, the Angpt2: Angpt1 ratio was calculated for all groups (Figure 1.16C). Whilst there was no difference in the ratios between the control and pre-dialysis groups, the ratio was significantly increased in patients undergoing dialysis as compared with both pre-dialysis patients and controls; this suggests that the balance of the angiopoietins favours increased Angpt2 in this cohort (Figure 1.16C) (Shroff *et al* 2013). Angpt2 levels were shown not to correlate with age, gender, the length of CKD duration, or mode of dialysis; however, Angpt2 did show a positive linear relationship with the length of time spent on dialysis (Shroff *et al* 2013). Additionally, samples taken from before and after dialysis showed no significant difference between circulating levels of Angpt2 ($p = 0.7$), indicating that Angpt2 is not cleared by dialysis; this is likely due to the multimeric protein structure of Angpt2 (Shroff *et al* 2013).

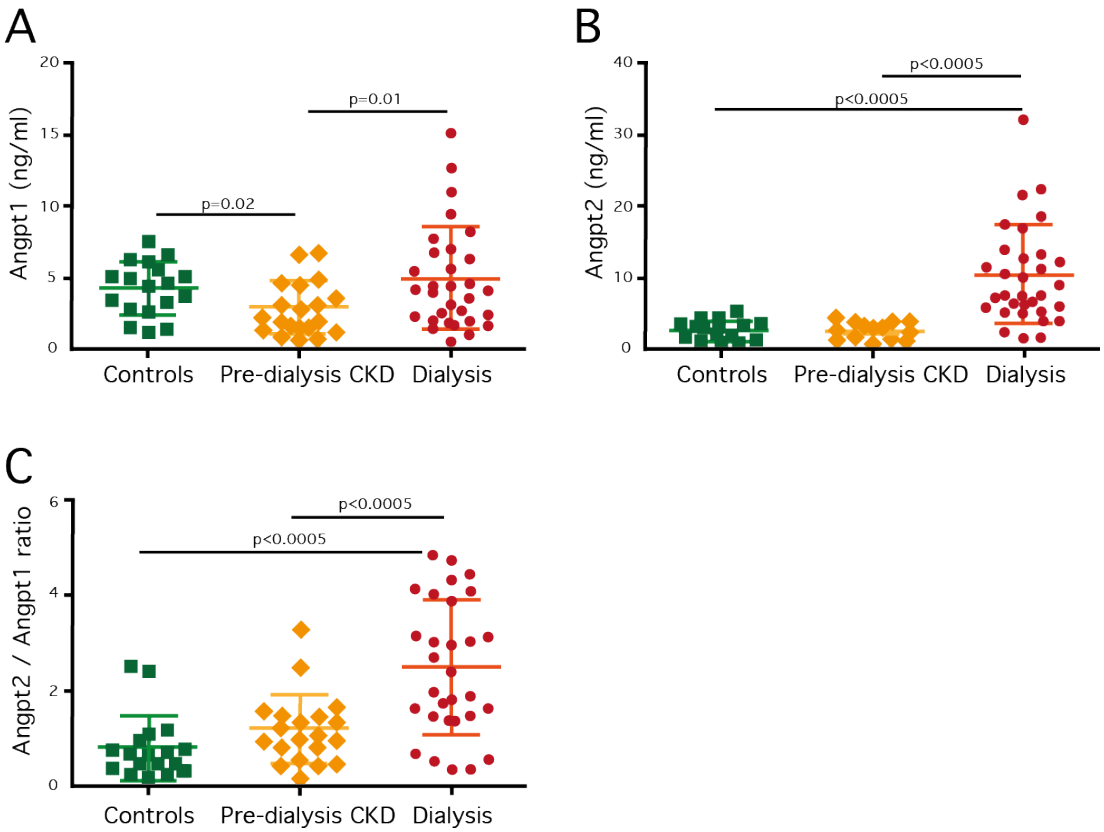

Figure 1.16: Circulating levels of Angpt1 and Angpt2 in CKD patients

A: Circulating Angpt1 is modestly but significantly reduced in pre-dialysis CKD patients, whilst there is no significant change between dialysis patients and healthy controls. **B:** Circulating Angpt2 is significantly increased in CKD patients on dialysis, whilst there is no change between pre-dialysis CKD patients and healthy controls. **C:** The Angpt2: Angpt1 ratio is significantly increased in patients undergoing dialysis, compared with healthy controls, with a tendency for levels to be elevated in pre-dialysis CKD patients; this suggests that Tie2 binding of Angpt2 is favoured over the binding of Angpt1. Results are presented as mean ± standard deviation, and *p*-values were calculated using analysis of variance (ANOVA) to compare between groups. Figure redrawn from Shroff *et al* (2013).

To determine whether the elevated levels of Angpt2 were accompanied by a surrounding milieu which favoured vascular regression or sprouting, circulating levels of VEGFA and the soluble VEGFA receptor (sFlt-1) were also measured in both pre-dialysis and dialysis patients (Figure 1.17 A and B) (Shroff *et al* 2013). sFlt-1 has been previously shown to be elevated in patients with CKD; this soluble receptor inhibits

angiogenic activity by binding VEGFA with similar affinity to the VEGFA receptor, as it contains the same VEGFA binding domain as VEGFR but without the transmembrane and cytoplasmic regions (Di Marco *et al* 2009).

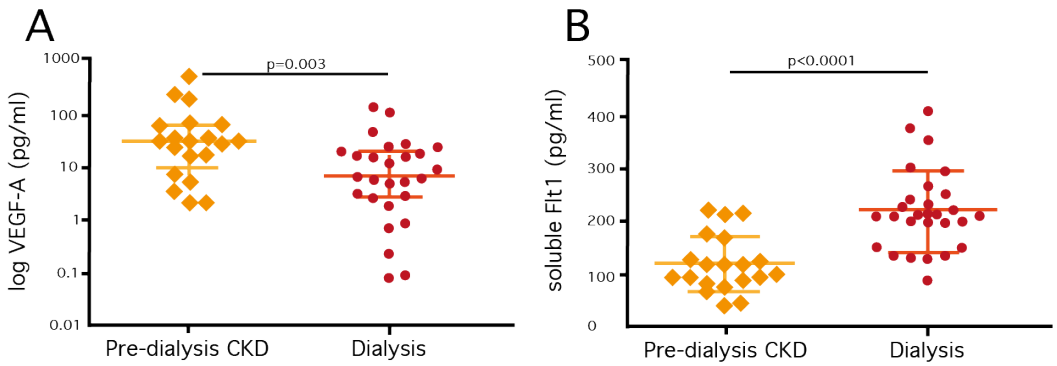

Figure 1.17: Angpt2 correlates with markers of vascular health

A: VEGFA levels were measured in the patient cohort; mean VEGFA levels are significantly decreased in patients on dialysis, compared to pre-dialysis CKD patients. **B:** Levels of VEGFA receptor (sFlt1) were also measured in the patient cohort and sFLT1 was significantly increased in patients on dialysis compared to pre-dialysis CKD patients. The decreased VEGFA levels along with the increase of sFlt1 favour the destabilising effects of Angpt2 in patients on dialysis. Results are presented as mean ± standard deviation, and *p*-values were calculated using ANOVA to compare between groups. Figure redrawn from Shroff *et al* (2013).

In dialysis patients, endogenous VEGFA levels were significantly lower than in pre-dialysis patients ($p = 0.003$), whilst sFlt-1 levels were significantly higher ($p<0.0001$) (Shroff *et al* 2013). Although neither VEGFA nor sFlt1 exhibited correlation with any physiological markers of CVD, circulating Angpt2 itself was shown to positively correlate with several markers in dialysis patients, namely systolic blood pressure, serum urate levels and cIMT (Shroff *et al* 2013). This positive correlation was not observed in healthy controls or pre-dialysis patients (Shroff *et al* 2013). Interestingly, Angpt2 did not correlate with PWV, suggesting that an alteration in the angiopoietins may occur prior to early signs of endothelial dysfunction.

Given that Angpt2 is known to have pro-inflammatory effects, inflammatory factors E-selectin, P-selectin, sVCAM-1, and ICAM-1 were measured and correlated with circulating Angpt2. Whilst the former three molecules were significantly elevated in children on dialysis, there was no change in ICAM-1 (Shroff *et al* 2013). Additionally, Angpt2 showed a positive correlation with VCAM-1 but not with any of the other factors (Shroff *et al* 2013). The results of this study indicate that Angpt2 may act as a biomarker for CVD in children undergoing dialysis; however, it is also questioned as to whether Angpt2 may also play a role in actively driving vascular calcification in these patients given the close correlation between the growth factor and some markers of vascular health.

1.4 Summary

Vascular calcification is a key manifestation of CVD, caused by hydroxyapatite deposition within the blood vessel. Although calcification can occur in either the tunica intima or the tunica media, the main form observed in paediatric CKD patients is medial calcification. This highly regulated process is similar to bone formation and is driven by a combination of matrix vesicle release, cellular apoptosis and osteogenic gene expression.

Endothelial dysfunction is one of the first events in the development of CVD and precedes any clinical symptoms. One cause of endothelial dysfunction is change in vascular growth factors, such as the angiopoietins, which help to maintain vascular stability. The angiopoietins are shown to be altered in CKD, in both adult and paediatric patients, and have been correlated with some markers of vascular damage.

1.5 Aims and Hypothesis

1.5.1 Overall Aim of this Thesis

The overall aim of this PhD thesis was to examine the role of the vascular growth factor Angpt2 in the progression of CVD in paediatric CKD patients on dialysis.

1.5.2 Hypotheses

Hypothesis 1: Angpt2 is not simply a biomarker of CVD, but a promoter of vascular calcification. This hypothesis will be tested by stimulating intact arterial rings and cultured VSMCs from paediatric CKD patients with Angpt2. Calcification levels will be quantitatively determined using the *o*-cresolphthalein colorimetric assay, and visually examined using histological staining.

Hypothesis 2: VSMCs express Tie2 providing a direct pathway by which Angpt2 acts on these cells (Figure 1.18). Tie2 expression will be investigated using both intact arterial rings, and isolated SMCs from dialysis patients. This will utilise a combination of molecular and historical techniques.

Hypothesis 3: Targeting the Angpt2 pathway can alter vascular calcification. Angpt2 binding will be targeted using siRNA specific to the Tie2 receptor in cells, whilst Tie2 of intact vessels will be targeted using a chemical inhibitor. Calcium deposition will be quantified using the *o*-cresolphthalein colorimetric assay.

Hypothesis 4: Angpt2-mediated calcification is mediated by an increase in osteogenic gene expression accompanied by vesicle release and apoptosis (Figure 1.18). The mechanism by which Angpt2 mediates calcification will be examined using histological stains to detect cell number and apoptotic cells, while qRT-PCR will be used to detect changes in gene expression levels in *in-vitro* monolayer VSMC studies.

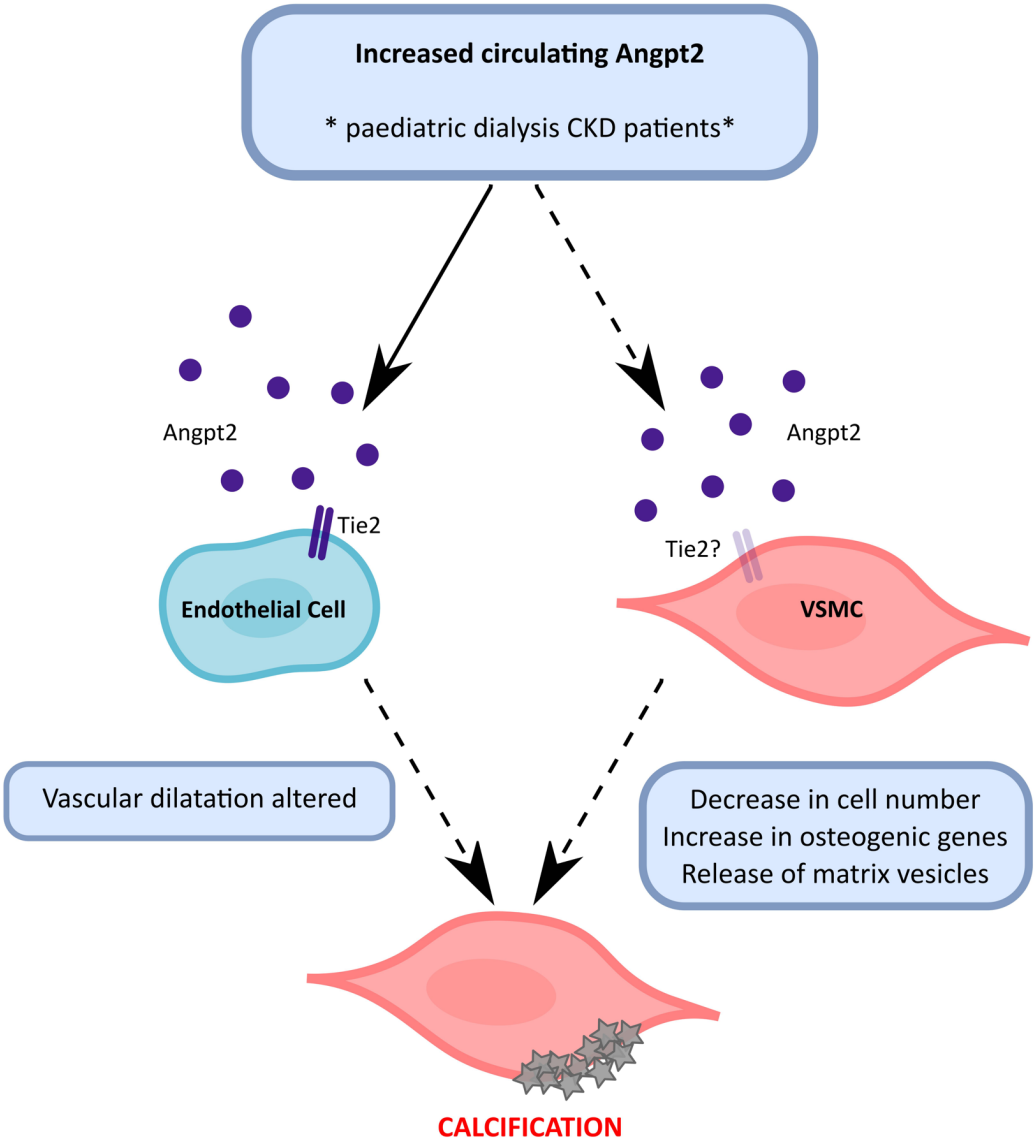

Figure 1.18: Hypothesis – Angpt2 promotes vascular calcification

Increased circulating Angpt2 in paediatric CKD patients on dialysis may act through a Tie2-dependent mechanism on the endothelial cells of the vasculature, decreasing vasodilation and increasing systolic blood pressure, which may indirectly contribute to the progression of vascular calcification. Alternatively, it may act directly upon the SMCs of the vasculature through a combination of mechanisms including cellular apoptosis, upregulation of osteogenic gene expression, and release of matrix vesicles.

Chapter 2: Materials and Methods

2.1 Statement of Materials

Unless otherwise specified, experimental reagents have been obtained from Sigma-Aldrich (St. Louis, MO).

2.2 Acquisition of Human Vessel Samples

2.2.1 Definition of Vessel Types

All human tissue used in this study was obtained from paediatric patients at GOSH NHS Foundation Trust. Paediatric vessels were classified into three primary categories, depending on the health of the patient – this designation will be used throughout the thesis:

1) **Healthy (non-renal) controls – 'Control'**
   These vessels were obtained from children with functional kidneys and no underlying cardiac disease. These children were recruited through the GOSH general surgery list on the basis that they were receiving intra-abdominal surgery.

2) **Pre-dialysis CKD patients – 'Pre-dialysis'**
   These vessels were obtained from patients undergoing PD catheter insertion or from patients receiving renal transplants who had not previously been on dialysis. These patients were recruited through the Nephrology Unit at GOSH.

3) **Dialysis CKD patients – 'Dialysis'**
   These vessels were obtained from patients who were receiving renal transplants and had spent a time on dialysis. Again, these patients were recruited from the Nephrology Unit at GOSH.

2.2.2 Obtaining Paediatric Vessels from Surgery

Informed written consent was obtained from the patient's guardian prior to surgery, and the project was ethically approved by the London Research Ethics Committee and GOSH Research and Development, Ref 12/LO/1186. None of the patients were on anti-hypertension medication at the time of the study.

Vessels were obtained for intact arterial ring *in vitro* modelling, and for isolation of VSMCs. The medium-sized muscular arteries obtained from paediatric CKD patients during renal transplantation were all inferior epigastric arteries. The inferior epigastric artery is a medium-sized muscular artery located in the lower abdominal cavity that arises from the iliac artery. Surgical procedures requiring lateral incisions rather than medial incisions routinely ligate this artery when accessing the abdominal cavity, which makes it a suitable target to remove for research purposes. Additionally, the muscularity of this artery makes it a suitable comparative artery to the carotid artery that is usually measured during vascular scans in patients.

If a midline incision was used rather than a lateral incision, the accessible arteries were obtained from excised omental tissue. As paediatric controls were undergoing bowel surgery, the accessible vasculature was obtained from excised mesentery, which was removed from dissected tissue. Under most circumstances, the omentum only contained small vessels that were suitable for isolation of VSMCs but were not suitable for intact vessel ring modelling. Medium-sized muscular arteries from control patients were obtained from the mesentery. Although different blood vessels (inferior epigastric arteries versus mesenteric arteries) were collected for each group, both types of arteries are medium-sized muscular arteries and exhibit no significant differences in their histology (Shroff *et al* 2008). Overall, I collected 32 samples. A list of samples and their subsequent use is provided (Table 2.1).

Sample ID	Disease State	Artery	Vessels	Cells
1	Dialysis	Inferior Epigastric	7 days	-
2	Pre-dialysis	Omental	7 days	-
3	Dialysis	Inferior Epigastric	7 days	-
5	Pre-dialysis	Omental	7days	-
6	Pre-dialysis	Omental	7 days	-
13	Pre-dialysis	Omental	7 days	-
14	Dialysis	Inferior Epigastric	x	x
15	Pre-dialysis	Omental	x	x
16	Dialysis	Inferior Epigastric	-	x
17	Pre-dialysis	Omental	x	-
22	Pre-dialysis	Omental	-	x
23	Pre-dialysis	Omental	-	x
24	Dialysis	Inferior Epigastric	-	x
26	Pre-dialysis	Omental		x
28	Control	Mesenteric	x	x
29	Pre-dialysis	Omental	-	x
31	Control	Mesenteric	-	x
32	Control	Mesenteric	-	x
33	Control	Mesenteric	-	x
34	Pre-dialysis	Omental	-	x
36	Pre-dialysis	Omental	x	x
37	Dialysis	Inferior Epigastric	x	-
39	Pre-dialysis	Omental	x	-
40	Dialysis	Inferior Epigastric	x	x
41	Dialysis	Inferior Epigastric	x	x
42	Dialysis	Inferior Epigastric	x	-
43	Control	Mesenteric	x	-
44	Control	Mesenteric	x	x
45	Control	Mesenteric	-	x
46	Dialysis	Inferior Epigastric	x	-
47	Dialysis	Inferior Epigastric	x	-
48	Dialysis	Inferior Epigastric	x	-

Table 2.1: Samples collected and their use in vessel or cell experiments

In total, 32 samples were collected. The first six samples that were collected (two dialysis, four pre-dialysis) were cultured for seven days, rather than 14 days, and were used to determine that a longer culture timeline was necessary. The sample numbering is not sequential; this is because patient blood samples were obtained simultaneously and added to the same list. This table is colour-coded with green representing control patients, yellow representing pre-dialysis patients and red representing dialysis patients. This same colouring is used in all subsequent graphs.

2.3 Whole Vessel Ring Modelling

2.3.1 Experimental Design

Arteries were obtained directly from theatre following surgical excision; intact arteries were both collected and cultured in serum-free medium 199 (M199, M2154). The basal level of calcium in M199 is 1.8 mM, whilst the basal level of phosphate is 1.0 mM. Whenever possible, vessels were set up for *in vitro* modelling and VSMC explants immediately following collection (within 1 hour); however, vessels occasionally had to be left refrigerated overnight.

Inferior epigastric arteries were obtained with minimal fat attached. However, mesenteric arteries and omentum samples required dissection from surrounding adipose tissue using individually packed sterile scalpels (Swann-Morton, Sheffield, UK) carried out in a Safe FAST Elite Class 2 biological safety cabinet (Faster S.R.L, Ferrara, Italy). The artery was stripped of the adventitia and cut into 1mm wide rings; these rings were then placed in a 6-well plate (Falcon, Newcastle, UK) with the culture medium (Figure 2.1). Due to the varying arterial length, 10–15 rings were typically obtained from each vessel. When these vessel rings were divided between the culture conditions, this typically equated to 1 arterial ring from each vessel (for each subsequent assay (calcium assay, paraffin histology, cryosections) per culture condition, including the rings collected for baseline measurements. Any remaining tissue was used for explant culture of VSMCs.

Calcium and phosphate concentrations (2.7 mM and 2.0 mM) were chosen as the pro-calcaemic conditions, as these have been previously shown to be the minimum concentrations required to induce calcification of vessel rings *in vitro* (Shroff *et al* 2010). In a patient, these concentrations would equate to a serum calcium concentration of 10.8 mg/dL and a serum phosphate concentration of 6.2 mg/dL, levels at the high end of what one would expect after prolonged HD (Block *et al* 1998).

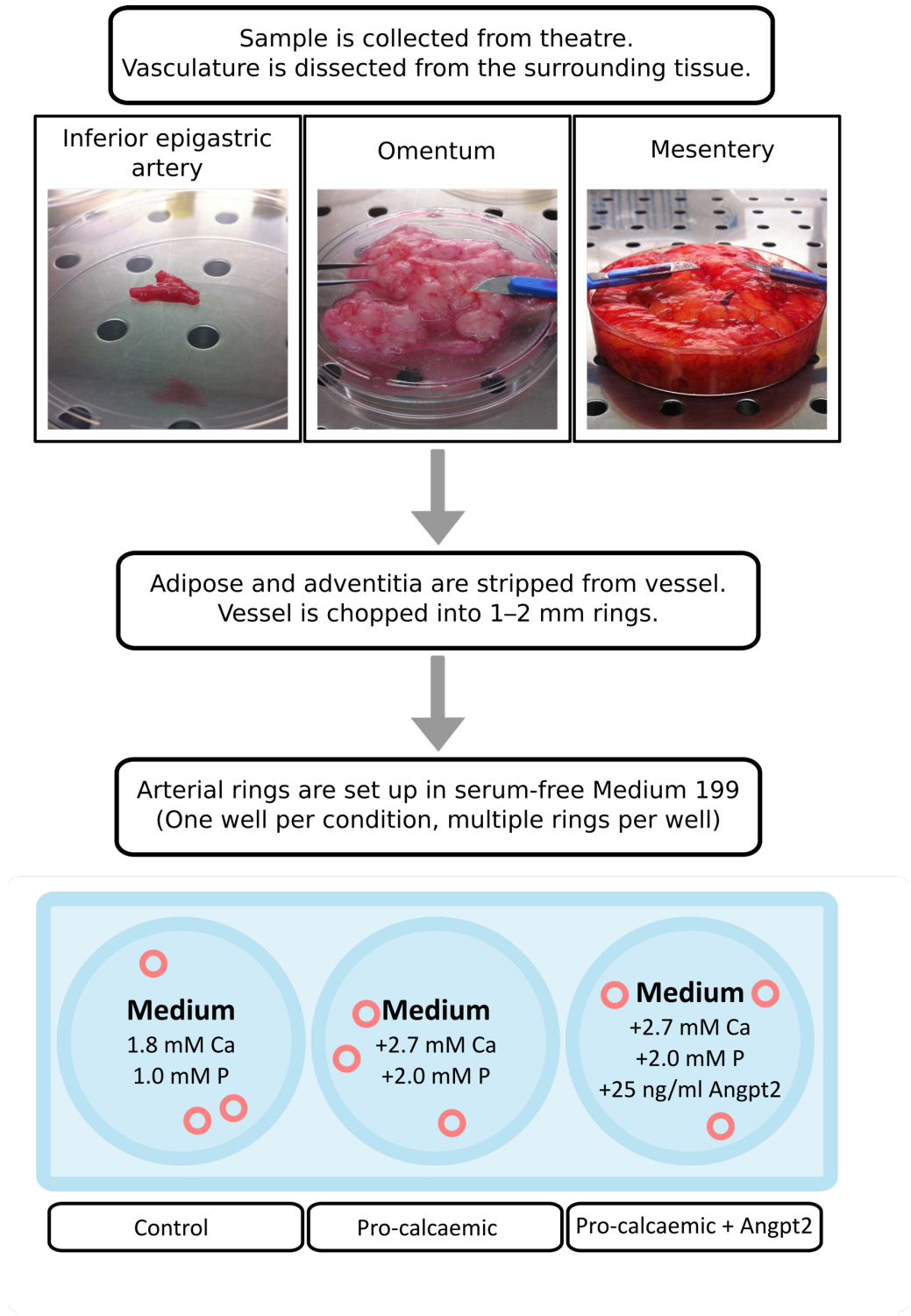

Figure 2.1: Dissection of artery from mesentery and culture set-up

The vessel was obtained from surgery and dissected down to the bare vessel. It was then diced into 1–2 mm rings, and cultured for 14 days. Each well contains three vessel rings, with one for each subsequent experiment: calcium assay, paraffin histology, and cryosections.

Carrier-free human recombinant Angpt2 (923-AN-025/CF; R&D Systems, Abingdon, UK) was added to the pro-calcaemic medium (at a final concentration of 25 ng/mL) to test the effects of Angpt2 in the presence of high calcium and phosphate. This dose of Angpt2 was chosen as the dose for the *in vitro* experiment as it was the maximum circulating level measured in paediatric CKD patients on dialysis (Shroff *et al* 2013). Angpt2 was obtained as a lyophilised protein, reconstituted at 100 µg/mL in sterile Dulbecco's phosphate-buffered saline (DPBS, 14190-094; Invitrogen, Paisley, UK), and stored in aliquots at -20ºC; the predicted molecular mass of Angpt2 is 50 kDa.

For most experiments, vessel rings were left for 1 day in a New Brunswick Galaxy®S series CO_2 incubator (Eppendorf, Hamburg, Germany) and maintained at 37°C with 5% CO_2. The medium was replaced every 3 to 4 days, over a period of 14 days (Figure 2.2). This time-course was established following preliminary experiments that indicated that there were no quantifiable differences between calcium deposition in vessel rings cultured in pro-calcaemic medium with and without Angpt2 after 7 days in culture, whilst reproducible differences could be quantified after 14 days in culture. It has been previously determined that vessel rings can survive for up to 28 days under these culture conditions (Shroff *et al* 2008). Note that unless otherwise specified, all media and wash solutions used in tissue culture were pre-warmed to 37ºC in a water bath prior to use to avoid vessel rings being exposed to rapid changes in temperature.

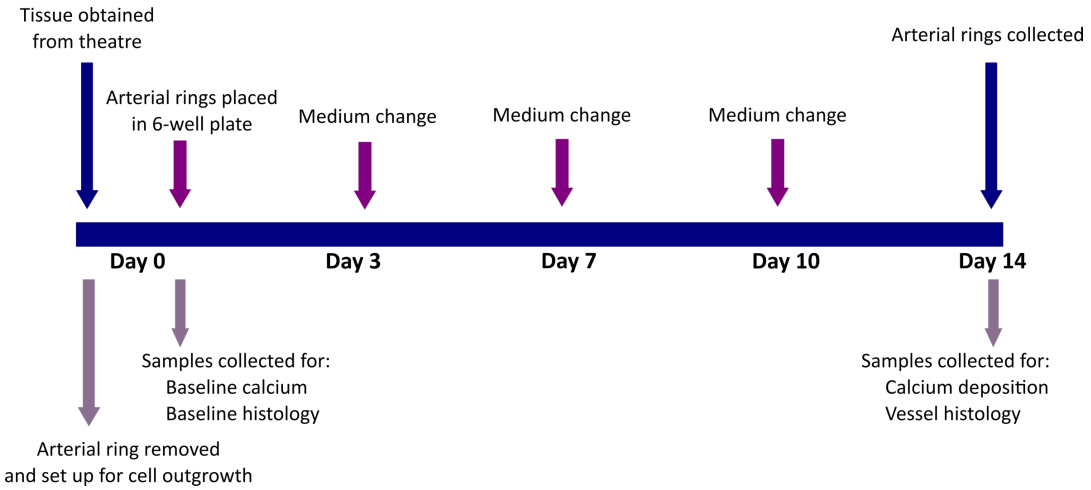

Figure 2.2: Timeline of *in vitro* intact vessel ring culture experiment

2.3.2 Extraction and Quantification of Calcium from Intact Arterial Rings

Following 14 days in culture, arterial rings were removed from the medium and frozen at -80ºC for later quantification of calcium content. The calcium content was measured quantitatively by the *o*-cresolphthalein colorimetric assay, which was then normalised to the protein content of each individual ring. Each patient was run individually, with all vessel rings from the same patient run at the same time to maintain consistency across a single patient.

Arterial rings were defrosted at room temperature, washed 3 times in DPBS and gently blotted to remove excess liquid. Each arterial ring was then placed in an individual 3 mL borosilicate glass homogeniser (1153243; Fisher Scientific, Loughborough, UK), along with 200 µL 0.1M hydrochloric acid (HCl). Arterial rings were ground every 15 minutes over the course of 2 hours to decalcify the samples, as per the protocol used by Shroff *et al* (2008, 2010). For each experiment, a single arterial ring was used per homogeniser; homogenisers were acid-washed and autoclaved between samples.

Following this homogenisation step, the supernatant and all arterial remnants were transferred into 1.5 ml microcentrifuge tubes (Eppendorf) and centrifuged at 17000*g* for 2 minutes in an AccuSpin™ microcentrifuge (Fisher Scientific). The calcium-containing supernatant was transferred to a fresh 1.5 mL microcentrifuge tube; the remaining arterial tissue was washed 3 times with DPBS and saved for protein quantification.

To quantitatively measure the calcium content of the supernatant, samples were loaded in duplicate on a 96-well flat-bottomed plate (Falcon) alongside a calcium chloride ($CaCl_2$) standard curve. The standard curve was run in triplicate, and consisted of serial dilutions of 1 mg/mL $CaCl_2$. Each individual well contained 55 µL of sample or standard, 200 µL ammonium chloride buffer (NH_4Cl, 0.48 g NH_4Cl dissolved in 191 mL distilled water and 9 mL 1M sodium hydroxide (NaOH) titrated to pH 10.5), 25 µL MilliQ water, and 10 µL fresh 0.1% cresolphthalein solution. Cresolphthalein solution (0.1%) consisted of 50 mg phthalein purple dissolved in 14 mL NH_4Cl and made up to 50 mL with distilled water. Given that this solution is light sensitive, it was wrapped in aluminium foil and dissolved on a rolling rack. Solution was made fresh

for each experiment and discarded after use. The plate was immediately read at 540 nm on a Synergy HT spectrophotometer (Bio-Tek, Winooski, VT), and absorbance values were exported to Microsoft Excel (Microsoft, Redmond, WA) for subsequent analysis.

The arterial remnants from the calcium extraction were used to determine the amount of protein present in each individual arterial ring. This allowed me to normalise μg of calcium to μg of protein, thereby allowing direct comparison of calcium content across samples. After the arterial remnants were washed in DPBS to remove traces of acid, they were transferred into clean glass homogenisers and 100 μL 0.1M NaOH/1% sodium dodecyl sulphate (SDS) was added to each sample. Samples were homogenised every 10 minutes over the course of 1 hour, as per the protocol used by Shroff *et al* (2008; 2010). The supernatant and remaining material were then transferred to 1.5 mL microcentrifuge tubes and spun at 17000*g* for 1 minute. The protein-containing supernatant was transferred to a clean 1. 5mL microcentrifuge tube for quantification using a Pierce™ bicinchoninic (BCA) Protein Assay Kit (Thermo Scientific, Waltham, MA).

To quantitatively measure the protein content, samples were loaded in duplicate on a 96-well flat-bottomed plate alongside a BSA standard curve. In each well, 25 μL of sample or standard was loaded along with 200 μL of 'working solution' (BCA Protein Assay Kit). The working solution contains two components, A and B (as labelled in the kit), in a 50:1 ratio (20 μL in 1 ml), which were mixed just prior to use. Working solution was added to the plate using a multichannel pipette to ensure that the colorimetric reaction began simultaneously in all wells. All bubbles were removed, and the plate was incubated at 37ºC for 30 minutes. The plate was shaken well (5 seconds, variable speed) before reading at 562 nm on a spectrophotometer. Absorbance readings were exported to Microsoft Excel, where data was subsequently analysed.

A standard curve was created using the absorbance readings (plotted along the x-axis) and the known concentration of the standards (plotted along the y-axis). The equation of the linear trend line was then used as the formula for which all other concentrations were calculated using the absorbance value. The calcium content of an individual ring

was then divided by the protein content of that vessel ring to give μg of calcium per μg protein. The data has been presented as both 'raw calcium values' as calculated and as 'fold-change' from the vessel ring cultured in the control medium (M199 alone).

2.3.3 Paraffin Histology

Arterial rings for paraffin embedding were removed from culture, washed in DPBS and fixed overnight in 10% formalin. The following day, the arterial rings were transferred to 70% ethanol and dehydrated through a gradient of increasing ethanol (Haymankimia, Witham, UK) concentrations (two 30-minute washes in 70%, 80%, 90% and 100% ethanol). Vessel rings were cleared in two 30-minute Histoclear II (National Diagnostics, Atlanta, Georgia) washes, followed by two 30-minute 50:50 Histoclear: paraffin wax washes, and finally two 30-minute liquid paraffin washes.

When rings were fully paraffin-permeated, they were embedded in paraffin blocks (one ring per block) taking care to position the vessel as to allow for a cross-section of lumen and tissue layers. Blocks were stored at room temperature; however, blocks were chilled on ice prior to sectioning. Sections (5 μm) were cut using an HM330 microtome (Microm, Bicester, UK), floated on a water bath, and mounted on SuperFrost Plus slides (BDH, Poole, UK). Slides were left on a warming tray to allow the wax to adhere to the slides; sections were then stored at room temperature until use.

2.3.4 Preparation of Frozen Sections

Arterial rings for frozen sections were removed from culture, washed in PBS, fixed for 1 hour in 10% formalin and washed again in PBS. The rings were then left in 30% sucrose (w/v) in PBS overnight. When initially placed into sucrose, the arterial rings floated; when completely saturated with sucrose solution, the arterial rings sank. Excess sucrose was delicately blotted off, the vessel ring was placed into a plastic embedding cup containing Tissue-Tek® Optimal Cutting Temperature (O.C.T.; Sakura Finetek, Torrance, California) medium, and the sample was rapidly frozen in dry ice. Blocks were stored at -80ºC until sectioning, at which point they were allowed to warm to -20°C. Sections (5 μm) were cut using a cryostat (Leica Microsystems, Milton

Keynes, UK), and mounted on SuperFrost Plus slides. Slides were stored at -20ºC until use. Slides were brought to room temperature and rehydrated in PBS for 10 minutes prior to staining.

2.3.5 Immunohistochemistry

For immunohistochemistry (IHC) procedures, all paraffin slides were deparaffinised before staining using the same protocol. Slides were first heated in a 56ºC oven to melt the paraffin, followed by two 5-minute Histoclear immersions and rehydration through an ethanol gradient (two 5-minute washes in 100% ethanol and two 5-minute washes in 70% ethanol). The deparaffinised slides were then left in distilled water until use.

Citrate buffer (2.94 g sodium citrate, dissolved in 22 mL 0.2 M HCl and 978 mL water) was used as the method of antigen retrieval. Citrate buffer was heated until boiling (10 minutes on HIGH in an 800W microwave); the slides were then added to the boiling solution and microwaved for a further 15 minutes on MEDIUM. The slides were cooled down to room temperature, washed twice in PBS, and incubated in 1.6% hydrogen peroxide block (10.6 mL 30% hydrogen peroxide made up to 200 mL PBS) for 10 minutes.

Slides were washed in running water for 5 minutes and dipped in 0.1% PBS-Tween. Each sample was marked with a wax pen to form a hydrophobic barrier around the sample, and 100 µL block (10% FBS, 2% BSA, and 0.1% Tween-20 in PBS) was added to cover the sample for 30 minutes at room temperature in a humid chamber. Block was tipped off the slide, and 50 µL of the primary antibody alpha (α) smooth muscle actin [Clone 1A4] (70 mg/mL, M0851, DAKO, Glostrup, Denmark) (1:150, diluted in block) was added to the sample. Slides were incubated overnight at 4ºC in a humid chamber.

The following day, the slides were washed 3 times for 5 minutes each with PBS-Tween. The secondary antibody diluted in block (100 µL) was then added to each sample, and the slides were incubated in a humid chamber for 30 minutes at room temperature. Horseradish peroxidase (HRP)-conjugated anti-mouse secondary antibody (K4006; DAKO) was used from the Mouse EnVision® Kit (DAKO). The

HRP-conjugated anti-rabbit secondary antibody was used from the Rabbit EnVision® Kit (DAKO). The slides were then washed three times for 5 minutes each in PBS-Tween, and HRP was visualised using 3,3'-diaminobenzidine (DAB) made up in 5 mL distilled water. Development of the brown colour was initially watched under a light microscope, and when the optimal time was determined, all other slides (for that antibody) were developed for the same length of time. The slides were placed in distilled water to stop the reaction and washed for 5 minutes in running water. Slides were counterstained with Mayer's Haematoxylin for 1 minute to indicate the nuclei and were then washed in running water for 5 minutes to clear excess haematoxylin from the slides. The slides were dehydrated through an ethanol gradient, and coverslipped using Histomount as the mounting medium. Slides were visualised under a Zeiss Axiophot II light microscope (Carl Zeiss, Oberkochen, Germany).

2.3.6 Fluorescent Immunohistochemistry

Tissue sections were permeabilised with 0.1% Triton-X in PBS for 5 minutes, incubated in block for 1 hour, and the primary antibody was applied overnight at 4°C in a humidified chamber. The following primary antibodies were used for immunofluorescence: alpha (α) smooth muscle actin [Clone 1A4] (70 mg/mL, M0851, DAKO), and an affinity-purified rabbit polyclonal IgG raised against a peptide mapping to the C-terminus of Tie2 (C-20) (200 µg/mL, c-324; Santa Cruz Biotechnology, Dallas, TX). The α-smooth muscle actin antibody was used at a 1:500 dilution, for a final concentration of 140 µg/mL. The Tie2 antibody was used at the recommended starting dilution of 1:200, for a final concentration of 1 µg/mL.

Slides were washed three times in PBS, and secondary antibody was applied for 1 hour in a dark humidified chamber. The secondary antibodies used for immunofluorescence were: AlexaFluor®594 (donkey anti-rabbit IgG, 2 mg/mL, A21207, Invitrogen), and AlexaFluor®488 (goat anti-mouse IgG, 2 mg/mL, A11001, Invitrogen). Both antibodies were used at a 1:150 dilution, for a final concentration of 13.3 µg/mL.

Slides were washed three times with PBS, incubated in 0.1% Sudan black in 70% ethanol for 10 minutes, washed twice with PBS, and incubated in 32 µL Hoechst

33342, trihydrochloride trihydrate (10 mg/mL, H3570, Life Technologies, Carlsbad, CA) in 200 mL PBS for 5 minutes. Slides were washed 3 times in PBS, dipped in distilled water, and mounted using aqueous mounting solution SlowFade Gold (S36936, Life Technologies). Slides were visualised under a Zeiss Axioplan II fluorescent microscope (Carl Zeiss).

A blocking peptide for Tie2 (200 µg/mL, sc-324P, Santa Cruz Biotechnology) was used to ensure that the secondary antibody was specifically binding to the Tie2 antibody. The Tie2 antibody was incubated overnight at 4°C with an equal volume of blocking peptide; this mixture of the Tie2 antibody and blocking peptide was used in place of the primary antibody as a negative control. For this experiment, both the Tie2 antibody and blocking peptide were used at a 1:200 dilution, for a final concentration of 1 µg/mL.

2.3.7 Quantification of Nuclei Number and Morphology

For each vessel ring, the number of nuclei was quantified per 0.25 mm^3 of the tunica media. To do this, one section per vessel ring was stained using only Hoechst 33342 (10 mg/mL) and 6–8 regions of the tunica media (per section) were photographed under a fluorescent microscope. The internal and external elastic laminas are autofluorescent and clearly denote the boundaries of the tunica media (Figure 2.3).

Fiji Is Just ImageJ (FIJI), an open source image-processing package (Schindelin *et al* 2012), was used to outline the tunica media and calculate the area in pixels, which could then be converted to millimetres. The nuclei within the tunica media were counted to give the total number of nuclei; these were then divided into two groups (elongated or condensed) based on the nuclear morphology. The nuclei number has therefore been presented as the total number of nuclei, the number of elongated nuclei and the number of condensed nuclei within 0.25 mm^2 of the tunica media for each vessel ring.

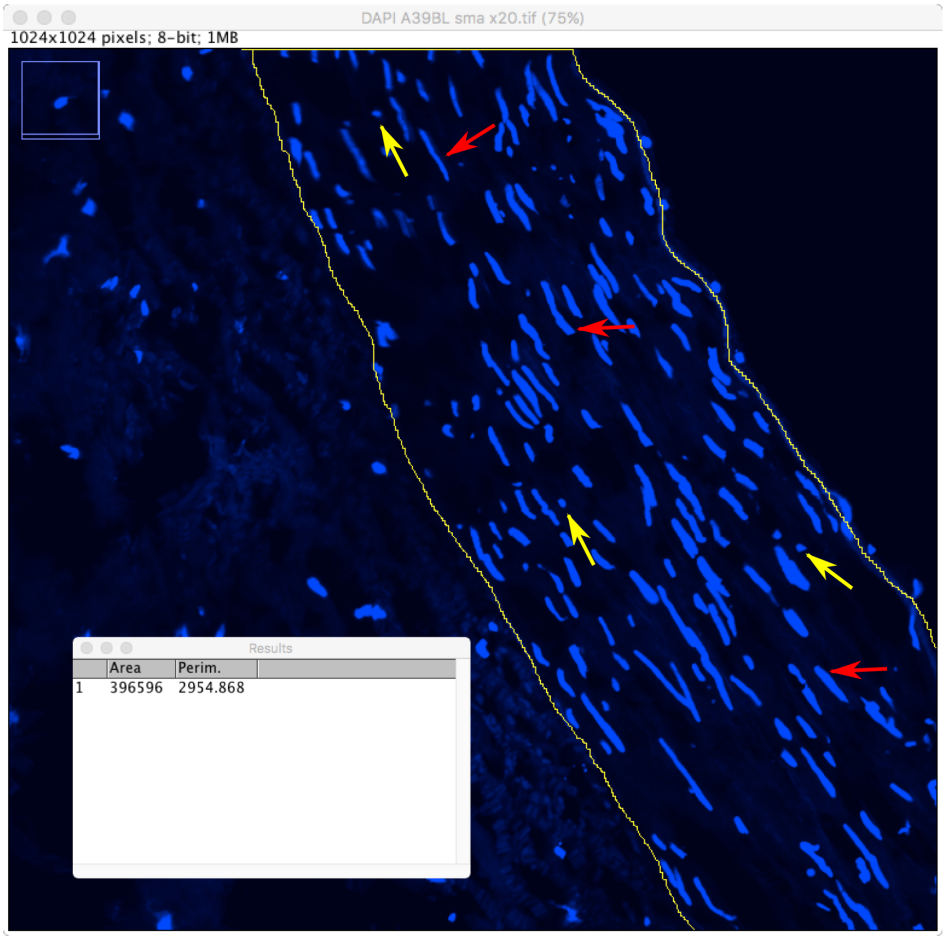

Figure 2.3: Representative region of tunica media as utilised for the quantification of nuclei

The tunica media of fluorescently stained (using Hoechst) was traced in FIJI to select the area to quantify (highlighted in yellow). This area was then measured in pixels (output is shown in the inset). The nuclei (which appeared bright blue when visualised under a fluorescence microscope) were counted and distinguished based upon their morphology. Nuclei that appeared small and rounded (as indicated by yellow arrows) were assessed separately to those that were elongated (as indicated by red arrows).

2.3.8 Haematoxylin and Eosin

Arterial rings were stained with haematoxylin and eosin (H&E) to examine the basic morphology of the vessels. The tissue sections were rehydrated and washed in running tap water for 5 minutes. They were then incubated in Harris's haematoxylin for 5 minutes, and rinsed well in tap water until the water ran clean. To differentiate the

haematoxylin, the slides were dipped in acid alcohol (1% HCl in 70% ethanol). Slides were then washed in running water for 5 minutes before staining with eosin for 3 minutes. Slides were briefly washed in tap water and then dehydrated, cleared in Histoclear, and mounted using Histomount.

2.3.9 Von Kossa

Von Kossa staining acts through replacing the calcium ions with silver ions, which is subsequently reduced to produce a black-brown stain. Von Kossa alone does not indicate the presence of calcium but rather indicates a substitution reaction, and is therefore typically used in conjunction with further stains or tests to confirm osteogenic changes. Following rehydration, slides were rinsed in several changes of distilled water and incubated with 2% silver nitrate solution in a clear glass Coplin jar under a 150W light bulb for 1 hour. To amplify the light, the Coplin jar was wrapped in aluminium foil with the reflective side inwards. Slides were then rinsed in several changes of distilled water, rinsed twice in 3% sodium thiosulfate and rinsed again in distilled water. Slides were counterstained in neutral red for 30 minutes, rinsed in distilled water and dehydrated to mount. Vessels cultured in calcium and phosphate have low levels of extraneous calcium surrounding the adventitia; this calcium stains positive for Von Kossa, acting as an internal positive control.

2.3.10 VasoTACs Apoptosis Staining

Staining for apoptosis was done using a commercially-available VasoTACS™ *In Situ* Apoptosis Detection Kit (4826-30-K; Trevigen, Gaithersburg, MD). Like terminal deoxynucleotidyl transferase dUTP nick end labelling (TUNEL), this kit works to detect apoptotic cells by detecting DNA end-labelling using terminal deoxynucleotidyl transferase (TdT). Though originally fluorescent labelling was attempted, the natural auto-fluorescence of the vessel elastic tissue provided a high background that made it difficult to determine which cells were truly apoptotic. Therefore, an HRP conjugate was utilised.

Slides were rehydrated and washed twice in PBS. Samples were incubated in a 1:50 dilution of 100 µg/mL Proteinase K (from the kit) for 1 hour (50 µL per section), before

being washed twice in distilled water for 2 minutes each. Sections were then incubated for 5 minutes in a methanol-hydrogen peroxide solution to quench any endogenous HRP activity. Sections were washed twice in distilled water to remove the peroxide solution, and immersed in the TdT labelling buffer (from the kit) for 5 minutes. Slides were then covered with the labelling reaction mix (50 μL per slide) and incubated in a humidified chamber for 1 hour at 37°C. To stop the reaction, slides were immersed for 5 minutes in TdT stop buffer (from the kit) and again washed twice in distilled water. Each section was then covered with 50 μL of HRP-Strep and incubated for 10 minutes at room temperature. Slides were washed 3 times with distilled water and covered with the labelling solution (from the kit) for 10 minutes; this development time was initially determined after watching a few slides develop under the microscope. Slides were washed several times in distilled water. Slides were immersed in Red Counterstain C for 5 minutes, washed briefly in distilled water to remove excess counterstain and dehydrated through an increasing alcohol gradient. Slides were cleared with Histoclear and mounted using Histomount.

As a positive control, one vessel section was treated for 1 hour with a nuclease (from the kit) to artificially induce breaks in the DNA before continuing the protocol from the incubation in the methanol-hydrogen peroxide solution. For each vessel ring collected and stained, 6–8 regions of the tunica media were photographed under a bright field microscope and analysed in FIJI. TUNEL was quantified by counting the number of TUNEL-positive (blue-stained) nuclei within a given region of the tunica media. This region of the tunica media was defined as the area between the internal and the external elastic lamina (Figure 2.4), which was measured (in pixels) using the Analyse > Measure function, and converted to millimetres based on the scale of the microscope. The number of positive nuclei was then calculated per 0.25 mm^2, and the mean of the 6–8 photographs was taken per each vessel.

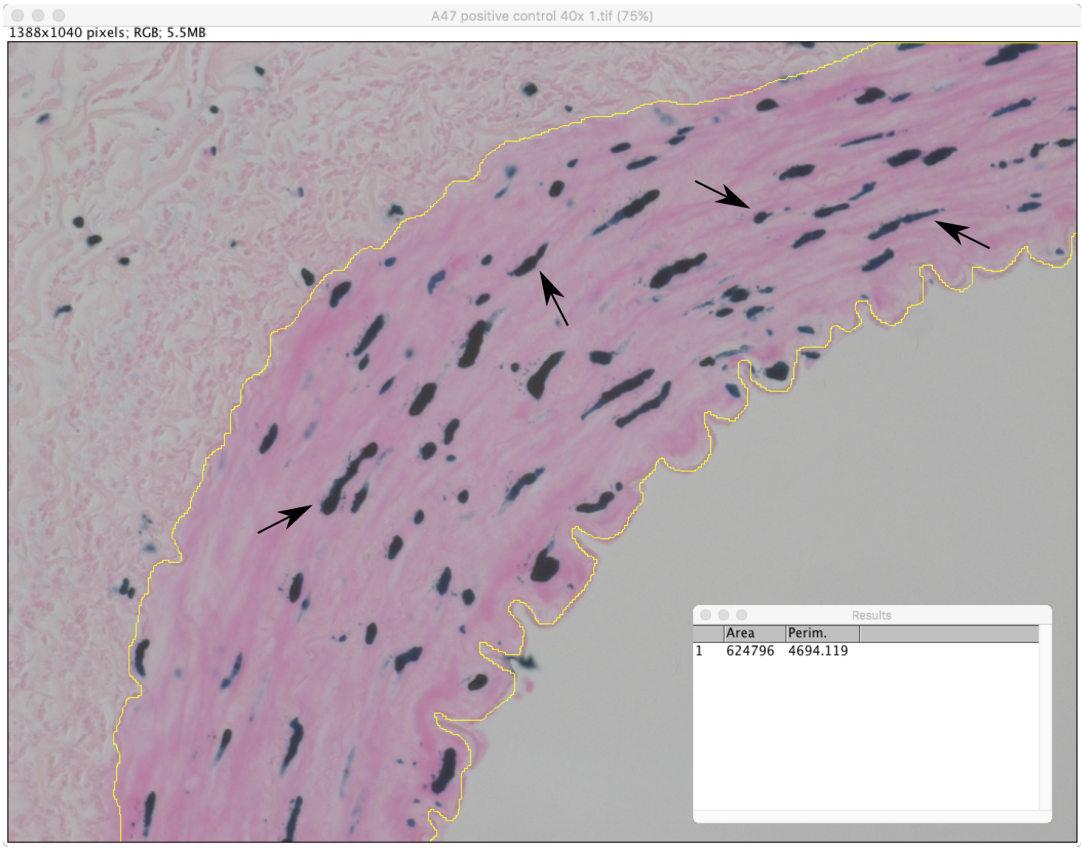

Figure 2.4: Representative area of tunica media in a nuclease-treated section
The tunica media was traced in FIJI to select the area to quantify (outlined in yellow), and this area was then measured in pixels (output is shown in the inset). The positive nuclei (stained dark blue, some of which are indicated by the black arrows) were counted within this region. Unlike the vessel sections stained with Hoechst, the nuclei in the TUNEL-stained sections were counted, but not further distinguished based on their morphology. Note that as this section is nuclease-treated, all nuclei are positive for TUNEL—including elongated nuclei.

2.4 Isolation and Culture of VSMCs

2.4.1 VSMC Culture Medium

Primary VSMC cultures were grown in M199 supplemented with 20% (v/v) heat-inactivated South American-derived foetal bovine serum (FBS, 10500-064; Gibco, UK), 1% (v/v) penicillin/streptomycin (5000 units of penicillin and 5 mg streptomycin

per ml, 4458), and 0.1 g/L L-glutamine (G7513). This complete medium will be referred to as 'VSMC growth medium' throughout this thesis.

2.4.2 Isolation of VSMCs from Intact Arteries

VSMCs were isolated from medium-sized muscular arteries and omental vasculature using the explant method previously described by Proudfoot and Shanahan (2012). Vessels were gently scraped to remove as much of the adventitial layer as possible; the vessel was then bisected along the longitudinal axis of the vessel to reveal the endothelium (Figure 2.5). Endothelium was gently removed with a pipette tip; this was observed as a thin gelatinous membrane that was pulled away from the elastic smooth muscle layer. The tissue was then dissected into 1 mm x 1 mm segments. A minimal amount of VSMC growth medium was added to the 60 mm tissue culture dish (430166, Corning, Corning, NY) so as to not disrupt or detach the explants; the tissue was then left for 3–5 days to allow it to adhere to the dish. VSMC growth medium was then replaced every few days until the plate was confluent with cells proliferating from the explants. The initial culture of proliferating cells was labelled P0, and any subsequent passages were P0+1 (therefore referred to as Px, where x = the number of passages).

2.4.3 Passaging of VSMCs

VSMCs require close proximity to one another to allow for optimal growth; therefore, harsh splits (in which the resulting cells are not in close proximity to each other) are inadvisable as they result in reduced proliferation and cells often do not recover from the trauma. As such, cells were passaged when 70% confluent at a 1:2 split. When passaging, cells were washed twice in Earle's Basic Salt Solution (EBSS, E6267) and detached from the culture surface using an appropriate amount (0.5 mL in a T25/60 mm^2 dish, 2 mL in a T75/100 mm^2 dish) of 0.25% Trypsin-ethylenediaminetetraacetic acid (Trypsin-EDTA, 25200-072; Life Technologies). Trypsin is a protease, which cleaves the adhesion proteins that attach cells to the culture surface; EDTA is a chelator and mops up divalent cations, such as Ca^{2+} and Mg^{-}. Together, this is a potent disassociation treatment and therefore cells were left in trypsin-EDTA only until detached (3–5 minutes). Cells were deemed detached when they rounded up from the plate and were free-floating in the medium. Following detachment, protease activity

was neutralised with an equivalent or greater volume of medium as the calcium and magnesium ions inhibit further enzymatic activity. The cell suspension was divided to new tissue culture plates, and fresh VSMC growth medium was added.

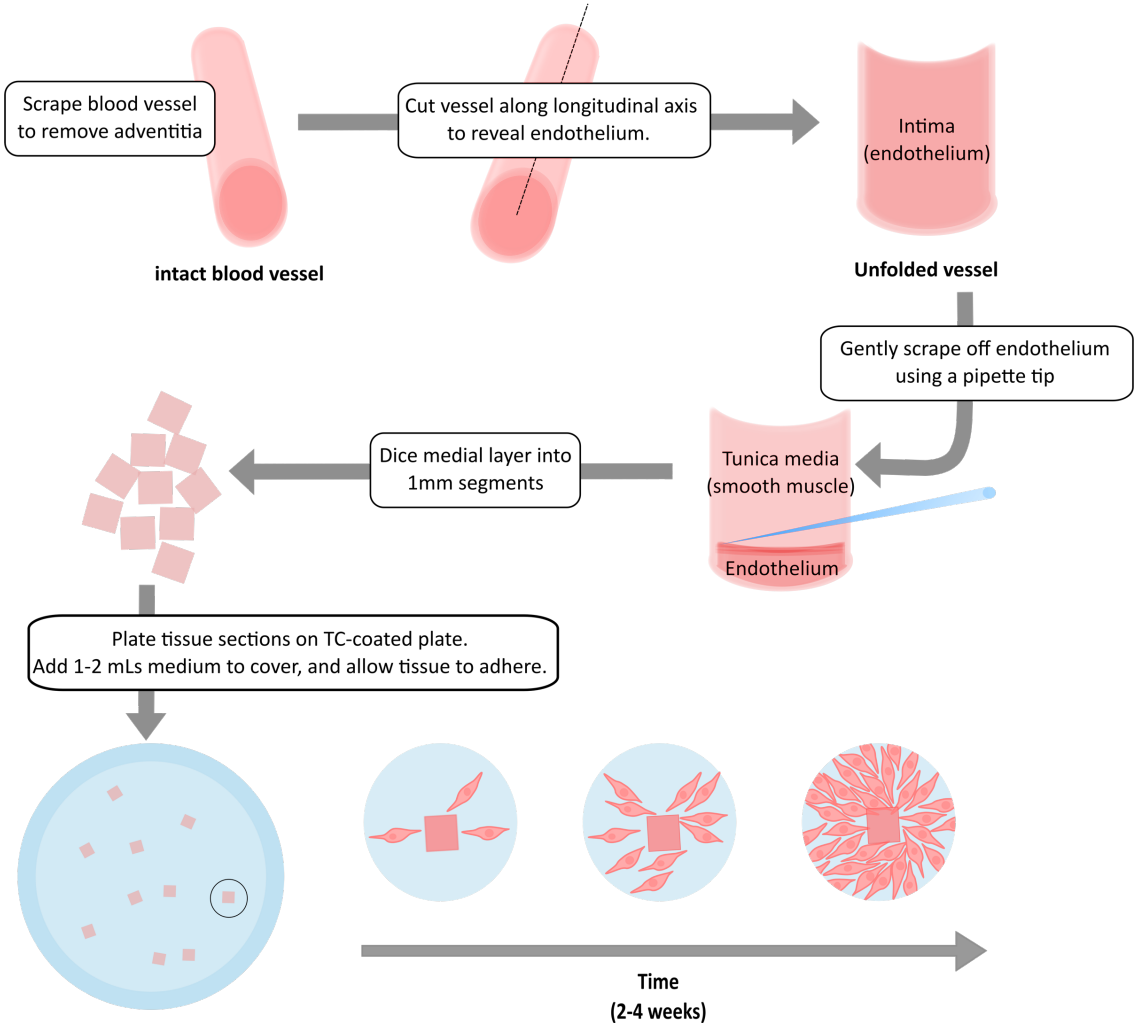

Figure 2.5: Isolation of VSMCs from arterial explants

When arteries had been dissected from surrounding tissue and stripped of all extraneous material, they were sliced longitudinally, stripped of the endothelium, and placed lumen side down. They were then finely diced, and tissue pieces were distributed in a small tissue culture dish with just enough VSMC growth medium to cover the sections. VSMC growth medium was initially changed only after tissue had adhered to the culture surface, usually 3–5 days after tissue was dispersed. Migration of cells from the tissue usually began within 1–2 weeks of tissue attachment.

2.4.4 Cell Counting

Determining cell number is important for seeding cells in the same density across experiments; this allows for reproducibility across samples, and limits variation in results due to varying cell number. A well-mixed cell suspension (10µL) was added to 90µL 0.4% trypan blue (15250-061; Life Technologies) and allowed to stand for 2 minutes. When cells are incubated with trypan blue, the live cells appear bright and refractive, as the dye cannot penetrate the intact cell membrane. However, dead cells will take up the dye and appear dark blue when visualised under a light microscope. The cell count should be done within 5 minutes of incubating cells as trypan blue is also a toxin and will instigate cell death in the sample. Cell-trypan blue suspension (10µL) was added to each counting chamber of a Bright-Line™ haemocytometer (Z359629) of a depth of 0.1 mm (Figure 2.6). Live cells within the red squares were counted, and the total number of cells was determined using the following formula:

Total viable cell number:

$$\frac{number\ of\ viable\ counted\ cells}{number\ of\ red\ squares\ counted} \times 10^4 \times dilution\ factor \times volume\ of\ original\ cell\ suspension\ (mL)$$

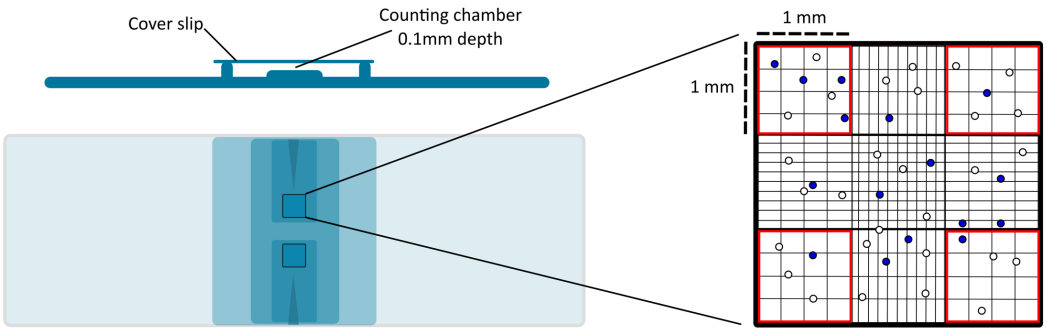

Figure 2.6: Counting cells and determining total cell number

A: A haemocytometer consists of a counting chamber, containing a 3 mm x 3 mm grid, which has a total depth of 0.1 mm when a cover slip is affixed. When the cell suspension is added to the edge of the cover slip, the suspension is pulled into the counting chamber using capillary action. **B:** Counting chamber consists of 9 squares, 4 of which are counted (outlined in red) and included in the calculation.

2.4.5 Cryopreservation of Cells

To cryopreserve cells for future use, cells were first trypsinised and neutralised as per the passaging protocol (Section 2.4.3). The cell suspension was then centrifuged in a Labofuge 400 centrifuge (Heraeus, Hanau, Germany) at 1950*g* for 5 minutes to obtain a pellet. After removing the supernatant, the cell pellet was resuspended in cold (4ºC) fresh 'freezing medium' consisting of 70% (v/v) FBS, 20% (v/v) VSMC growth medium and 10% (v/v) tissue culture grade dimethyl sulfoxide (DMSO, D2438). Cryovials (1.8mL) were obtained from Thermo Scientific. Vials were quickly wrapped in paper towels taking care to keep the cells upright, and the cell parcel was left at -80ºC for three days to allow cells to freeze slowly. Cryovials were then transferred to the vapour phase of liquid nitrogen for long-term storage.

2.4.6 Defrosting Cryostocks

Cryovials from liquid nitrogen storage were rapidly defrosted at 37ºC in a water bath, and the cell suspension was transferred to a 15mL centrifuge tube (Falcon). VSMC growth medium (9mls) was added slowly to the DMSO suspension. The suspension was then centrifuged at 1950*g* for 5 minutes, the supernatant was gently aspirated and the cell pellet was agitated to disrupt the cells. The pellet was resuspended in fresh growth medium and seeded into a fresh T25 vented cap flask (430639, Corning). The cells were left to attach and proliferate; VSMC growth medium was changed every 2–3 days to encourage proliferation.

2.4.7 HUVEC and HuAoFib Culture

HUVECS (2519; Lonza, Walkersville, MD) were cultured in Endothelial Basal Medium-2 (EBM-2, 3156; Lonza) and supplemented with 5% FBS (v/v) and Endothelial Growth Medium™-2 SingleQuots® (EGM-2, 4176; Lonza). SingleQuots were composed of recombinant long R insulin-like growth factor 1 (R3-IGF-1), ascorbic acid, recombinant human (rh) fibroblast growth factor B (FGF-B), VEGFA, hydrocortisone, epidermal growth factor (rhEGF), and gentamycin sulphate amphotericin-B (GA-1000). The exact concentrations of these growth factors are not

defined as it is a proprietary blend. These HUVECs were pooled cells, obtained from multiple umbilical cords.

Human aortic fibroblasts (HuAoFibs, C-12380; PromoCell, Heidelberg, Germany) were cultured in Dulbecco's modified Eagle's medium/Ham's F-12 medium (DMEM/F12; 12634-010; Life Technologies), supplemented with 10% (v/v) FBS and 1% (v/v) penicillin/streptomycin. All wash steps for both HUVECs and HuAoFibs were done using DPBS. Otherwise, all protocols for culturing these cells were the same as outlined for VSMCs.

2.5 Characterisation of VSMCs

2.5.1 Examination of VSMCs in this Thesis

Isolated cells were assessed for their SMC characteristics through PCR, real-time PCR, western blotting and immunocytochemistry. All investigations were done with low passage (<6 passages) cells, and both ribonucleic acid (RNA) and protein were isolated from flasks at 70–80% confluence.

2.5.2 Extraction and Assessment of RNA

There were two methods of RNA extraction used in this thesis. RNA was extracted using either guanidinium thiocyanate-phenol-chloroform extraction (TRI Reagent®, T9424), or an RNeasy Mini Kit (74106; Qiagen, Venlo, Netherlands). When using the RNeasy kit, an on-column DNase digestion was carried out for all samples using an RNase-free DNase set (79254; Qiagen). While the protocol for RNA extraction using TRI Reagent® is outlined below, the protocol for RNA extraction using the RNeasy Mini Kit is outlined in Section 2.6.4 as the TRI Reagent® method did not work well if cells were treated with calcium.

All centrifugations in the RNA extraction method using TRI Reagent® were done at 17000*g* using a Centrifuge 5414 R microcentrifuge (Eppendorf) at 4ºC. The medium was aspirated, and cells were washed twice with ice-cold DPBS. All DPBS was removed, and 1 mL TRI Reagent® was added to each dish. The dish was left for 2–3

minutes at room temperature to lyse the cells; the cells were scraped down using a sterile cell scraper (Greiner Bio-One, Stonehouse, UK), and the suspension was transferred to an RNase/DNase-free 1.5 mL microcentrifuge tube. The tubes were left at room temperature for 10 minutes. Chloroform (200 µL) was added to each tube, vortexed to mix, and left for 15 minutes. The tubes were centrifuged for 40 minutes to separate the organic, interface, and aqueous phases containing the protein, DNA and RNA, respectively. The aqueous phase was then transferred to a new tube, mixed well with 500 µL isopropanol, allowed to stand for 15 minutes and centrifuged for 40 minutes. RNA formed a 'feather-like' pellet at the bottom and side of the microcentrifuge tube. The supernatant was removed, the pellet was washed with RNase-free 70% ethanol and the sample was vortexed. The sample was spun for 10 minutes at 4^{o}C, and ethanol was removed to allow the pellet to air dry. The pellet was resuspended in 30 µL of RNase-free water, and RNA was stored at -80^{o}C until use.

2.5.3 Quantification of RNA Quality and Quantity

The quality and quantity of the extracted RNA were assessed using agarose gel electrophoresis and spectrophotometric analysis, both of which are detailed below.

Agarose gel electrophoresis: The physical quality of RNA was determined by running a RNA sample (1 µL RNA, 1 µL loading dye, 8 µL distilled water) on a gel composed of 2 g UltraPure™ agarose (16500-500; Invitrogen) in 100 mL of 1x Tris-Acetate-EDTA (TAE) buffer. TAE buffer is composed of 0.04 M Tris-Acetate and 0.0001 M EDTA. The gel was run at 100V for 30 minutes. When run on an agarose gel, high-quality RNA exhibits two crisp bands corresponding to the 28S and 18S ribosomal RNAs. Ideally, the 28S band is approximately twice as intense as the 18S band due to their relative ratios.

Spectrophotometric analysis: Absorbance levels of RNA were measured at the wavelengths 260 nm and 280 nm. For each RNA sample, 2 µL RNA was loaded into a well of a 96-well UV star plate (Greiner Bio-One), and diluted with 98 µL distilled water (1:50 dilution). Blank (100 µL distilled water) was loaded into 3 wells. Absorbance at 260 nm and 280 nm was measured using a spectrophotometer, and the

mean blank absorbance was subtracted from each sample. The concentration of RNA was calculated as follows:

$$\text{Concentration of RNA (μg/mL)} = A_{260} \times \frac{1}{n} \times C$$

Where n = dilution factor; $C = 40$.

For some experiments, RNA concentrations were measured using a NanoDrop™ (Thermo Scientific), which only required 1 μL of RNA.

2.5.4 Synthesis of cDNA

Complementary deoxyribonucleic acid (cDNA) was synthesised from extracted RNA using reverse transcriptase. All reactions were conducted using the iScript cDNA synthesis kit (170-8891, Bio-Rad, Hercules, CA). Each reverse transcription reaction to produce cDNA contained 4 μL 5x iScript reaction mix, 1 μL iScript reverse transcriptase and the desired quantity of RNA (100–500ng). The total reaction volume was made to 20 μL using nuclease-free water. The reverse transcription synthesis reaction utilised the following cycling program: 5 minutes at 25ºC, 30 minutes at 42ºC, and 5 minutes at 85ºC. The reaction was held at 4ºC until samples were removed and subsequently stored at -20ºC. All cDNA reactions and subsequent polymerase chain reactions (PCRs) were run in a Mastercycler Epgradient S thermocycler (Eppendorf), using 0.2 mL low profile thin-walled PCR tubes (Thermo Scientific).

2.5.5 Primer Design

Primers for each gene investigated were designed from the mRNA transcripts, as found on the online database ENSEMBL (ensembl.org). ENSEMBL is a joint project between the Wellcome Trust Sanger Institute and the European Molecular Biology Laboratory – European Bioinformatics Institute and compiles information on targeted eukaryotic genomes. Ideal primers were designed to be between 18–22 base pairs (bp) in length, 50–55% GC content, and have low self-complementarity. To ensure single sequence homology, forward and reverse primers were run through the Basic Local Alignment Search Tool (BLAST), produced by the National Centre for Biotechnology Information (NCBI). Reverse e-PCR (also by NCBI) was used to test that the primers were specific to the human transcript, as well as verify the expected amplicon size.

Where possible, primers were designed to be exon spanning and given that the same primers were to be used for both conventional PCR and qRT-PCR, all primers were designed to produce amplicons less than 300 base pair in length.

Primers arrived as lyophilised nucleic acids (Sigma); DNase/RNase-free water was added to make 100 µM stock solutions. The volume of DNase/RNase-free water required was given for each primer on the manufacturer's specification sheet. Working primer solutions were made up at 10 µM by adding 20 µL stock solution to 180 µL DNase/RNase-free water (1:10 dilution). Both stock and working primer dilutions were stored at -20ºC until use. All primer details are given in Table 2.2.

Gene	Full Name	Forward Primer	Reverse Primer	Size (bp)	T_m (°C)
ACTA2	alpha smooth muscle actin (*αSMA*)	TACTACTGCTGAGCGTGAGATT	CATGATGCTGTTGTAGGTGGTT	247	60
ANGPT1	angiopoietin-1	GAAGGGAACCGAGCCTATTC	GCTCTGTTTTCCTGCTGTCC	108	60
ANGPT2	angiopoietin-2	TGCAAGTGCTGGAGAACATC	GTTAACTTCCGCGTTTGCTC	190	60
BMP2	bone morphogenic protein 2	TCAAGCCAAACACAAACAGC	ACGTCTGAACAATGGCATGA	197	60
CNN1	calponin	GTGAAGCCCCACGACATTTT	TGATGTTCCGCCCTTCTCTT	193	60
FETUA	fetuin-A (*AHSG*)	TCTACACCCAAGTTCCACATCA	CAATCGCCTTGTCCTTCTGAAT	176	60
HPRT	hypoxanthine phosphoribosyltransferase 1	CCACGAAGTGTTGGATATAAGC	GGCGATGTCAATAGGACTCCAGATG	205	60
MGP	matrix gla protein	CCCTCAGCAGAGATGGAGAG	CGCTTCCTGAAGTAGCGATT	162	60
OCN	osteocalcin	CTCACACTCCTCGCCCTATT	GTCAGCCAACTCGTCACAGTC	246	60
OPN	osteopontin	AGCTGGATGACCAGAGTGCT	TGAAATTCATGGCTGTGGAA	151	60
PECAM1	platelet endothelial cell adhesion molecule 1 (*CD31*)	TCTACACCCAAGTTCCACATCA	CAATCGCCTTGTCCTTCTGAAT	136	60
RUNX2	runt-related transcription factor 2	CCTTGACCATAACCGTCTTCAC	GGACACCTACTCTCATACTGGG	192	60
SP7	transcription factor SP7 (osterix)	CATGGTGTTCCAAACACAGC	CTGGAGGAGCTGCCAGTAAC	161	60
TAGLN	transgelin (*SM22α*)	GGCTGAAGAATGGCGTGATT	CTGCCATGTCTTTGCCTTCA	210	60
TIE1	tyrosine-protein kinase receptor Tie1	GACTGACCCAGCTTTTGCTC	CTGCAATCTTGGAGGCTAGG	182	60
TIE2	tyrosine-protein kinase receptor Tie2	TACACCTGCCTCATGCTCAG	ATGGCAGACACCATTGTTCA	176	60
VEGFA	vascular endothelial growth factor A	GGAGGAGGGCAGAATCATCACG	CTCAGTGGGCACACACTCCAG	201	60
VEGFR1	vascular endothelial growth factor receptor 1	TTACTTGCAGGGGACAGAGG	TTCCCGGTAGAAGCACTTGT	221	60
VEGFR2	vascular endothelial growth factor receptor 2	TGGGACTGTGGGAAGAAACATA	GCTCCTTAGTGATGGCCATTTT	170	60

Table 2.2: Primers used in this thesis

2.5.6 PCR and qRT-PCR

All PCRs were run using an iTaq DNA polymerase kit (170-8870; Bio-Rad), supplemented with deoxynucleotide triphosphates (dNTPs, 201900; Qiagen). Each individual reaction contained 2.5 µL iTaq buffer, 0.75 µL $MgCl_2$, 0.5 µL dNTPs, 1µL of 10 µM forward and reverse primers, 18.125 µL RNase/DNase-free water, 0.125 µL iTaq DNA polymerase and 1 µL cDNA. A gradient PCR programme was carried out for all primers to determine the optimum run temperature; the annealing temperatures tested were (in ºC) 51.1, 52.5, 54.3, 56.2, 58.3, 60.3, 62.0 and 63.5. The gradient cycling programme was composed of: 3 min at 95ºC, followed by 40 cycles of denaturation at 95ºC for 30 seconds, annealing at one of the queried temperatures (as given above) for 30 seconds, and extension at 72ºC for 30 seconds. PCR products, supplemented with loading dye (Promega, Madison, WI), were run on a 2% agarose gels. SYBR® Safe DNA Gel Stain (2 µL, S33102; Life Technologies) was added to each gel to visualise PCR products; gels were imaged on a Gel Doc EZ system (Bio-Rad). A 100 bp DNA ladder (G210A; Promega) was run alongside all samples to determine product band size.

Quantitative real-time PCRs (qRT-PCR) were run on a CFX96 Touch Real-Time PCR Detection System (Bio-Rad), using SsoAdvance Universal SYBR® Green Supermix (172-5271; Bio-Rad) and 96-well qRT-PCR plates (HSP-9601; Bio-Rad). A standard qRT-PCR well contained 10 µL SYBR® Green, 1 µL forward primer, 1 µL reverse primer, 7 µL RNase/DNase-free water, and 1 µL cDNA for a total volume of 20 µL. *HPRT* was used as the housekeeping gene to which all other genes were normalised, and was run for each sample on every plate. The amplification curves of samples with *HPRT* remained consistent across experimental conditions, and thus this gene was determined to be a suitable housekeeping gene. Each sample was run in duplicate to account for any pipetting inaccuracies; any further calculations were done using the mean of these replicates. The RT cycle was composed of 3 minutes at 95ºC, followed by 45 cycles of denaturation at 95ºC for 30 seconds, annealing at either 64ºC /62.5ºC for 30 seconds, and extension at 72ºC for 30 seconds.

Whole human adult kidney cDNA was made from MVP Total Human Kidney RNA (Agilent Technologies, Santa Clara, CA). Human kidney RNA was derived from a

single 71-year old male donor, and provided by Agilent in 0.1 mM EDTA (pH 8.0). This cDNA was used to establish the optimal annealing temperature for each primer and was used as a positive control in each qPCR. DNase/RNase-free distilled water was used in all reactions as a negative control.

qRT-PCR files were exported as cfx files for analysis with CFX manager (Bio-Rad). Melting curves were examined before analysing the data to ensure that all reactions had worked and that there was a single peak corresponding to a single product. The number of cycles chosen for quantitative analysis was based on the amplification curve and the number of cycles was picked within the exponential of the PCR amplification, rather than the plateau. mRNA levels of each gene of interest were assessed relative to *HPRT* expression levels using the Δ ΔCt (dCt) method.

qRT-PCR was conducted for: (i) contractile genes *αSMA*, calponin (*CNN1*), and transgelin (*SM22α*); (ii) endothelial and angiogenic genes angiopoietins 1 and 2 (A*NGPT1, ANGPT2)*, receptor tyrosine kinases (*TIE1, TIE2),* vascular endothelial growth factor (*VEGFA)*, and cluster of differentiation marker 31 (*CD31*); and (iii) osteogenic genes runt-related protein-2 *(RUNX2)*, osteopontin *(OPN),* matrix Gla protein *(MGP),* fetuin-A *(AHSG)*, bone morphogenic protein-2 *(BMP2)*, and osterix *(SP7)*.

Firstly, expression levels of these genes were compared between HUVECs, HuAoFibs, human aortic smooth muscle cells (HuAoSMCs) and isolated VSMCs from healthy controls (n = 3). This experiment examined the relative expression of these genes between cell types, therefore expression levels are presented as dCt values, indicating the difference in amplification cycles between the gene of interest and the housekeeping gene *HPRT.* When reading these values, it should be noted that negative dCt values indicate that the gene of interest is expressed at higher levels than *HPRT*, whilst positive dCt values indicate that the gene of interest is expressed at lower levels than *HPRT*.

The second qRT-PCR experiment compared gene expression between VSMCs isolated from paediatric controls (n = 4), pre-dialysis CKD patients (n = 4), and dialysis

CKD patients (n = 4). The number of amplification cycles was normalised to the housekeeping gene *HPRT* to give dCt values. Each sample was then compared with the mean of the control VSMCs, which was given an arbitrary value of 1. Therefore, all gene expression is shown as fold-change as compared with paediatric control VSMCs.

Finally, the third qRT-PCR experiments examined relative levels of gene expression in cells transfected with control siRNA (n = 3) and Tie2 siRNA (n = 3), across different medium conditions. This experiment was analysed as above; however, the baseline to which all other cells were compared was the expression level in cells that were transfected with control siRNA and cultured in control medium (M199, containing no supplemental calcium, phosphate, or Angpt2). All gene expression is therefore shown as fold-change as compared with control-cultured control-transfected VSMCs.

2.5.7 Sequencing

PCR products were purified before sequencing using the protocol provided with the QIAquick PCR purification kit (28106; Qiagen). Five volumes (100 µL) Buffer PB were added to 1 volume (20 µL) of the PCR reaction and mixed well. This mixture was then added to the QIAquick column, which was placed in a 2ml collection tube and centrifuged at 17000*g* for 1 minute; flow-through was discarded. The column was then washed twice with 750 µL Buffer PE. It was centrifuged at 17000*g* for 1 minute between washes, with flow-through discarded after each centrifugation. The column was then removed from the collection tube, placed in a 1.5 mL microcentrifuge tube, and the purified product was eluted from the column using 50 µL DNase/RNase-free water. Product concentrations were measured using the NanoDrop™ and diluted with DNase/RNase-free water to 1 ng/µL per 100 bp of product (~1.7 ng/µL). Purified products were sent, along with the forward primer, to the Wolfson Institute for Biomedical Research (part of UCL core facilities; Gower Street, London) for sequencing; primers were diluted to 5 pM/µL. Sequencing results were obtained as .ab1 files and viewed using 4Peaks (Nucleobytes, Aalsmeer, Netherlands).

2.5.8 Protein Extraction, Quantification, and Western Blotting

To extract protein, growth medium was first aspirated and cells were washed twice with ice-cold DPBS. Protein was then extracted in radioimmunoprecipitation assay (RIPA) buffer, which was composed of 150 mM sodium chloride, 1% Iqepal CA-630 (I3021), 0.5% sodium deoxycholate (D6750), 0.1% SDS, and 50 mM Tris buffer (pH 8.0). Stock RIPA buffer was stored at 4ºC, and fresh inhibitors (66 µg/mL aprotinin, 100 µg/mL sodium orthovanadate, and 0.1 mM phenylmethylsulfonyl fluoride (PMSF)) were added immediately before use. The volume of RIPA buffer used in each extraction was dependent on the size of the dish (100 µL for 60 mm^2 dishes/T25 flasks, 300 µL for 100 mm^2 dish/T75 flasks). The dish was left on ice for 5 minutes, and cells were scraped down using individually packaged cell scrapers. The cell suspension was transferred to a 1.5 mL microcentrifuge tube, and passed 5–6 times through a 25-gauge needle to mechanically shear the cells; the resulting lysate was centrifuged at 17000*g* for 30 minutes at 4ºC. A pellet, consisting of non-soluble cellular debris, was formed at the base of the tube, and the protein-containing supernatant was transferred to a clean 1.5 mL microcentrifuge tube. All protein samples were stored at -80ºC until use.

Protein concentrations were calculated using the Pierce™ BCA Protein Assay Kit as described for the calcium assay protocol (Section 2.3.2) with two notable exceptions. First, the standard curve was diluted in RIPA buffer, rather than NaOH/SDS. Second, the samples were diluted 1:4 with RIPA buffer to ensure that the reaction occurred slowly and fit within the range of the standard curve. Protein samples were denatured using 6x electrophoresis buffer, which was composed of 60% glycerol, 12% SDS, 60 mM Tris-HCl, 0.03% bromophenol blue, and 5% β-mercaptoethanol. Volume equating to 20 µg of protein was added to a PCR tube and the equivalent volume of electrophoresis buffer was added. Samples were heated for 10 minutes at 95˚C using a thermocycler and cooled for 5 minutes on ice.

Gel electrophoresis was conducted in a Bio-Rad Mini-PROTEAN® electrophoresis chamber, using pre-cast 10-well 4–15% Mini-PROTEAN® TGX denaturing polyacrylamide gradient gels (456-1084, Bio-Rad). Running buffer (1x) was composed of 25 mM Tris, 190 mM glycine, and 0.1% SDS, pH of 8.3. Protein samples were loaded into the individual wells of the gel, with care taken to ensure that each

sample was added in its entirety. Additionally, 5µL 100 kDa Precision Plus Protein Dual Xtra protein ladder (161-0377, Bio-Rad) was loaded into the first well of every gel. This ladder has 12 pre-stained protein bands with molecular weights of 2, 5, 10, 15, 20, 25, 37, 50, 75, 100, 150, and 250 kDa. Each gel was run for 50 minutes at 150V, which allowed the loading dye to reach the bottom of the gel. Earlier gels were run at 200V for 30 minutes; however, by decreasing the voltage and thus the speed at which the proteins migrated, the curvature of the bands was reduced.

Gels were then removed from the tank, drained of the residual buffer, and removed from the plastic casing. Proteins were transferred from the gel to a nitrocellulose membrane using the Trans-Blot® Turbo™ transfer system (Bio-Rad). For most proteins, the Turbo function (1.3A, 25V, and 7 min) was sufficient for adequate transfer; however, to improve the transfer of higher molecular weight proteins (i.e. Tie2) the amperage and transfer time was increased to 1.3A, 25V, and 10 min. The efficacy of transfer was observed by staining the membrane briefly (~5 minutes) in Ponceau S.

The membrane was briefly washed in PBS to remove excess Ponceau S stain, before blocking with 5% Marvel in PBS-0.01% Tween at room temperature for 1 hour. The membrane was transferred to a 50 mL centrifuge tube (Falcon), and the primary antibody diluted in 5 mL 5% Marvel in PBS-0.01% Tween was added. This was left to incubate overnight at 4°C on a rolling platform. In this thesis, primary antibodies specific to Tie2 and glyceraldehyde-3-phosphate dehydrogenase (GADPH) were used where Tie2 was the protein of interest and GAPDH was the loading control. The antibody used for Tie2 was the same antibody that was used for immunohistochemistry and immunofluorescence (sc-324; Santa Cruz Biotechnology). Although the molecular weight of Tie2 is 125 kDa, the observed protein size was 140 kDa as a result of glycosylation. It was used at a dilution of 1:200 for Western blotting, for a final concentration of 1 µg/mL. To ensure that it worked correctly, samples were run alongside an equivalent volume of HUVEC protein that was known to be positive for Tie2. Mouse monoclonal antibody to Anti-GAPDH (MAB374; Merck Millipore) was chosen as a loading control, and was used at a dilution of 1:2000 for a final concentration of 1 ng/mL. The non-reduced GAPDH protein size is 46 kDa, while the

reduced product is 36 kDa. This antibody is known to react in pig, dog, human, mouse, rabbit, fish and cat.

The following day, membranes were washed twice in PBS-T for 20 minutes each; this was followed by one wash with 5% Marvel in 0.01% PBS-Tween for 20 minutes. The secondary antibody (1:1000 dilution in 10 mL 5% Marvel in 0.01% PBS-Tween) was then added and rotated for 30 minutes at room temperature. The secondary antibody used against Tie2 (raised in rabbit) was HRP-conjugated Rabbit EnVision® (DAKO), whilst the secondary antibody used against GAPDH was anti-mouse (DAKO). The membranes were then washed three times in PBS-T (20 minutes each), followed by two washes in PBS (30 minutes each). The membrane was removed from the 50 mL centrifuge tube, gently blotted to remove excess PBS, and placed on plastic wrap.

Proteins were detected using the SuperSignal West Pico Chemiluminescent Substrate Kit (Thermo Scientific) using a 1:1 working solution of Solution A (Stable peroxide solution) and Solution B (Luminol/Enhancer solution). When mixed, 4 mL working solution was added directly to the membrane and left for 5 minutes. Excess liquid was removed, and the membrane was wrapped in a smooth layer of plastic wrap. As chemiluminescence is time-limited, the wrapped membrane was quickly exposed to Amersham Hyperfilm ECLB film (GE Healthcare Life Sciences, Pittsburgh, PA) in a darkroom; the length of film exposure was initially set at 1 minute and increased/decreased depending on the signal intensity. Maximum exposure time was set at 30 minutes. For Tie2, the best results were obtained following a 30-minute exposure to film, although weak bands could be detected after 10 minutes of exposure. For GAPDH, results were obtained with a 15-second exposure to film. The film was developed in an ECOMAX X-ray film processor (PROTEC, Oberstenfeld, Germany). For strong signals, such as those emitted by housekeeping genes, the film was exposed to chemiluminescence for seconds before developing.

To re-blot a membrane with a different antibody, the membrane was stripped of the initial antibody and chemiluminescence. To do this, the membrane was first washed in PBS for 10 minutes followed by a 10-minute wash in ReBlot Plus Strong Solution (1:10 dilution of a 10x solution, 2504; Merck Millipore, Temecula, CA). This was

followed by three 10-minute washes in PBS, and a 30-minute wash in 5% Marvel. The next primary antibody was then added as described earlier.

2.5.9 Immunofluorescent Cell Staining

Cells for immunofluorescence staining were cultured in 4- or 8-well glass chamber slides (PEZG50416, PEZG50816; Merck Millipore) and were fixed in ice-cold methanol for 10 minutes. The cells were washed twice in DPBS, and stained using the immunofluorescence protocol described in Section 2.2.6; however, unlike the vessel sections, the cells were not incubated in Sudan black. The primary antibody for αSMA was earlier described in Section 2.2.6, and it was used at a 1:150 dilution for immunocytochemistry. The primary antibody specific to fibroblast specific protein [1B10] (FSP; 200 μg/mL, ab11333, Abcam) was a mouse monoclonal antibody and was utilised at a 1:150 dilution. Two secondary antibodies (described previously in Section 2.2.6) were used, both at 1:250 dilutions: AlexaFluor® 594 (donkey anti-rabbit IgG), and AlexaFluor® 488 (goat anti-mouse IgG). Slides were coverslipped using the aqueous mounting medium SlowFade Gold and visualised under a fluorescent microscope.

2.6 Stimulation of Cells

2.6.1 Experimental Set-up and Design

Cell culture experiments were designed to mirror the conditions experienced by the intact vessel rings *in vitro* in a monolayer culture environment. As such, the calcium, phosphate, and Angpt2 concentrations remained the same as in the intact vessel ring studies. Serum was reduced from 20% (v/v) FBS in the VSMC growth medium to 5% (v/v), as previously done by Reynolds *et al* (2004); however, the time period for stimulation was reduced to 5 days as the VSMCs would not survive in the low-serum culture medium for any longer duration. Attempts to reduce the serum further resulted in extensive cell death with the addition of calcium and phosphate and no quantifiable data. Due to this time-frame, the medium was changed on day 2.5 of the experiment, as shown in the experimental timeline (Figure 2.7).

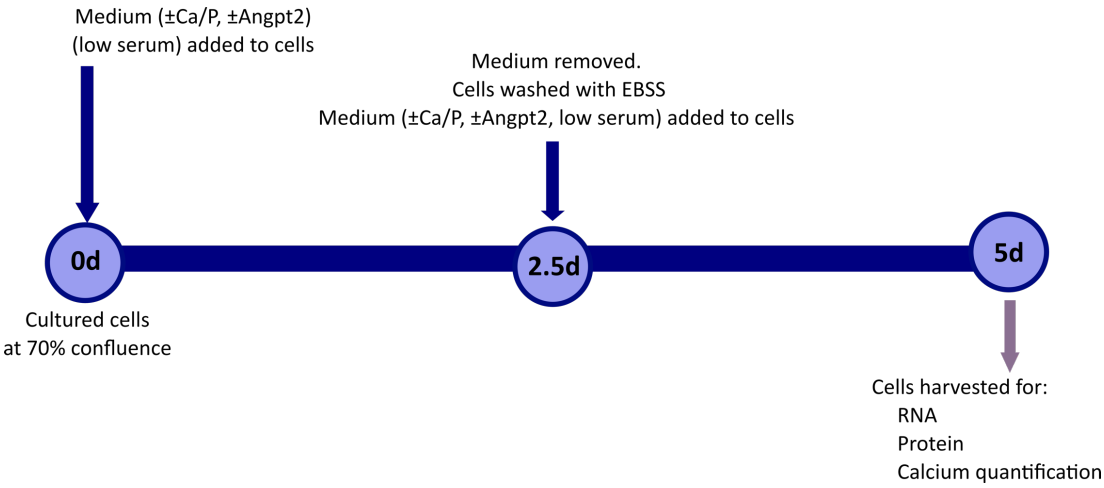

Figure 2.7: Experimental set-up and timeline for VSMCs stimulated with Angpt2 in a pro-calcaemic medium

In this figure, the medium was M199 containing low serum (5% FBS), penicillin, streptomycin and L-glutamine. Calcium concentration was 2.7 mM, phosphate concentration was 2.0 mM and Angpt2 concentration was 25 ng/mL.

2.6.2 Quantitative Measurement of Calcification

Calcium in cells was quantitatively measured by the *o*-cresolphthalein complexosome colorimetric assay as performed in the vessels. While the majority of the protocol is the same, the original extraction of supernatant differs. Ten thousand cells per well were seeded in flat-bottomed 24-well tissue culture plates (353047, Falcon). Once the cells had attached, VSMC growth medium was removed, wells were washed, and 500µL medium was added per well. The medium was changed halfway through the 5-day time-course, and cells were collected after 5 days. HCl (200 µL, 0.1M) was added to each well and the cells were left to decalcify for 45 minutes at room temperature; the supernatant was collected and centrifuged at 17000*g* for 5 minutes. The supernatant was then used in the calcium assay as previously described (Section 2.3.2). Wells were washed with PBS and incubated with 0.1% NaOH in 10% SDS to lyse cells and retain protein. Protein was then quantified using the BCA kit (as described in Section 2.3.2); calcium was normalised to the amount of protein across the course of the experiment.

2.6.3 Alizarin Red Cell Staining

VSMCs were seeded in 6-well plates and treated with pro-calcaemic medium with or without 25 ng/mL Angpt2, alongside an untreated control. The cells were cultured for 5 days before being fixed in 4% paraformaldehyde (PFA) in PBS for 10 minutes, washed with DPBS, and incubated in Alizarin red stain for 30 minutes at room temperature. Alizarin red stain was removed, and cells were washed in DPBS before visualising under a light microscope (as mentioned in Section 2.3.5; Carl Zeiss).

2.6.4 Extraction of RNA and qRT-PCR

Isolating RNA from calcium-stimulated cells proved difficult as calcium precipitated with the RNA pellet when using TRI Reagent®, thus decreasing both the yield and the purity of the RNA. Additionally, these cells could not be trypsinised for subsequent RNA extraction as the presence of calcium impeded the activity of trypsin. Therefore, RNA was extracted from these cells by lysing them directly in culture and using an RNeasy extraction column. Cells were washed twice in ice-cold DPBS; DPBS was removed completely before adding 350 µL Buffer RLT (from the Qiagen RNeasy Mini Kit) containing 3.5 µL β-mercaptoethanol per well of a 6-well plate. Cells were then scraped off the culture surface using a sterile cell scraper, and cell-containing RLT was then transferred to a 1.5 mL microcentrifuge tube. Samples in lysis buffer were frozen at -80˚C until ready to process.

Samples stored at -80°C were defrosted, and the cell suspension was passed 5–6 times through a fine 26-gauge (26G) needle attached to a 1 mL syringe to homogenise cells. Ethanol (350 µL, 70%) was added to the suspension, mixed well, and the total volume was added to the RNeasy spin column. The spin column was then centrifuged at 6500*g* for 15 seconds and flow-through was discarded. The column was then washed with 350 µL Wash Buffer RW1, centrifuged at 6500*g* for 15 seconds, and flow-through discarded.

On-column DNase-digestion was carried out for all samples using an RNase-free DNase set (79254; Qiagen); 80 µL DNase mixture (10 µL DNase, 70 µL Buffer RDD) was added to the O-ring of the spin column and left at room temperature for 15

minutes. Wash Buffer RW1 (350 µL) was then added to the column and spun at 6500*g* for 15 seconds; flow-through was discarded. Buffer RPE (500 µL), made up with ethanol, was added to the column and spun at 6500*g* for 15 seconds; again, the flow through was discarded. Another 500 µL Buffer RPE was added, and the column was spun at 17000*g* for 2 minutes. The column was transferred into a new collection tube and centrifuged at 17000*g* for 1 minute to remove all traces of ethanol. RNase-free water (30 µL) was then added to the column and allowed to sit for 5 minutes before spinning at 6500*g* for 1 minute. The eluted 30 µL sample was run through the column again and spun at 17000*g* for 1 minute. The eluted RNA was stored at -80˚C.

2.6.5 Effect of Exogenous Angpt1 on Vascular Calcification

In most biological contexts, Angpt1 and Angpt2 act as an agonist-antagonist pair (Maisonpierre *et al* 1997, Yuan *et al* 2009). To explore this relationship with regard to vascular calcification, VSMCs exposed to pro-calcaemic conditions were stimulated with Angpt1. Cells were stimulated with calcium and phosphate as described in Section 2.5.1; however, some cells were also supplemented with an additional 25 ng/mL carrier-free recombinant human Angpt1 (923-AN-025/CF; R&D Systems). Angpt1 was obtained as lyophilised protein, reconstituted prior to use at 100µg/mL in sterile DPBS and stored in aliquots at -20ºC. Calcium content was then measured as described in Section 2.6.2.

2.6.6 Tie2 Inhibition Using siRNA

To inhibit the expression of the Tie2 receptor, cells were transfected with small interfering RNA (siRNA) specific to human Tie2 (sc-33677; Santa Cruz Biotechnology). Tie2 siRNA (human) contains three 19–25 nucleotide siRNA sequences specific to *TIE2*. Cells transfected with Tie2 siRNA were compared with cells transfected with control siRNA-A (sc-37007; Santa Cruz Biotechnology); siRNA-A is a non-targeting scrambled sequence of 20–25 nucleotides. Control siRNA and Tie2 siRNA arrived lyophilised, and were resuspended to give a final concentration of 10 µM.

Cells were set up in 24- or 6-well plates as for previous stimulation experiments (Section 2.6.1) and left overnight to attach. VSMC growth medium was removed, cells were washed twice with EBSS, and 500 µL Opti-MEM®I (1x) reduced serum medium (31985-062; Gibco), containing 4-(2-hydroxyethyl)-1-piperazineethanesulfonic acid (HEPES), 2.6 g/L sodium bicarbonate, and L-glutamine was added to each well. Lipofectamine RNAiMax (Invitrogen) was used as the lipid carrier, and 3.3 µL was added to each well, along with *x* µL (dependent on the desired siRNA concentration) of either control siRNA or Tie2 siRNA.

To determine the optimal concentration of siRNA, a preliminary experiment was conducted with four different concentrations (10 nM, 30 nM, 50 nM, or 100 nM), from which the concentration was chosen for subsequent experiments. The concentration (10 nM) was chosen, as this provided a 75% knockdown of *TIE2* mRNA at the lowest possible concentration. The effect of lipofectamine was compared against VSMCs with no lipofectamine added to verify that the chosen concentration had no effects on cell survival. Furthermore, to determine how frequently the cells needed to be transfected to ensure *TIE2* mRNA downregulation was maintained throughout the experiment, a brief time-course experiment was conducted in which cells were collected at 48 hours, 72 hours, and 5 days post-transfection.

This preliminary experiment indicated that, whilst *TIE2* was downregulated at the 48-hour time-point, cells needed to be transfected again to maintain downregulation across the 5-day period. Two hours post-transfection, Opti-MEM®I was removed and replaced with low-serum (5% FBS) VSMC medium and in the final protocol cells were cultured for 48 hours before removing the medium. Cells were washed in EBSS and re-transfected. Fresh medium was added 2 hours post transfection, and cells were left until the 5-day time-point. RNA and protein were harvested. The experimental timeline is shown in Figure 2.8 and the medium conditions are shown in Figure 2.9.

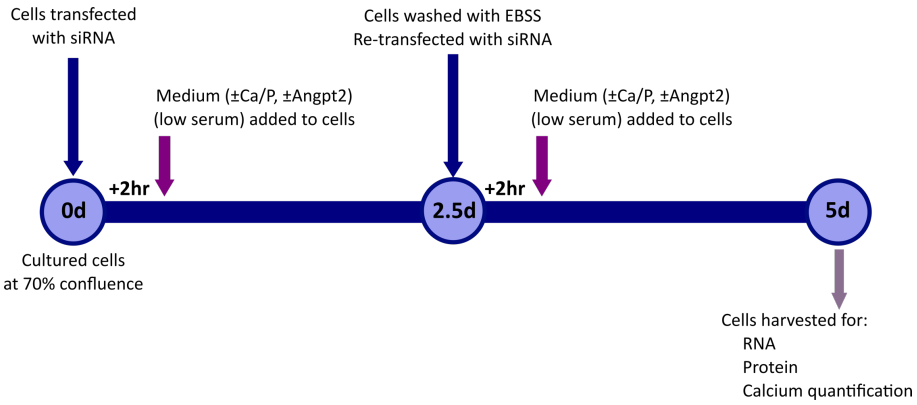

Figure 2.8: Experimental set-up and timeline for VSMCs transfected with control siRNA and *TIE2* siRNA

Cells were transfected with siRNA twice in the duration of the 5-day experiment, on Day 0 and Day 2.5. Medium was M199 containing low serum (5% FBS), penicillin, streptomycin, and L-glutamine. Calcium concentration was 2.7 mM, phosphate concentration was 2.0 mM, and Angpt2 concentration was 25 ng/mL.

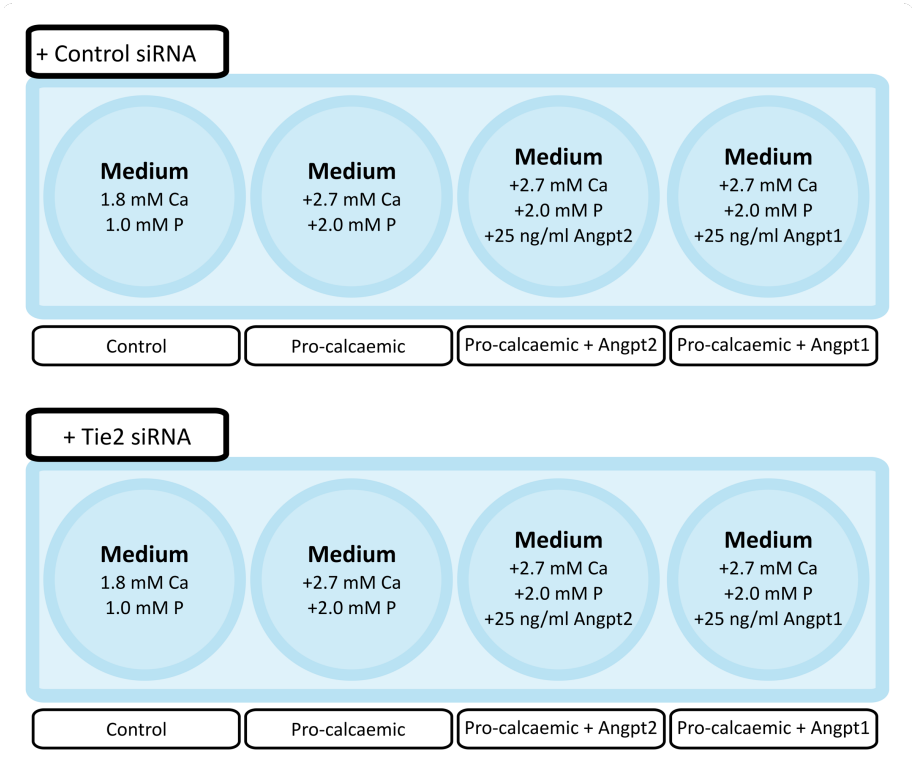

Figure 2.9: Medium conditions for transfection studies

In each well, cells were transfected with 500 µL Opti-MEM®I, 3.3 µL Lipofectamine, and 2 µL of either control or Tie2 siRNA. The experimental groups (medium only [1.8

mM Ca, 1.0 mM P], pro-calcaemic medium [+2.7 mM Ca, +2.0 mM P], and pro-calcaemic medium with Angpt2 [+2.7 mM Ca, +2.0 mM P, +25 ng/mL Angpt2]) were the same as those outlined in Figure 2.1, barring the addition of a single well stimulated with Angpt1 rather than Angpt2 (pro-calcaemic + Angpt1 [+2.7 mM Ca, +2.0 mM P, +25 ng/mL Angpt1]).

2.6.7 TUNEL Staining to Detect Apoptosis in VSMCs

VSMCs were seeded in 4-well chamber slides and treated with either control siRNA or Tie2 siRNA before adding pro-calcaemic medium with or without 25 ng/mL Angpt2. The cells were cultured for 24 hours or 5 days before being fixed in 4% PFA in PBS for 10 minutes, washed with DPBS, and stained for apoptosis using a Fluorescein *In Situ* Cell Death Detection Kit (11684795910, Roche, Mannheim, Germany). The cells were washed twice with DPBS and permeabilised using 0.1% Triton-X in 0.1 M citrate buffer (500 µL per well, for 2 minutes at room temperature). The cells were again washed twice with DPBS and 50µL 'TUNEL Reaction Mixture' ('Enzyme Solution' diluted 1:30 in 'Label Solution', both from the Roche kit) was added for 1 hour in a humidified chamber. The slides were then washed twice with PBS, followed by incubation in 32 µL Hoechst 33342 (10 mg/mL) in 200 mL PBS for 5 minutes, and washed twice more in PBS. Slides were mounted using SlowFade gold and sealed with nail polish. All slides were examined using a fluorescent microscope.

2.7 Inhibition of Tie2 in Vessel Rings

Tie2 kinase inhibitor (sc-356156, Santa Cruz Biotechnology), otherwise known as 4-(6-methoxy-2-naphthyl)-2-(4-methylsulfinylphenyl)-5-(4-pyridyl)-1H-imidazole, was used as a synthetic chemical inhibitor of Tie2 activity in the vessel rings, rather than siRNA (Semones *et al* 2007). The Tie2 kinase inhibitor (100 µg/mL) was added to the vessel culture medium, along with 2.7 mM calcium, 2.0 mM phosphate, and 25 ng/mL Angpt2. The vessel rings were cultured for 14 days, with medium changed every 3–4 days, and rings were taken for calcium quantification and histology.

2.8 Statistics

Within this thesis, I have utilised two-tailed Student's *t*-tests in preference to ANOVA tests to compare the means between experimental groups. By choosing a two-tailed Student's *t*-test, I have chosen to examine the possibility that the mean of one group is either significantly greater or significantly less than the mean of the other group, using a significance level of 0.05.

When using an ANOVA test, two of the underlying assumptions are that the data are normally distributed, and that variance is heteroscedastic – the data within this thesis do not comply with these assumptions, due to the small sample size and large degree of biological variance between individual samples. Whilst I could have used non-parametric tests, which have no distributional assumptions, the Student's *t*-test is robust to departures from normality; this is partially due to the fact that the *t*-test utilises the standard error of the sample means, and remains consistent irrespective of the distribution of the data. Increasing the sample size would bring the standard error closer to standard deviation; however, the distribution of the data does not affect this and, given the small number of samples from each disease state (control, pre-dialysis CKD, or dialysis CKD) and the large degree of variation between individual samples, this was a crucial consideration.

Although my small sample size was one reason as to why the Student's *t*-test was chosen, this test was also chosen in preference to a non-parametric test given that I wanted to compared the means of the sample groups, rather than the median values (which is what the non-parametric tests would have compared). An artefact of the small sample size is the high variation between samples. As an ANOVA test utilises a test statistic based upon the difference between the variance of the samples, it is more readily affected by outliers than the Student's *t*-test. Comparatively, the Student's *t*-test utilises a test statistic that is based upon comparison of the mean values. Where a non-parametric test would be more robust with respect to issues arising from data quality, the small sample sizes would continue to have a noticeable effect.

The small sample size also increases the likelihood of inducing a Type-I error, in which the data falsely suggests that there is a difference between groups. However, a larger

number of samples would be required to reduce this risk. All of the possible tests have their flaws and, given the multiple considerations discussed, the Student's *t*-test was chosen for the analyses in this thesis. However, given a larger sample size, I would reassess the utilised statistical test potentially in favour of an ANOVA test.

All calculations were done using Microsoft Excel, and all graphs were made using GraphPad Prism® 6 (GraphPad Software Inc., La Jolla, California). In this thesis, all graphs present the mean of *n* samples (specific *n* is denoted in each figure), as well as the standard error of the mean.

Chapter 3: Results — The Effect of Angpt2 on Calcification

3.1: Quantification of Calcium Deposition in Intact Vessel Rings

3.1.1 Experimental Overview: Calcium Quantification

The first aim of this thesis was to determine whether exogenous Angpt2 had any effect on calcification deposition using intact vessel rings. To examine this, medium-sized muscular arteries were obtained from control, pre-dialysis, and dialysis paediatric patients (as described in Section 2.2). These arteries were cut into 10–15 1 mm rings. One ring was used to assess baseline calcium content in each individual. The remaining rings were cultured in one of three conditions: control medium (medium only), pro-calcaemic medium (2.7 mM Ca/2.0 mM P), and pro-calcaemic medium with 25 ng/mL Angpt2 (as described in Section 2.3.1).

The concentrations of calcium and phosphate used for the 'pro-calcaemic' medium were chosen as they are the minimum concentrations required to induce calcification in dialysis vessels *in vitro* (Shroff *et al* 2010). Similarly, the Angpt2 dosage was determined from the results of the paper leading to this studentship (Shroff *et al* 2013), which indicated that 25 ng/mL was the highest level of circulating Angpt2 observed in paediatric dialysis patients.

3.1.2 Baseline Calcium Content

One arterial ring was collected prior to culture from each patient's vessel to determine the baseline level of calcium in that individual. Shroff and colleagues (2010) have previously shown that paediatric patients on dialysis exhibit a significantly higher baseline level of calcium than healthy paediatric controls.

Comparatively, the baseline calcium measurements in this study (Table 3.1) suggested that there was a tendency for calcium deposition to be increased in arterial rings from pre-dialysis (36.3±21.1 μg calcium/ μg protein, $n = 3$) and dialysis (36.8±35.9 μg calcium/μg protein, $n = 8$) patients when compared with healthy paediatric controls (15.7±13.7 μg calcium/ μg protein, $n = 3$). However, there were no statistically

significant differences between the groups (Figure 3.1). The discrepancy between these findings and those of Shroff and colleagues (2010) is likely due to the wide variability between patients and the low patient number.

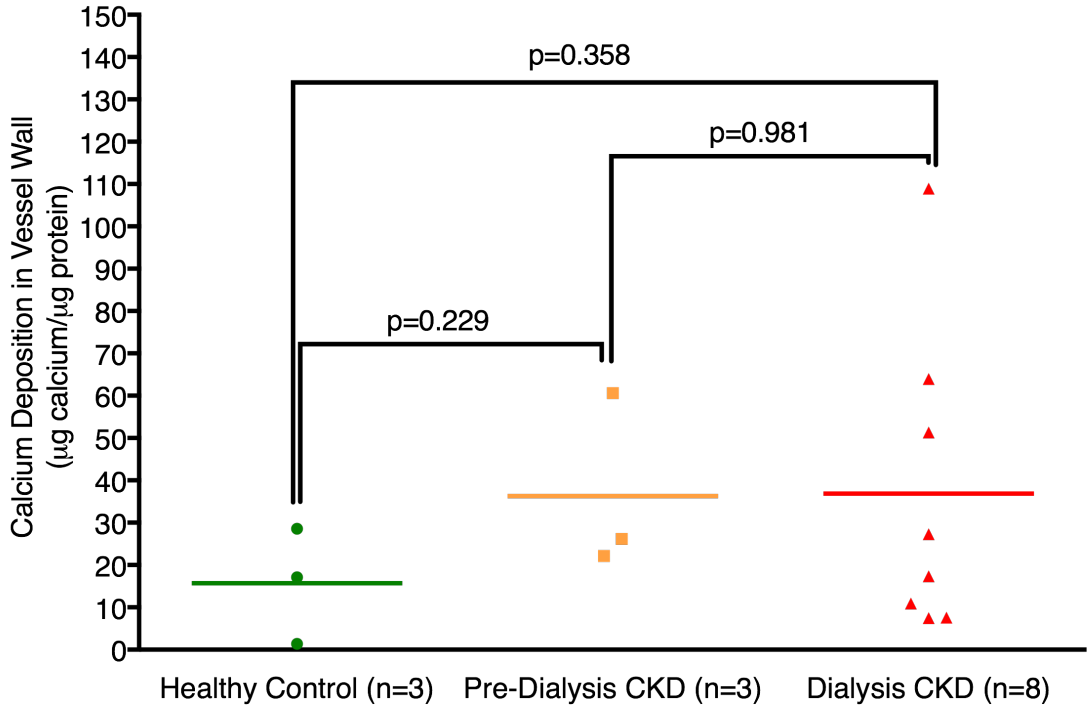

Figure 3.1: Baseline calcium levels in arterial rings

Calcium loads of arterial rings obtained at baseline are shown in µg calcium per µg protein for healthy renal controls ($n = 3$), pre-dialysis CKD patients ($n = 3$), and dialysis CKD patients ($n = 8$). Only one ring was obtained per patient due to the limited quantity of vessel rings. Note that baseline calcium levels could not be obtained from one pre-dialysis sample due to the technical difficulties when the vessel rings were cut. There are no statistically significant differences between the groups.

Sample ID	Type of Artery	Baseline (µg /µg)	M199 (µg /µg)	CaP (µg /µg)	CaP+Angpt2 (µg /µg)
Control A28	Mesenteric	28.54	29.28	30.32	41.91
Control A43	Mesenteric	17.13	21.22	21.14	20.68
Control A44	Mesenteric	1.35	3.00	2.81	2.80
CKD A15	Omental	60.61	87.98	117.75	120.83
CKD A17	Omental	-	54.82	95.51	114.86
CKD A36	Omental	22.12	130.03	173.82	150.35
CKD A39	Omental	26.18	27.38	33.37	32.92
Dialysis A14	Inf. Epi.	51.32	32.85	122.94	171.74
Dialysis A37	Inf. Epi.	27.30	40.26	136.23	355.97
Dialysis A40	Inf. Epi.	108.90	128.85	343.73	604.28
Dialysis A42	Inf. Epi.	10.91	12.02	85.53	118.45
Dialysis A41	Inf. Epi.	63.96	65.63	211.60	424.43
Dialysis A46	Inf. Epi.	7.56	11.03	36.40	57.73
Dialysis A47	Inf. Epi.	7.47	10.20	23.07	75.37
Dialysis A48	Inf. Epi.	17.34	42.12	61.24	91.54

Table 3.1: Calcium deposition in control, pre-dialysis CKD and dialysis vessel rings at baseline and following 14 days in culture under treated conditions

Types of arteries utilised are the mesenteric artery, the omental artery, and the inferior epigastric artery (shortened to 'Inf. Epi.' in the table above). All raw calcium values are given in µg calcium per µg protein. M199 = serum-free M199.

3.1.3 Stimulation with Exogenous Angpt2

Initially, a pilot study was performed to assess the time-course of calcium deposition in pre-dialysis ($n = 3$) and dialysis vessels ($n = 2$) exposed to pro-calcaemic medium with and without Angpt2, using the *o*-cresolphthalein colorimetric assay (as described in Section 2.3.2). Due to the limited length of the vessel, only one ring was available for each condition; therefore, for all calcium assays, *n* equals the number of patients in the given category (i.e. healthy control, pre-dialysis, or dialysis). However, the digested vessel ring was measured in duplicate for both the calcium assay and protein assay to account for any pipetting variation observed in the measured absorbance levels. After 7 days of exposure, there was no statistically significant difference in the calcium deposition in either pre-dialysis or dialysis vessels cultured in control or pro-calcaemic medium with or without Angpt2 (Figure 3.2).

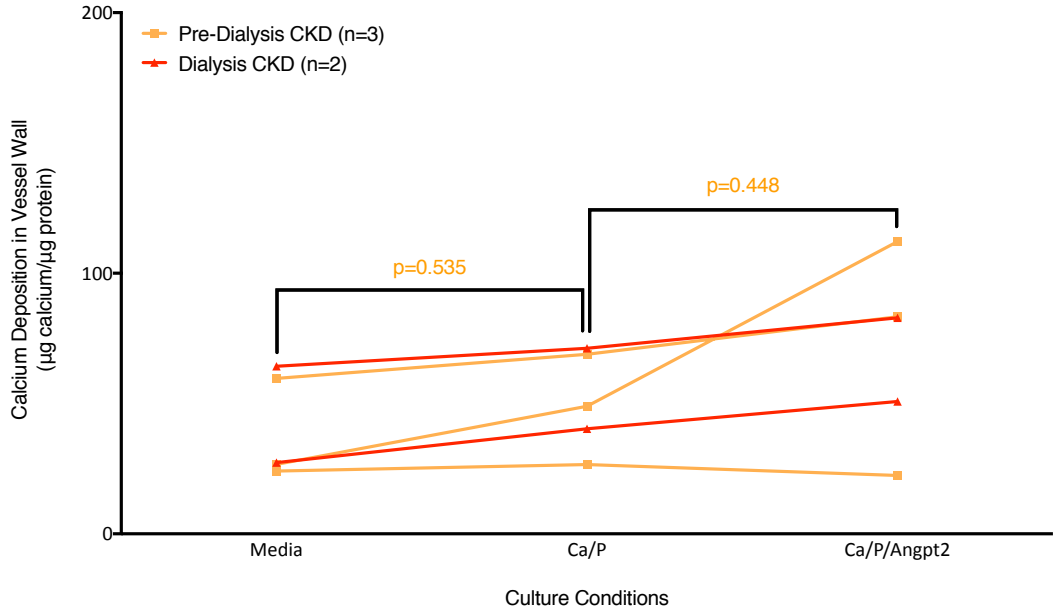

Figure 3.2: Calcium deposition in arterial rings after 7 days in culture

Calcium content, normalised to the protein content, of arterial rings from pre-dialysis ($n = 3$) and dialysis ($n = 2$) patients was measured (µg calcium per µg protein) after 7 days exposure. There were no statistically significant differences in calcium deposition between conditions in pre-dialysis vessels. As there were only two dialysis samples, *p*-values were not calculated between the conditions due to the problems that such a small sample would cause with the underlying assumptions of the test.

I subsequently extended the duration of my experiments and examined the effect of 14 days exposure to a pro-calcaemic environment with, and without, 25 ng/mL of Angpt2 on the arterial rings (Table 3.1, Figure 3.3).

Control vessels (*n = 3*) cultured in the pro-calcaemic medium had a similar calcium load to those exposed to control medium (18.09±8.09 µg calcium/ µg protein versus 17.83±7.77 µg calcium/ µg protein respectively, *p = 0.983*). The addition of Angpt2 to the pro-calcaemic media did not have any effect on calcium deposition in control vessels (21.80±11.31 µg calcium/ µg protein, *p = 0.803*).

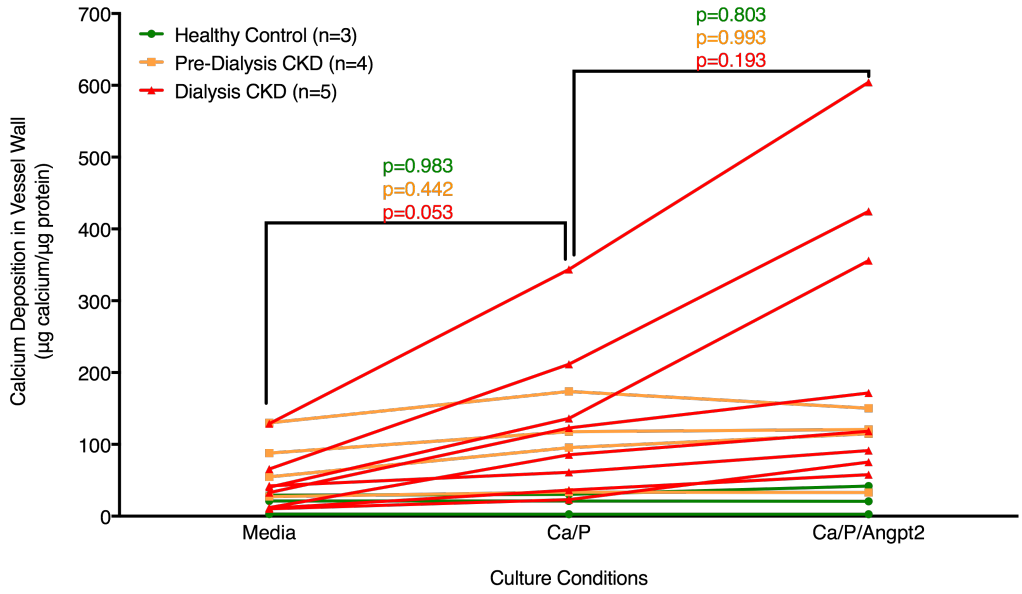

Figure 3.3: Calcium deposition of intact arterial rings (µg Ca/µg protein)
Calcium content, as measured using the *o*-cresolphthalein colorimetric assay, was normalised to the protein content of the respective arterial ring after 14 days in culture. Control (*n = 3*) and pre-dialysis CKD (*n = 4*) vessels do not exhibit any significant difference in calcium load between culture in M199 medium alone and culture with calcium and phosphate (control: *p = 0.983*, pre-dialysis: *p = 0.442*). There was a strong trend for calcium deposition to be increased in dialysis vessels exposed to pro-calcaemic conditions, which nearly reached significance (p = 0.053), compared with M199 medium alone. Dialysis vessels (*n = 8*) also exhibit a further increase in calcium load when treated with 25 ng/mL Angpt2 in pro-calcaemic medium, although this trend is not statistically significant (*p = 0.193*).

Each pre-dialysis vessel (*n = 4;* Figure 3.3) cultured in pro-calcaemic media had an increased calcium load compared with vessel rings incubated in normal media, though this was not significant (105.12±29.04 µg calcium/ µg protein versus 75.05±22.12 µg calcium/ µg protein respectively, *p = 0.442*). The addition of Angpt2 to the pro-calcaemic media had no further effect on calcium deposition in pre-dialysis vessels when compared with pre-dialysis vessels cultured in pro-calcaemic media alone (104.74±25.17 µg calcium/ µg protein, *p = 0.993*).

Each dialysis vessel (*n = 8;* Figure 3.3) also had an increased calcium load when exposed to pro-calcaemic media (as compared with dialysis vessels cultured in control medium); this was very close to statistical significance (127.59±37.63 µg calcium/ µg protein versus 42.97±14.05 µg calcium/ µg protein, *p = 0.053*). Furthermore, when each dialysis vessel was exposed to Angpt2, calcium deposition in the pro-calcaemic medium was further enhanced, compared with dialysis vessels cultured in pro-calcaemic media alone, although this did not reach significance (237.44±70.95 µg calcium/ µg protein, *p = 0.193).*

Displaying the data as raw values has the limitation of not taking into account the variation in baseline calcium levels between patients. Therefore, I re-examined the data using each vessel as its own internal control. In this analysis, the change in calcium content is represented as the fold-change compared with the vessel rings cultured in medium alone, which was given an arbitrary value of 1 (Figure 3.4).

The control vessels (*n = 3*) showed no increase in fold-change of calcium load when exposed to a pro-calcaemic medium (0.99±0.03, *p = 0.746*); similarly, fold-change remained the same with the addition of 25 ng/mL Angpt2 to control vessels in pro-calcaemic medium (1.11±0.16, *p = 0.491*). The pre-dialysis vessels (*n = 4*) exhibited a 1.4±0.11-fold increase in the calcium load when cultured in the pro-calcaemic medium, compared with pre-dialysis vessel rings cultured in control medium (*p = 0.012*). However, the calcium load was not further enhanced in the pre-dialysis vessel rings cultured with the addition of Angpt2 (1.46±0.22, *p = 0.853* when compared with pre-dialysis vessel rings cultured in pro-calcaemic media alone). The culture of the dialysis vessels (*n = 8*) in a pro-calcaemic medium resulted in a significant fold increase in calcium load (3.39±0.59, *p = 0.001*), compared with dialysis rings cultured

in control medium. Calcium deposition in dialysis vessels was further augmented with the addition of Angpt2 to the pro-calcaemic medium; there was a significant fold-change (6.23±0.87), compared to vessels cultured in pro-calcaemic medium without Angpt2 ($p = 0.019$).

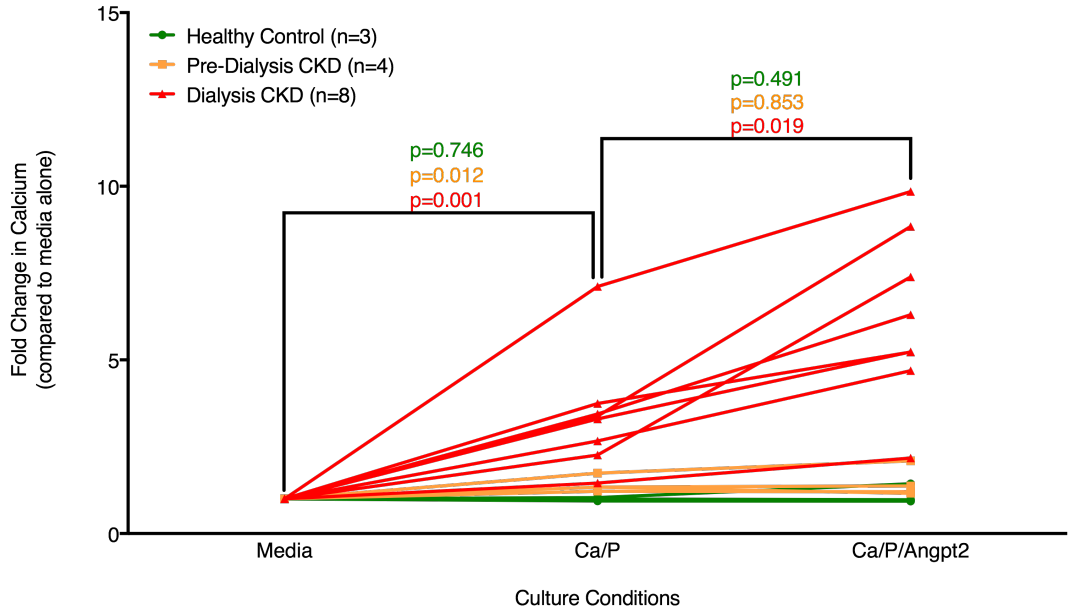

Figure 3.4: Calcium deposition of intact arterial rings (fold-change)

Calcium content, normalised to the protein content, of each arterial ring was measured (µg calcium per µg protein). Each vessel was used as its own control, and the calcium content in each arterial ring was compared to the calcium content in the arterial ring that was cultured in the medium alone, which was given an arbitrary value of 1. Control ($n = 3$) and pre-dialysis ($n = 4$) blood vessels exhibited no significant changes in calcium load when treated with pro-calcaemic medium with and without Angpt2 (control: $p = 0.491$, pre-dialysis: $p = 0.853$). Vessel rings from patients on dialysis ($n = 8$) exhibited a significant increase in calcium load when cultured in a pro-calcaemic medium, compared with normal medium ($p = 0.001$); treatment with Angpt2 further increased the calcium load in these vessels significantly compared with calcium and phosphate alone ($p = 0.019$).

As the calcium assay indicated that calcium deposition increased within arterial rings from dialysis patients with the addition of calcium and phosphate to the culture medium, I then examined the cultured arterial rings that had been fixed for immunohistochemistry for localisation of the calcium deposition using the Von Kossa

staining method. However, staining of the vessel rings (Figure 3.5) indicated that none of the arterial rings contained any visually detectable calcium depositions, even when the arterial rings were cultured in pro-calcaemic medium with or without Angpt2. Shroff and colleagues (2008) have previously found that very few paediatric patients exhibit calcium deposition in the tunica media as detected using the Von Kossa staining method; instead, this method appears to be preferable for detection of large calcium depositions in the atherosclerotic plaques of adult patients.

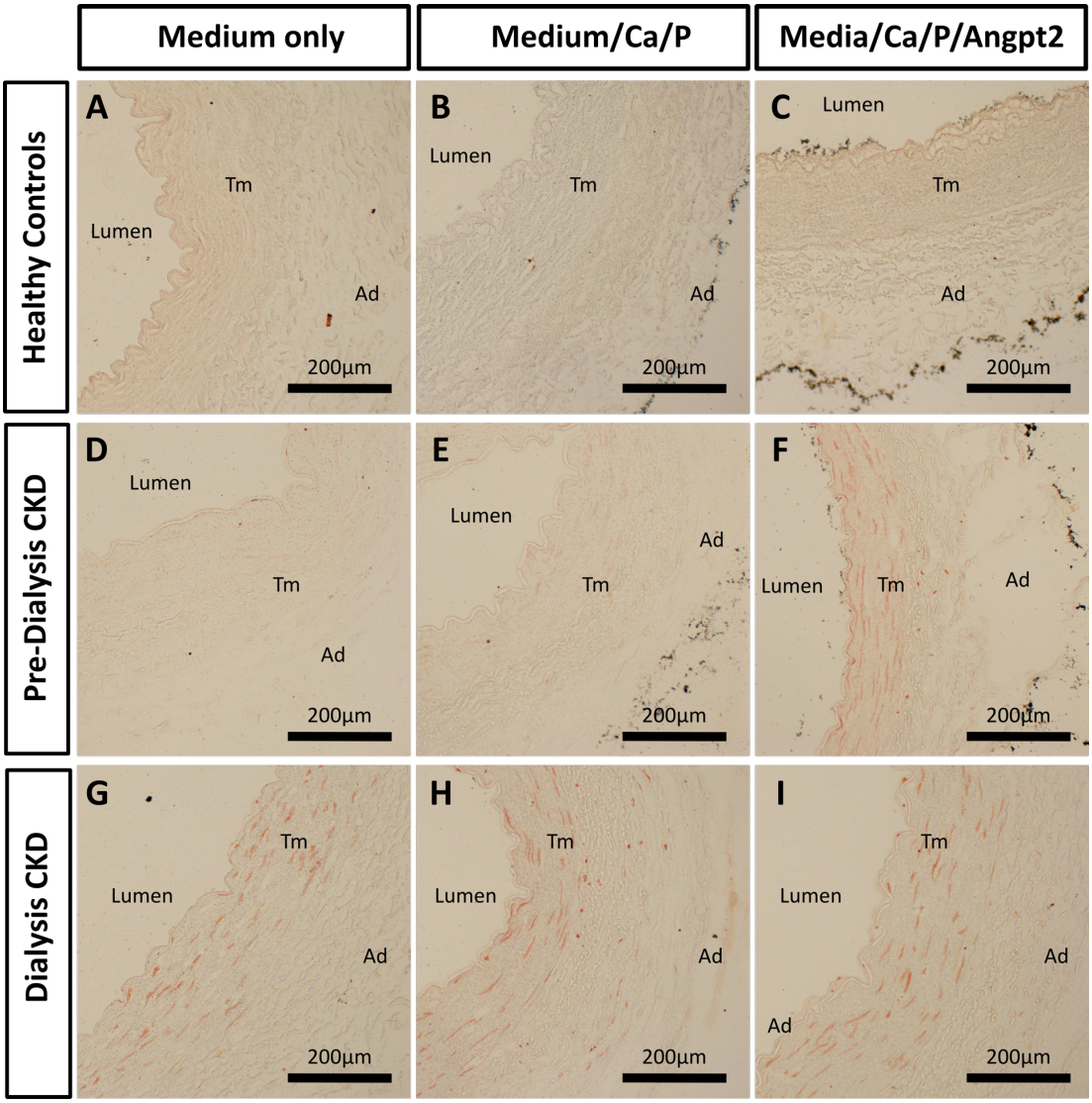

Figure 3.5: Von Kossa staining of intact vessels to detect calcium

Arterial rings cultured from healthy control vessels, pre-dialysis vessels, and dialysis vessels were negative for Von Kossa staining to detect calcium deposition when cultured for 14 days in control medium alone (**A**, **D**, **G** respectively). Arterial rings

from healthy control vessels stained positive for Von Kossa along the outer edge of the adventitia when cultured in pro-calcaemic medium (**B**) and when cultured in pro-calcaemic medium with Angpt2 (**C**). However, this staining is not localised within the arterial ring itself. Positive staining is also observed along the edge of the adventitia in pre-dialysis patients cultured in calcium-containing medium, with and without, Angpt2 (**E**, **F)**. Arterial rings obtained from dialysis vessels exhibit minimal Von Kossa positive staining when cultured in the pro-calcaemic medium, with and without, Angpt2 (**H**, **I**). Although Von Kossa positive staining along the adventitia indicates that the protocol worked, the vessels themselves are negative for detectable calcium depositions within the tunica media.

3.2: Isolation and Immunocytochemistry of Primary VSMCs

3.2.1 Experimental Overview: VSMCs

Given that arterial rings from paediatric patients on dialysis exhibited an increase in calcium deposition when treated with exogenous Angpt2 for 14 days under pro-calcaemic conditions, compared with pro-calcaemic conditions alone, I decided to investigate whether exogenous Angpt2 would increase calcium deposition in isolated VSMCs. VSMCs were explanted from the medial layer of fresh patient vessels (as described in Section 2.4.2). All VSMCs used in this project are primary cells; however, each individual cell population (cells isolated from one particular patient) will be referred to as a cell 'line'.

3.2.2 Isolation of Primary Paediatric VSMCs

Nineteen vessels were set up for explant cell isolation (as shown in Table 2.1). Of these, two did not attach and were discarded. Explants from 17 vessels attached and resulted in proliferating cells. Of these, two lines were destroyed due to a systemic incubator malfunction at passage one while a third line was infected at passage one. This left 14 independent cell lines: five control lines, four pre-dialysis lines, and five dialysis lines.

For each sample, VSMCs proliferated in a radial manner outwards from the attached medial explants (Figure 3.6A, B, and C). The cell density was highest near the explant and became increasingly sparse as the distance from the explant increased (Figure 3.6C). VSMCs isolated from the healthy controls proliferated at a more rapid rate (2–3 weeks to reach confluence) than VSMCs obtained from either pre-dialysis or dialysis vessels (4–6 weeks to reach confluence). The cells were visualised using light microscopy, and all isolated VSMCs exhibited classical SMC morphology (Figure 3.6D, E, F); that is, the cells appeared spindle-like and elongated and, when confluent, formed a 'hill and valley' structure. These cells were also mono-nucleated, with small rounded nuclei. There were no obvious morphological differences between control, pre-dialysis, and dialysis VSMCs.

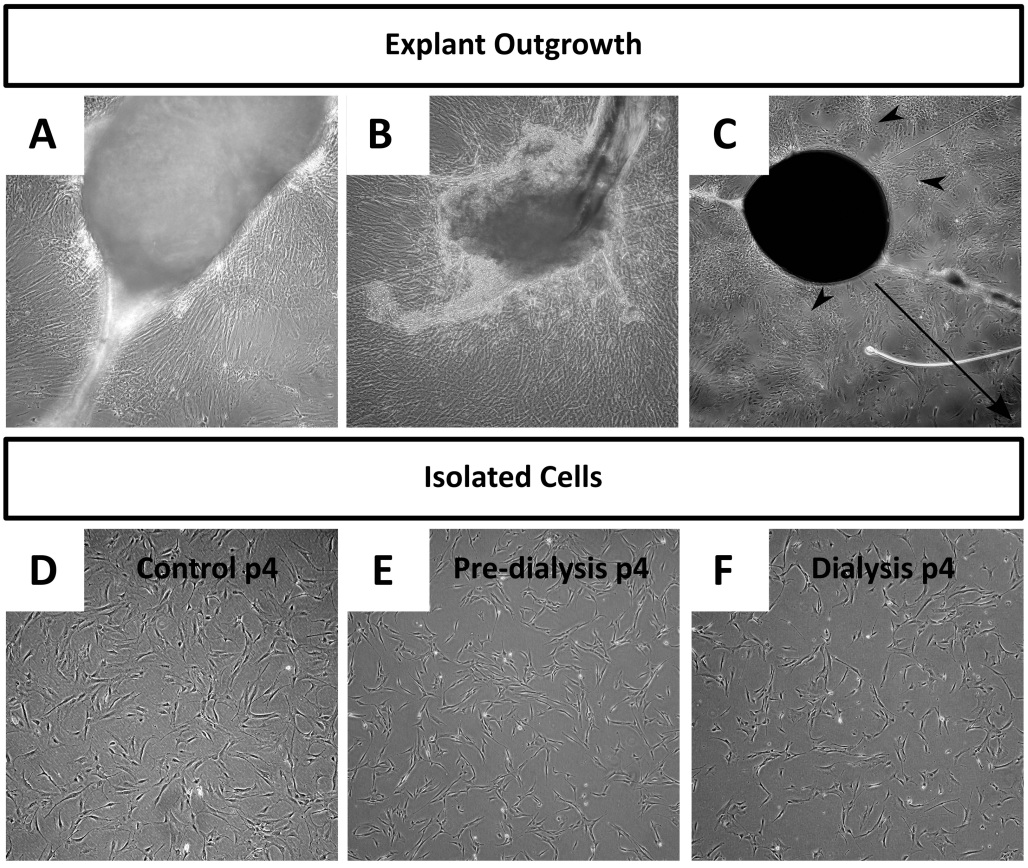

Figure 3.6: Isolation of VSMCs from explants of paediatric tunica media

VSMCs were isolated from the explants of the tunica media obtained from paediatric arteries. VSMCs were isolated from medial explants obtained from dialysis vessels (**A**, **B**, **C)**. Photos were taken 4 weeks after seeding the tissue, highlighting the different patterns that these cells can take as they reach confluence. Arrowheads in **C** indicate

regions in which the cells are beginning to condense; when this begins to occur, cells need to be passaged immediately to prevent the release of apoptotic bodies and spontaneous calcification due to over confluence. The long arrow in **C** denotes the decreasing density of the cell population as the distance from the explant increases. Control, pre-dialysis, and dialysis VSMCs exhibit typical VSMC morphology at low passages (shown here at passage 4; **D**, **E**, **F**). Cells are representative of their respective populations (control: $n = 5$, pre-dialysis: $n = 4$, dialysis: $n = 5$). Cells were passaged and utilised in experiments until passage 9 as long as they retained this morphological phenotype. All cells were photographed at 40x magnification.

3.2.3 Immunocytochemistry of VSMCs

Blood vessels contain several different cell types (VSMCs, endothelial cells, and fibroblasts). Therefore, I wanted to check the purity of the cells that I had isolated before using them for detailed experiments. I utilised immunocytochemistry to compare the expression pattern of αSMA and FSP1 between my isolated cell populations and a commercially purchased population of primary huAoFibs. Differentiating between VSMCs and fibroblasts is difficult, as there is no clear marker that differs between them; both αSMA and FSP1 are expressed in both cell types. However, literature has suggested that the pattern and localisation of these proteins differ between VSMCs and fibroblasts and therefore by using immunocytochemistry, the identity of the cells could be indicated (Brouty-Boye *et al* 1992, Chamley *et al* 1977).

The isolated VSMCs (all lines) express αSMA in discrete filamentous structures, with strong staining in the stress fibres of the cells (Figure 3.7A, C). In contrast, αSMA staining is more diffuse across the HuAoFibs (Figure 3.7D, F). FSP1 expression is condensed around the nucleus in the isolated VSMCs (Figure 3.8A, C), whilst the HuAoFibs exhibit diffuse FSP1 positivity throughout the cytoplasm (Figure 3.8D, F). Although not a definitive indicator, these staining patterns suggest that the isolated cells are indeed VSMCs (Brouty-Boye *et al* 1992, Chamley *et al* 1977).

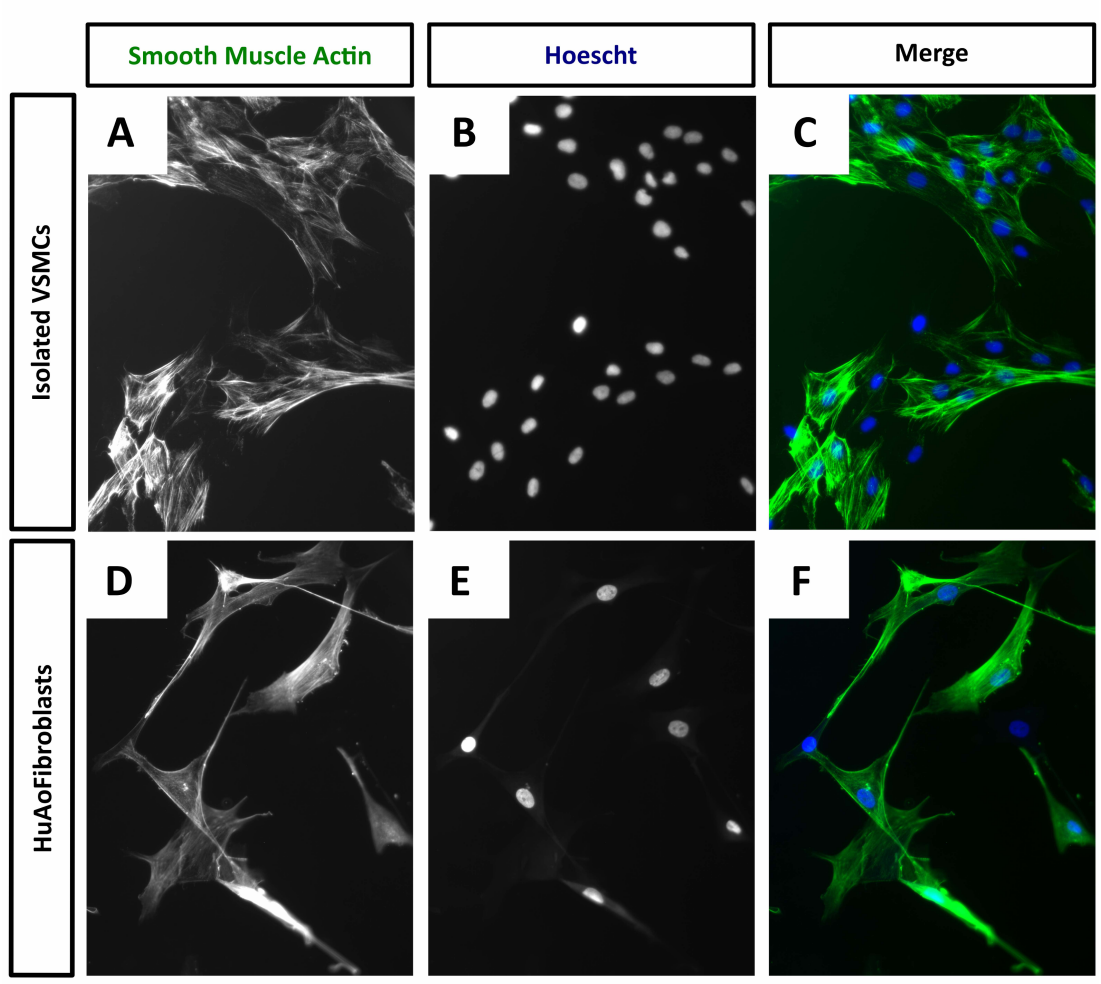

Figure 3.7: Immunocytochemistry for αSMA in VSMCs and HuAobFibs

Isolated dialysis VSMCs and HuAoFib were stained for αSMA, to highlight the characteristic actin structures of the cells. Both VSMCs **(A, B, C)** and fibroblasts (**D, E, F)** stain positive for αSMA (**A, D**); however, when staining VSMCs the actin fibres are clearly defined along the stress fibres in the isolated VSMCs (**A)** in comparison to the filamentous structures observed in HuAoFib (**D**). VSMC staining is representative of nine independent cell lines (control: $n = 3$, pre-dialysis: $n = 3$, dialysis: $n = 3$), while fibroblast staining is representative of a single commercial cell line. All cells were photographed at 200x magnification.

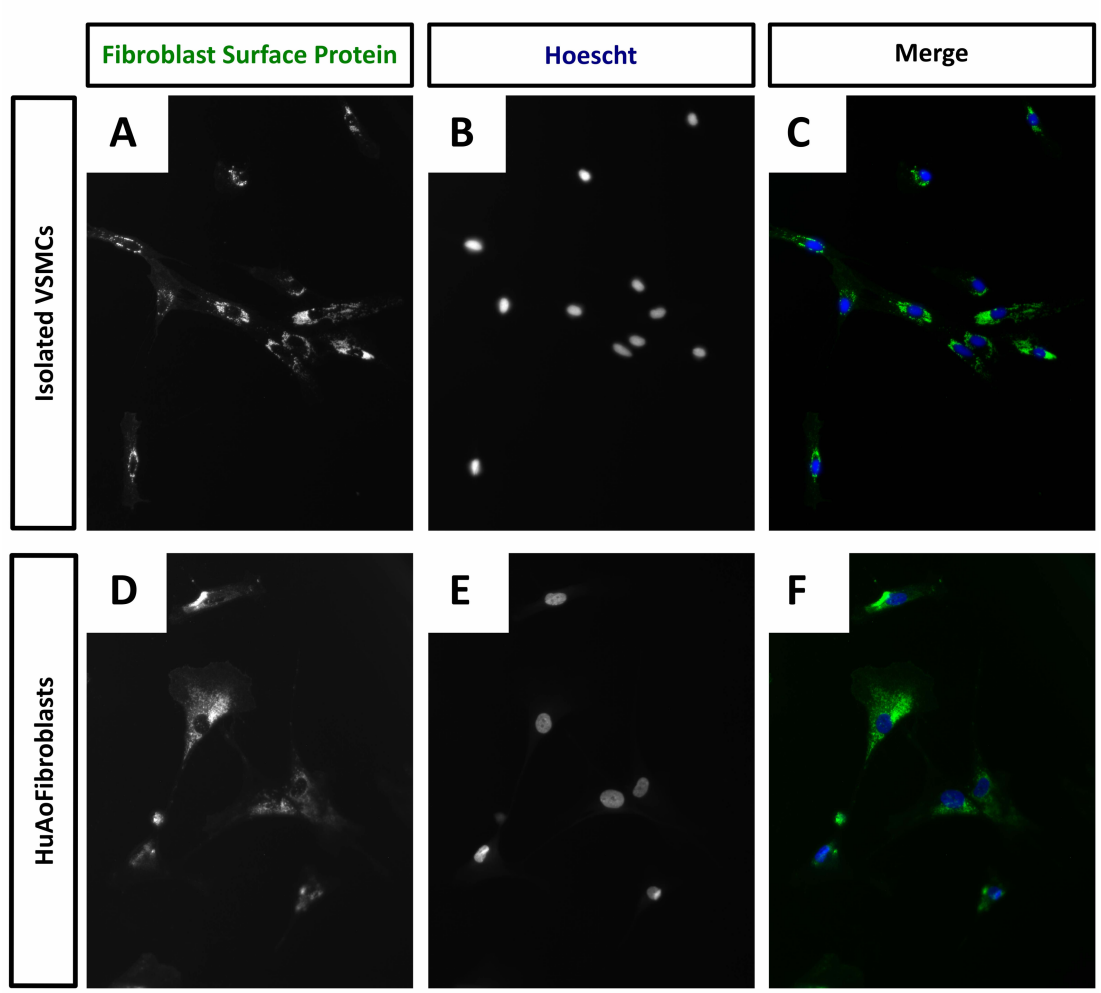

Figure 3.8: Immunocytochemistry for FSP1 in VSMCs and HuAoFibs

Isolated VSMCs and HuAoFib were stained for FSP1 to indicate the overlap in markers between the two cell types. VSMCs (**A, B, C**) and HuAoFib (**D, E, F)** both stained positive for FSP1, with strong nuclear exclusion in the staining. VSMC staining is representative of nine independent cell lines (control: $n = 3$, pre-dialysis: $n = 3$, dialysis: $n = 3$), while fibroblast staining is representative of a single commercial cell line. All cells were photographed at 200x magnification.

3.3: Gene Expression Profiling of VSMCs from Healthy Controls

3.3.1 Experimental Overview: Gene Expression Analysis

VSMCs have a propensity to lose some markers of SMC identity in culture; therefore, it was also important to ensure that these isolated VSMCs expressed transcripts which encode markers of smooth muscle identity following isolation.

Using qRT-PCR (as described in Section 2.5.6), I constructed an expression profile for isolated control VSMCs that I then examined with respect to HUVECs, HuAoFibs, and human aortic VSMCs (HuAoVSMCs). I examined mRNA expression of genes indicative of SMC lineage (*αSMA, CNN1, SM22α,*), markers of the endothelium (*CD31, TIE1, TIE2*), angiogenic growth factors and their receptors (*ANGPT1, ANGPT2, VEGFA)*, and regulators of osteogenesis (*AHSG, BMP2, MGP, RUNX2, OPN, SP7)*. The expression levels were normalised to the expression of the housekeeping gene *HPRT* for each individual cDNA sample. For each primer, RNase/DNase-free distilled water was run as a negative control whilst whole adult human kidney cDNA was used as a positive control.

3.3.2 RNA Quality and Concentration

RNA was extracted from four healthy control VSMC cell lines and subsequently examined for RNA quality and quantity prior to use in PCR and qRT-PCR (as described in Sections 2.5.2 and 2.5.3). The concentration of RNA obtained from control VSMCs was typically between 100–250 ng/μL. When run on an agarose gel, high-quality RNA samples exhibit two distinct bands corresponding to 28S ribosomal RNA and 18S ribosomal RNA. The 28S band should appear approximately twice the intensity of the 18S band (Figure 3.9A). The purity of the sample is also measured using spectrophotometry in which the absorbance ('A') of the sample is measured at wavelengths 260 nm and 280 nm. The absorbance ratio ($A_{260/280}$) should ideally be ~2.0 for pure RNA (Figure 3.9B). All of the samples isolated from control VSMCs yielded high-quality RNA.

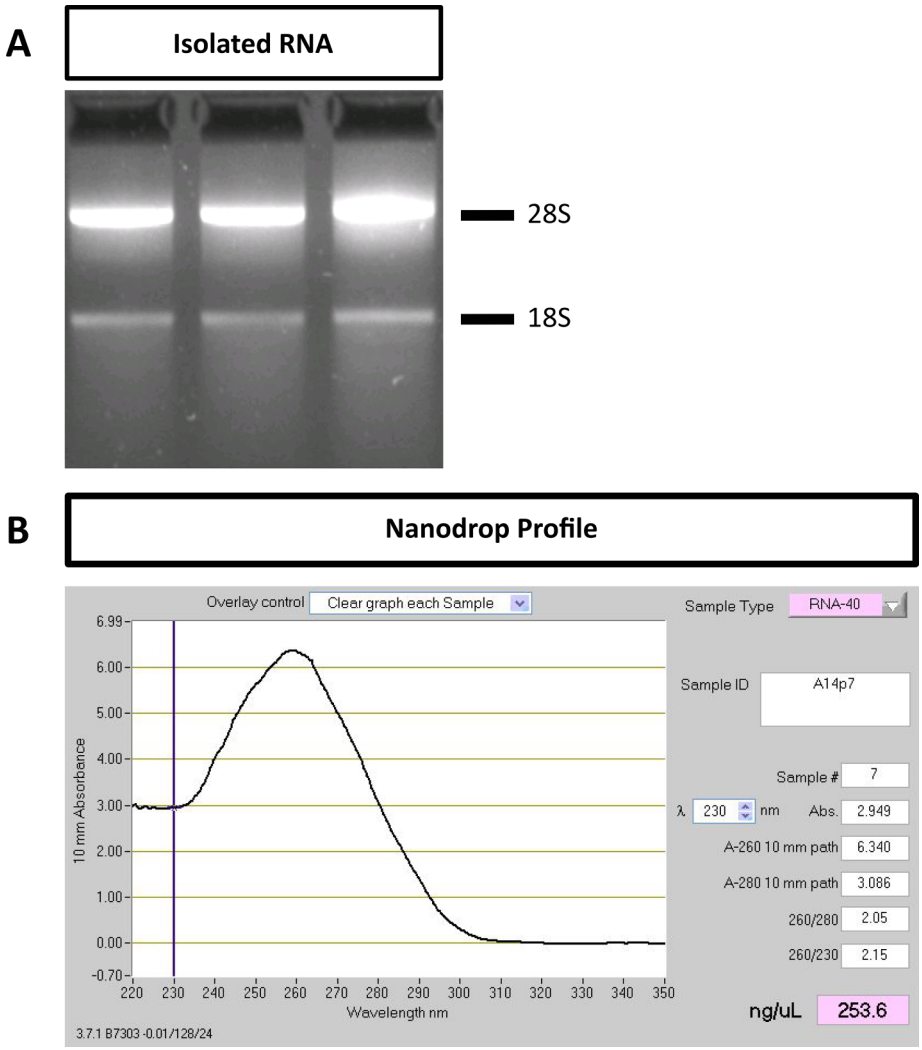

Figure 3.9: RNA isolated from primary VSMC cultures

RNA quality was assessed by two primary methods: agarose gel electrophoresis and spectrophotometry. **A:** Three RNA samples from healthy control VSMCs (2µL for each sample) were run on a 2% agarose gel. These three samples demonstrate high-quality RNA, as both the 28S and the 18S band are strong, distinct, and exemplify the 2:1 28S/18S ratio. **B:** A spectrophotometric reading of an RNA sample from a NanoDrop™ shows a smooth curve, with a single peak. $A_{260/280}$ is near 2.0, indicating that the RNA sample is free of protein contaminants while $A_{260/230}$ is above 2, which indicates that the sample is free of chemical contaminants such as the phenol utilised for extraction. This sample yielded high quality, high quantity RNA; this is representative of the typical RNA sample obtained from control VSMCs.

3.3.3 Optimising PCR Conditions

Each primer pair (as described in Section 2.5.5) was optimised on whole adult human kidney RNA prior to use in qRT-PCR. Gradient PCR results indicated the ideal annealing temperature necessary to produce a simple specific amplicon and reveal any non-specific amplification or excessive primer-dimer formation; examples of primer gradients for *TIE1* and *ANGPT1* are given in Figure 3.10. All primers that were subsequently used for this thesis produced single products; however, the strongest bands (suggesting increased product) were observed between 60–62ºC. Following this, primers were used in qRT-PCR. For each primer in an individual 96-well plate, two wells were allocated for the positive control (whole human kidney), and two wells were allocated for the negative control (RNase/DNase-free distilled water). Upon completion of the qRT-PCR cycle, the melt curves for these samples were examined to ensure that only a single peak was observed; representative melt curves for *TIE2*, *αSMA*, *RUNX2* and *HPRT* are given in Figure 3.11.

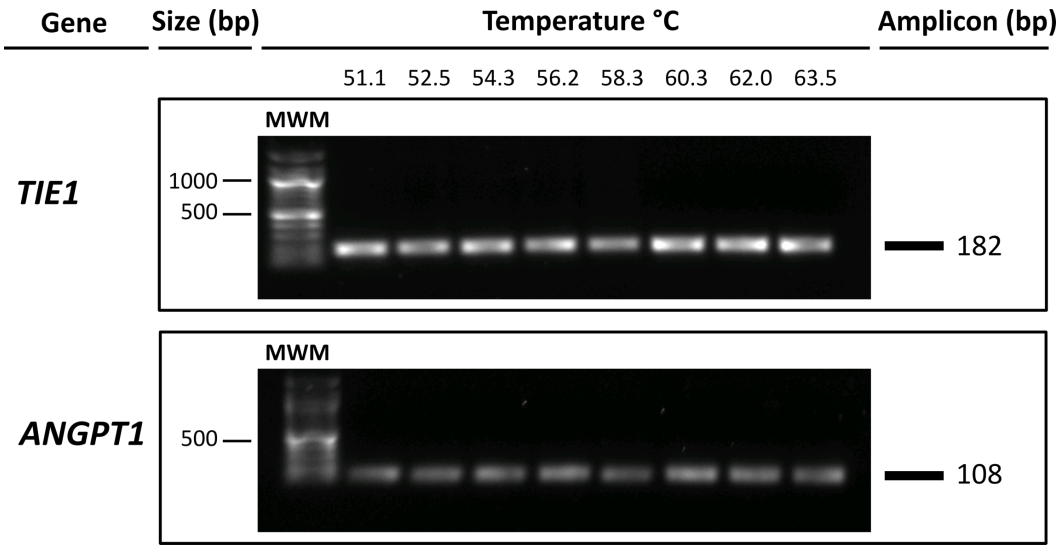

Figure 3.10: Representative gradient PCR results from *TIE1* and *ANGPT2*

The temperature gradient ran from 51.1°C to 63.5°C. The optimal annealing temperature was chosen based on the ability to produce a strong single product of correct length. In these examples, the optimal temperature was between 60.3°C and 62°C for *TIE1* and *ANGPT1*.

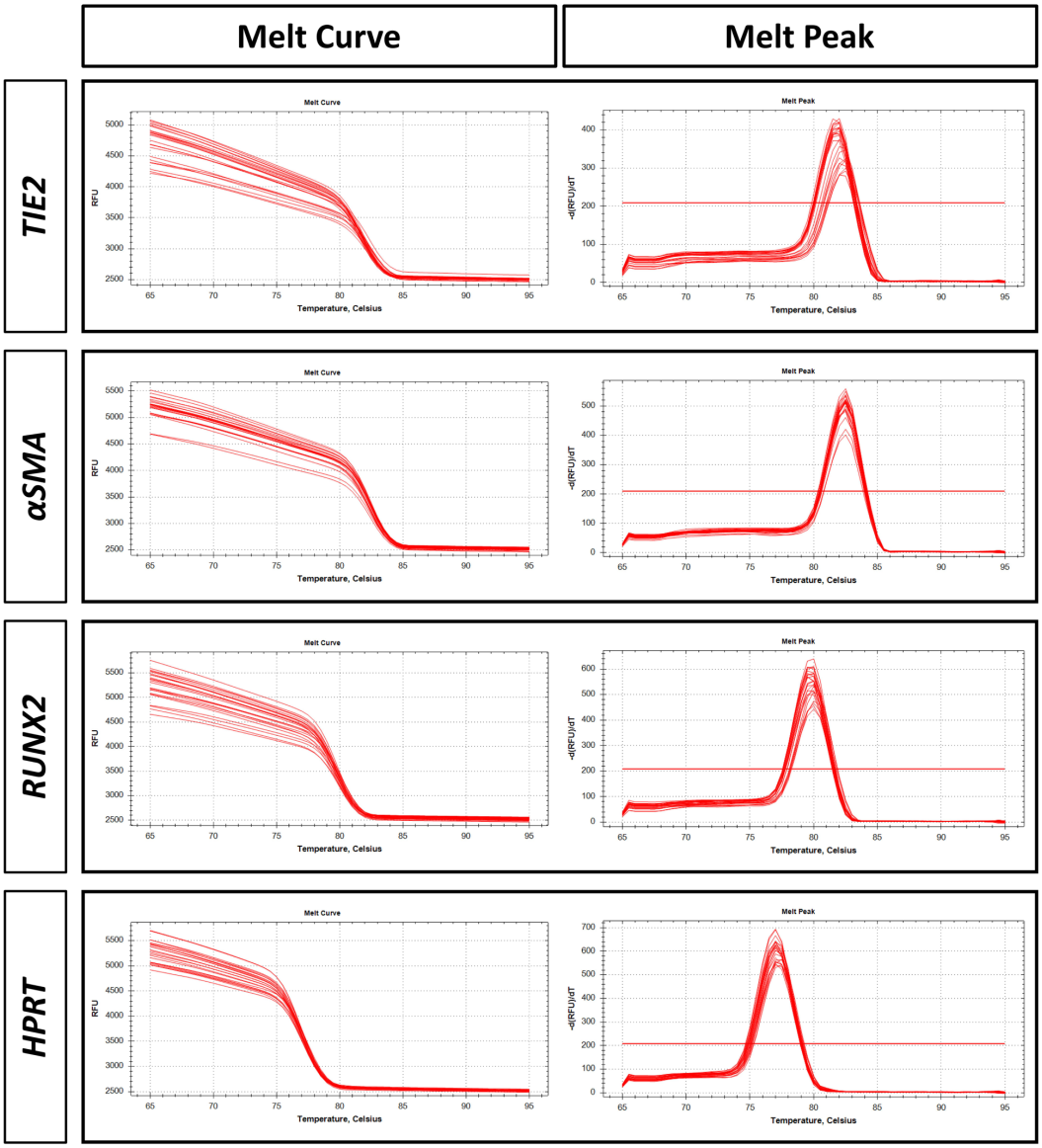

Figure 3.11: Representative qRT-PCR melting curves from four primers

The quality of the qRT-PCR was determined by the quality of the melt curve. A good quality melt curve as seen above for *TIE2*, *αSMA*, *RUNX2* and *HPRT* exhibited a single peak, corresponding to a single product.

3.3.4 Contractile Gene Expression

I then compared the expression of contractile genes (*αSMA, CNN1,* and *SM22α*) between paediatric control VSMCs, HuAoVSMCs, HuAoFibs, and HUVECs. To do this, I used the dCt method, which provided an expression level for each gene relative

to the housekeeping gene *HPRT*. A negative dCt indicated that a gene was more highly expressed relative to *HRPT*, whilst a positive Ct showed lower expression relative to *HPRT*. HuAoVSMCs expressed high levels of *αSMA* and transgelin (*SM22α*) mRNA relative to *HPRT*, with similar levels of calponin relative to *HPRT* (Figure 3.12A). HuAoFibs expressed higher levels of all three contractile proteins relative to *HPRT* (Figure 3.12B) as compared with HuAoVSMCs. Comparatively, HUVECs expressed lower mRNA levels for *CNN1*, *αSMA* and *SM22α* relative to *HPRT* (Figure 3.12C) as compared with both HuAoVSMCs and HuAoFibs. The expression in the VSMCs isolated from paediatric controls was similar to HuAoVSMCs and HuAoFibs with high levels of αSMA, transgelin and calponin mRNA relative to *HPRT* (Figure 3.12-D).

3.3.5 Angiogenic and Endothelial Gene Expression

Next, I examined markers of the endothelium (*CD31, TIE1, TIE2*) and vascular growth factors (*ANGPT1*, *ANGPT2* and *VEGFA*). As expected, HUVECs expressed high levels of *CD31* and *TIE1* relative to *HPRT*, with *TIE2* expressed at similar levels to *HPRT* (Figure 3.13C). HUVECs expressed similar levels of *ANGPT2* relative to *HPRT*, indicative of Angpt2 production in the Weibel-Palade bodies of the endothelial cells. These HUVECs also express low levels of both *ANGPT1* and *VEGFA* (Figure 3.13C). HuAoVSMCs (Figure 3.13A) and HuAoFibs (Figure 3.13B) had a similar expression profile with low expression of *CD31*, *TIE1* and *TIE2* compared with HUVECs. These cells both expressed higher levels of *VEGFA* and ANGPT1 relative to *HPRT*, compared with HUVECs, and lower levels of *ANGPT2* (Figure 3.13A and B). In VSMCs isolated from paediatric controls (Figure 3.13D), the majority of the expression profile resembled HuAoVSMCs and HuAoFibs with low *TIE1*, *ANGPT2*, *CD31* and high *VEGFA* relative to *HPRT*. Interestingly, the levels of *TIE2* relative to *HPRT* were higher than either HuAoVSMCs or HuAoFibs, whilst the expression of *ANGPT1* was low.

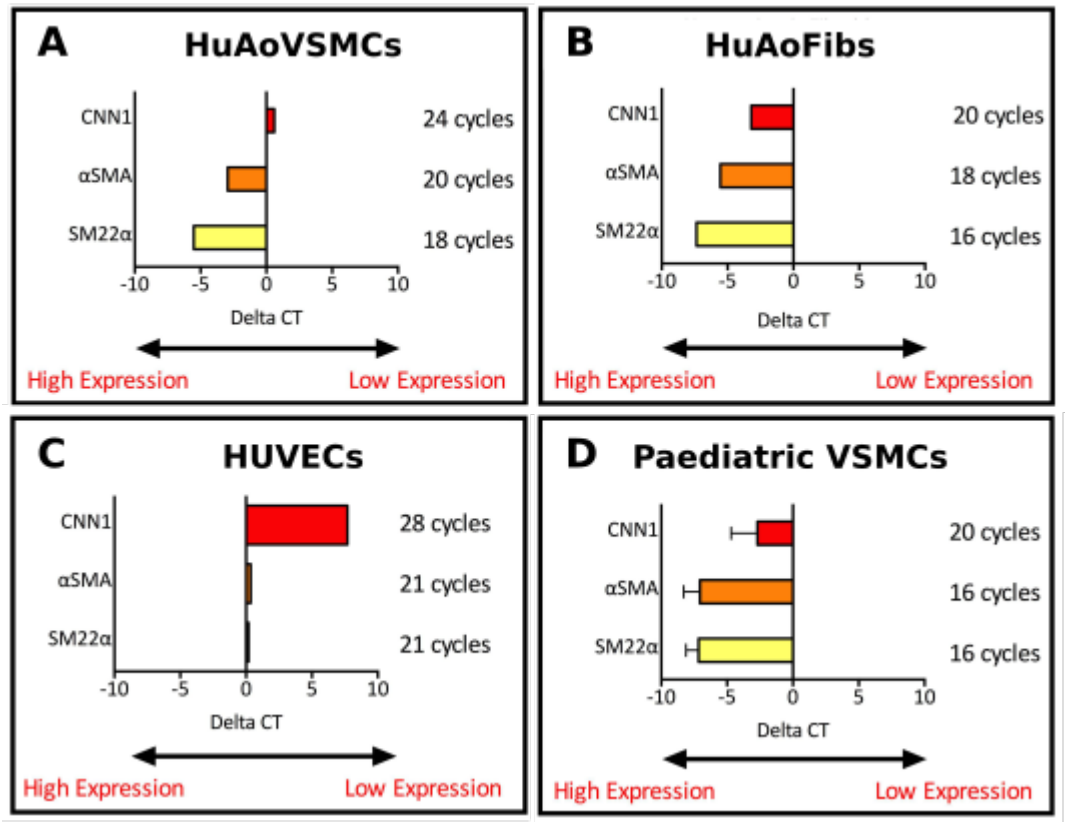

Figure 3.12: Expression of contractile genes

ΔCt values have been plotted to show mRNA expression levels of genes normalised to *HPRT*, where no difference to *HPRT* is equal to 0. Low values (negative dCt values) indicate high levels of gene expression relative to *HPRT* whilst high values (positive dCt values) indicate low levels of gene expression relative to *HPRT*. HuAoVSMCs exhibit decreased *CNN1* expression relative to *HPRT* when compared to other VSMCs; however, *αSMA* and *SM22α* expression levels remain increased relative to *HPRT* (**A**). HuAoFibs (**B**) and control VSMCs (**D**) express increased levels of contractile genes *αSMA*, *CNN1*, and *SM22α* relative to *HPRT*. HUVECs exhibit decreased levels of *CNN1* relative to *HPRT*, whilst *αSMA* and *SM22α* are expressed at similar levels to *HPRT* (**C**). Mean expression levels were plotted for control ($n = 3$) VSMCs, and error bars indicate standard error of the mean. HUVECs, HuAoVSMCs, and HuAoFibs were all obtained commercially and therefore only one independent line was tested. Each cDNA sample was run in duplicate during qRT-PCR, and the mean value was used in dCt calculations.

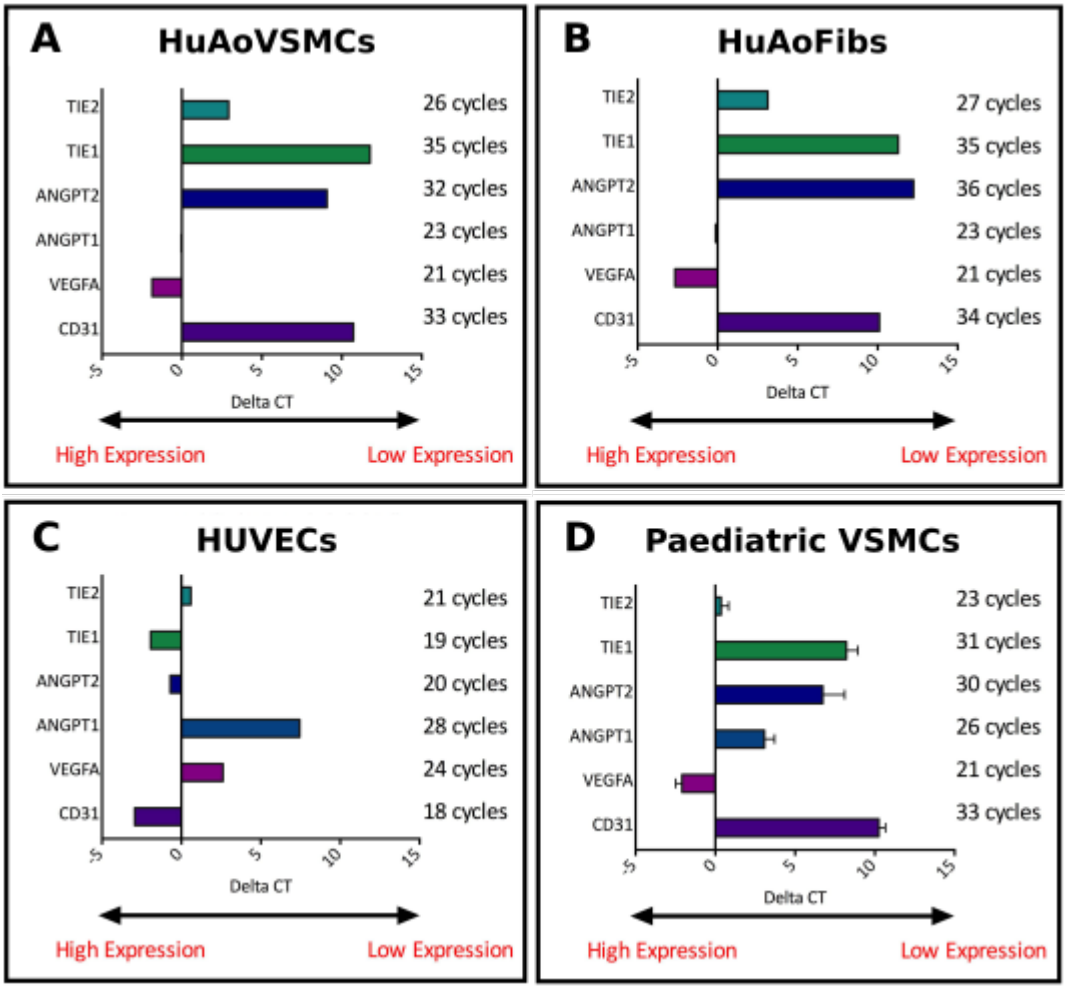

Figure 3.13: Expression of endothelial and angiogenic genes

ΔCt values have been plotted to show mRNA expression levels of genes normalised to *HPRT*, where no difference to *HPRT* is equal to 0. Low values (negative dCt values) indicate high levels of gene expression, and low values (positive dCt values) indicate low levels of gene expression. HuAoVSMCs (**A**) express decreased levels of *CD31*, *TIE1*, and *ANGPT2* with respect to *HPRT,* as do the HuAoFibs (**B**). HUVECs (**C**) express increased levels of *CD31* relative to *HPRT*, while expression of *TIE2* is similar to *HPRT*. HUVECs are the only cells examined to express increased *ANGPT1* and *TIE1* with respect to *HPRT*; all VSMC populations express decreased *TIE1* with respect to *HPRT* (**A**, **D**). Mean expression levels were plotted for control ($n = 3$) VSMCs, and error bars indicate standard error. HuAoVSMCs, HuAoFibs, and HUVECs were all obtained commercially and therefore only one independent line was tested. Each cDNA sample was run in duplicate during qRT-PCR, and the mean value was used in dCt calculations.

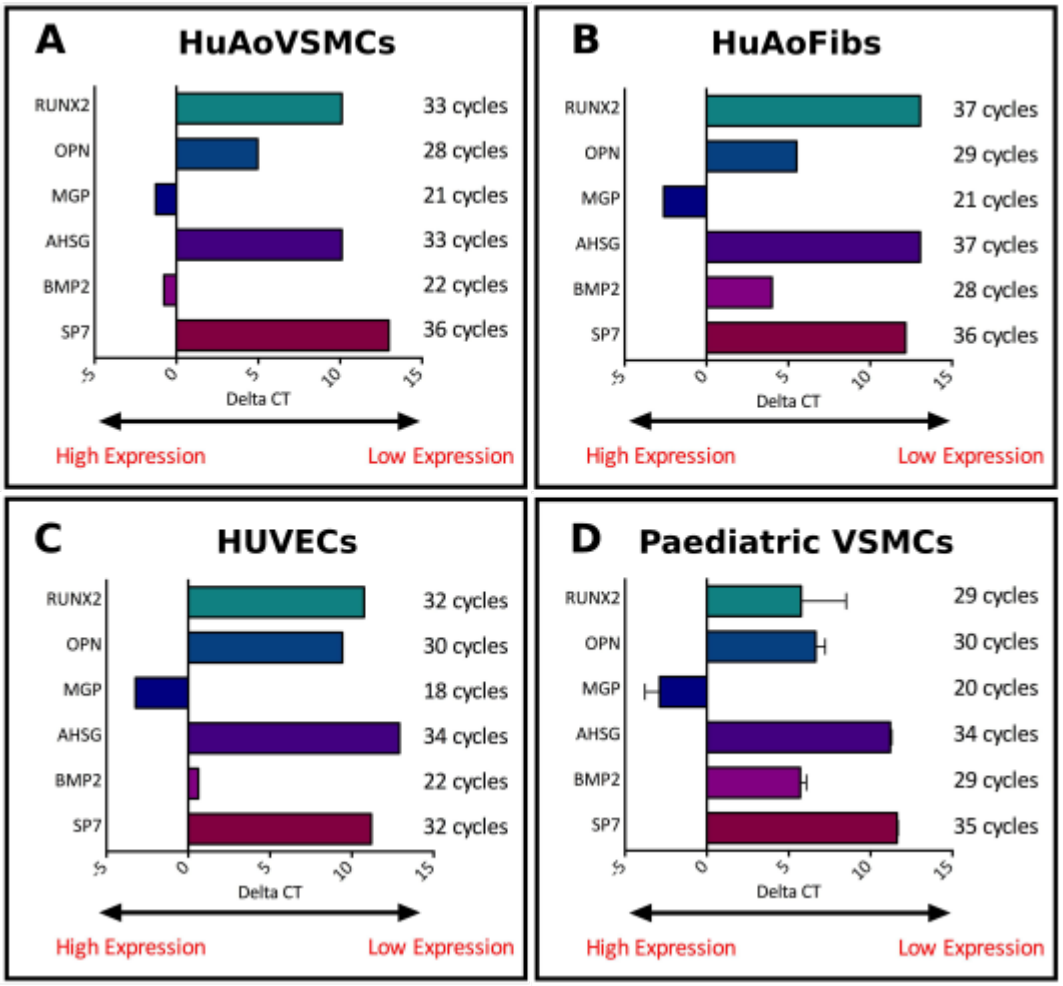

Figure 3.14: Expression of osteogenic genes

ΔCt values have been plotted to show mRNA expression levels of genes normalised to *HPRT*, where no difference to *HPRT* is equal to 0. Low values (negative dCt values) indicate high levels of gene expression, and low values (positive dCt values) indicate low levels of gene expression. All cell types express increased mRNA levels of anti-osteogenic *MGP* with respect to *HPRT* (**A**, **B**, **C**, **and D**). Apart from the HuAoVSMCs (**A**), which expressed increased mRNA levels of pro-osteogenic factor *BMP2* with respect to *HPRT*, all cell types express very low levels of pro-osteogenic genes. Mean expression levels were plotted for control ($n = 3$) VSMCs, and error bars indicate standard error. HUVECs, HuAoVSMCs, and HuAoFibs were all obtained commercially and therefore only one independent line was tested. Each cDNA sample was run in duplicate during qRT-PCR, and mean value was used in dCt calculations.

3.3.6 Osteogenic Gene Expression

HuAoVSMCs expressed low levels of the pro-osteogenic genes *OPN, RUNX2, SP7* relative to *HPRT* (Figure 3.14A). In contrast, expression of another pro-osteogenic gene *BMP2* was higher relative to *HPRT*. In these HuAoVSMCs, *MGP* mRNA expression was high relative to *HPRT* suggesting that these cells actively maintain an anti-osteogenic phenotype. Additionally, HuAoVSMCs expression of the anti-osteogenic gene *AHSG* (fetuin-A) was very low relative to *HPRT* (Figure 3.14A). Given that fetuin-A is produced in the liver and is actively taken up by VSMCs as an osteoprotective mechanism, we expect to see low levels of expression in these cells (Reynolds *et al* 2005).

The majority of the profile of HuAoFibs was similar to HuAoVSMCs, with equivalent levels of *OPN, MGP* and *SP7* relative to *HPRT* (Figure 3.14B). The levels of *BMP2*, *RUNX2* and *AHSG* relative to *HPRT* in HuAoFibs were lower than in HuAoVSMCs. The expression levels of *RUNX2*, *OPN*, *AHSG* and *BMP2* relative to *HPRT* in HUVECs were similar to HuAoVSMCs (Figure 3.14C), whilst *MGP* and *SP7* were higher. Finally, paediatric control VSMCs contained similar levels of *OPN*, *MGP*, and *SP7* relative to *HPRT* compared with both HuAoVSMCs and HuAoFibs (Figure 3.14D). The level of *RUNX2* relative to *HPRT* in paediatric control vessels was higher than both HuAoVSMCs and HuAoFibs, whilst the expression level of *AHSG* was similar to the expression level observed in the HuAoVSMCs. Interestingly, the paediatric control vessels also exhibited lower levels of *BMP2* relative to *HPRT* when compared with the HuAoVSMCs.

3.4: Effects of Angpt2 on Calcium Deposition in VSMCs

3.4.1 Experimental Overview: Angpt2 Calcification in VSMCs

The intact arterial ring experiments indicated that exogenous Angpt2 promoted calcium deposition in vessels obtained from dialysis patients in the presence of calcium and phosphate when compared with vessels cultured in calcium and phosphate alone. The aim in using monolayer primary VSMC cultures was to determine whether this same augmentation of calcification occurred when the VSMCs were isolated from

the tunica media. To investigate this, VSMCs isolated from control and dialysis patients were cultured for 5 days under the same conditions that the intact arterial rings were cultured in: (i) control (media only), (ii) pro-calcaemic medium (2.7 mM Ca/2.0 mM P), and (iii) pro-calcaemic medium with 25 ng/mL Angpt2. Cells from pre-dialysis vessels were not used, as they did not respond to Angpt2 in the vessel ring experiments. Similarly to the vessels, calcium content was measured using the *o*-cresolphthalein colorimetric assay and normalised to the protein content of each well (as described in Section 2.6.2). For both control and dialysis individuals, three independent patient VSMC lines were examined and each patient cell line was run in triplicate for each condition.

3.4.2 Angpt2 Increases Calcium Deposition in Dialysis VSMCs

When cultured in medium alone (M199 containing 1.8 mM Ca and 1.0 mM P), VSMCs isolated for paediatric controls exhibit very low levels of calcification (Figure 3.15). Comparatively, VSMCs isolated from paediatric CKD patients exhibit increased calcium deposition when compared with the control VSMCs, even when cultured under control conditions. However, under baseline conditions (M199 only), there is no significant difference in calcium content between control and dialysis cell populations. When cultured in the presence of high calcium (2.7 mM) and high phosphate (2.0 mM), both control and dialysis VSMCs calcify significantly when compared to cells cultured in medium alone ($p = 0.043$ and $p = 0.0002$ for control and dialysis cells respectively; Figure 3.15). The dialysis cells calcify more readily than the control cells when cultured in the pro-calcaemic medium; the difference between the two populations is near statistical significance ($p = 0.065$). When cultured in pro-calcaemic medium with addition of 25 ng/mL Angpt2, the control VSMCs calcify to the same degree as in the pro-calcaemic environment alone ($p = 0.0852$). Comparatively, when VSMCs from dialysis patients are cultured in pro-calcaemic medium containing exogenous Angpt2, the VSMCs accumulate almost twice the calcium than when cultured in the pro-calcaemic medium alone ($p = 0.005$). The differential response between the control and dialysis VSMCs when cultured in pro-calcaemic medium ($p = 0.065$) and pro-calcaemic medium with exogenous Angpt2 ($p = 0.001$) suggests that there is an intrinsic element of the dialysis cells that heightens their propensity to calcify in response to Angpt2.

Dialysis VSMCs cultured in pro-calcaemic medium, with and without Angpt2, clearly exhibit the formation of calcium-containing nodules (Figure 3.15 B).

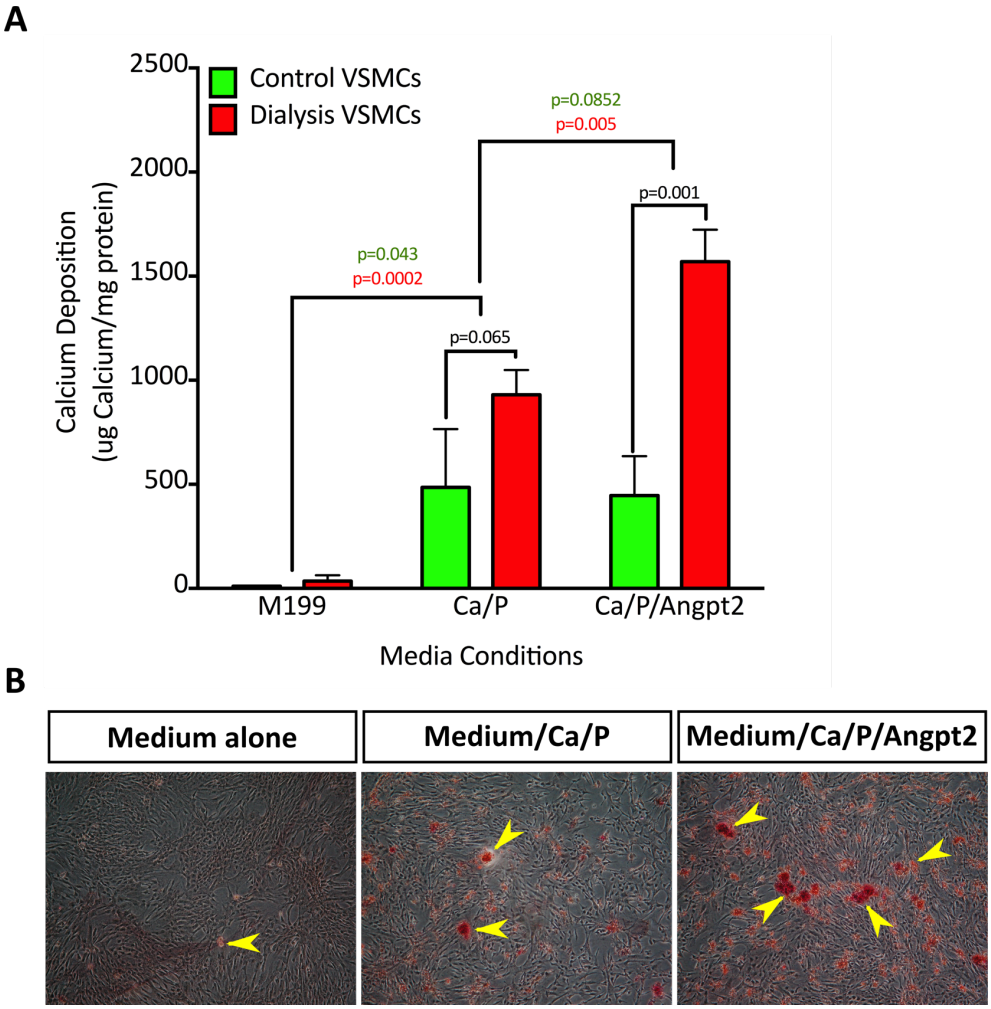

Figure 3.15: Calcium deposition in monolayer VSMC cultures

Calcium deposition in VSMCs after 5 days in culture was measured using the *o*-cresolphthalein colorimetric assay and normalised to protein content (**A**). Three independent cell lines for each group (control: $n = 3$, dialysis: $n = 3$) were used, and each of these was run in triplicate to ensure reproducibility within the cell line. Both control and dialysis VSMC populations exhibited a significant increase in calcium deposition when cultured under pro-calcaemic conditions; however, only dialysis cells exhibited a significant further increase when stimulated with 25 ng/mL Angpt2 under pro-calcaemic conditions. Dialysis VSMCs were stained with Alizarin red to highlight calcium-containing nodules, indicated by the yellow arrows (**B**). Images are representative of three dialysis VSMC lines, and cells were visualised at 40x magnification.

3.5: Conclusion

Using the intact arterial ring model, I have shown that there is a trend towards an increase in baseline levels of calcium deposition in arterial rings in patients with CKD, both pre-dialysis and on dialysis. This corroborates with previous research conducted by Shroff *et al* (2010) but suggests that an increased number of samples would be beneficial in this study as, although there was a trend for calcium deposition to increase in patients with CKD, there was no statistical significance between the groups.

Preliminary experiments showed no significant differences in calcium deposition between pre-dialysis vessels and dialysis vessels cultured with and without the addition of exogenous Angpt2 after 7 days in pro-calcaemic media. In contrast, after 14 days in culture, the arterial rings from control patients exhibited no significant increases in calcium deposition when exposed to a pro-calcaemic medium with or without Angpt2 when compared with control arterial rings cultured in media alone. Pre-dialysis arterial rings exhibited a significant increase in calcium deposition when cultured in pro-calcaemic conditions but did not exhibit a further increase in calcium deposition when cultured in pro-calcaemic conditions with the addition of Angpt2. However, arterial rings obtained from dialysis patients calcified significantly when cultured in the pro-calcaemic media and this calcification was further augmented to a significant degree when cultured with the addition of Angpt2.

These data suggest that Angpt2 may potentiate calcification in a calcium- and phosphate-rich environment. However, as this effect is only observed in the dialysis vessels and not observed in either the control or pre-dialysis vessels, this augmentation effect may potentially be mediated by intrinsic changes that occur in the vessels themselves because of dialysis.

VSMCs were readily isolated from the tunica media of paediatric medium-sized muscular arteries. This allowed this project to utilise a rare resource for further *in vitro* work. Unlike commercially-available VSMCs, these isolated cells have been exposed to the uremic environment and the environmental stressors induced by dialysis. Additionally, the healthy control VSMCs are isolated from age-matched (paediatric) controls, making them a more appropriate comparison than healthy adult VSMCs. The

staining patterns of αSMA and FSP1 in the isolated VSMCs were indicative of this SMC lineage. These isolated paediatric control VSMCs express high levels of mRNA for SMC markers *CNN1,* α*SMA,* and *SM22*α relative to *HPRT*. However, these VSMCs also express *TIE2*, a transmembrane receptor that is typically associated with endothelial expression. Despite this, they do not express *CD31*, another marker of the endothelium, and otherwise exhibit SMC morphology.

In a pro-calcaemic environment, both control and dialysis VSMCs calcify. However, the dialysis VSMCs exhibit twice the calcium deposition as the control VSMCs and this calcification is further augmented with the addition of Angpt2; Angpt2 does not further increase calcium deposition in control VSMCs. This response is similar to the response observed in the paediatric vessel rings and suggests that Angpt2 may be a driver of calcification in children on dialysis.

Chapter 4: Results — Pathological and Molecular Mechanisms Following Angpt2 Stimulation

4.1: Gene Expression Between Disease States

4.1.1 Experimental Overview: Gene Expression in VSMCs

Vessels from healthy paediatric patients do not calcify in culture, and it has been suggested that these vessels possess the intrinsic ability to protect against vascular calcification (Shroff *et al* 2010). One potential suggestion is that VSMCs from healthy control patients express higher baseline levels of contractile genes (*αSMA, SM22α*) whilst VSMCs from dialysis patients express higher levels of pro-osteogenic genes (*RUNX2, BMP2*). Similarly, there is potential for a discrepancy between the expression levels of osteogenic inhibitors such as *MGP*. To test this hypothesis, I compared the expression of contractile, angiogenic, and osteogenic genes in VSMCs as categorised by disease state from control, pre-dialysis, and dialysis individuals.

cDNA was isolated from control (*n = 4*), pre-dialysis (*n = 3*), and dialysis VSMCs (*n = 4*). Primers for angiogenic growth factors (*ANGPT1, ANGPT2*) and their receptors (*TIE1, TIE2*), smooth muscle marker *SM22α* and endothelial cell marker *CD31*, as well as osteogenic genes (*BMP2, MGP, SP7, OPN*) were used in qRT-PCR. Each sample was run in duplicate and normalised to the expression level of *HPRT*. Mean dCt value was taken from the control VSMCs, and all other dCt values were subsequently compared to this value. For each primer, RNase/DNase-free distilled water was run as a negative control while whole human kidney was run as a positive control.

4.1.2 Baseline Gene Expression in Paediatric VSMCs

VSMCs isolated from healthy paediatric vessels, pre-dialysis CKD vessels, and dialysis CKD vessels exhibited no significant differences in gene expression levels in the tested angiogenic genes (*TIE1, TIE2, ANGPT1, ANGPT2;* Figure 4.1 A, B, C, D).

No significant differences in gene expression were detected between VSMCs populations for either receptor tyrosine kinase, *TIE1* (Figure 4.1A) or *TIE2* (Figure 4.1B). Additionally, there were no significant differences in expression levels for either angiopoietin, *ANGPT1* (Figure 4.1C) or *ANGPT2* (Figure 4.1D), between VSMC populations. There was a trend towards a mean increase in contractile SMC marker *SM22α* (Figure 4.1E) as disease severity increased; however, the difference was not statistically significant. Similarly, the endothelial marker *CD31* remained present across all isolated VSMCs despite the disease state (Figure 4.1F).

Next, I explored the hypothesis that the VSMCs from patients on dialysis might express differential levels of the osteogenic genes *BMP2*, *MGP, OPN*, or *SP7*. Although no statistically significant differences in osteogenic gene expression (of the measured genes) were detected between these VSMC populations, the mean fold-change of pro-osteogenic gene *BMP2* (Figure 4.2A) was marginally increased in VSMCs from vessels obtained from patients on dialysis. Pro-osteogenic genes *OPN* (Figure 4.2B) and *SP7* (Figure 4.2C) are minimally higher in VSMCs from control vessels, whilst the pre-dialysis VSMCs exhibit an increase in *MGP* (Figure 4.2D) when compared with both control and dialysis VSMCs. There was wide variation in expression levels between individual patients within a given category, suggesting that each patient has an individual baseline level of expression from which any deviation may qualify as an increase or decrease. Due to the wide variation in expression levels in individual patients within a given category, the standard error for each sample is very large.

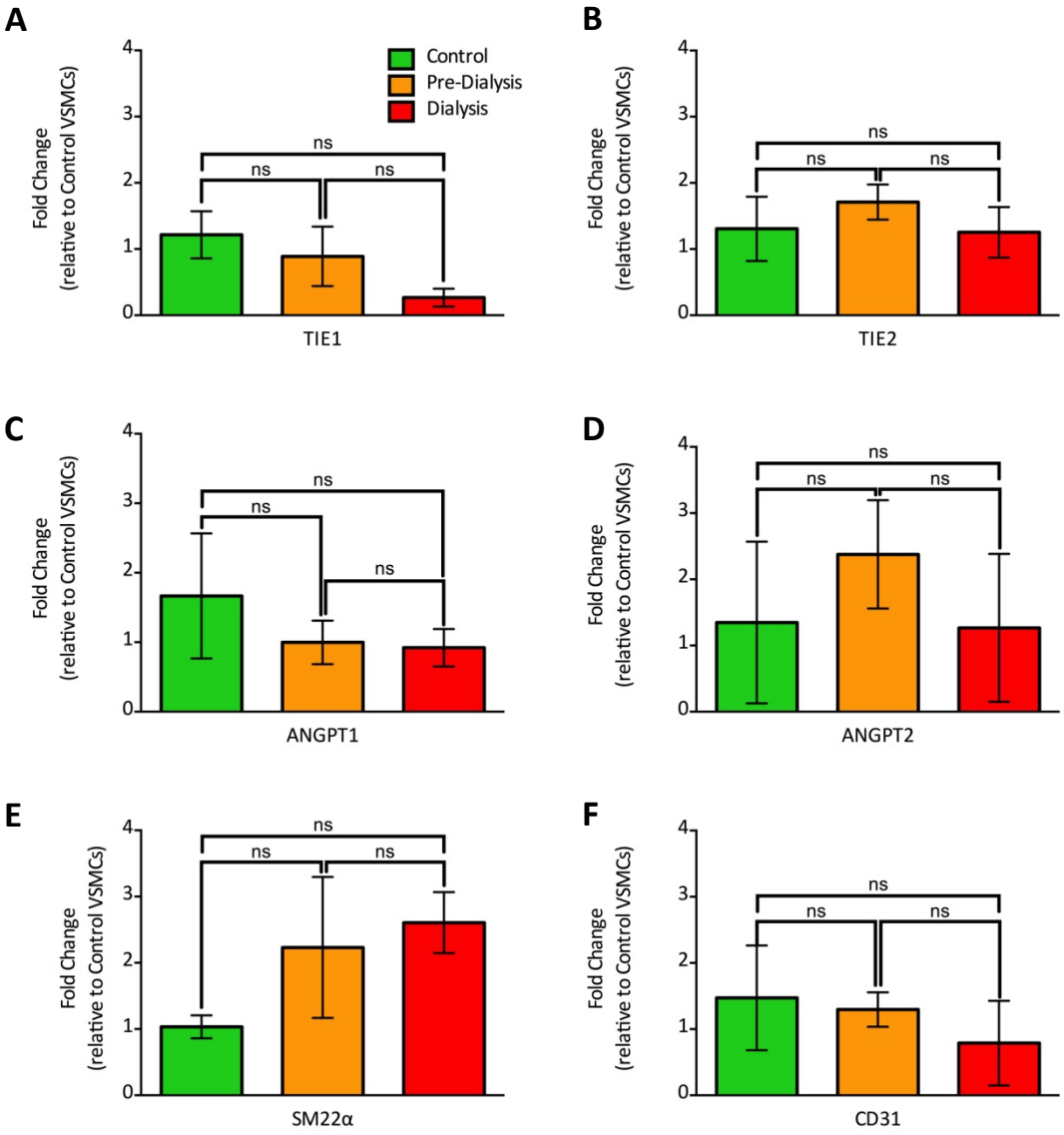

Figure 4.1: Expression of angiogenic genes in VSMCs across disease states

Expression levels of angiogenic-related genes (*TIE1, TIE2*, *ANGPT1, ANGPT2*) and markers *SM22α* and *CD31* were quantified in cultured (baseline, untreated) paediatric VSMCs isolated from control ($n = 4$), pre-dialysis ($n = 3$) and dialysis ($n = 4$) vessels. Note that the endothelial expression level is low (35–36 cycles compared to 20–21 cycles of *HPRT*) and has been included to determine if the cells acquired any endothelial-like characteristics (given that they express *TIE2*). Bars represent the mean fold-change in gene expression, relative to the control VSMCs. Error bars indicate standard error; note that there is a large variation between individual patients, thus increasing the size of the error bars.

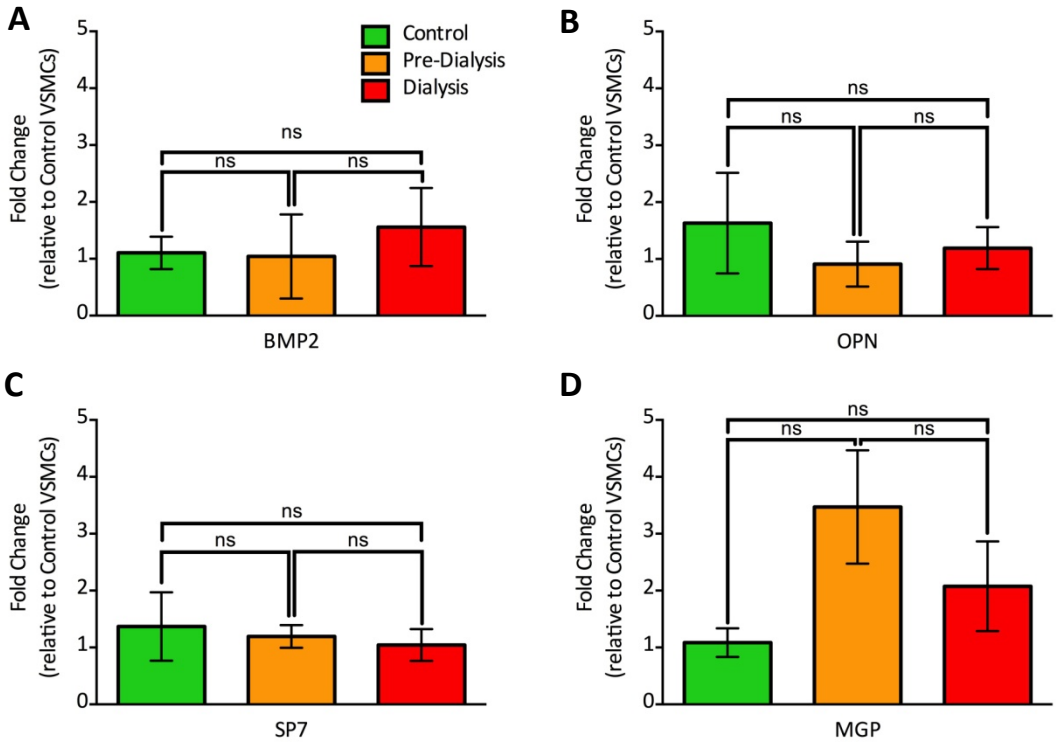

Figure 4.2: Expression of osteogenic genes

Expression levels of osteogenic-related genes (*BMP2, OPN, SP7*, and *MGP)* were quantified in cultured (baseline, untreated) paediatric VSMCs isolated from control (*n* = 4), pre-dialysis (*n* = 3) and dialysis (*n* = 4) vessels. Bars represent the mean fold-change in expression relative to control VSMCs. Error bars indicate standard error. Note that there is a large variation between individual patients, thus increasing the size of the error bars.

4.2: Effects of Angpt2 on Vessel Histology and Apoptosis

4.2.1 Experimental Overview: Histology of Intact Arterial Rings

The previous experiments (Chapter 3) have indicated that exogenous Angpt2 increases the calcium deposition in both VSMCs and intact vessels from patients on dialysis and that, given the presence of the Tie2 receptor on the VSMCs in both culture and *in vivo*, Angpt2 may potentially act through the Tie2 receptor. However, the pathological mechanism through which this occurs is not known. To explore this, when vessel rings were set up in culture for calcium quantification, additional rings were also cultured for embedding in paraffin and O.C.T (Sections 2.3.3 and 2.3.4). Sections (5µm) were

cut from each vessel ring, and H&E staining was performed to examine vessel morphology (as described in Section 2.3.8).

4.2.2 Dialysis Vessels Exhibit Disrupted VSMC Arrangement

In a normal vessel, there are three defined structures: the tunica intima, the tunica media, and the adventitia. After the vessel is collected and dissected from surrounding tissue, the vessel is scraped with a scalpel in an attempt to remove the adventitia. There is inevitably residual tissue, which can be observed in all of the histological images. However, stripping the vessel of the adventitia also places stress on the thin endothelial lining of the vessel causing the endothelium to be damaged and often removed from the vessel prior to explant culture. As such, very few endothelial cells are observed in the histological images.

In a healthy vessel ring, the VSMCs of the tunica media exhibit elongated nuclei that run parallel to the external elastic lamina; these maintain a well-organised linear arrangement (Figure 4.3A, Moe *et al* 2002). I found that healthy control paediatric vessels maintain this morphology, even when challenged with a high calcium and phosphate environment with, and without, Angpt2 (Figure 4.3B and C, respectively). Pre-dialysis vessels again exhibit this well-aligned arrangement of VSMCs (Figure 4.3D), although they begin to exhibit a slightly haphazard arrangement of nuclei following treatment with calcium and phosphate with and without Angpt2 (Figure 4.3E and F, respectively). Dialysis vessels exhibit increased disarrangement of nuclei (Figure 4.3G); this disarrangement is further increased following culture in high calcium and phosphate media (Figure 4.3H). Along with the misaligned nuclei, dialysis vessels also exhibit an increase in regions devoid of cells (as depicted by the black arrows, Figure 4.3G, H, and I) and rounded condensed nuclei that are believed to be apoptotic (as depicted by the red arrows, Figure 4.3).

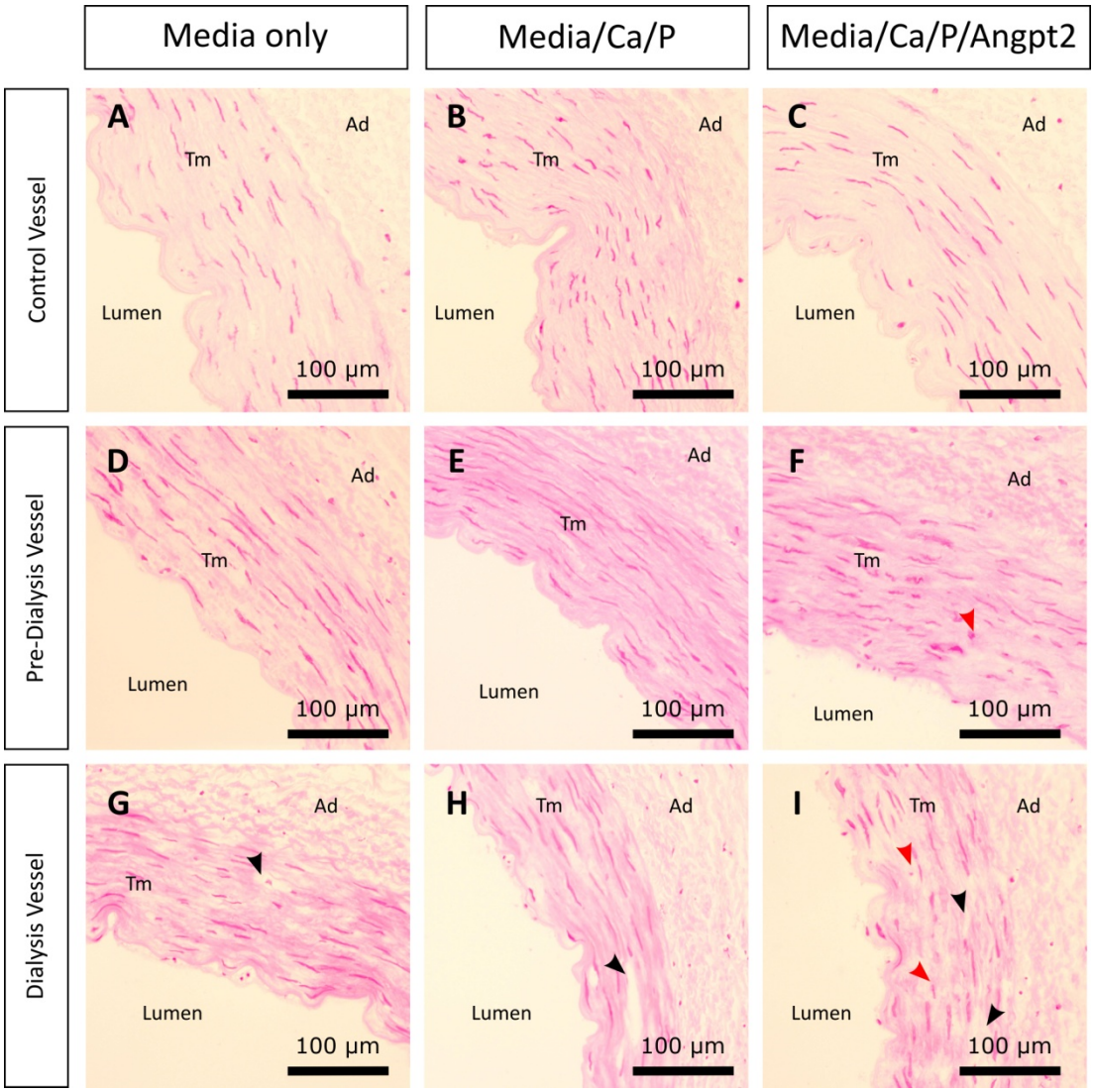

Figure 4.3: H&E staining of intact vessel rings

Vessel rings from control patients exhibit even medial staining and aligned elongated nuclei, even following treatment with pro-calcaemic medium and Angpt2 (**A, B, C**). Vessel rings obtained from pre-dialysis CKD patients still exhibit elongated nuclei when cultured in control medium (**D**) and pro-calcaemic medium (**E**). However, with the addition of Angpt2 (**F**), there are an increased number of condensed nuclei (as indicated by the red arrow). The alignment of nuclei within the tunica media is also less organised than when cultured in medium alone. Rings from dialysis vessels (**G, H, I**) exhibit disorganised nuclei alignment when cultured in medium alone (**G**), and have regions of cell loss (as indicated by black arrowheads). When cultured in pro-calcaemic medium (**H**), vessels exhibit large areas of cell loss; with the addition of Angpt2 in the pro-calcaemic medium, there are large areas of cell loss along with an increase in condensed nuclei (**I**). Tm = tunica media, Ad = adventitia.

Initially, the total nuclei were counted per vessel (represented as the number of cells per 0.25 mm^3, Figure 4.4A) with 6–8 images counted per arterial ring. Despite the phenotypic differences between the arterial rings from patients at different stages of disease (as visualised in Figure 4.3), no significant differences in total nuclei number were observed between disease states or culture conditions although there was a high degree of variation in cell numbers between individual vessels. Although not significant, each individual vessel exhibited a downward trend in the total number of nuclei with the addition of calcium and phosphate, and the number of nuclei further decreased with the addition of Angpt2 (control: 185.51±39.00, 180.66±33.00, 163.44±27.64; pre-dialysis: 197.26±32.77, 194.45±32.08, 181.47±27.54, dialysis: 212.65±34.86, 180.38±30.30, 172.04±28.19; where *x, y, z* are the total number of counted nuclei cultured in control medium, medium with calcium and phosphate, and medium with calcium, phosphate and Angpt2 respectively).

To reconcile the difference between the phenotypic observations and the quantified nuclei, I then classified each nucleus, based on its morphology, into one of two groups: elongated, or condensed (Figure 4.4B, C). The elongated nuclei followed the same downward trend observed when quantifying the total number of nuclei in which the addition of calcium and phosphate reduced the number of elongated nuclei in the vessel ring (Figure 4.4B). Again, this trend was further augmented with the addition of Angpt2 to the arterial rings (control: 171.24±37.40, 164.44±31.15, 141.33±27.96; pre-dialysis: 175.39±32.90, 166.11±29.65, 147.29±24.06; dialysis: 188.55±35.38, 145.80±31.46, 124.55±23.92; where *x, y, z* are the total number of counted nuclei cultured in control medium, medium with calcium and phosphate, and medium with calcium, phosphate and Angpt2 respectively). However, despite this trend, there were no statistically significant differences between groups.

Most of the nuclei appeared elongated and phenotypically normal; however, small numbers of nuclei appeared condensed and rounded, potentially indicative of cells undergoing apoptosis. Quantification of these rounded and condensed nuclei indicated that they increased in response to two variables: 1) disease severity and 2) supplementation with 25 ng/mL Angpt2 (Figure 4.4C).

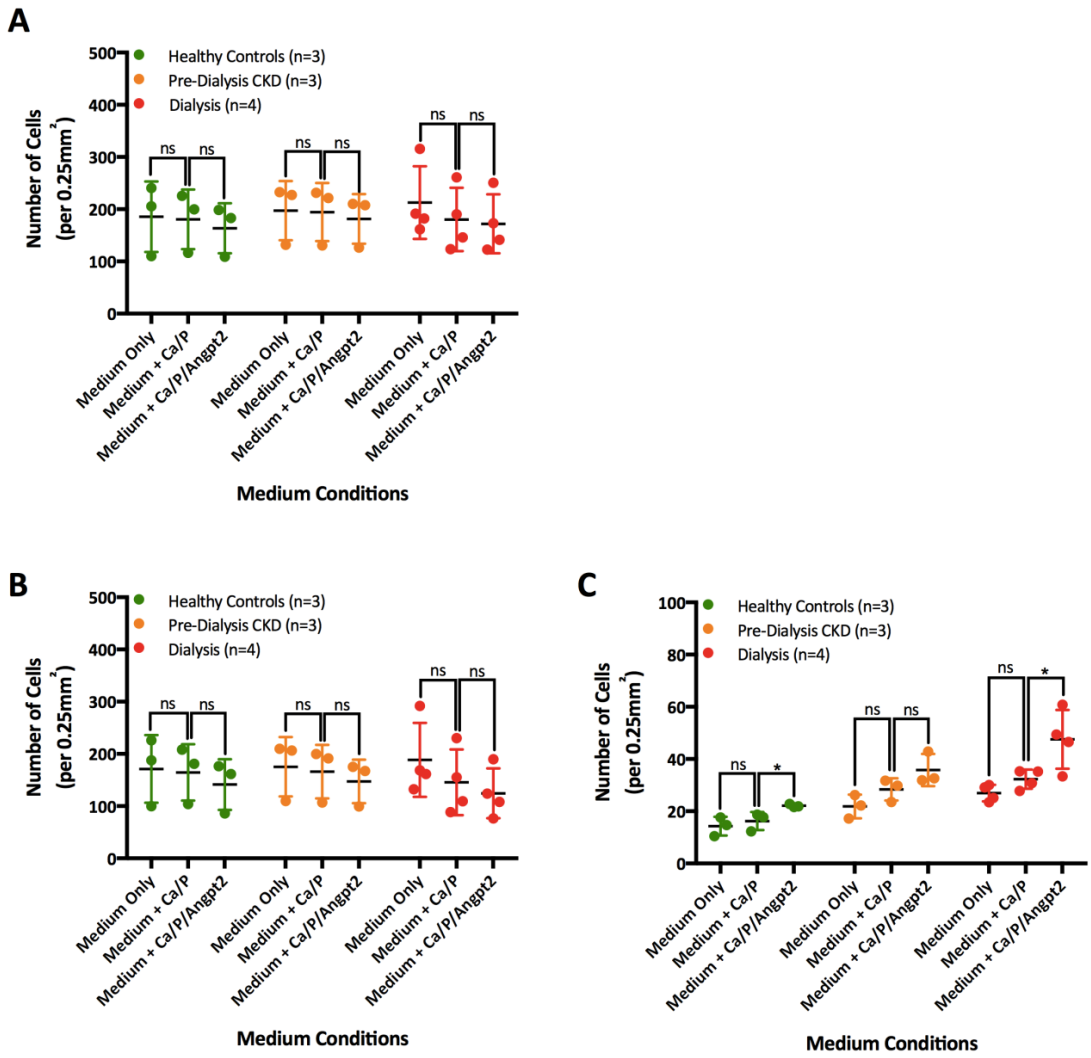

Figure 4.4: Quantification of nuclei in intact vessel rings

A: After 14 days, the total number of nuclei remains consistent between intact arterial rings cultured from paediatric vessels, despite the disease state of the patient or the culture conditions. **B:** The number of elongated and aligned nuclei decreases as disease severity increases; the number of elongated and aligned nuclei also decreases across culture conditions (medium alone, pro-calcaemic medium, and pro-calcaemic medium with 25 ng/mL Angpt2). **C:** The number of small rounded nuclei (suggestive of apoptotic nuclei) increases in patients on dialysis, when compared to both healthy control and pre-dialysis patients. There are an increased number of these phenotypically smaller nuclei in arterial rings cultured in the pro-calcaemic medium, and an even greater number in the arterial rings cultured in pro-calcaemic medium with the addition of 25 ng/mL Angpt2. All cell numbers are represented as the number of nuclei per 0.25 mm^2, and have been counted from 6–8 images of the arterial ring. *<0.05

When arterial rings were cultured under control conditions (M199 only) for 14 days, there was a trend towards an increase in condensed nuclei as CKD severity increased (control: 14.27±2.08 nuclei/0.25mm^2, pre-dialysis: 21.87±2.62 nuclei/0.25mm^2, dialysis: 26.97±1.57 nuclei/0.25mm^2). When cultured in medium alone, there were no significant differences between the number of condensed nuclei between control and pre-dialysis vessels (p = 0.086), or pre-dialysis and dialysis vessels (p = 0.137). However, there was a significant difference in condensed nuclei between the control and dialysis vessels (p = 0.004).

When arterial rings were cultured in the presence of calcium and phosphate, there was a trend towards an increased number of condensed nuclei across all disease states (control: 16.22±2.00 nuclei/0.25 mm^2, pre-dialysis: 28.35±2.45 nuclei/0.25 mm^2, dialysis: 32.38±1.83 nuclei/0.25 mm^2). However, while there were significant differences in the number of condensed nuclei between control vessels and pre-dialysis vessels (p = 0.019) as well as between control vessels and dialysis vessels (p = 0.002), no significant difference was observed between the number of condensed nuclei pre-dialysis and dialysis vessels (p = 0.245) when cultured in medium with calcium and phosphate.

When arterial rings were cultured in medium supplemented with calcium and phosphate with the addition of 25 ng/mL Angpt2, the same trend towards an increased number of condensed nuclei held with increased disease severity (control: 22.12±0.35 nuclei/0.25 mm^2, pre-dialysis: 35.79±3.55 nuclei/0.25 mm^2, dialysis: 47.54±5.64 nuclei/0.25 mm^2). Significant differences in the number of condensed nuclei were observed between control and pre-dialysis (p = 0.019), as well as between control and dialysis vessels (p = 0.013), and between pre-dialysis and dialysis vessels (p = 0.017*)*.

Interestingly, when the number of condensed nuclei was compared by culture condition within a single disease status, significant differences were not observed between vessel rings cultured in M199 vs. vessel rings cultured with calcium and phosphate in control and pre-dialysis vessels (p = 0.536 and p = 0.160, respectively; depicted in Figure 4.4C). However, significant differences were observed between vessel rings cultured with calcium and phosphate vs. those supplemented with exogenous Angpt2 in the presence of calcium and phosphate for both control and

dialysis vessels ($p = 0.044$ and $p = 0.042$, respectively; depicted in Figure 4.4C). These data suggest that, along with the disease state of the patient, Angpt2 plays a contributing role in the condensation and potential apoptosis of these VSMCs in the vessel rings.

Vessels were also examined for increased apoptosis by terminal deoxynucleotidyl transferase dUTP nick end-labelling (TUNEL) staining. Many different kits were utilised prior to obtaining these images, as the arterial ring has a high level of autofluorescence in the FITC spectrum. Most TUNEL kits use fluorescent staining to identify apoptotic nuclei; however, this results in numerous false positive nuclei in arterial rings. Therefore, I used the VasoTACS™ *In Situ* Apoptosis Detection Kit as outlined in Section 2.3.10. In this kit, apoptotic nuclei are stained dark blue (Figure 4.5); the images presented are representative of an individual vessel cultured from each media condition. Note that most apoptotic cells are near the intimal edge of the tunica media. This is likely due to increased exposure to the pro-calcaemic medium. Vessels were treated with a nuclease to create a positive control with artificial DNA damage (Figure 4.5J). These nuclei are elongated (like healthy nuclei) because the artificially-induced damage does not result in condensation of the DNA. Comparatively, the apoptotic nuclei shown in Figure 4.5 are mostly small and rounded. The negative control (Figure 4.5K) omitted the nick-end labelling enzyme; therefore, any positive staining in this sample is due to the non-specific reaction of the HRP labelling mix.

To determine whether the data showing an increase in condensed nuclei represented apoptotic cells in vessels treated with Angpt2 and vessels from patients on dialysis, the number of apoptotic nuclei in intact arterial rings after 14 days in culture was quantified utilising TUNEL staining. However, quantification of the number of apoptotic cells per unit area (μm of tunica media) indicated that there was no consistent relationship between the number of apoptotic nuclei and the culture condition (Figure 4.6).

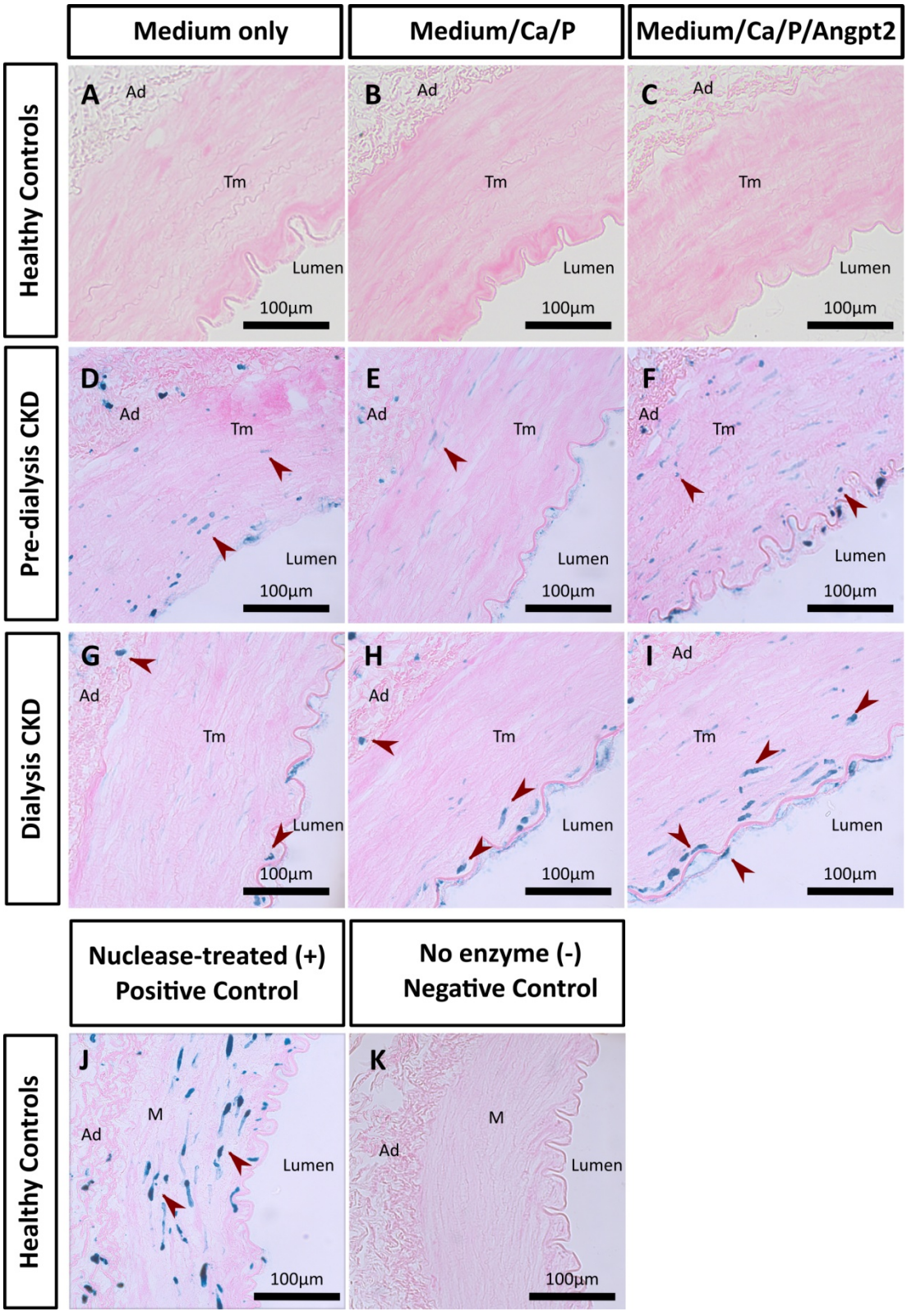

Figure 4.5: Vessel sections stained with TUNEL

Paraffin-embedded histological sections of arterial rings were stained with TUNEL following 14-day culture. Arterial rings obtained from healthy controls exhibited little to no TUNEL-positive nuclei when cultured in medium only (**A**), pro-calcaemic medium (**B**), or pro-calcaemic medium with Angpt2 (**C**). Both arterial rings obtained

from pre-dialysis (**D, E, F)** and dialysis patients (**G, H, I)** exhibited apoptotic nuclei within the tunica media across all culture conditions (as indicated by blue, rounded nuclei and highlighted by the red arrows). To ensure that the reaction was specific, a positive control (control vessel, pre-treated with nuclease to induce artificial DNA damage) was run alongside each set of samples (**J**); conversely, a negative control (control vessel, stained without an active [nick-labelling] enzyme) was run to ensure that non-specific labelling did not occur (**K**).

Arterial rings from healthy paediatric controls exhibited a mean number of 1.16×10^{-6} $\pm1.16\times10^{-6}$ apoptotic cells per unit area (as indicated by TUNEL positivity) when cultured in medium alone (Figure 4.6). Comparatively, healthy paediatric control arterial rings cultured in pro-calcaemic medium exhibited $2.51\times10^{-6}\pm1.40\times10^{-6}$ apoptotic cells per unit area. This decreased to $0.8\times10^{-6}\pm0.45\times10^{-6}$ apoptotic cells per unit area when cultured in pro-calcaemic medium with the addition of Angpt2.

When cultured in medium alone, the pre-dialysis CKD vessels exhibit 3.52×10^{-5} $\pm3.47\times10^{-5}$ apoptotic cells per unit area, and this increases to $4.58\times10^{-5}\pm4.26\times10^{-5}$ apoptotic cells per unit area when cultured in pro-calcaemic medium (Figure 4.6). The number of apoptotic cells further increases when pre-dialysis rings are cultured in pro-calcaemic medium with the addition of Angpt2, to a total of $7.86\times10^{-5}\pm6.58\times10^{-5}$ apoptotic cells per unit area. Again, the difference between conditions is not significant.

Finally, the number of TUNEL-positive cells in cultured arterial rings from patients on dialysis is $5.10\times10^{-5}\pm3.61\times10^{-5}$ apoptotic cells per unit area when cultured in medium alone, as compared with $4.33\times10^{-5}\pm2.85\times10^{-5}$ apoptotic cells per unit area when cultured in pro-calcaemic medium (Figure 4.6). This further decreases when cultured in pro-calcaemic medium with the addition of Angpt2, as the total number of apoptotic cells per unit area is $3.21\times10^{-5}\pm1.94\times10^{-5}$.

Each individual vessel has considerable variation from the next, even when from the same disease state. Although both pre-dialysis and dialysis CKD arterial exhibit slightly higher levels of apoptosis when compared with arterial rings from the healthy

controls across all culture conditions, there is no significant difference between disease states for any of the culture conditions.

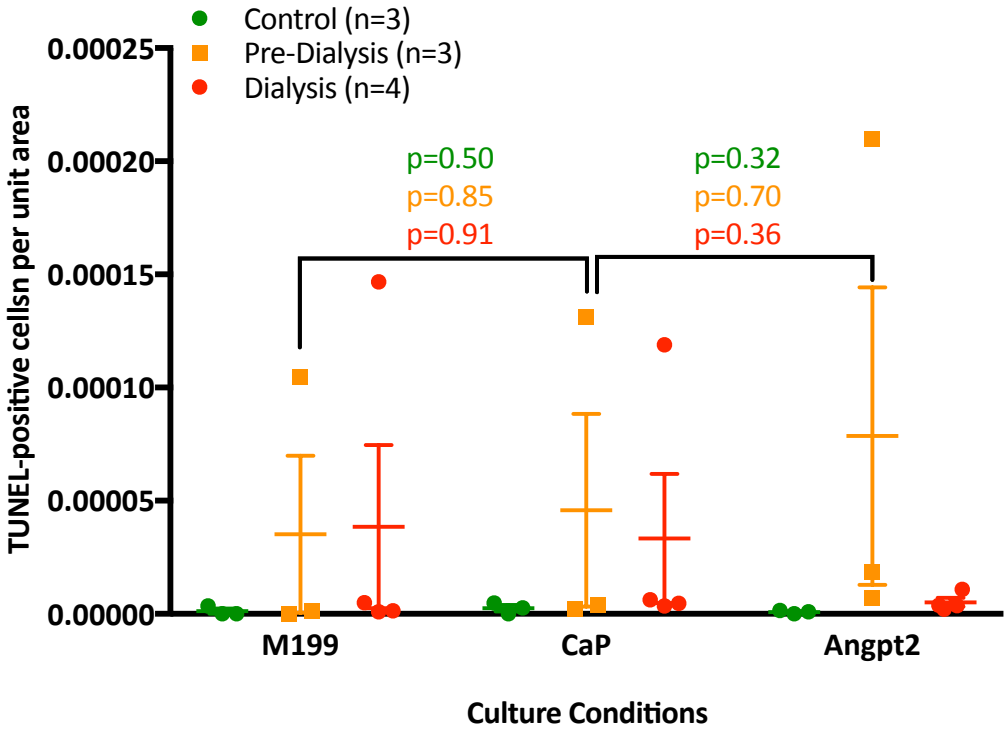

Figure 4.6: Quantification of apoptosis using TUNEL in arterial rings

TUNEL staining has been quantified as the number of apoptotic cells per unit area (μm^2), where bright blue staining of the nucleus indicates a TUNEL positive cell. Both pre-dialysis and dialysis VSMCs exhibited outlying samples, and there was no significant difference between groups.

4.2.3 Apoptosis in Cultured VSMCs

Isolated VSMCs from healthy paediatric controls and dialysis vessels were then examined to determine whether cultured cells could provide any additional insight into the apoptotic response (Figure 4.7 and 4.8). Interestingly, the cultured cells exhibited the inverse response as to what was expected as there was a decrease in the percentage of apoptotic cells in cultured VSMCs isolated from patients on dialysis, when compared with VSMCs isolated from healthy paediatric controls. This held true across all culture conditions, although the difference was not significant between populations and there was large variation between individual samples (Figure 4.8).

When cultured in medium alone, 5.93±5.76% of control VSMCs were TUNEL-positive. Comparatively 0.61±0.08% of dialysis VSMCs were TUNEL-positive (p = 0.41). When cultured in pro-calcaemic medium, 9.47±6.54 of control VSMCs were TUNEL-positive whilst only 3.14±1.40% of dialysis VSMCs were TUNEL-positive (p = 0.40). Finally, control VSMCs cultured in pro-calcaemic medium with the addition of Angpt2 were 13.95±6.25% TUNEL-positive while the dialysis VSMCs were only 5.38±0.15% TUNEL-positive (p = 0.24). However, it should be noted that the number of TUNEL-positive cells increased with pro-calcaemic medium, and was further increased with the addition of Angpt2 in both disease states.

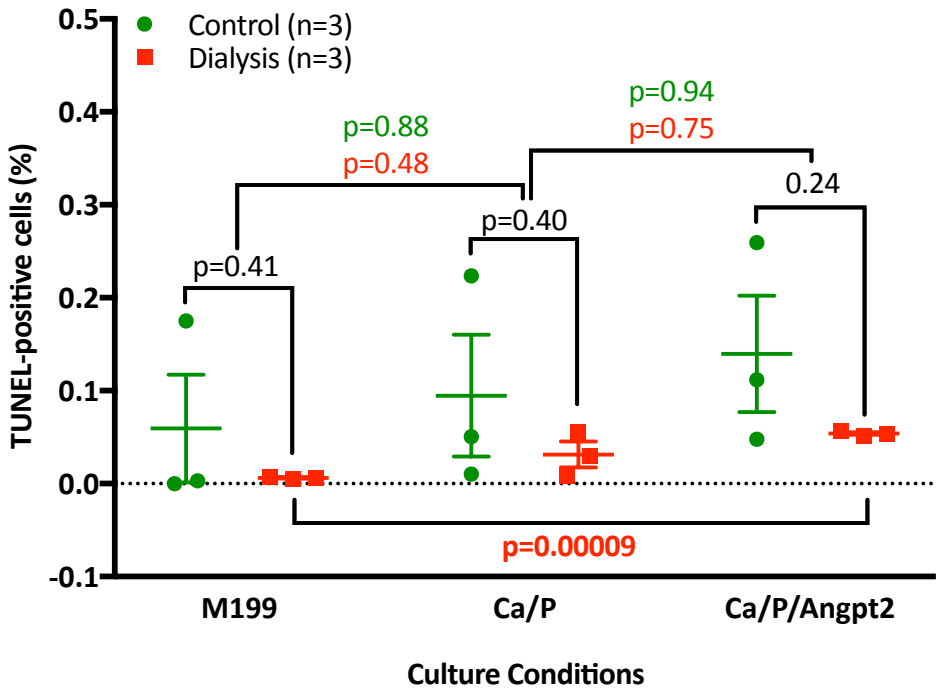

Figure 4.7: Quantification of apoptosis in cultured VSMCs treated with pro-calcaemic medium and Angpt2

VSMCs were cultured in pro-calcaemic medium with and without Angpt2, and apoptosis was quantified using TUNEL. Large variation between samples was exhibited in VSMCs isolated from control children, whilst VSMCs isolated from dialysis patients exhibited little variation but lower levels of apoptosis. Although there is no significant difference in apoptosis between control and dialysis patients, a significant difference in apoptosis is observed when directly comparing dialysis VSMCs cultured in medium alone, and pro-calcaemic medium.

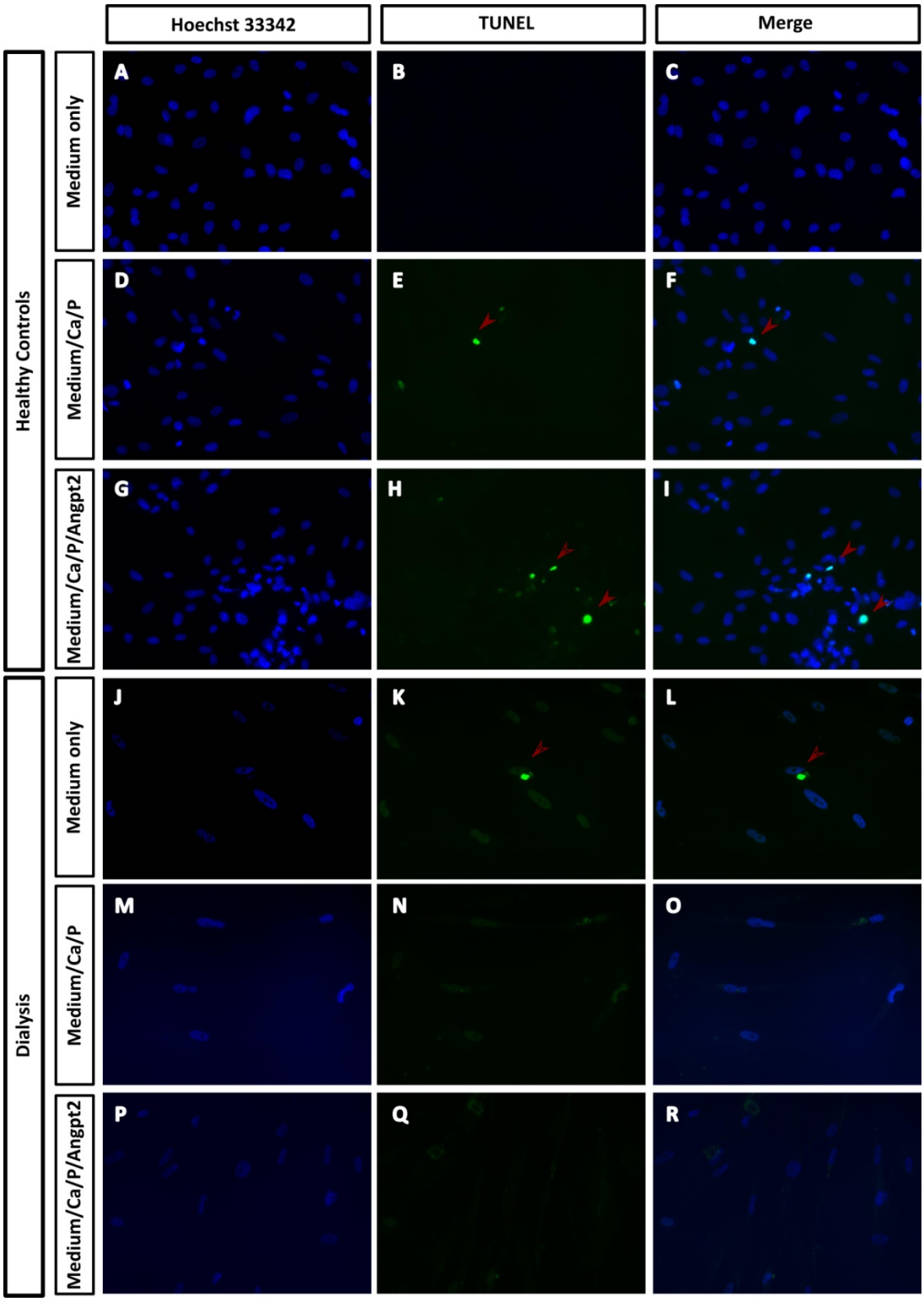

Figure 4.8: TUNEL quantification of apoptosis in control and dialysis VSMCs

Control (**A–I**) and dialysis (**J–R)** VSMCs were cultured in M199, pro-calcaemic medium, and pro-calcaemic medium with the addition of 25 ng/mL exogenous Angpt2. Few cells stained positive for apoptosis using TUNEL staining. Cells were viewed at 40x magnification.

4.2.4 Smooth Muscle Actin Staining in Paediatric Arterial Rings

Vessel rings were stained with an antibody specific to αSMA (Figure 4.9). This highlights the SMCs of the tunica media, as these cells express the contractile smooth muscle protein, which is a key marker of smooth muscle cells. Previous studies have indicated that increased expression of osteogenic genes, such as *RUNX2* and *BMP2* correlate with a loss of αSMA positivity (Shroff *et al* 2008). The healthy control vessel exhibits intense αSMA staining in the tunica media (Figure 4.9 A, B, C) across culture conditions with few regions devoid of staining, indicative of strong positive expression. Comparatively, the staining observed in pre-dialysis vessels (Figure 4.9 D, E, F) is much weaker and, when cultured in calcium and phosphate with the addition of 25 ng/mL Angpt2 (Figure 4.8 F), there are small regions of the tunica media that lack αSMA staining that would otherwise be expected to express the contractile protein. Finally, expression of αSMA in the dialysis vessel is notably weaker with large regions devoid of staining across culture conditions (Figure 4.9 G, H, I). This loss of αSMA positivity is indicative of SMC cell loss, or osteogenic changes resulting in the loss of αSMA expression and SMC identity.

4.3: Effects of Angpt2 on Gene Expression

4.3.1 Experimental Overview: Examining the Role of Gene Expression

Although the findings in Section 4.1.2 indicated that, at baseline, there were no differences in gene expression between control, pre-dialysis and dialysis VSMCs, changes in gene expression in response to pro-calcaemic medium with the addition of exogenous Angpt2 remained a potential mechanism for which calcification could occur. Additionally, as the apoptosis findings (Section 4.2.3) indicated that vessel rings did not undergo significant loss of total cell number, osteogenic conversion (i.e. the increase in osteogenic genes and the loss of smooth muscle cell markers) was a potential explanation for this result alongside an increase in calcium content.

To determine if these changes in calcium deposition in the dialysis cells were related to changes in osteogenic gene expression, RNA was isolated from VSMCs cultured in medium alone, pro-calcaemic medium, and pro-calcaemic medium with 25 ng/mL

exogenous Angpt2. A concurrent experiment in which RNA was isolated from vessel rings would have been beneficial; however, the volume of artery required to do so would have prohibited any further experiments on the vessel.

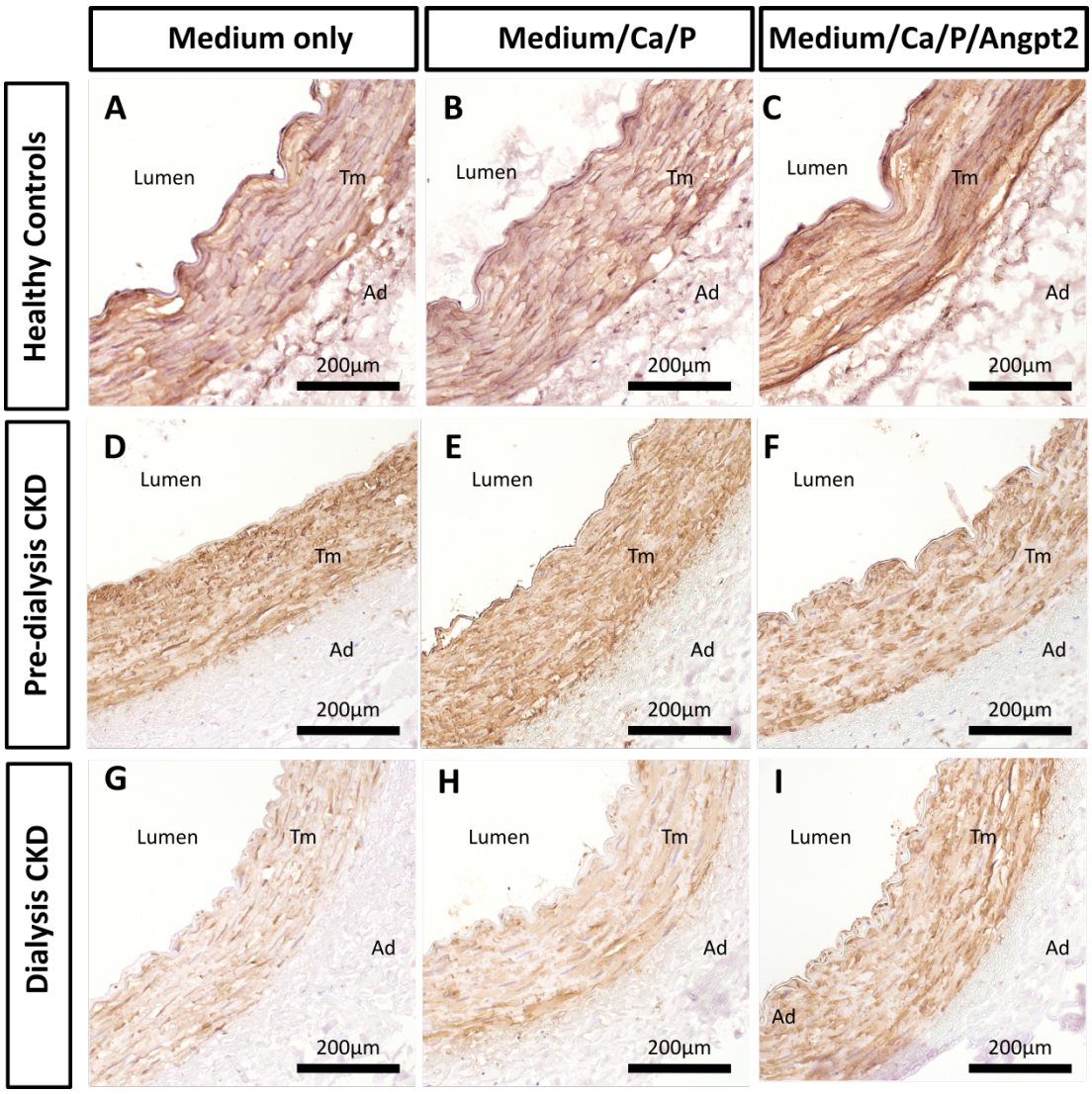

Figure 4.9: Vessel sections stained with αSMA

Paraffin-embedded histological sections of arterial rings were stained for αSMA following 14-day culture. Vessel rings obtained from healthy paediatric controls exhibited positive αSMA staining across culture conditions (medium only [**A**], pro-calcaemic medium [**B**], and pro-calcaemic medium with the addition of Angpt2 [**C**]). The intensity of αSMA staining decreased in arterial rings obtained from pre-dialysis CKD patients when cultured in medium alone (**D**) or pro-calcaemic medium **(E**). Vessels cultured in pro-calcaemic medium containing Angpt2 (**F**) exhibited small

regions lacking αSMA-positive staining, although these regions were infrequent. Dialysis vessels exhibited decreased αSMA staining when cultured in medium only (**G**), pro-calcaemic medium (**H**), and pro-calcaemic medium containing Angpt2 (**I**), as well as increased regions of tunica media devoid of αSMA positivity.

4.3.2 Osteogenic Gene Expression with Addition of Angpt2

There is a significant difference in the fold change of expression levels for contractile marker *αSMA* in the dialysis VSMCs (n = 5) cultured in pro-calcaemic medium with and without Angpt2, when compared to dialysis VSMCs cultured in media alone (n = 5, Figure 4.10A). However, there is no significant difference in the fold change of *αSMA* between the dialysis VSMCs cultured in pro-calcaemic medium with Angpt2 and the dialysis VSMCs cultured in pro-calcaemic medium without Angpt2.

Given that the action of Angpt2 is traditionally through the receptor tyrosine kinases Tie1 and Tie2, I also examined mRNA expression of these receptors. There were no significant differences in *TIE1* expression between dialysis VSMCs cultured in medium alone, pro-calcaemic medium, and pro-calcaemic medium with 25 ng/mL Angpt2 (Figure 4.10B). Although there was a slight increase in *TIE2* expression in dialysis VSMCs cultured in pro-calcaemic medium with and without Angpt2, there were no significant differences in expression levels between culture conditions (Figure 4.10C).

There is a significant increase in pro-osteogenic factor *BMP2* in dialysis VSMCs cultured in pro-calcaemic medium with and without Angpt2 (Figure 4.10D), when compared to dialysis VSMCs cultured in medium alone. Whilst there is a trend towards an increase in *BMP2* expression in the dialysis VSMCs cultured in pro-calcaemic medium with the addition of Angpt2, there is no significant difference when compared to dialysis VSMCs cultured in pro-calcaemic medium alone.

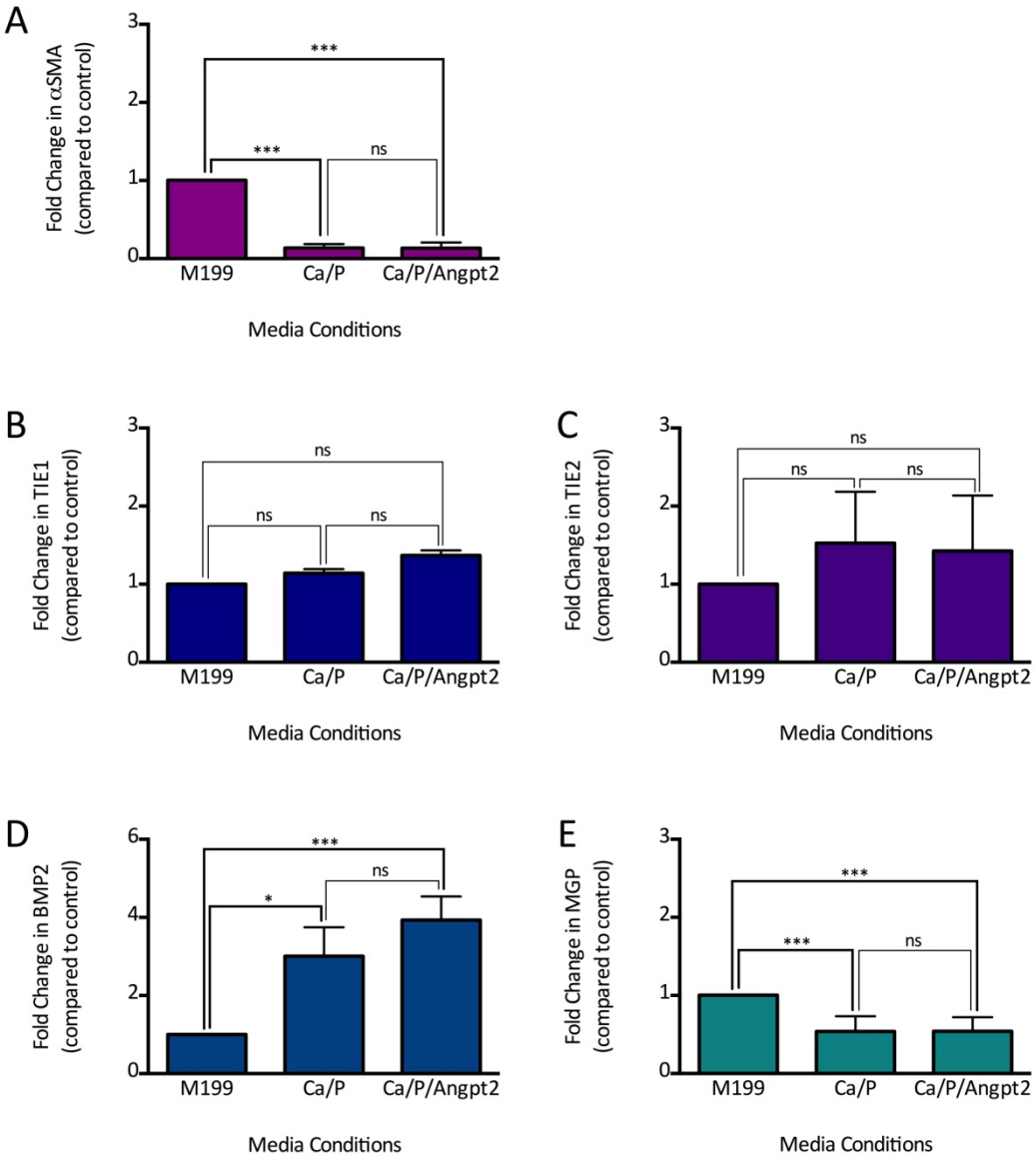

Figure 4.10: Gene expression in Angpt2-stimulated VSMCs.

Expression levels of genes *αSMA*, *TIE1, TIE2*, *BMP2* and *MGP* were quantified in cultured VSMCs isolated from patients undergoing dialysis (n = 5) following culture in medium alone, pro-calcaemic medium, and pro-calcaemic medium with the addition of 25 ng/mL Angpt2. Bars represent the mean fold-change in gene expression, relative to the dialysis VSMCs cultured in medium alone. Error bars indicate standard error; note that there is a large variation between individual patients, thus increasing the size of the error bars.

Conversely, there was a significant decrease in anti-osteogenic gene *MGP* in dialysis VSMCs cultured in pro-calcaemic medium with and without Angpt2 (Figure 4.10E), when compared to dialysis VSMCs cultured in medium alone. However, there is no significant difference in *MGP* expression between VSMCs cultured in pro-calcaemic medium with the addition of Angpt2, and VSMCs cultured in pro-calcaemic medium without Angpt2.

4.4: Conclusion

Using primary VSMCs isolated from paediatric controls, pre-dialysis CKD patients, and CKD patients on dialysis, I have shown that there are no significant changes in the baseline levels of gene expression for either angiogenic genes (*TIE1, TIE2, ANGPT1* and *ANGPT2*) or osteogenic genes (*BMP2*, *MGP, OPN,* or *SP7*), as well as indicators of smooth muscle identity *SM22*α and α*SMA*. However, the large variation in expression between individual samples suggests that an increased sample size is essential.

One of the potential mechanisms that propagate calcification of the tunica media is apoptosis; therefore, I quantified the level of apoptosis in both arterial rings and cultured primary VSMCs following stimulation with pro-calcaemic medium with and without Angpt2. Whilst there were no significant changes in the total number of nuclei, there was a trend towards an increase in condensed nuclei (suggesting apoptotic cells) with the addition of Angpt2 across disease states. However, further quantification of apoptosis using TUNEL staining gave variable results showing no clear association between the addition of Angpt2 and calcification.

One of the potential reasons behind the static nuclear number was that, rather than undergoing apoptosis, the cells were undergoing osteogenic changes. However, whilst expression of osteogenic gene *BMP2* increased and anti-osteogenic *MGP* decreased following culture in pro-calcaemic medium (and α*SMA* decreased correspondingly), there were no significant changes in expression between VSMCs cultured with Angpt2 and those cultured without.

Chapter 5: Results — Tie2 Binding and Inhibition in Vascular Calcification

5.1: Expression of Tie2 in VSMCs

5.1.1 Experimental Overview: Expression of Tie2

qRT-PCR analysis (Figure 3.12) indicated that the isolated paediatric VSMCs express high levels of contractile proteins, indicative of their identity as VSMCs. Furthermore, the paediatric VSMCs also express αSMA incorporated into stress fibres of the cell (Figure 3.7). However, this data has indicated that although these paediatric VSMCs express low levels mRNA for the endothelial marker *CD31,* they also express *TIE2* at levels similar to those recorded in endothelial cells (Figure 3.13). Given that *TIE2* is traditionally described as marker of endothelial cells, I wanted to confirm the expression in these VSMCs using a range of alternative techniques.

5.1.2 Expression of TIE2 RNA in VSMCs

Firstly, a standard PCR was run for the genes *TIE1, TIE2, ANGPT1,* and *ANGPT2* to confirm that they were indeed present in VSMCs (Figure 5.1). VSMCs from dialysis were used in these experiments, whilst HUVEC RNA was used as a positive control and RNase/DNase-free water was used as a negative control. The HUVEC RNA produced three strong bands at the correct size for *TIE1, TIE2,* and *ANGPT2*, while the intensity of the band for *ANGPT1* was much weaker. Comparatively, both the HuAoVSMC and the dialysis VSMCs exhibited strong bands at the correct size for *TIE2* and *ANGPT1*. The absence of bands in the wells containing the negative controls indicates that the results of these PCRs can be taken as valid and are not false positives due to contaminated reagents.

To further confirm that the qRT-PCR previously performed in this thesis for *TIE2* amplified the correct gene, I sequenced 4 products from the PCR plate following qRT-PCR for *TIE2*. Each product was from a difference cell population with one sample each from HUVECs, control VSMCs, pre-dialysis VSMCs, and dialysis VSMCs.

Remnant dNTPs and polymerases from the amplification reaction were removed (as described in Section 2.5.7), and the products were sequenced using the forward primer from the *TIE2* amplification. The product sequence was then compared to the sequence of the intended *TIE2* amplicon (Figure 5.2).

Purified qRT-PCR products were run on a NanoDrop™ prior to sequencing to confirm that they were of high quality and to measure the quantity (Figure 5.2A). All 4 sequencing reactions were 100% homologous to *TIE2* (Figure 5.2B), indicating that the products produced in the qRT-PCR experiment were representative of *TIE2*. The full product of the qRT-PCR reaction is exon-spanning; as each of these sequencing reactions exhibits clear single peaks, indicative of a single product, none of the amplicons are DNA-derived, as a mismatch would otherwise be observed. The sequenced region shown (Figure 5.2B) corresponds to the segment highlighted in red (Figure 5.2C).

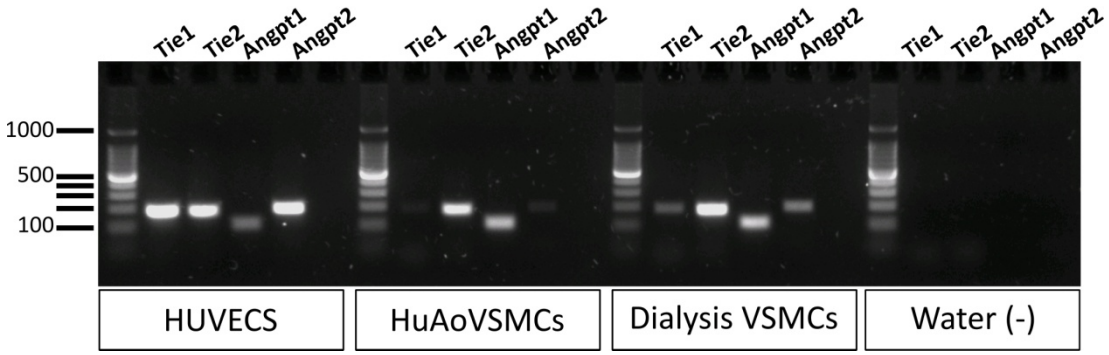

Figure 5.1: Standard PCR for *TIE1, TIE2, ANGPT1* and *ANGPT2*

Standard PCR for *TIE1, TIE2, ANGPT1,* and *ANGPT2* indicate that *TIE2* is expressed by both HuAoVSMC and dialysis VSMCs, as well as by HUVECs. As there are no bands in the negative control (distilled water), these products are not due to contamination of the reagents.

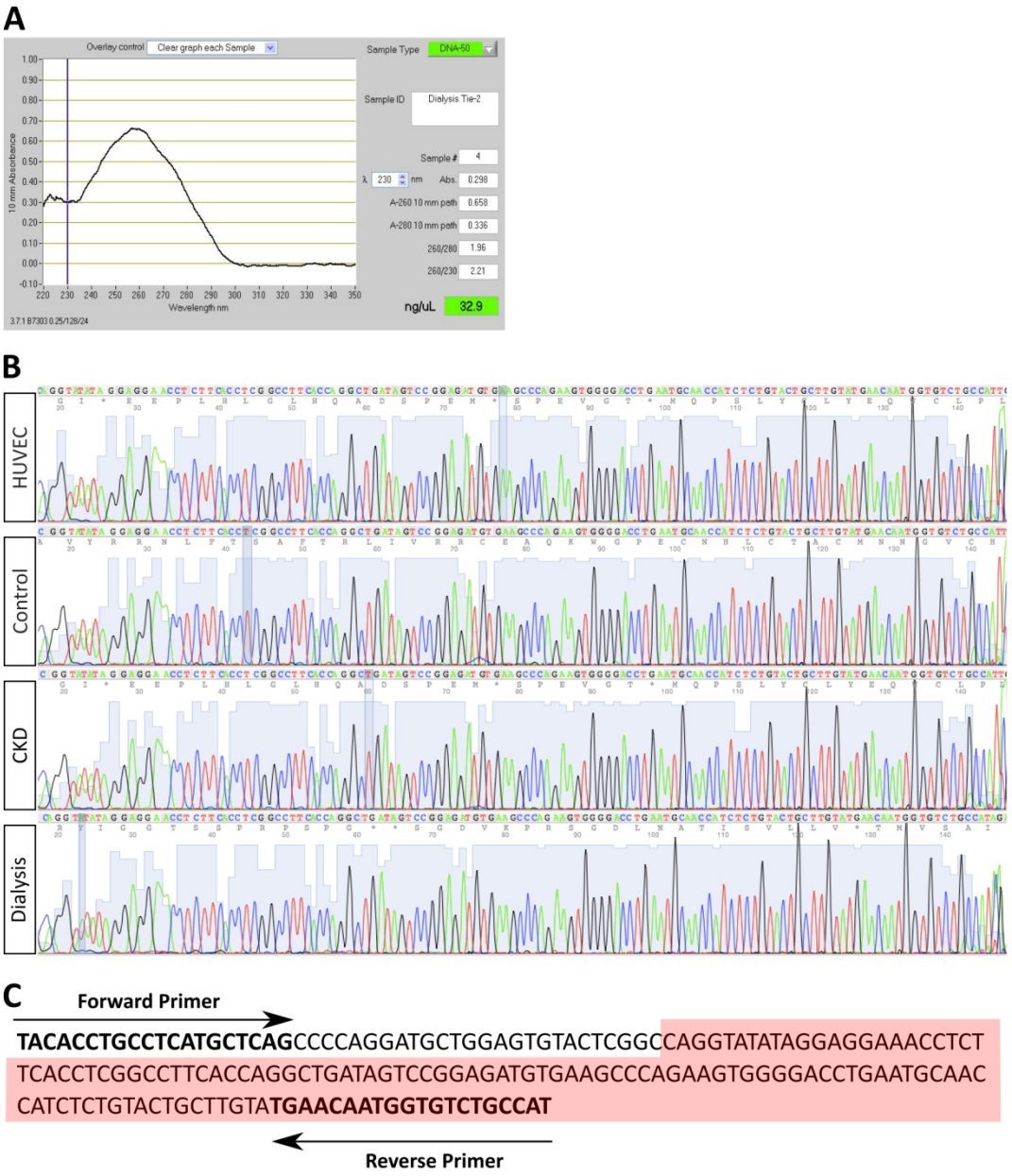

Figure 5.2: *TIE2* sequencing products

A: Extraneous dNTPs were removed from the PCR products prior to sequencing; the concentrations of cleaned-up products were measured using NanoDrop™ spectrophotometric software, and products were diluted to 1.7 ng/µL before sequencing. **B:** The sequencing results for amplicons from HUVEC, control VSMC, pre-dialysis VSMC, and dialysis VSMCs all correspond to the *TIE2* sequence spanning exons 4 and 5. **C:** The expected *TIE2* sequence, as given by the forward and reverse primer. The area highlighted in red corresponds to the sequence shown in the sequencing products above.

5.1.3 Expression of TIE2 protein in VMSCs

Expression of *TIE2* RNA in the isolated VSMCs does not guarantee translation of the gene into protein. Therefore, protein isolates from control ($n = 4$), pre-dialysis ($n = 4$), and dialysis ($n = 4$) VSMCs were run on a Western blot and probed for TIE2 (as described in Section 2.5.8). HUVEC protein isolate was run with these samples as a positive control; RIPA buffer (with no cell extract) was run with these samples as a negative control. Note that the Western blot shown in Figure 5.3A shows only two of four VSMC samples for each patient population; this was because the gel could only fit 10 samples. Therefore, in this blot I have chosen to show the protein ladder as well as both a positive and negative control. However, densitometry has been conducted on 4 samples from each patient population, utilising GAPDH as the loading control.

This Western blot for TIE2 (Figure 5.3 A) indicates that TIE2 is present across all VSMCs isolated from paediatric patients. The mean expression level of TIE2/GAPDH decreased as the level of disease severity increased (control: 1.49±0.46, pre-dialysis CKD: 1.35±0.27, dialysis CKD: 0.75±0.25). Following densitometric analysis, there were no significant differences between groups as determined by 2-tailed *t*-tests (control versus pre-dialysis CKD, $p = 0.802$; control versus dialysis CKD, $p = 0.207$; pre-dialysis CKD versus dialysis CKD, $p = 0.155$). There were also no statistical differences in expression levels between any of the patient VMSCs and the commercially obtained HUVECs (control, $p = 0.383$; pre-dialysis CKD, $p = 0.356$; dialysis CKD, $p = 0.274$).

5.2: Tie2 Localisation in the Intact Vessel Ring

5.2.1 Experimental Overview: Tie2 Localisation

The presence of TIE2 protein was detected in the isolated paediatric control, pre-dialysis and dialysis VSMCs by Western blot. However, culture conditions can trigger expression of genes in primary cells that may not otherwise be expressed *in vivo* (Dozmorov *et al* 2007, Rensen *et al* 2007, Zaitseva *et al* 2006). Therefore, Tie2 expression was examined in frozen sections of intact vessel rings (as described in Section 2.3.6) to determine if expression was localised to the endothelium, as indicated

in the literature, or whether it was also expressed in the tunica media as indicated by the primary cell data.

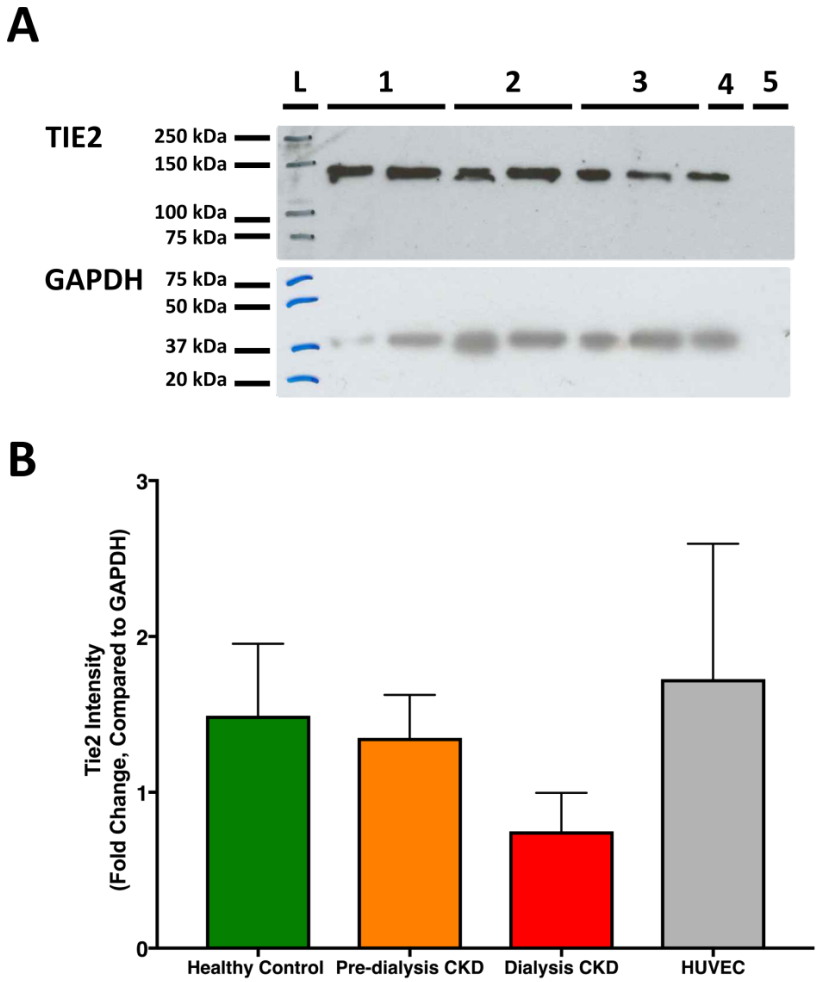

Figure 5.3: Western blot for TIE2

A: Representative samples from protein isolated from paediatric control VSMCs (labelled '1', shown $n = 2$; actual $n = 4$), pre-dialysis VSMCs (labelled '2', shown $n = 2$; actual $n = 4$), and dialysis VSMCs (labelled '3', shown $n = 2$; actual $n = 4$) was examined for TIE2 expression using Western blotting. HUVEC protein isolate was used as the positive control (labelled '4', shown $n = 1$; actual $n = 3$) while the negative control consisted of RIPA buffer that had gone through the same pre-loading process as the samples (labelled '5'). The protein ladder is given in the first lane, labelled 'L'. GAPDH was used as a loading control for comparative purposes, and therefore loading variability is accounted for in the densitometry. **B:** Densitometry was conducted to determine the fold-change in intensity between bands, in relation to the loading control GAPDH (control $n = 4$, pre-dialysis CKD $n = 4$, dialysis CKD $n = 4$, HUVEC $n = 3$). *t*-tests were conducted between groups; however, there were no significant differences between groups.

5.2.2 Immunofluorescent Staining of the Blood Vessel

Tie2 staining of intact arterial rings exhibited specific expression of Tie2 within the tunica media, with no staining in the adventitia of the vessel (Figure 5.4). Although the shown figure is a representative image from a dialysis vessel, Tie2 staining was also observed in vessel rings from paediatric controls. Incubating the Tie2 antibody with a commercially-available blocking peptide to Tie2 prior to staining acted as a negative control for Tie2 staining; the secondary antibody was then added, and staining was carried out as described in Section 2.3.6. No staining was observed in the samples treated with the blocking peptide, showing that the signal (of the utilised Tie2 antibody) could be specifically inhibited and that positive staining was not due to non-specific binding of the secondary antibody (Figure 5.4 G, I). Hoechst was utilised to highlight the nuclei of the cells which, when merged with the Tie2 staining (Figure 5.4 C) indicated that Tie2 expression was localised outside the nucleus.

The tunica media of the arterial rings also exhibited positive staining for αSMA (Figure 5.5). As indicated by the extensive staining in the tunica media (Figure 5.5 A, D), αSMA is highly expressed in the tunica media of the arterial rings. When merged with Hoechst, the staining indicates cytoplasmic localisation of αSMA (Figure 5.5. C, F). A paediatric kidney sample was utilised as a positive control for αSMA. The tunica media of these arterial rings stain positive for both Tie2 and αSMA, confirming the gene expression data from the primary VSMCs, derived from the paediatric vessels.

Whilst one would expect to see Tie2 expressed in the tunica intima, the intima of these cultured vessels is damaged during processing of the vessel, and during culture of the intact rings. As such, very few endothelial cells are detected in these sections, and CD31 staining of vessel rings indicated lack of CD31 positive cells in the tunica intima (Figure 5.6). It should be noted that, despite positive expression of Tie2, the tunica media also exhibits no positive staining for CD31. A paediatric kidney biopsy sample was used as a positive control, as CD31 stains the renal microvasculature (Figure 5.6 G, I).

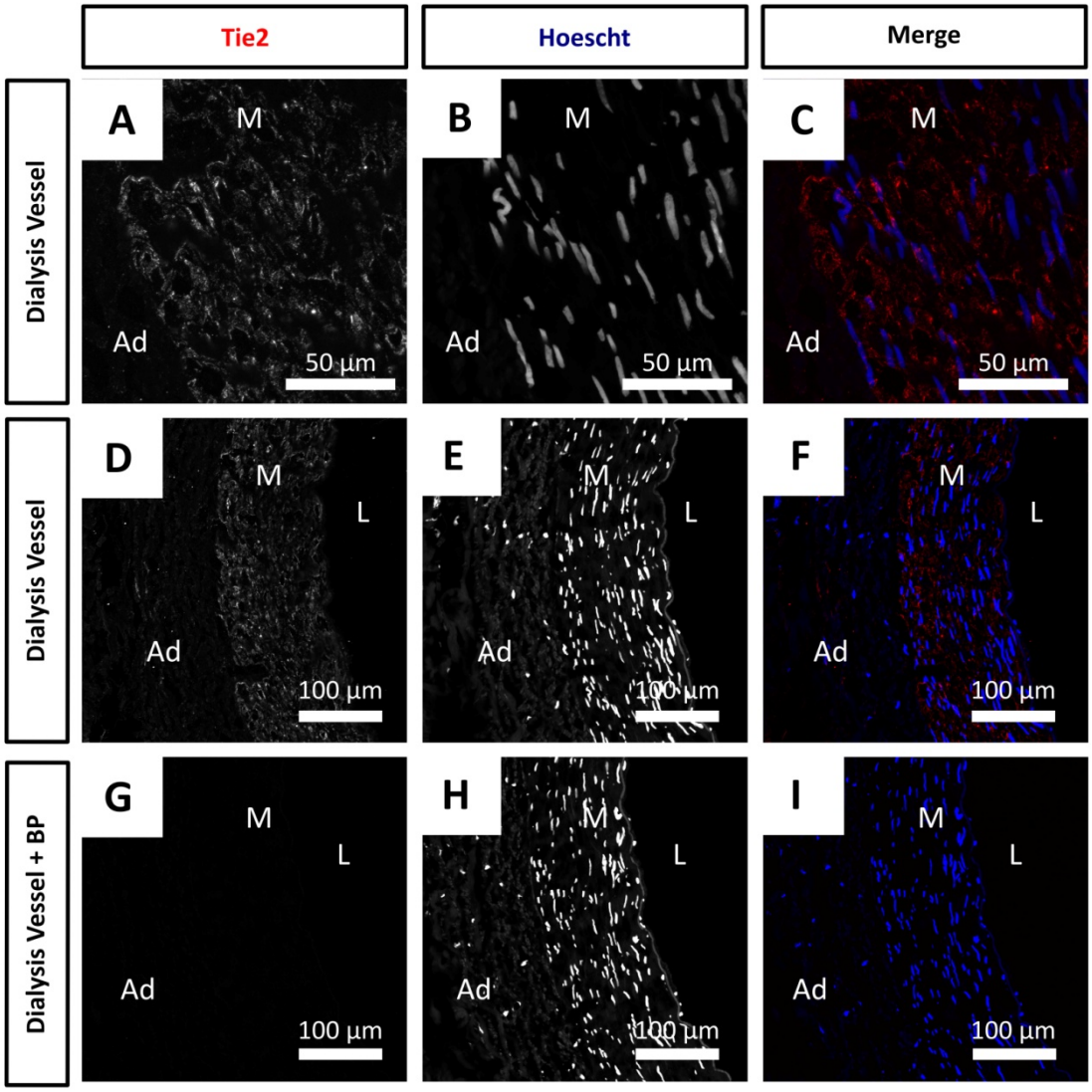

Figure 5.4: Intact arterial rings stained for TIE2

Frozen sections of intact arterial rings stained positive for TIE2 in the tunica media, (**A–F**). Vessel adventitia did not show positive staining. Nuclei are stained with Hoechst (**B**, **E**, **H**) and the merged TIE2 (red) and Hoechst (blue) images are shown in **C**, **F**, and **I**. Tunica intima in arterial rings was damaged during explant culture and processing, therefore few endothelial cells are observed in arterial sections for which to compare Tie2 expression even at high (x630) magnification (**A, B, C**). Incubating Tie2 antibody with a blocking peptide (BP) specific to Tie2 prior to staining completely obliterated positive staining for Tie2 (**G–I**). Images **D–I** were visualised at 400x magnification. Ad = adventitia, M = tunica media, and L = lumen.

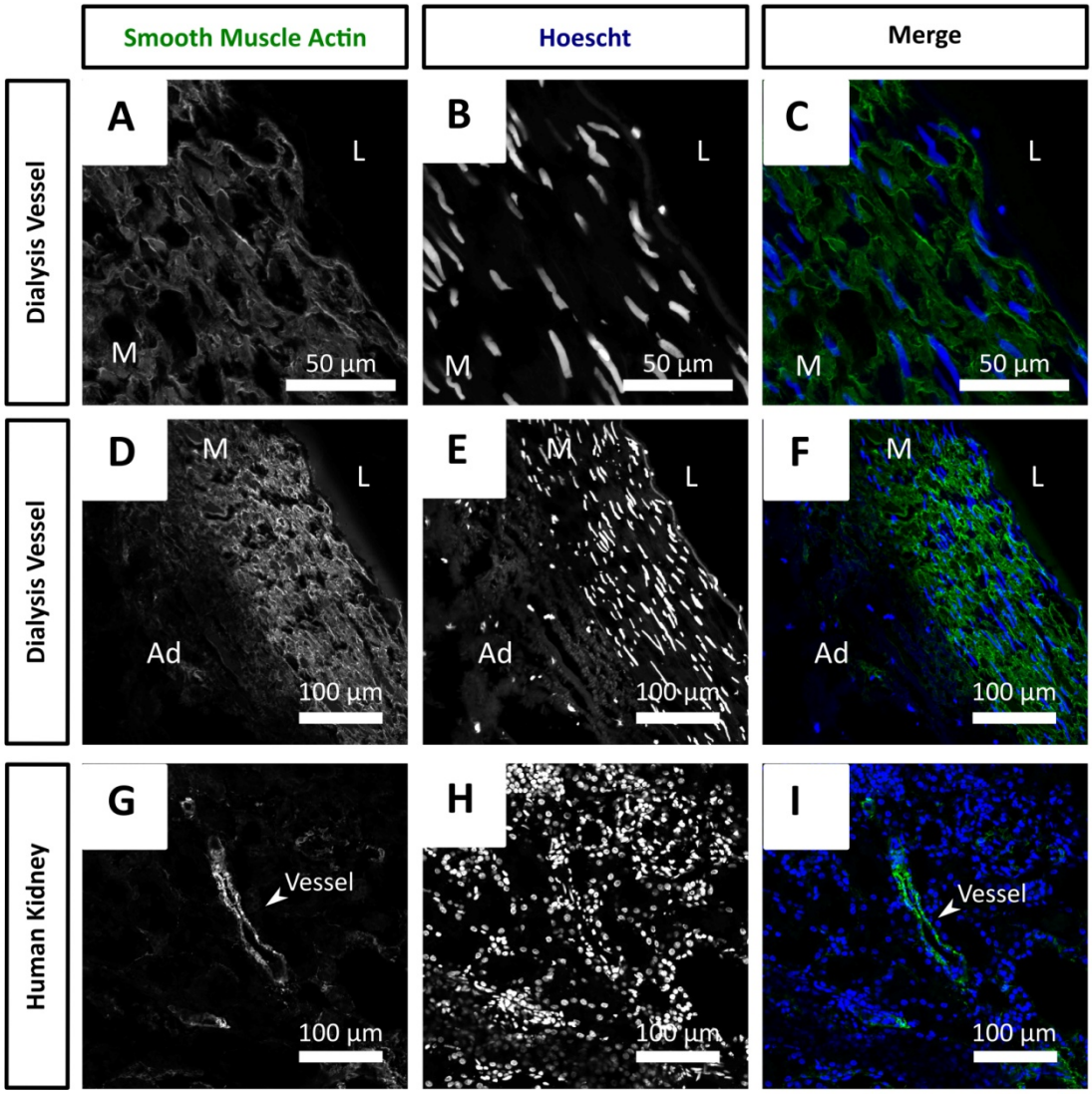

Figure 5.5: αSMA staining of dialysis vessels

Frozen sections of intact arterial rings stained positive for αSMA in the tunica media. αSMA (**A, D**) can be seen spanning the cell body with clear nuclear exclusion. Nuclei are stained with Hoechst (**B, E**) and the merged αSMA (green) and Hoechst (blue) images are shown in **C** and **F**. A paediatric kidney biopsy sample (**G**, **H**, **I**) was used as a positive control for αSMA, as αSMA stains the large vessels in the renal structure as indicated by the white arrowhead in **G** and **I** while the nuclei are detected by Hoechst (**H**). The vessel adventitia does not exhibit positive staining for αSMA, unlike cultured fibroblasts. Ad = adventitia, M = tunica media, and L = lumen.

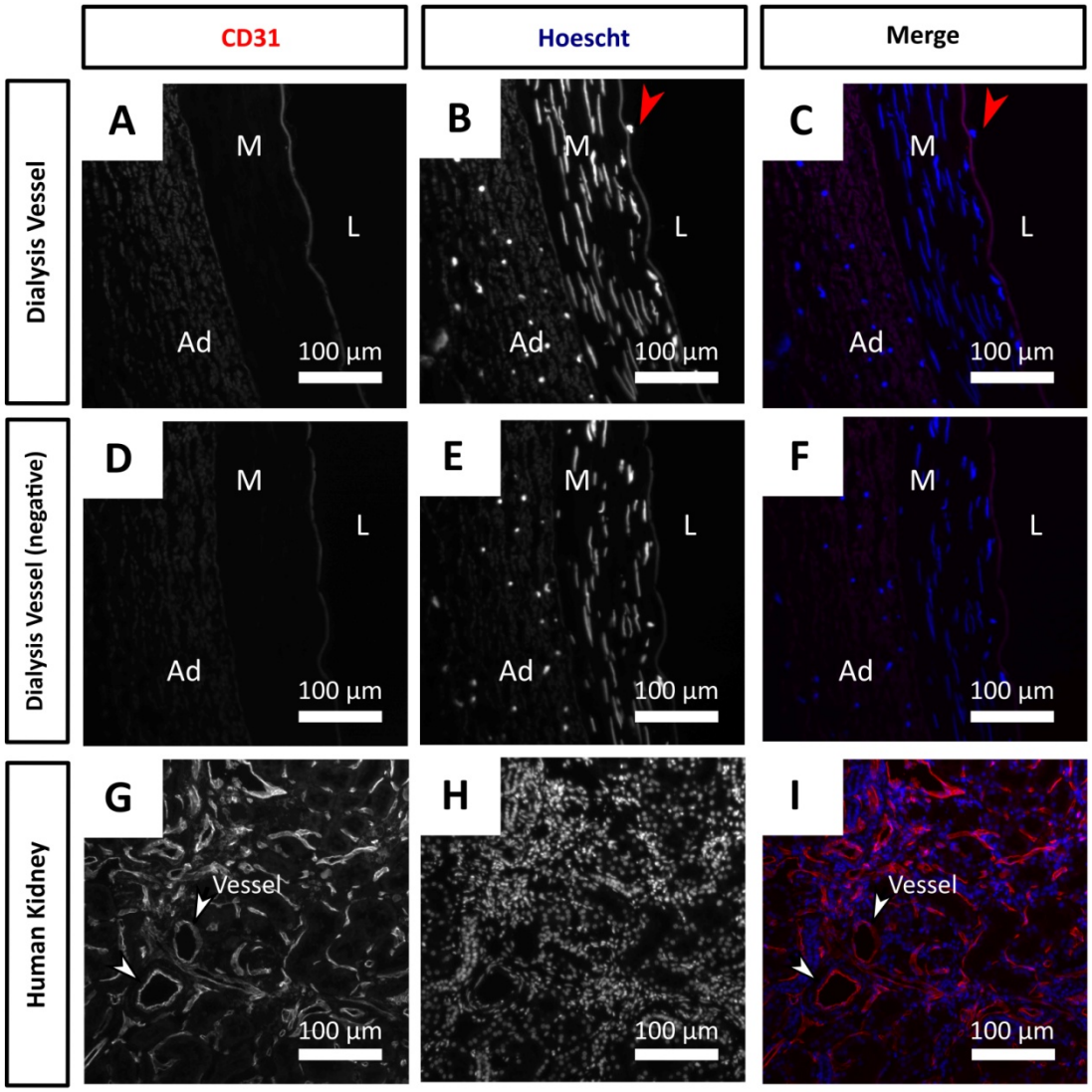

Figure 5.6: Intact arterial rings stained for CD31

Frozen sections of intact arterial rings did not exhibit CD31 staining (**A**, **D**) along the tunica intima. The weak signal observed in **A** is due to high autofluorescence of the internal elastic lamina. The vessel nuclei are stained with Hoechst (as shown in **B** and **E**) and the merged CD31 (red) and Hoechst (blue) images are shown in **C** and **F.** Although a few individual nuclei were detected on the lumen side of the internal elastic membrane (as indicated by the red arrows in **B** and **C**), an intact monolayer of endothelial cells was not detected. A paediatric kidney biopsy sample (**G**, **H**, **I**) was used as a positive control for CD31, as CD31 stains the microvasculature in the kidney (as indicated by white arrowheads in **G** and **I)**. Nuclei in the kidney are stained with Hoechst **(H**). Ad = adventitia, M = tunica media, and L = lumen.

5.3: Targeting Tie2 in VSMCs and Intact Vessel Rings

5.3.1 Experimental Overview: Knockdown of Tie2

The work in this thesis has shown Angpt2 to have an additive effect on calcium deposition within both intact blood vessels and VSMCs from patients undergoing dialysis, when cultured in a pro-calcaemic environment. Furthermore, I have demonstrated that Tie2 is expressed in the tunica media of paediatric inferior epigastric arteries as well as in cultured VSMCs. Here, I will aim to determine whether the acceleration in VSMC calcification (as induced by exogenous Angpt2) can be modulated through alteration of Tie2 signalling.

My strategy was to modulate expression of the receptor Tie2 by downregulating transcription of *TIE2*, using siRNA specific to this gene (as described in Section 2.6.6). If, as hypothesised, Angpt2 were to act through Tie2 to drive calcification, downregulating the expression of *TIE2* (and thus limiting the production of TIE2) should limit calcification in response to stimulation with exogenous Angpt2.

5.3.2 Optimising siRNA Conditions

siRNA transfection conditions were first optimised on a single dialysis VSMC population to determine two primary objectives necessary for use in subsequent calcification experiments:

1) Optimal siRNA concentration
   → The lowest concentration of siRNA that would produce an effective knockdown of *TIE2*
2) Length of knockdown effect
   → To determine how frequently cells would need to be re-transfected to maintain *TIE2* downregulation over a 5-day experiment.

Each optimisation experiment was conducted in triplicate to show reproducibility of the findings.

Optimising Concentration: Addition of control siRNA to the culture media had low-level effects on *TIE2* expression; at 10 nM control siRNA, *TIE2* expression was decreased to 81% of total *TIE2* expression (as compared to non-transfected cells) (Figure 5.7). *TIE2* expression decreased in a linear fashion as the concentration of control siRNA increased, with the maximum concentration of control siRNA (100 nM) corresponding to an almost 50% decrease in *TIE2* expression. Comparatively, the specific effects of *TIE2* siRNA at a concentration of 10 nM resulted in an 88% decrease in *TIE2* expression; this remained fairly consistent as *TIE2* siRNA concentration increased, with the maximal dose of *TIE2* siRNA (100 nM) corresponding to a 93% decrease in *TIE2* expression. Given that the minimum concentration of control siRNA (10 nM) had the least non-specific reduction of *TIE2* expression (as compared with the non-transfected cells) while the *TIE2* siRNA at this concentration provided a near 90% reduction in *TIE2* expression, 10 nM was chosen as the optimal concentration of siRNA for further experiments.

Optimising Time-Course: All previous stimulation experiments with exogenous Angpt2 on the VSMCs had used a 5-day time-course. Therefore, it would be ideal that the inhibition experiments maintained the same conditions and timing. A brief experiment was conducted to ensure that the knockdown effects of the *TIE2* transfection could be maintained over the full 5-day period (Figure 5.8). Following a single transfection, RNA was harvested after 48 hours, 72 hours, and 5 days to determine *TIE2* expression levels. While *TIE2* expression was still reduced by 80% after 48 hours (using 10 nM Tie2 siRNA), there was only a 62% reduction after 72 hours and a 40% reduction after 5 days. This indicated that a single transfection could not maintain a strong reduction over the full 5-day time-course as the effects were partly diminished by the 3rd day. Therefore, to maintain reduced *TIE2* expression across the course of 5 days, cells were transfected twice during the time-course: once at the beginning of the experiment, and once at the midpoint of the experiment. *TIE2* expression was checked using qRT-PCR following each experiment to confirm that the transfection had worked efficiently.

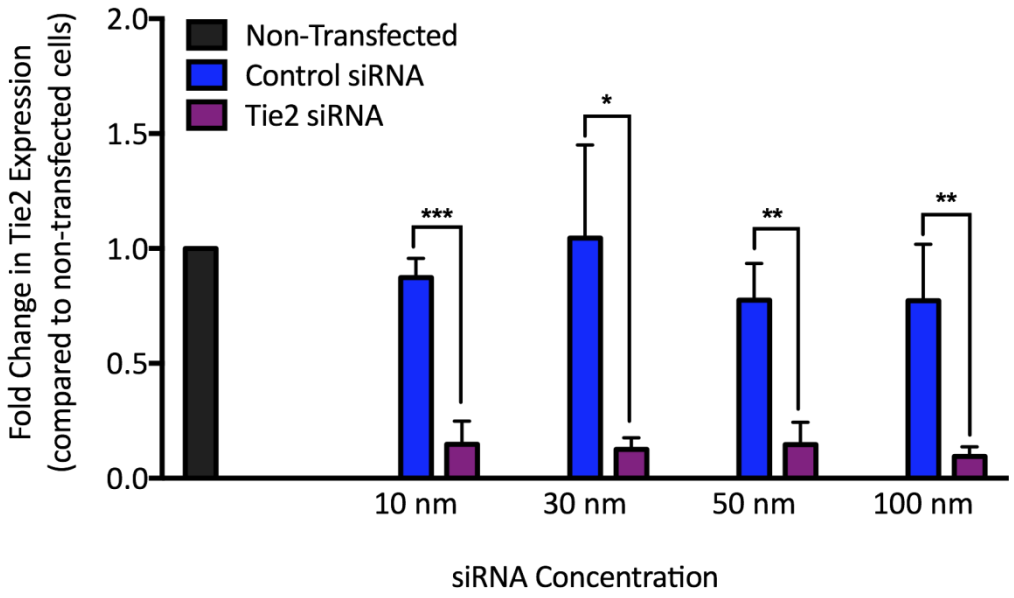

Figure 5.7: Determination of the optimal concentrations of Tie2 siRNA

Four different siRNA concentrations – 10 nM, 30 nM, 50 nM, and 100 nM – of both control siRNA and *TIE2* siRNA were added to plated VSMCs that had reached 70% confluence. Each well (of a 6-well plate) contained low-serum medium Opti-MEM®I. All wells with siRNA also contained Lipofectamine, and one well contained Lipofectamine only. One well contained medium alone (no transfection reagents). After 48 hours, cells were harvested and RNA was extracted, reverse-transcribed, and analysed for *TIE2* expression using qRT-PCR. Fold-change in *TIE2* expression was calculated as compared with non-transfected cells. Each experiment was done in triplicate, and the mean value was used in dCt calculations ($p<0.0005$ ***, $p<0.005$ **, $p<0.05$*).

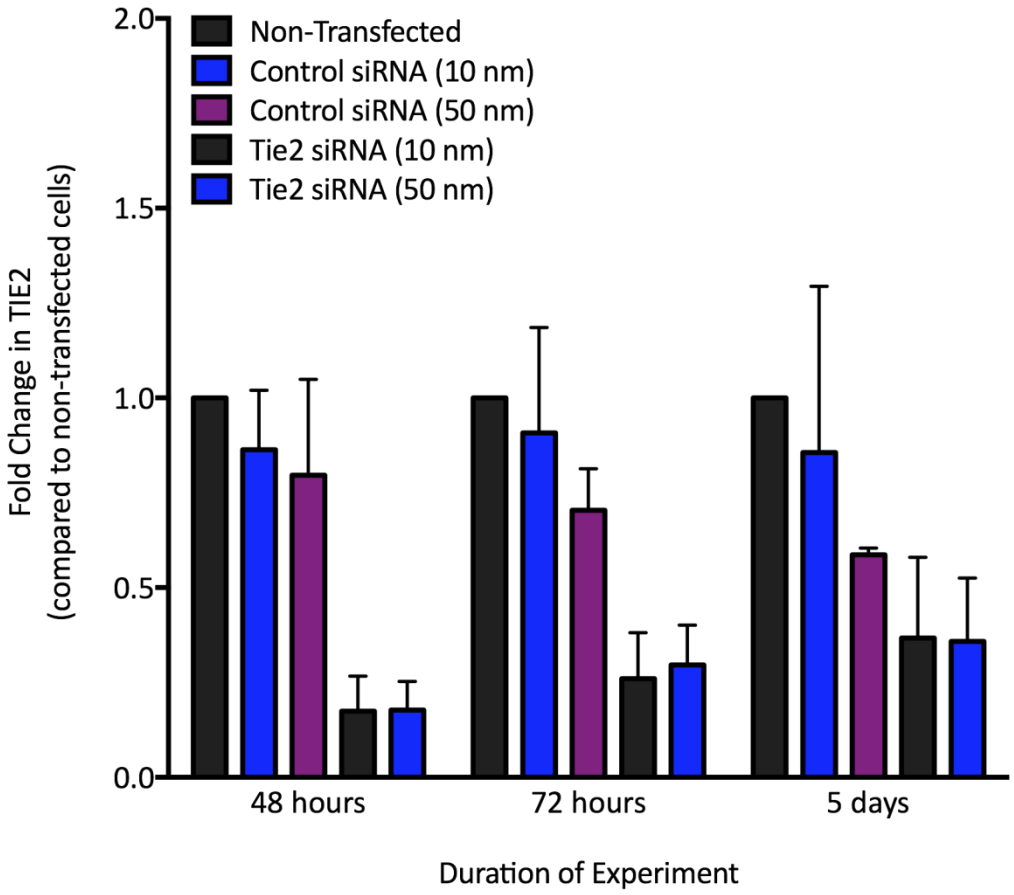

Figure 5.8: Time-course of transfected primary VSMCs

The effectiveness of two different doses of siRNA (10 nM, 50 nM) was tested at three different time-points (48 hours, 72 hours, and 5 days after transfection) to determine the duration for which the siRNA was effective at each dose. RNA collected at 48 hours exhibited reduced *TIE2* expression in cells transfected with either 10nM or 50nM *TIE2* siRNA (compared to non-transfected cells). At 72 hours, *TIE2* expression was greater than at 48 hours; however, expression was still reduced compared to non-transfected cells. At 5 days post-transfection, *TIE2* expression was similar in both control siRNA and *TIE2* siRNA transfected cells. Each experiment was done in triplicate, and the mean value was used in dCt calculations.

5.3.3 Calcium Deposition in Transfected VSMCs

Like in previous calcification experiments with non-transfected cells (Chapters 3 and 4), cells from healthy control and dialysis patients were treated with pro-calcaemic media (containing 2.7 mM calcium and 2.0 mM phosphate) with or without exogenous Angpt2 over a 5-day time-course (as described in Section 2.6.6).

Control VSMCs (*n = 3*) transfected with a scrambled sequence (control) siRNA exhibited a significant increase in calcium deposition when cultured in a pro-calcaemic medium with or without Angpt2, as compared with those cultured in media alone. When control VSMCs (*n = 3*) were transfected with *TIE2* siRNA and cultured in pro-calcaemic medium with or without Angpt2, they also exhibited a significant increase in calcium deposition compared with *TIE2* transfected control VSMCs (*n = 3*) cultured in medium alone (Figure 5.9A). There was no significant difference between VSMCs cultured in pro-calcaemic medium without Angpt2 as compared with those cultured in pro-calcaemic medium with Angpt2.

Comparatively, dialysis VSMCs transfected with a scrambled (control) siRNA sequence exhibited a significant increase in calcium deposition when cultured in the pro-calcaemic medium, as compared with control-transfected dialysis VSMCs cultured in medium alone (Figure 5.9B). This increase in calcium deposition was further and significantly increased when cells were cultured in the pro-calcaemic medium with exogenous Angpt2.

When dialysis VSMCs were transfected with siRNA specific to *TIE2*, there was again a significant increase in cells cultured in the pro-calcaemic medium compared to medium alone (Figure 5.9B). However, unlike the VSMCs transfected with the scrambled siRNA, there was no significant difference between VSMCs cultured in pro-calcaemic medium with Angpt2 and those cultured in pro-calcaemic medium without Angpt2. Most importantly, the difference between control-transfected and *TIE2*-transfected cells was significant, indicating that inhibiting *TIE2* may attenuate the increase in calcium deposition induced by exogenous Angpt2.

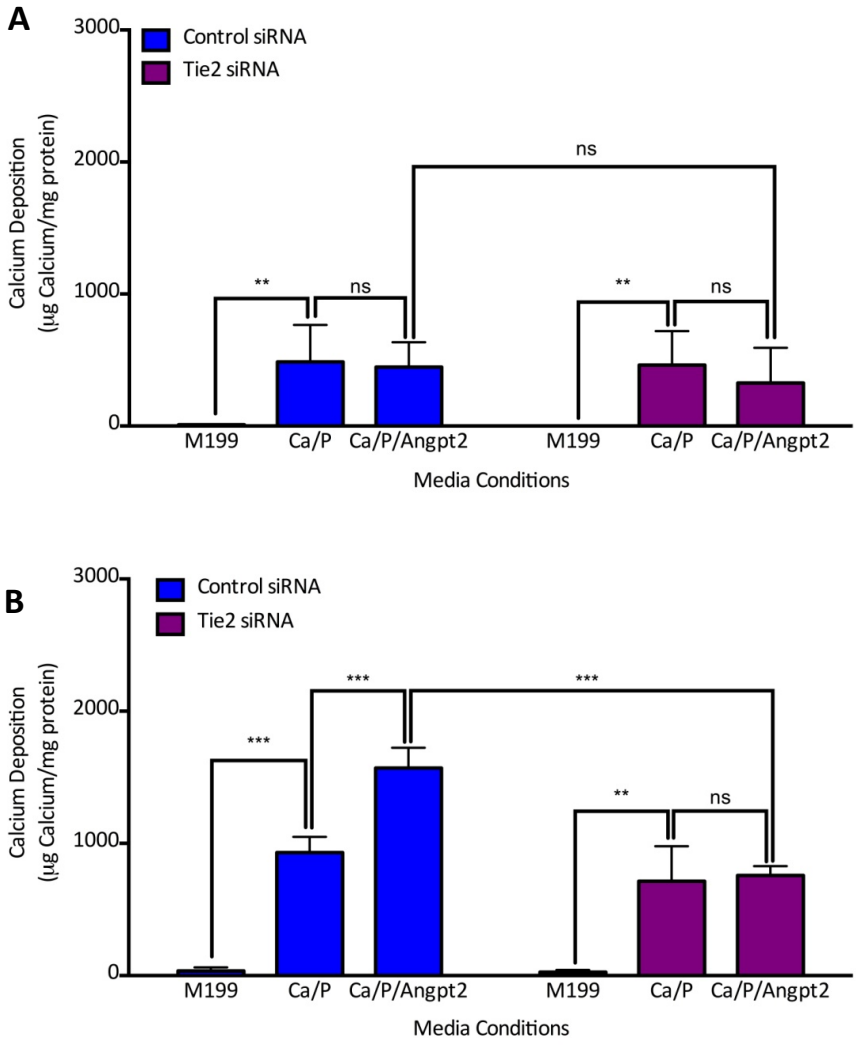

Figure 5.9: Control and dialysis VSMCs transfected with control and Tie2 siRNA
Calcium deposition was measured using the *o*-cresolphthalein colorimetric assay and normalised to protein content. **A:** Control VSMCs (*n = 3* independent cell lines) calcified when exposed to a pro-calcaemic milieu, but did not calcify further when stimulated with 25 ng/mL Angpt2; this did not change when cells were transfected with either a control siRNA or *TIE2* siRNA. **B:** Dialysis VSMCs (*n = 3*) calcified when exposed to pro-calcaemic medium; this was further enhanced in VSMCs transfected with control siRNA when stimulated with 25 ng/mL Angpt2. VSMCs transfected with *TIE2* siRNA exhibited no significant increase in calcium deposition when stimulated with 25 ng/mL Angpt2 when compared to pro-calcaemic medium alone. Each sample was run in triplicate, and the mean value was taken ($p<0.0005$ ***, $p<0.005$ **, $p<0.05$.)

These changes in calcification can also be observed visually, as depicted in the bright-field images of VSMCs in culture shown in Figure 5.10. Panels A, B, and C show dialysis VSMCs culture under low calcium and phosphate conditions (medium only), high calcium and phosphate conditions, and high calcium and phosphate conditions with exogenous Angpt2.

Using the same culture conditions, I cultured VSMCs transfected with control siRNA and Tie2 siRNA. Transfection had no obvious effect on cell proliferation, morphology, or attachment and all populations appeared healthy and proliferative after culture in medium only (Figure 5.11 A, D, G). However, nodule formation is indicated by black arrows at sites of cell interaction in all populations cultured in pro-calcaemic medium (Figure 5.11 B, E, H). Finally, non-transfected dialysis VSMCs and control-transfected VSMCs exhibited large calcium depositions (as indicated by red arrows) when cultured in the presence of Angpt2 under pro-calcaemic conditions (Figure 5.11 C, F).

When cultured in pro-calcaemic conditions containing exogenous Angpt2, dialysis VSMCs transfected with *TIE2* siRNA exhibit reduced calcium deposits as compared to those seen in the non-transfected or control siRNA-transfected VSMCs populations (Figure 5.11 I). The images in this figure are representative of three dialysis VSMC lines and confirm the quantitative differences given in Figure 5.9.

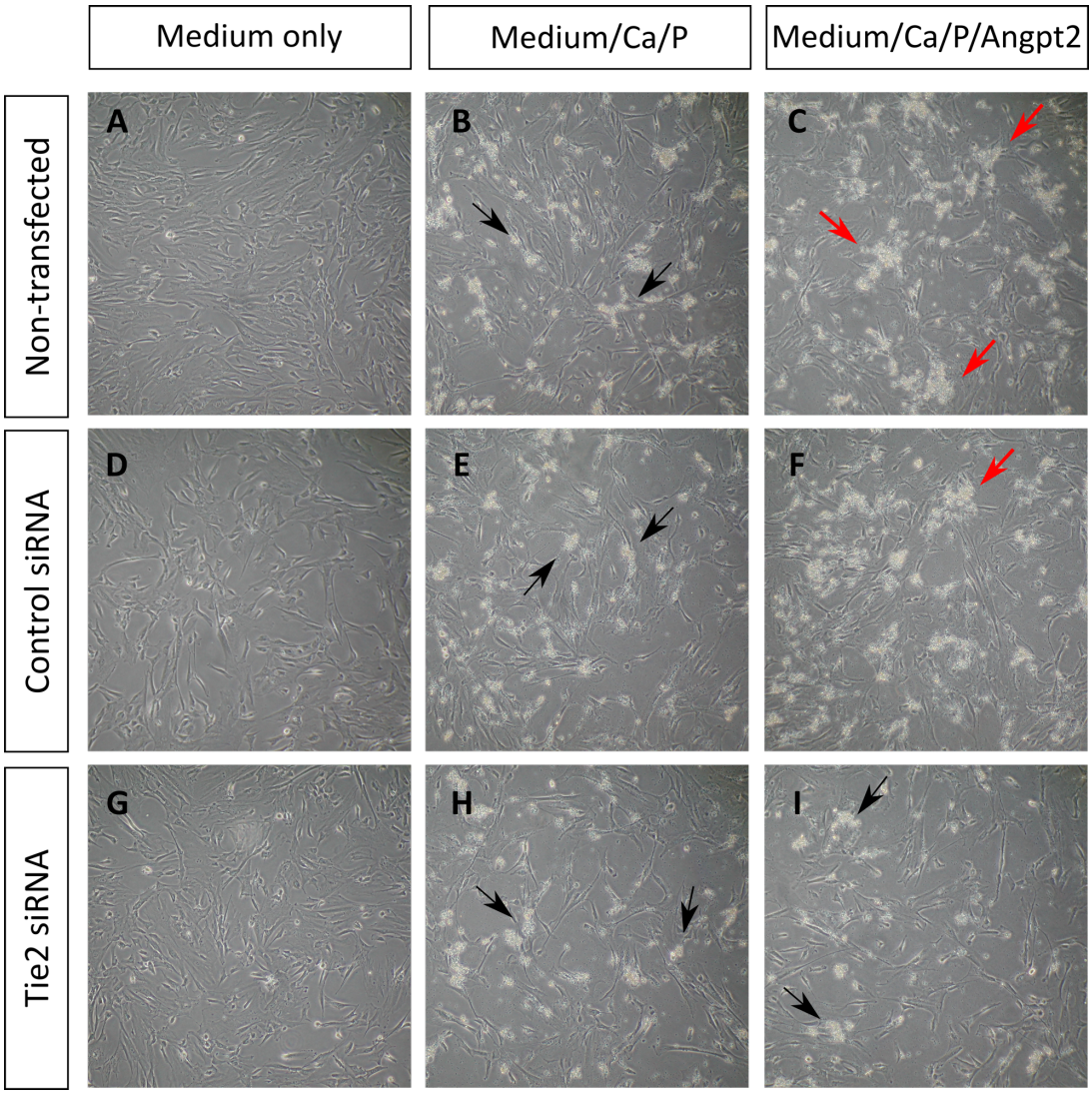

Figure 5.11: Calcium deposition in non-transfected and transfected cells

Hydroxyapatite deposits can be visualised by bright field microscopy. For these images, all medium was removed and cells were washed twice with PBS. Therefore, all depositions observed in this image are attached rather than being precipitates in the media. **A**, **D**, and **G** show cells from a patient on dialysis that are cultured in M199; no phenotypic changes are detectable between non-transfected and transfected cells. **B**, **E** and **H** show cells stimulated with 2.7 mM Ca and 2.0 mM P. The black arrows indicate examples of calcium depositions. **C** and **F** exhibit regions of heightened calcium deposition, as indicated by red arrows. Images are representative of three dialysis VSMC lines.

5.3.4 Gene Expression in Transfected VSMCs

Following transfection of the dialysis VSMCs with control and *TIE2* siRNA, the expression of both receptor tyrosine kinases (*TIE1, TIE2*), as well as the contractile gene *αSMA* and osteogenic genes *OPN, BMP2,* and *MGP* were examined to determine if any of these genes were altered by downregulating *TIE2*.

Firstly, I examined *TIE2* mRNA to determine the efficiency of my transfection (Figure 5.12A). *TIE2* mRNA was significantly decreased in cells transfected with *TIE2* siRNA as compared with cells transfected with control siRNA; this indicated that the transfection was successful and *TIE2* expression remained downregulated at the end of the experiment. However, transfection with *TIE2* siRNA also appears to result in decreased expression of *TIE1* (Figure 5.12B). Whether this is an off-target effect of the siRNA given the close homology of the two sequences, or an example of TIE2 controlling the expression of *TIE1*, is unclear. *TIE1* is downregulated under all medium conditions and this suggests that the change in expression occurs because of the siRNA.

The contractile marker *SM22α* was decreased in both dialysis VSMCs transfected with Tie2 or scrambled (control) siRNA exposed to the pre-calcaemic medium. Transcript levels of *SM22α* were significantly increased in dialysis VSMCs exposed to a pro-calcaemic medium when compared with control siRNA (Figure 5.12C). This may indicate a decreased osteogenic state; however, both *OPN* and *BMP2* show slight (but non-significant) increases in expression when transfected with *TIE2* siRNA when the VSMCs are cultured in either M199 or pro-calcaemic conditions with/without exogenous Angpt2 (Figure 5.12D, E). Similarly, there are no significant changes in *MGP* expression levels between calcification conditions (Figure 5.12F) although mean *MGP* expression is increased in the VMSCs transfected with *TIE2* siRNA in pro-calcaemic conditions with/without exogenous Angpt2. These results again support the idea that, although Angpt2 promotes calcium deposition, it does not act through enhancing these osteogenic genes.

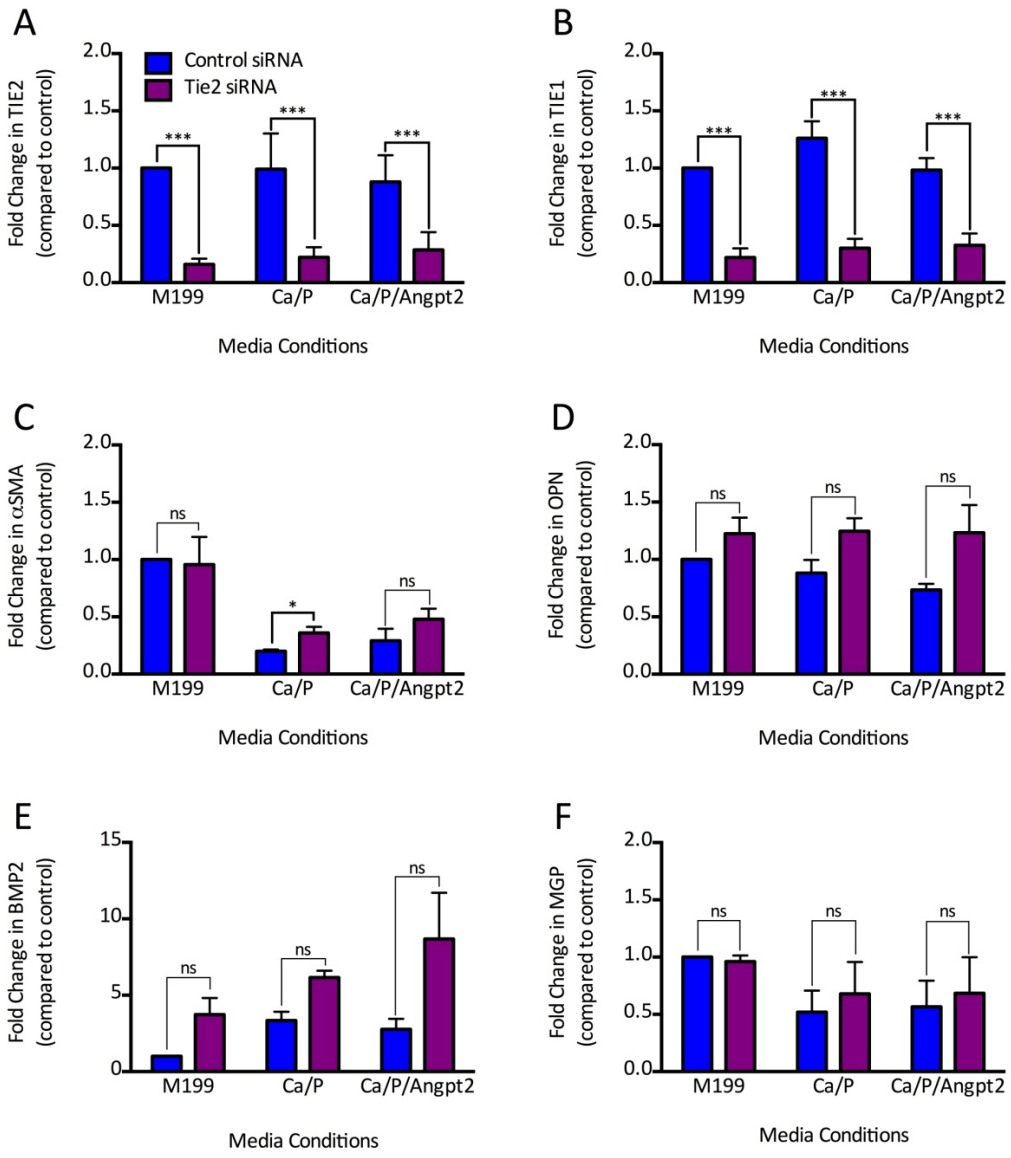

Figure 5.12: Gene expression in transfected dialysis VSMCs

Gene expression levels of *TIE1* (**A**), *TIE2* (**B**), *αSMA* (**C**), *OPN* (**D**), *BMP2* (**E**), and *MGP* (**F**) were measured in siRNA-transfected dialysis VSMCs cultured in control medium, pro-calcaemic medium, and pro-calcaemic medium with 25 ng/mL Angpt2. Each bar was based on $n = 3$, and error bars indicate standard error; note that there is a large variation between individual samples, accounting for the large error bars ($p<0.0005$***, $p<0.005$**, $p<0.05$*).

5.3.5 Targeting Tie2 Using Angpt1 Manipulation

Under most conditions, Angpt1 and Angpt2 have an agonist/antagonist relationship (Maisonpierre *et al* 1997, Yuan *et al* 2009). Therefore, I hypothesised that the addition of exogenous Angpt1 to the medium may have the opposite effect of Angpt2 and potentially reduce calcification levels. To test this, VSMCs were transfected with either control or Tie2 siRNA and stimulated with control, pro-calcaemic medium, and pro-calcaemic medium with 25 ng/mL Angpt1. Cells were harvested after 5 days and measured for calcium deposition and gene expression.

In control VSMCs, the addition of Angpt1 had no significant effect on calcium deposition compared with VSMCs cultured in pro-calcaemic medium without Angpt1. This held true if cells were transfected with either control siRNA or Tie2 siRNA (Figure 5.13). Dialysis VSMCs transfected with control siRNA exhibited a significant increase in calcium deposition when compared with cells cultured in low calcium and low phosphate medium; however, there was no significant change between control VSMCs cultured in pro-calcaemic medium with or without Angpt1 (Figure 5.13). Dialysis VSMCs transfected with Tie2 siRNA again exhibited an increase in calcium deposition when cultured in pro-calcaemic media with and without Angpt1 compared to medium alone. However, there was no difference between VSMCs culture with and without Angpt1 (Figure 5.13).

I then went on to look at gene expression levels of *αSMA, TIE1, TIE2, BMP2* and *MGP* in VSMCs stimulated with Angpt1 in the presence of high calcium and phosphate as measured using qRT-PCR (Figure 5.14). As expected, *TIE2* expression was significantly downregulated across all media conditions with the addition of *TIE2* siRNA (Figure 5.14A). In accord, with my previous findings, I also found that *TIE1* expression was also significantly downregulated across conditions with the addition of *TIE2* siRNA (Figure 5.14B). Interestingly, the expression level of *αSMA* was significantly increased in *TIE2* siRNA transfected cells stimulated with calcium and phosphate, and there was a slight, but not significant, increase in *αSMA* expression in pro-calcaemic conditions with the addition of Angpt1 VMSCs when transfected with *TIE2* siRNA (Figure 5.14 C). This suggests that inhibiting Tie2 signalling within these

culture conditions has the potential to attenuate the level of *αSMA* loss due to high calcium and phosphate.

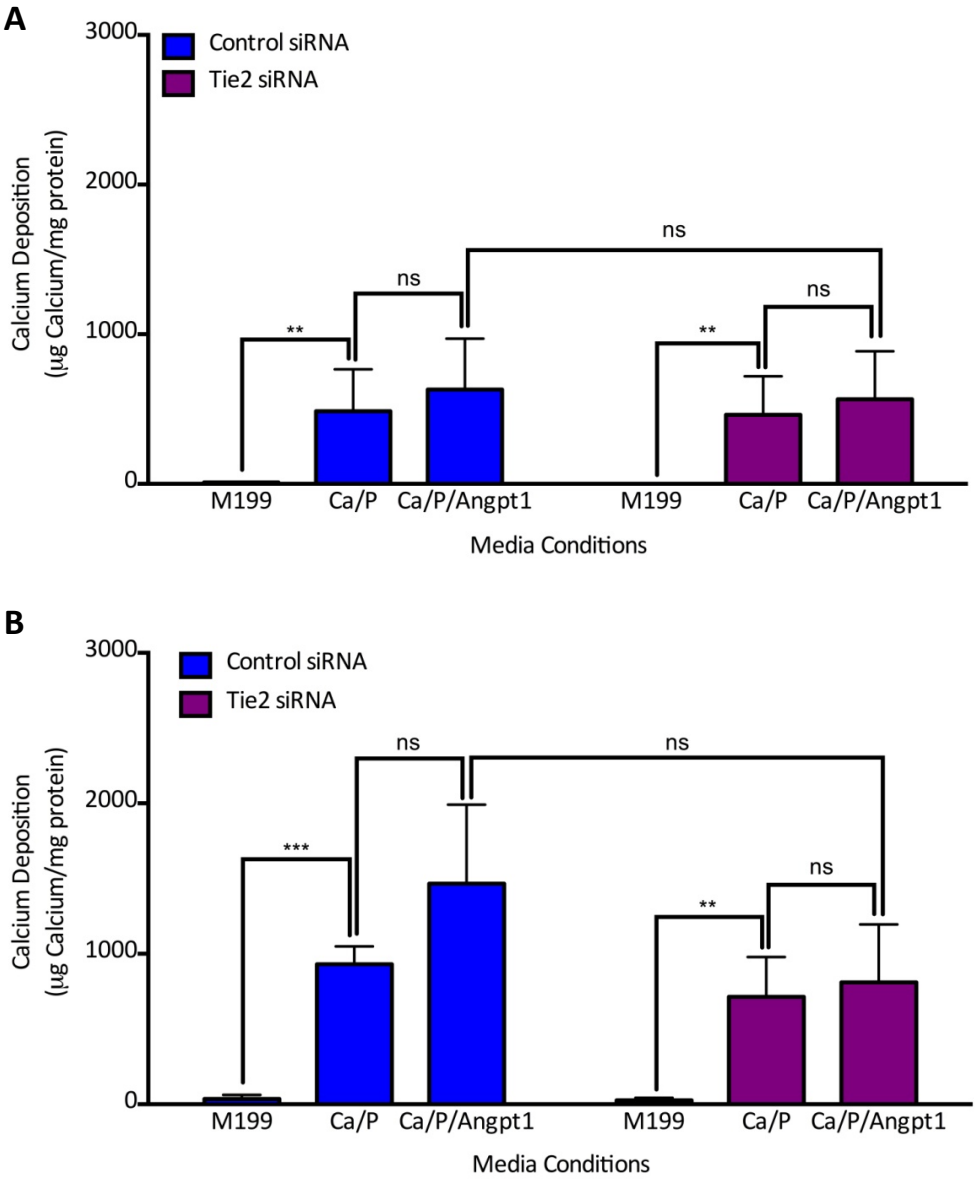

Figure 5.13: Calcium deposition in VSMCs stimulated with Angpt1

Control VSMCs (*n = 3*) transfected with either control or Tie2 siRNA exhibit no significant changes when stimulated with 25 ng/mL Angpt1. This does not differ between cells transfected with control or Tie2 siRNA. Dialysis VSMCs (*n = 3*) transfected with control or Tie2 siRNA exhibit no significant change when stimulated with Angpt1, although there is a trend towards increased calcium deposition with Angpt1 stimulation in cells transfected with control siRNA. Each sample was run in triplicate ($p<0.0005$***, $p<0.005$**, $p<0.05$*).

There is no significant difference between *OPN* expression in VSMCs transfected with either control siRNA or *TIE2* siRNA in either VMSCs cultured in M199 alone, or those cultured with calcium and phosphate. However, there is a significant increase in the level of *OPN* expression in those cells transfected with siRNA to *TIE2* when stimulated with calcium, phosphate and Angpt1 (Figure 5.14 D). Finally, transfection of VSMCs with siRNA to *TIE2* appears to have no significant effect on the expression level of osteogenic promoter *BMP2* or osteogenic inhibitor *MGP* in VMSCs cultured in M199 alone, or those cultured with calcium and phosphate with or without the addition of exogenous Angpt1 (Figure 5.14 E and F, respectively).

5.3.6 Inhibition of Tie2 Activity in Intact Vessel Rings

A second Tie2 inhibition method was utilised on the intact vessel rings when cultured *in vitro* over a 14-day time-period. Rather than utilising siRNA, a synthetic inhibitor of Tie2 was utilised in an attempt to reduce calcium deposition. When arterial rings from vessels obtained from dialysis patients ($n = 5$) were cultured for 14 days in pro-calcaemic medium containing both 25 ng/mL Angpt2 and the Tie2 inhibitor, four of the vessels exhibited reduced calcium content when compared with their corresponding rings cultured in pro-calcaemic medium with 25 ng/mL Angpt2 (without the Tie2 inhibitor); one of the dialysis vessels exhibited no change in calcium deposition between these culture conditions (Table 5.1, Figure 5.15). However, the decrease in mean calcium deposition (172.51±68.14 µg Ca/µg vs. 259.29±108.37 µg Ca/µg, with, and without, the Tie2 inhibitor respectively) – as measured using µg Ca/µg protein – was not statistically significant ($p = 0.517$); this is likely due to the large variation between individual samples.

Two control vessels were treated with the Tie2 inhibitor for the course of the 14-day experiment, and cultured in pro-calcaemic media with and without Angpt2. However, as the vessels rings did not calcify in the presence of high calcium and phosphate and there was low vessel availability, there are no statistics for this experimental group (Table 5.1, Figure 5.15).

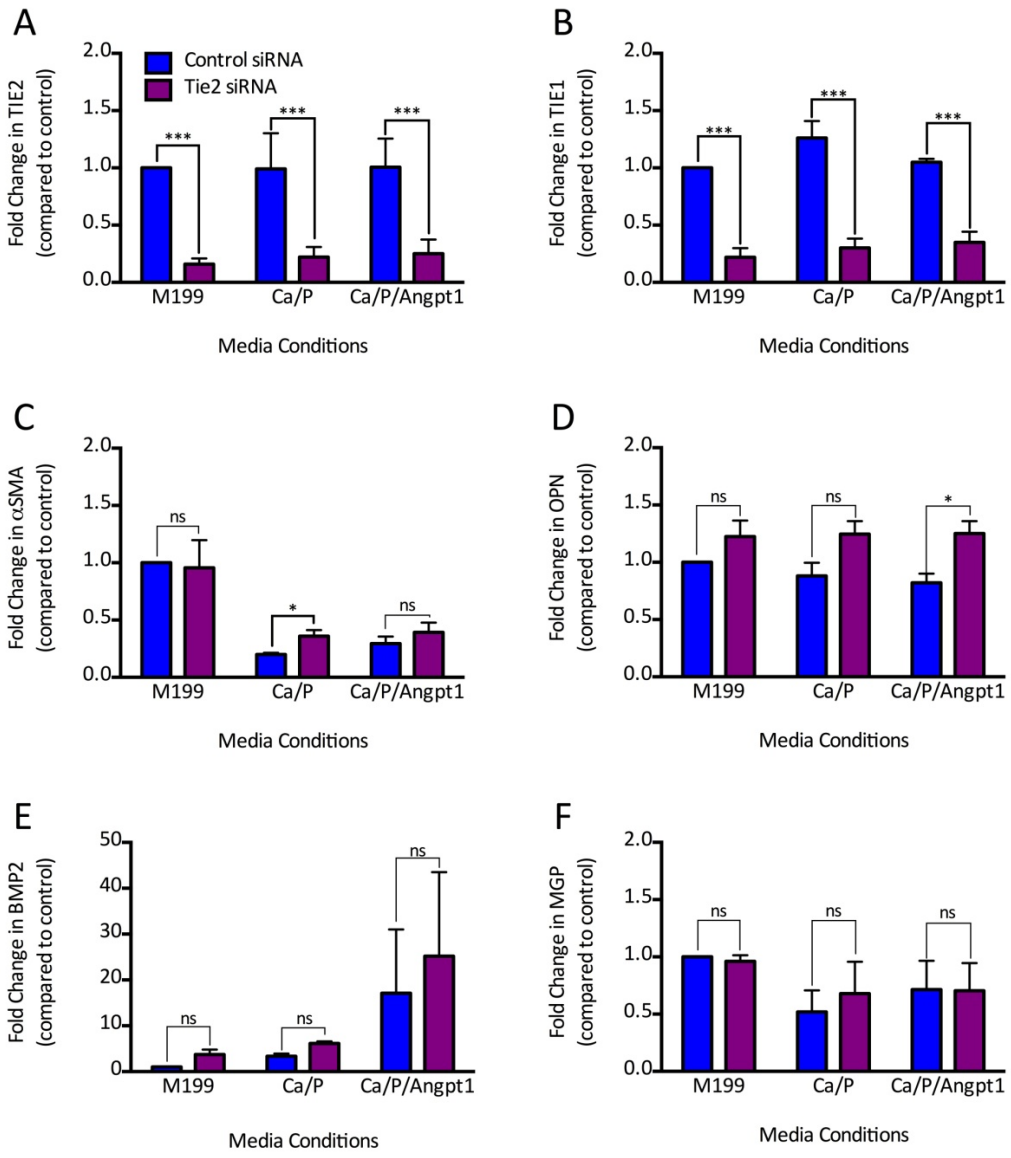

Figure 5.14: Gene expression in transfected dialysis VSMCs

Gene expression levels of *TIE1* (**A**), *TIE2* (**B**), *αSMA* (**C**), *OPN* (**D**), *BMP2* (**E**), and *MGP* (**F**) were measured in siRNA-transfected dialysis VSMCs cultured in control medium, pro-calcaemic medium, and pro-calcaemic medium with 25 ng/mL Angpt1. Each bar represents the mean ± standard error of three individual VSMC samples (n = 3), equating to three different patients on dialysis. Each sample was run in duplicate to ensure consistency of the qPCR. Note that there is a large variation between individual samples, accounting for the large error bars ($p<0.0005$ ***, $p<0.005$ **, $p<0.05$*).

	Type of Artery	Baseline (µg /µg)	M199 (µg /µg)	CaP (µg /µg)	CaP +Angpt2 (µg /µg)	CaP+Angpt2 +Tie2Inh (µg /µg)
Control A43	Mesenteric	17.13	21.22	21.14	20.68	32.21
Control A44	Mesenteric	1.35	3.00	2.81	2.80	6.10
Dialysis A40	Inf. Epi.	108.90	128.85	343.73	604.28	281.23
Dialysis A42	Inf. Epi.	10.91	12.02	85.53	118.45	60.37
Dialysis A41	Inf. Epi.	63.96	65.63	211.60	424.43	386.06
Dialysis A46	Inf. Epi.	7.56	11.03	36.40	57.73	47.67
Dialysis A48	Inf. Epi.	17.34	42.12	61.24	91.54	87.24

Table 5.1: Calcium deposition in control and dialysis vessel rings, following culture in pro-calcaemic conditions, treated with Angpt2 and a Tie2 inhibitor
Arteries utilised are: the mesenteric artery, and the inferior epigastric artery (shortened to 'Inf. Epi.' in the table above). All raw calcium values are given in µg calcium per µg protein. M199 = serum-free M199, Ca = 2.7 mM calcium, P = 2.0 mM phosphate, Angpt2 = 25 ng/mL, and Tie2Inh = a synthetic Tie2 inhibitor. Note that data is repeated from Table 3.1, with the addition of the last column, which shows calcium levels following treatment with the synthetic Tie2 inhibitor.

However, as with the calcium deposition data in Section 3.1.3, the fold-change was calculated for each vessel to account for individual patient variation. This standardises the patient data and reflects the proportional magnitude of the changes. Change in calcium content is therefore represented as the fold-change, compared with the vessel rings cultured in medium alone, which was given an arbitrary value of 1 (Figure 5.16). Again, there are no statistical calculations based upon the controls due to low sample numbers (*n = 2)*. However, there was a 3.9±0.76 fold increase in calcium deposition in dialysis vessels cultured with 25 ng/mL Angpt2 in a pro-calcaemic medium when

treated with a Tie2 inhibitor, compared to dialysis vessels cultured in control medium. Although this is a significant increase compared to arterial rings cultured in medium alone ($p = 0.012$), this fold-change is decreased from the arterial rings cultured under the same conditions without Tie2 inhibition (5.68±1.26), but not significantly different between these two groups.

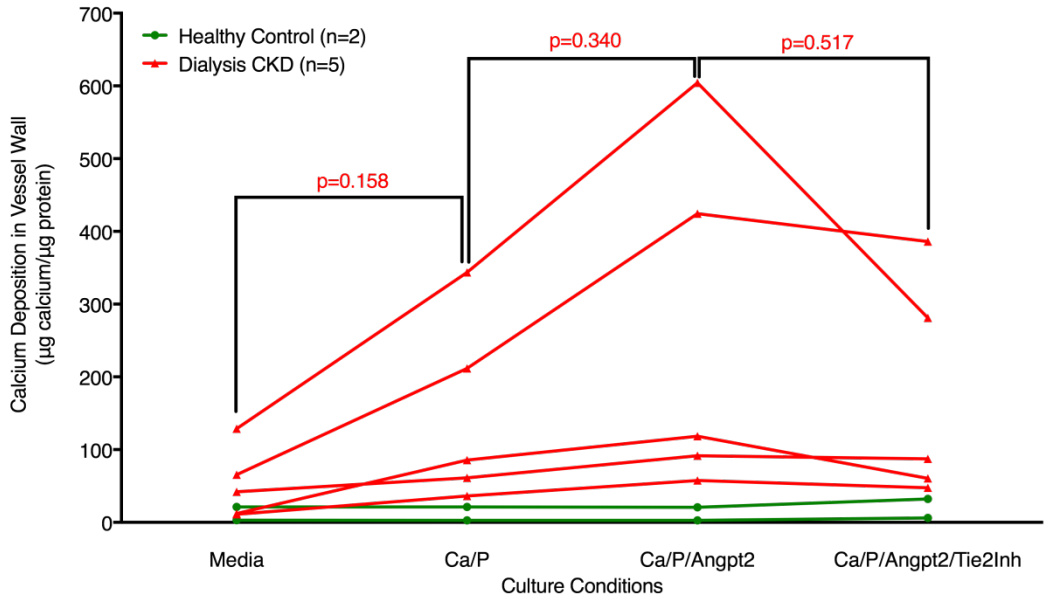

Figure 5.15: Calcium deposition of intact arterial rings, treated with Tie2 inhibitor (µg Ca/µg protein)

Calcium content, as measured using the *o*-cresolphthalein colorimetric assay, was normalised to the protein content of the respective arterial ring after 14 days in culture. The synthetic Tie2 inhibitor was only utilised on two control samples, of which one sample calcium load increased while in the other calcium load decreased. All dialysis samples ($n = 5$) showed either a reduction in calcium load when treated with the Tie2 inhibitor over the 14-day experiment, or no change ($p = 0.517$). Each sample was run in duplicate to obtain an absorbance value.

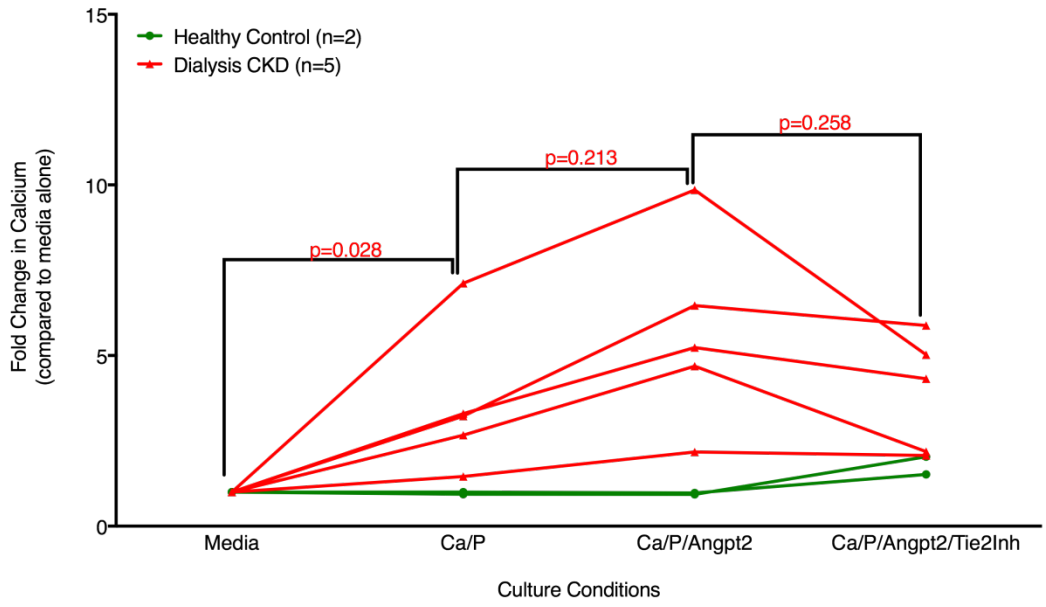

Figure 5.16: Calcium deposition in arterial rings treated with a synthetic Tie2 inhibitor (fold-change)

Calcium content, normalised to the protein content, of each arterial ring was measured (µg calcium per µg protein). Each vessel was used as its own control, and the calcium content was compared to the calcium content in the ring that was cultured in the medium alone, which was given an arbitrary value of 1. Control (n = 2) and dialysis vessels (n = 5) exhibited no significant differences in calcium load between key conditions of interest (Ca/P/Angpt2 and Ca/P/Angpt2/Tie2Inh; dialysis: p = 0.258); however, this may be due to the small sample size. No p-values are given for control vessels as there were only two samples tested.

5.4: Conclusion

My previous work in this thesis indicated that *TIE2* (typically an endothelial marker) was detected in isolated VSMCs from the paediatric population. Therefore, the presence of this receptor was further examined to confirm the legitimacy of its expression. To do so, a combination of conventional PCR, qRT-PCR, sequencing of the amplified production, and Western blotting of paediatric VSMC protein isolates was utilised; each test indicated that Tie2 was indeed present in the isolated VSMCs, which suggests that the receptor may be a potential pathway through which vascular growth factor Angpt2 may act upon smooth muscle. Furthermore, immunostaining indicated that the intact arterial rings also express TIE2 within the tunica media;

therefore, the expression observed in the isolated VSMCs is not likely to be an artefact induced during explant culture.

In vitro downregulation of TIE2, utilising siRNA specific to *TIE2*, indicated that reduction of the receptor did not reduce overall calcification in response to culture in a pro-calcaemic environment. However, when VSMCs were cultured in a pro-calcaemic environment with 25 ng/mL Angpt2, the dialysis VSMCs transfected with *TIE2* siRNA did not exhibit the augmentation in calcium deposition that was otherwise observed in the VMSCs transfected with control siRNA. This suggests that Tie2 is a critical receptor with which Angpt2 interacts to enhance calcification in a pro-calcaemic environment.

However, subsequent *in vitro* experiments utilising intact arterial rings were less conclusive. Through use of a chemical inhibitor targeting Tie2 phosphorylation, a slight trend was observed in which the calcium deposition in dialysis arterial rings was decreased when the inhibitor was present in a 14-day culture in a pro-calcaemic containing 25 ng/mL Angpt2. However, this result was not statistically significant and it would be beneficial to look into this further with a larger sample size, as these preliminary results suggest that Tie2 may play a key role in signalling for an increase in calcium deposition in paediatric dialysis VSMCs.

Chapter 6: Conclusion and Discussion

6.1: Overall Conclusions

6.1.1 Main Conclusions

The main conclusions of the work performed in my PhD thesis are:

Conclusion 1: Exogenous Angpt2 significantly increases calcium deposition in arterial rings and VSMCs from dialysis CKD patients cultured in a pro-calcaemic environment. Under pro-calcaemic conditions (2.7 mM Ca, 2.0 mM P), representing hypercalcaemia and hyperphosphataemia *in vivo*, Angpt2 can drive calcification in both arterial rings and isolated VSMCs from patients with CKD that have undergone dialysis. Although, at a cellular level, I found no significant differences in gene expression between cells of control, pre-dialysis CKD patients, and dialysis CKD patients, the vessels of dialysis patients appear to be 'primed' to respond to exogenous Angpt2 which subsequently leads to augmentation of the calcification process.

Conclusion 2: The angiopoietin receptor Tie2 is expressed on VSMCs and in the tunica media of arterial rings. My data has also highlighted that both the vessels and VSMCs (across disease states) express the angiopoietin receptor Tie2, which has typically been denoted as an endothelial cell specific receptor. Given this, I propose that Angpt2 acts by binding and stimulating Tie2 on VSMCs. However, the downstream pathophysiological mechanisms are, as of yet, undetermined. In this thesis, examination of some of the pathophysiological processes implicated in vascular calcification including changes in osteogenic gene expression, the release of matrix vesicles, and apoptosis, have shown no clear lead as to the mechanism by which Angpt2 promotes this pathogenicity.

Conclusion 3: Decreasing *TIE2* expression reduces calcium deposition in dialysis VSMCs stimulated with Angpt2 to the level of pro-calcaemic medium alone. Downregulation of Tie2 expression using siRNA in VSMCs was shown to decrease

calcium deposition in the presence of Angpt2. This is an encouraging finding, as the potential to dampen Tie2 expression in VSMCs may provide a pathway for investigation into novel therapy for vascular calcification in CKD patients on dialysis.

Conclusion 4: Targeting Tie2 activity using a synthetic inhibitor shows a trend towards decreased calcium deposition. In vessel rings, the addition of a synthetic inhibitor of Tie2 activity slightly decreased the calcium content of the vessel rings though the result was not significant. It is possible that with a greater number of vessels, one could more conclusively determine the effects of this inhibitor.

Conclusion 5: Angpt2 and Angpt1 do not act in an agonist: antagonist relationship in calcification. Finally, it was initially proposed that restoring the balance of the angiopoietins to favour Angpt1 might negate the effects of Angpt2 in vascular calcification. However, when VSMCs were stimulated with exogenous Angpt1 in the presence of elevated calcium and phosphate, calcium deposition remained similar to cells cultured in the pro-calcaemic medium alone.

6.1.2 Summary of Conclusions

Collectively, the results of my thesis indicate that Angpt2 is not simply a biomarker of CVD in children with CKD, but also an active participant that enhances vascular calcification in these patients. Given that my work has focused on isolated VSMCs in culture and that I have also shown by immunostaining that vessel rings are devoid of CD31 positive staining, it is unlikely that the effects of Angpt2 on vascular calcification are due to changes in endothelial cells. On this basis, I believe that the enhanced calcium deposition associated with exogenous Angpt2 stimulation is a result of changes in the VSMCs (Figure 6.1). However, as the two populations co-exist *in vivo*, further examination of the interaction between the two systems would be beneficial to future work.

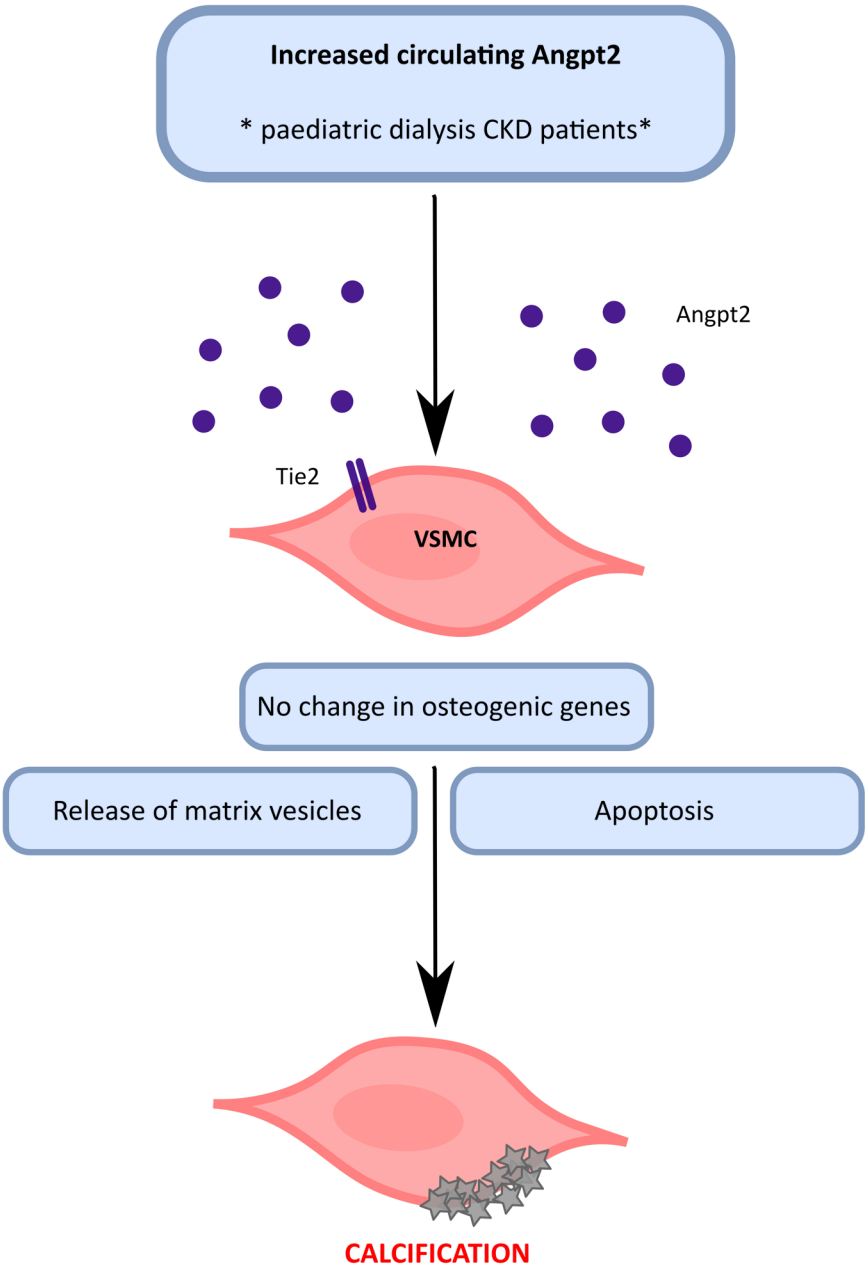

Figure 6.1: Summary of my findings

Paediatric patients on dialysis exhibit increased circulating levels of Angpt2 (Shroff *et al* 2013). As VSMCs express the transmembrane receptor tyrosine kinase Tie2, Angpt2 has the potential to act directly upon the SMCs of the vasculature. In the presence of elevated calcium and phosphate, Angpt2 induces calcification of VSMCs. Although the exact mechanism remains unknown, Angpt2 does not appear to drive vascular calcification through alterations in osteogenic genes.

6.2: Discussion

6.2.1 Angiogenic Growth Factors in VSMCs During CKD

The hypothesis for my thesis was derived from previous research from our laboratory, in which circulating Angpt2 was significantly increased in paediatric patients on dialysis (Shroff *et al* 2013). Immunostaining of intact arterial rings indicated that both the tunica media and the endothelium were potential sources of Angpt2; however, scoring of staining intensity indicated that there was no significant difference between Angpt2 expression in pre-dialysis vessels and dialysis vessels (Shroff *et al* 2013). While it has now been well established that Angpt2 increases in correlation with CKD severity in adults and children (Shroff *et al* 2013, David *et al* 2012), this thesis provides the first study that I am aware of that suggests that a vascular growth factor may be responsible for promoting vascular calcification through a smooth muscle-based mechanism.

To my knowledge, there is only one other study currently examining the relationship between Angpt2 and VSMCs in CKD. In this study Chang and colleagues (2014) found a correlation between increased circulating plasma Angpt2 and arterial stiffness in adult patients with CKD stages 3–5. The investigators went on to use animal models to attempt to tease-out the potential pathological consequences of elevated circulating Angpt2. Using adult male CD1 mice that had undergone a 5/6 subtotal nephrectomy, they showed that plasma Angpt2 was increased 4 and 8 weeks after surgery (Chang *et al* 2014). This was accompanied by an increase in transcript levels of *Col1al* and *Col3a1* in the thoracic aorta (Chang *et al* 2014); these genes are associated with the production of ECM, which is a feature of contractile VSMCs (Chen *et al 199,* Tsai *et al* 2009). The investigators then overexpressed Angpt2 by adenovirus in reporter mice expressing enhanced green fluorescent protein (GFP) under the regulation of the *Colla1* promoter and enhancer *Coll-GFP*$_{Tg}$. When Angpt2 was overexpressed in these mice, there was a notable increase in collagen transcripts in the VSMCs of the tunica media, whilst there was no change in collagen expression in the endothelial cells (Chang *et al* 2014). Comparatively, collagen expression was only exhibited in the adventitia of control vessels at a similar level to that observed in vessels from Angpt2 overexpressing mice (Chang *et al* 2014). These findings indicated that elevated

circulating Angpt2 could alter the biology of VSMCs. Future studies should examine components of ECM such as collagen, elastin, fibronectin and laminin in our VSMCs from children on dialysis exposed to exogenous Angpt2 in pro-calcaemic conditions.

6.2.2 Expression of Tie2 In Non-Endothelial Cells

Notably, the study described from Chang and colleagues (2014) highlighted that Tie2 expression was not observed within the VSMCs of the aorta in normal adult mice by immunohistochemical techniques, despite exhibiting an Angpt2-related increase in collagen expression. Instead, this study showed that both endothelial cells (by immunostaining) and a subpopulation of macrophages (by FACS analysis) expressed Tie2 (Chang *et al* 2014). Interestingly, the researchers also found that collagen transcription was not upregulated in isolated VSMCs exposed to exogenous Angpt2 (500 ng/mL) *in vitro*. They therefore proposed that the increase in collagen transcription might be related to an increase in pro-inflammatory cytokine release from the surrounding endothelial cells and macrophages, as well as the subsequent inflammation cascade (Chang *et al* 2014).

While Chang *et al* (2014) noted that Tie2 was not present on the VSMCs of the aorta of normal adult mice, one of the key findings of this thesis was that Tie2 expression can occur in the tunica media of paediatric blood vessels as well as in primary VSMCs isolated from the blood vessels of paediatric patients. Tie2 is traditionally known as an endothelial-specific receptor, and is used in many mouse models to generate *Cre* recombinase lines that target the endothelium (Kisanuki *et al* 2001). I was originally sceptical of these findings (thus accounting for my detailed examination into gene expression of the isolated VSMCs cells and the interest in determining whether they had a 'true' VMSC phenotype) but both RNA and protein for Tie2 were measured in my samples. To my knowledge, this is the first study highlighting Tie2 expression in human VSMCs.

There are several potential explanations for the apparent discrepancy between my human findings and the murine studies of Chang and colleagues (2014). Firstly, the expression of Tie2 in VSMCs might be restricted to childhood vessels. In the future, it would be informative to collect and explore Tie2 expression in adult human vessels

from CKD patients. Secondly, there is considerable heterogeneity in gene expression between different vascular beds (Aird 2007). Therefore, it is possible that smaller inferior epigastric vessels collected from the paediatric CKD patients might have a different expression pattern to the adult mouse aorta.

There is an increasing body of evidence that indicates that Tie2 can be expressed in non-endothelial sites in both humans and mice. Monocytes, a subpopulation of leukocytes derived from the bone marrow have, to-date, been the most well examined population of non-endothelial Tie2 expressing cells and possess increased vascularisation capabilities and are prevalent in cancer angiogenesis (De Palma *et al* 2005). A subset of pro-angiogenic myeloid cells, usually present in tumours, are termed 'TIE2-expressing monocytes/macrophages' and are shown to release high levels of IL-10, a cytokine that reduces T-cell activity and helps to suppress the immune system (Coffelt *et al* 2011). During tumorigenesis, increased Angpt2 appears to contribute to tumour vascularisation and metastasis by further augmenting release of IL-10 and encouraging pro-angiogenic signalling (Coffelt *et al* 2011; Welford *et al* 2011). Although not directly related to CKD, these studies highlight that Tie2 expression outside the endothelium is possible and can have detrimental effects.

The therapeutic potential of this TIE2-expressing monocyte population has been examined in patients requiring revascularisation of ischaemic limbs (Patel *et al* 2013). Patel and colleagues (2013) found that ANGPT2, VEGFA, and soluble TIE2 were significantly increased in patients with critical limb ischaemia when compared to age-matched controls, as were TIE2-expressing monocytes. Subsequent modelling in mice with severe hind limb ischaemia demonstrated that, following the induction of ischaemia, the proportion of circulating TIE-2-expressing monocytes increased; this increase in circulating TIE-2 monocytes increased with a linear relationship to the length of ischaemia (Patel *et al* 2013). When *Tie2* was silenced in bone marrow-derived haematopoietic stem cells (using a doxycycline-inducible lentiviral vector construct), the recovery of blood perfusion to the ischaemic limb was significantly decreased 28 days later. These functional experiments suggested that these TIE2-expressing monocytes were an important component of revascularisation (Patel *et al* 2013). Finally, when TIE2-expressing bone marrow-derived macrophages were

injected directly into the ischaemic hind limb, revascularisation was significantly improved (Patel *et al* 2013).

Glial cells in astrocytoma have also been shown to express Tie2, as detected by immunohistochemistry, while Tie2 expression is not observed in healthy brain tissue (Lee *et al* 2006). As with monocytes and pericytes, these astrocytoma glial cells are negative for CD31 (which would indicate an endothelial lineage). The cohort examined consisted of 25 adult histology samples; within these samples, the intensity of immunological expression strongly correlated with disease severity (Lee *et al* 2006). In these samples, the expression of Tie2 is believed to play into the disease pathologies of astrocytoma by increasing cell attachment to both collagen and the ECM in response to Angpt1 (Lee *et al* 2006). With these altered characteristics, these malignant glioma cells have an improved adherence capability that helps to ensure their proliferation and survival, thereby contributing to the aggressive nature of the disease (Lee *et al* 2006).

Whilst this thesis is the first study, to my knowledge, to examine Tie2 expression in human VSMCs, it is not the first study to suggest that Tie2 can be expressed in SMCs overall. The first known study to observe Tie2 expression in SMCs utilised a xenograft model of breast cancer, in which Angpt1 was used to stabilise the vasculature and prevent the formation of new blood vessels (Tian *et al* 2002). Upon observation of SMC infiltration into the Angpt1 overexpressing tumours, the investigators went on to examine Tie2 expression in cultured human coronary artery SMCs. Using Western blotting, this SMC population was determined to be Tie2 positive, although at a lower level than endothelial cells (Tian *et al* 2002).

A second study investigating Tie2 expression was again conducted in a mouse model, in which ‘mural precursor cells’ (which I believe to be pericytes) were isolated from mouse aortas using a non-enzymatic method (Iurlaro *et al* 2003). These ‘mural precursor cells’ migrated towards either Angpt1 or Angpt2 in chemotactic assays, and they did so in a dose-dependent manner (Iurlaro *et al* 2003). Tie2 was shown to be present in these cells, as detected using Western blotting and qRT-PCR (Iurlaro *et al* 2003). Staining of the intact vessel rings localised Tie2 to the intimal and sub-intimal layers of the tunica media (Iurlaro *et al* 2003). These mural precursor cells also

expressed αSMA, while not expressing the endothelial marker CD31 (Iurlaro *et al* 2003). Although both studies were in mice, the results that I have obtained using paediatric vessels suggest that Tie2 is similarly expressed in human vessels.

6.2.3 Plasticity of VSMCs in Culture

One of the contentious issues surrounding VSMC studies is the tendency of these cells to de-differentiate in culture, and take on a non-contractile, mesenchymal-like phenotype. In this study, I have purposely limited the use of commercially-obtained VSMCs to the role of a control VSMC line, to which gene expression is compared to for characterisation. Baseline characterisation of contractile, osteogenic, and angiogenic genes (Sections 3.3.4–3.3.6) suggested that there was only slight variation between control VSMCs isolated from paediatric patients and the commercially-obtained VSMCs; however, these expression levels were measured early on in culture and may not be representative of the lines as they age.

Limited availability of the tissue, for both isolation of cells and intact arterial ring culture, is one of the major restrictions to this work. Although isolating VSMCs allows for subsequent passaging and expansion of the primary cell population, VSMCs can dedifferentiate spontaneously in culture and take on a 'synthetic' phenotype (Chamleu *et al* 1974). This is almost an accepted aspect of VSMC culture and experimentation now, but in a concerted effort to maintain the contractile phenotype of the VSMCs all experiments in this thesis were done under passage 9. Similarly, if cells developed an immature phenotype with a flattened, multi-nucleated, and non-proliferative appearance, they were not used for subsequent experiments (Chamleu *et al* 1974). One of the key issues with commercially-obtained VSMCs is the age of the individuals from which they were isolated, as they are obtained from adults rather than children, and thus may not accurately represent the paediatric physiology. To avoid this conflict, paediatric VSMCs were utilised for all calcification experiments. One observation, although not quantitatively measured, was that VSMCs isolated from young (1–2 years of age) and healthy control patients maintained the contractile phenotype more readily in culture; dialysis VSMCs, on the other hand, were more likely to spontaneously calcify in culture, take on the synthetic phenotype, or enter senescence (Shanahan 2013). An increasing body of evidence points towards the protein prelamin A, a

precursor to the critical laminar protein lamin A, as a key player in VSMC senescence (Liu *et al* 2013; Ragnauth *et al* 2010; Shanahan 2013). *In vitro* culture experiments of healthy VSMCs have shown that oxidative stress (as simulated using both short-term, high-dose exposure and long-term, low-dose exposure to hydrogen peroxide) can lead to prelamin A accumulation and early cell cycle arrest (Ragnauth *et al* 2010). Similarly, Ragnauth and colleagues (2010) have shown that, following exposure to hydrogen peroxide, healthy paediatric arterial rings exhibit accumulation of prelamin A in over 90% of medial VSMCs. Liu and colleagues (2013) have gone on to show that prelamin A is accumulated in the VSMCs of paediatric dialysis patients when compared with healthy paediatric controls, as measured using both VSMC cultures and sectioned arterial rings. With these studies in mind, prelamin A is a potential protein to explore further in regard to differential expression between control and dialysis VSMCs as it would be interesting to see if accumulation was accelerated with the addition of Angpt2.

Another problematic aspect of VSMC culture was the wide variation between individuals, in regard to both baseline levels of gene expression and baseline levels of calcium deposition. For example, the baseline calcium level (Figure 3.1) in healthy paediatric controls (n = 3) was 15.7±13.7 µg calcium/ µg protein, compared with 36.3±21.1 µg calcium/ µg protein in pre-dialysis patients (n = 3) and 36.8±35.9 µg calcium/ µg protein in dialysis patients (n = *8*). This level of variation indicated that, even within our patient stratifications (healthy renal function, pre-dialysis CKD, and dialysis CKD), it is difficult to control for patient heterogeneity.

There is also debate as to whether other subpopulations of cells might exist alongside VSMC in the tunica media (Boström *et al* 1993, Doherty *et al* 1998, Tintut *et al* 2003). Interestingly, one of the first studies indicating *BMP2* expression in spontaneous VSMC calcified nodules also noted a third (non-endothelial, non-vascular smooth muscle) cell population in the tunica media, and proposed these cells to be pericyte-like cells (Boström *et al* 1993). While pericytes are involved in stabilisation of neovessels during angiogenesis, they also appear to be able to differentiate into osteoblasts, chondrocytes, adipocytes, and fibroblasts (Doherty *et al* 1998). These calcifying vascular cells have been named as a separate population by other researchers, and whilst not defined as pericytes, they are believed to be a subpopulation

of the medial VSMCs and are shown to express both contractile and osteogenic markers (Tintut *et al* 2003). One issue with these 'calcifying vascular cells' is that they are suggested to be 'self-renewing' and can maintain their proliferative capacity through 20 passages (Tintut *et al* 2003). Whilst the cells isolated in this thesis have not been pushed to proliferate through to this number of passages, the reduced rate of growth observed in later passages suggests that these cells do not possess this characteristic. Another possibility is that the VSMCs in paediatric vessels possess an immature phenotype, which allows for increased plasticity and repair of the vessel. This may account for the ability of healthy control vessels to resist calcification when stimulated with high calcium and phosphate media; however, this may be better examined using RNA isolated from fresh vessels rather than from isolated cells as was done in this thesis. To investigate this immature phenotype, genes and proteins associated with senescence (i.e. prelamin A, mentioned earlier) could be measured in these samples along with markers of DNA damage and cell cycle arrest (i.e. p53, p16) (Leopold 2015).

6.2.4 Differential Response to Calcification: Baseline Gene Expression

An interesting concept brought up by the work in this thesis is the differential response to a high calcium environment between control, pre-dialysis, and dialysis vessels and cells. It has previously been suggested by Shroff and colleagues (2010) that vessels from patients on dialysis may be 'primed' to calcify, due to changes in their vascular biology. Using intact arterial rings from paediatric CKD patients (both pre-dialysis and dialysis) alongside healthy paediatric controls, Shroff *et al* (2010) indicated that calcium deposition increased in arterial rings in proportion to an increase in environmental calcium and phosphate concentration. Similarly, prolonged exposure to a pro-calcaemic environment (with vessel rings collected at 7, 14 and 21 days) also increased calcium deposition in these vessels in a time-dependent manner (Shroff *et al* 2010). However, the crucial finding of the Shroff *et al* (2010) study was that the increase in calcium deposition was specific to the disease state of the vessel; namely, arterial rings from healthy controls showed no significant increase in calcium deposition whilst the increase in vascular rings from pre-dialysis CKD patients was minimal. Comparatively, the arterial rings obtained from paediatric dialysis patients calcified significantly in the pro-calcaemic medium.

The findings in this thesis mirror those found in the Shroff *et al* (2010) study, although this thesis has demonstrated that supplementing the pro-calcaemic medium with exogenous human Angpt2 (at a dose of 25 ng/mL) significantly enhances the calcium deposition in intact arterial rings from dialysis patients compared to the pro-calcaemic environment alone. In this thesis, I have also examined the response of both control and dialysis VSMCs to a pro-calcaemic environment, with and without Angpt2. The results with cells were slightly different to the intact arterial rings. I found that calcium deposition increased in control VSMCs exposed to increased calcium and phosphate in the culture media. However, dialysis VSMCs calcified to a greater extent as assessed by calcium extraction and quantification using the *o*-cresolphthalein colorimetric assay.

A potential explanation for these findings is that control, pre-dialysis and dialysis vessels and VSMCs may contain a different transcriptome profile. Comparative gene expression between healthy paediatric vessels, pre-dialysis CKD vessels and dialysis CKD vessels has the potential to reveal possible differences between these cell populations. Monroy and colleagues (2015) have quantitatively shown that the phenotype of VSMCs does indeed alter in response to CKD, and have hypothesised that this is due to the prolonged uremic conditions that these cells are subjected to. VSMCs exposed to short-term uremic conditions exhibited a significant (50–80%) reduction in contractile genes, namely αSMA and SM22α (Monroy *et al* 2015); these results corroborate the findings by both Shroff *et al* (2008, 2010) and those in this thesis, in which contractile genes are reduced following exposure to a pro-calcaemic (hyperphosphataemic and hypercalcaemic) milieu. Following 24-hour exposure to uremic serum from CKD patients on HD, otherwise healthy commercially-obtained VSMCs exhibited decreased migration, increased cell proliferation and no significant alteration in apoptosis (Monroy *et al* 2015).

In my study, I found that in paediatric vessels there were no significant differences in the baseline levels of contractile gene (*SM22α*) and osteogenic genes (*BMP2, MGP, SP7, OPN*) between control, pre-dialysis and dialysis VSMCs (Section 4.1.2). The clear heterogeneity between VSMC populations obtained from different patients made it difficult to observe any trends in the data; however, these samples highlight how variable gene expression – particularly in primary cells – can be. The relationship

between gene expression and the length of *in vivo* exposure to uraemia for both intact vessels and isolated primary cells would be another interesting aspect to explore, as Monroy *et al* (2015) exposed healthy VSMCs to the uremic milieu for a short period of time. The original dialysis vessels (from which the VMSCs utilised in this thesis were isolated) were exposed to uraemia in the *in vivo* environment for several months to years. Therefore, the slight trend towards increased *SM22α* in dialysis (as compared with control and pre-dialysis) cells could potentially be explained as a compensatory mechanism to counter a shift towards osteogenic differentiation.

6.2.5 Gene Expression in Response to Calcification

One of the limitations to this study is the small panel of genes chosen for expression profiling when cells are exposed to a pro-calcaemic milieu. The panel of osteogenic and contractile genes was chosen based on the literature surrounding VSMC calcification, with strong evidence implicating these genes in the calcification pathway and thus being the most likely to exhibit a substantial change in response to altered calcification. As such, the primary panel of genes included *RUNX2, BMP2, MGP, SM22α*, and *αSMA*. Significant changes in expression of these listed genes are likely to result in phenotypic alterations. Indeed, VSMCs cultured in pro-calcaemic medium did exhibit alterations in these genes when compared with VSMCs cultured in medium alone; however, we did not find any differences in the levels of gene expression in dialysis cells in pro-calcaemic conditions with/without Angpt2. The data in this thesis show a trend towards an increase in *BMP2* with the addition of Angpt2; however, the degree of variation between each individual sample within a given treatment group meant that the data failed to achieve statistical significance despite a visible trend. By increasing the number of patient samples analysed, the degree of variation may be reduced – thus potentially leading to significant differences between groups. Alternatively, the number of genes examined could be increased. However, unfortunately, we could not expand the panel of genes used for qRT-PR due to the low yield of RNA that was harvested from calcified cell cultures, as the presence of calcium and phosphate in the medium interfered with trypsin activity and partially blocked the column during RNA extraction. With this limited quantity of RNA, it would have been optimal to utilise an assay with the ability to examine multiple genes such as RNAseq which would have allowed for a broader examination of the expressed

genes than sequential qRT-PCRs. Alternatively, the protein could be explored at the molecular level; for example, the phosphorylation and glycosylation state of MGP may potentially impact the calcification pathway in response to exogenous Angpt2, as the dephosphorylated uncarboxylated form has previously been shown to increase in adult CKD patients with vascular calcification and correlate with vascular stiffness (Delanaye *et al* 2014; Thamratnopkoon *et al* 2017). Additionally, this desphosphorylated uncarboxylated form has been associated with markers of cardiovascular disease and increased mortality (Piven *et al* 2015).

While increasing the number of patient samples analysed may decrease variation between samples, increasing the number of tested time-points may highlight large-scale changes in gene expression or indicate a shift in expression of a single gene (or a set of genes) over time. In this study, a 5-day time-point was chosen based on previous *in vitro* VSMC experiments by Reynolds and colleagues (1998), as this point was one in which notable calcium depositions were observed. Although the expression of pro-calcaemic genes in VSMCs increased upon stimulation with pro-calcaemic medium, there were no significant changes in gene expression between those cells treated with or without Angpt2. One potential explanation for this lack of differential gene expression, despite differing levels of calcium deposition, is that a maximal level of gene expression is reached in both populations prior to the emergence of overt calcium depositions. By taking a sequential time-course following stimulation with pro-calcaemic medium with and without Angpt2 (for example, using daily intervals between RNA extractions), the changes in expression level could be measured prior to visible calcium depositions. However, the difficulty in conducting this experiment lies in the proliferation rate of the dialysis VSMCs as culturing the required volume of cells for such an experiment would require multiple passages, during which time there is a high likelihood of these valuable cells dedifferentiating.

6.2.6 Epigenetic Regulation of Osteogenic Genes

Although my data indicated that there were no significant changes in osteogenic gene expression in the presence of Angpt2 compared with the pro-calcaemic medium alone, I have only examined the mRNA expression of a small set of genes. Instead, a potential mechanism could be alterations in microRNAs (miRNA). In a study conducted by

Panizo and colleagues (2015), three distinct miRNAs were noted to play direct roles in VSMC high phosphate-induced calcification: miR-29b, miR-133b and miR-211. The aortic concentration of miR-29b was increased in nephrectomised male Wistar rats fed a high phosphate diet, whilst both miR-133b and miR-211 were decreased compared with controls (Panizo *et al* 2015). miR-133b is becoming increasingly well-characterised in its role in RUNX2 regulation, and it appears to interact with the 3' untranslated region to inhibit translation of the gene (Liao *et al* 2013). Numerous other miRNAs have been attributed to the regulation of different calcification genes. RUNX2, whilst downstream of BMP2, can also be regulated through both BMP2 activity and miR-30b and miR-30c; whilst BMP2 promotes expression of RUNX2, expression can be downregulated by the miRNAs as shown in monolayer adult aortic VSMC culture (Balderman *et al* 2012). *In situ* hybridisation for miR-30b has also shown this miRNA to be noticeably decreased in patients with arteriosclerotic plaques when compared to aortic donor vessels (Balderman *et al* 2012). Using small RNA obtained from fresh human vessels would provide a basis to examine the epigenetic regulation of the osteogenic genes by RNA sequencing.

Although a relatively new field, epigenetic changes have also been implicated in the progression of vascular calcification (Wu *et al* 2015). While examining the phenotypic changes of VSMCs in response to uremic serum, Monroy and colleagues (2015) noted that the acetylation of histone H4 was decreased at sites regulating contractility genes, thus reducing active chromatin for these genes and contributing to the phenotypic changes of these cells. Elevated phosphate has, *in vitro*, been shown to increase the methylation of the promoter region of the contractile gene *SM22α* (transgelin) that in turn reduces gene expression and subsequently promotes calcification (Oca *et al* 2010).

6.2.7 Pathological Changes During Calcification

Monroy *et al* (2015) also found that exposure to uremic serum had no effect on apoptosis of cultured VSMCs; however, another study utilising intact murine arterial rings indicated that VSMC loss (within the tunica media of the vessels) increases with exposure to uraemia (Pai *et al* 2011). However, the caveat for VSMC loss appears to be that exposure to uremic serum must be coupled with a high phosphate diet (Pai *et*

al 2011). As the commercially-obtained cultured cells used by Monroy *et al* (2015) were not previously phosphate-loaded, this may explain why these cells did not increase apoptosis. However, Pai *et al* (2011) did not observe any correlation between an increase in apoptosis and the level of calcification of the vessel. The authors propose that, in response to high calcium and phosphate, the VSMCs undergo phenotypic changes allowing them to take on an osteogenic-like phenotype. If the cells fail to take on this osteogenic phenotype, they are at high-risk to undergo apoptosis (Pai *et al* 2011, Shroff *et al* 2010).

6.2.8 Endothelial Co-culture and the Effects of VEGFA

Iurlaro *et al* (2003) also found that exposure to conditioned media from endothelial cells inhibited the chemotaxis of Tie2-positive mural cells. This response was not enhanced by further addition of exogenous Angpt1, indicating that the endothelial-SMC interaction may be the critical process in regulating the biology of Tie2-positive mural cells; the response to Angpt2 under these conditions was not examined (Iurlaro *et al* 2003).

Co-culture studies between endothelial and SMCs show alterations in the expression of angiogenic genes; for example, endothelial cells increase *VEGFA* expression when cultured in combination with VSMCs (Heydarkhan-Hagvall *et al* 2003). I have not examined the effects of VEGFA in this thesis, but this factor may be important regarding the actions of Angpt2 in vascular calcification. During angiogenesis, the environmental concentration of VEGFA determines whether the destabilisation of the endothelium (as induced by increased Angpt2) results in vascular regression or the branching of new vessels (Huang *et al* 2010). In the cohort of patients examined by Shroff *et al* (2013), VEGFA was found to decrease while its receptor, soluble Flt1 increased; this supports the destabilisation of the vasculature in these patients in the presence of increased Angpt2. In future studies, it would be ideal to measure the levels of circulating VEGFA as well as Flt1 in the culture medium both before and after addition of Angpt2.

Another interesting aspect of this study was the low concentration at which Angpt2 was able to increase calcium deposition. While the initial rationale behind choosing

25 ng/mL of Angpt2 was that it was the highest circulating level measured in dialysis patients, most studies investigating angiopoietin activity use concentrations from 100 ng/mL up to 800 ng/mL (Kim *et al* 2000, Scharpfenecker *et al* 2005, Sinnathamby *et al* 2015). However, most of these studies are single time-point studies that are conducted over a brief time period, usually between 5 minutes to an hour. Perhaps, as in this thesis, a long period of low-level exposure is necessary to observe a response. This scenario may be more representative of a chronic disease state. As the medium was replaced every 3–4 days during the 14-day intact vessel ring experiment and every 2.5 days for the 5-day VSMC experiments, any Angpt2 that was bound or internalised was later replenished. If one equates 4 media changes at 25 ng/mL to a single medium stimulation at 100 ng/mL, the dose is the same. However, if Angpt2 remains bound to Tie2, theoretically the number of active receptors would remain the same. However, by replenishing the medium every few days, these receptors are activated in a step-wise manner.

6.2.9 In Vivo Investigation of Calcification

To extend this project, an *in vivo* investigation is required and thus a mouse model for CKD would be beneficial. One model that has been considered is the *Enpp1* model, which has a mutation in the enzyme ectonucleotide pyrophosphatase (Li *et al* 2013). If bred on a BALB/C background, these mice develop extensive calcification throughout their arteries, which mirrors the effects of a similar *ENPP1* mutation that occurs in children. Progression of calcification can be monitored through the use of microCT, which reduces the number of animals culled at each stage, although the collection of organs at each time-point allows for quantitative measurement of calcium deposition as well as histological representation. However, we do not yet know if Angpt2 is altered in this model and this work would need to be done. Furthermore, as this model is intrinsically prone to calcification, a renal injury model such as a 5/6 nephrectomised mouse fed a high calcium and phosphate diet, may be more representative of the chronic disease state. Indeed, using CD1 mice, Chang and colleagues (2013) have shown that there is a significant increase in circulating Angpt2 following a 5/6 subtotal nephrectomy. Similarly, they also observed a significant increase in circulating Angpt2 following unilateral ureteral obstruction (Chang *et al* 2013).

Angpt2 can also be modulated in numerous ways *in vivo*. For example, there are now several studies utilising adenovirus expressing human Angpt2 to overexpress Angpt2 in mouse models (Chang *et al* 2013, Chen *et al* 2011, Lee *et al* 2006); this method is also used to induce Angpt2 overexpression in *in vitro* culture models (Mofarrahi and Hussain 2011). Inhibitors can also be utilised to block Angpt2 activity — this is particularly popular in cancer models to inhibit angiogenesis (Hu *et al* 2009); however, inhibitors have the potential to cause off-target effects (Shoshan and Linder 2008). Finally, transgenic mice – either over- or underexpressing Angpt2 – can also be utilised to modulate Angpt2; this has been the most popular technique utilised in previous studies in our laboratory as overexpression can be induced in specific vascular beds and at set time-points (Davis *et al* 2007).

6.2.10 Targeting Tie2 to Modulate Vascular Calcification

One potential means of modulating Angpt2 is through the agonist-antagonist relationship with Angpt1, or through the balance of these two angiopoietins (Brindle *et al* 2008). However, stimulating VSMCs with Angpt1 under pro-calcaemic conditions did not attenuate calcification—instead, although not significant, there was a trend towards increased calcification, similar to the effects of Angpt2. Targeting Tie2, either through downregulation of mRNA and subsequent receptor expression as in the transfected VSMCs or through chemical inhibition of the Tie2 phosphorylation activity as in the intact vessel rings, appears to be a more efficient way of regulating the activity of this pathway. In this thesis, transfection of VSMCs with *TIE2*-targeting siRNA had a dampening effect on calcification in dialysis VSMCs treated with Angpt2 when cultured in pro-calcaemic medium, compared with VSMCs treated with control siRNA cultured under the same conditions. However, whilst transfection with *TIE2* siRNA was shown to reduce expression *TIE2* in the VSMCs, the effect of the knockdown on translation and overall protein content was not measured. Therefore, the effects of residual TIE2 content on the experimental system cannot be determined. One of the other issues with *TIE2* siRNA is the similarity between the genetic sequence of *TIE2*, and *TIE1*. Although *TIE1* is frequently referred to as an orphan receptor, it can act to modulate *TIE2* activity. If, as was seen in Figure 5.12, *TIE1* expression is also decreased following transfection with *TIE2* siRNA, it is highly likely that the *TIE2* siRNA also had a knockdown effect on *TIE1*.

Inhibition of Tie2 activity utilising a synthetic inhibitor appears promising, but this needs to be done with several more vessels to determine if the inhibitor has a significant effect on calcium load and, if so, whether it is associated with any negative effects on the vessel. In future experiments, a control group containing the Tie2 inhibitor in the absence of Angpt2 would be interesting, as this would allow for investigation of the role of Tie2 signalling in the presence of elevated calcium and phosphate, but without exogenous Angpt2 stimulation.

This Angpt-Tie2 pathway is becoming increasingly targeted as a means for modulating angiogenesis in cancer, as recent studies in both humans and mice have demonstrated. Recently, Tuppurainen and colleagues (2017) targeted Tie2 and VEGFR in a human ovarian cancer xenograft model in immunodeficient mice using adenoviral therapy to inhibit these pathways, leading to a decrease in angiogenesis and a significant reduction in tumour weights ($p=0.007$) when compared with untreated controls. Trebananib, a recombinant peptide-Fc fusion protein, is also currently in Phase III clinical trials as a treatment for various cancers as it binds to the angiopoietins, thereby inhibiting their ability to engage with Tie2 (Mita *et al* 2010; Amgen NCT01493505). The effects of trebananib have also been recently examined *in vitro*, in which investigators have shown that the fusion protein is able to sensitise human carcinoma cells to the cytotoxic effects of T lymphocytes, potentially making them more responsive to subsequent immunotherapies (Grenga *et al* 2015).

6.3 Summary

By exploring the role of Angpt2 – and subsequently the role of Tie2 – in vascular calcification in paediatric patients on dialysis, the work described in this thesis opens a potential new pathway for which to target the pathogenic effects of dialysis. Both intact arterial ring studies and cultured VSMC studies indicate that exogenous Angpt2 increases calcium deposition in dialysis populations when under a pro-calcaemic environment as compared with dialysis vessels cultured in pro-calcaemic medium alone. However, this effect was strictly observed in vessels and VSMCs from patients on dialysis and was not observed in pre-dialysis CKD patients.

Nuclear staining of the intact arterial rings indicated that control, pre-dialysis and dialysis vessels maintained a consistent cell number across culture conditions; however, the number of condensed and thus potentially apoptotic nuclei increased in i) dialysis vessels, as compared with both pre-dialysis and control vessels and ii) vessel rings treated with Angpt2 under a pro-calcaemic medium, as compared with vessel rings cultured in pro-calcaemic medium or medium alone. As subsequent TUNEL staining to detect apoptosis exhibited no clear trend (in either vessels or VSMCs), the mechanism underlying the changes in nuclear phenotype is still unclear. In VSMCs, the changes in calcium deposition are accompanied by an increase in pro-calcaemic genes *BMP2* and *MGP*, alongside a decrease in contractile genes *SM22α*, and *αSMA*; however, whilst these changes in gene expression occur (and are significant when compared with VSMCs cultured in medium alone), the differences in expression are not significantly altered when compared with VSMCs cultured in the pro-calcaemic medium without Angpt2. However, these VSMCs are shown to express Tie2 and, although this receptor is typically seen as endothelial-specific, this thesis has utilised numerous tests to confirm the presence of the receptor and has subsequently shown that knockdown of *TIE2* using *TIE2* siRNA can reduce calcium deposition in cultured dialysis VSMCs, thereby suggesting that Tie2 is a potential modulator of Angpt2-driven vascular calcification.

Overall, whilst the mechanism by which Angpt2 drives vascular calcification remains unclear, the work in this thesis has provided insight into a previously unexplored means by which calcification may occur in the paediatric dialysis population. As CVD,

initiating with endothelial dysfunction and vascular calcification, is the leading cause of death in the CKD population, it is imperative that we continue to explore ways in which to target these physiological changes to improve the lives of patients (Steenkamp *et al* 2014).

References

Abbasian N, Burton JO, Herbert KE, Tregunna BE, Brown JR, Ghaderi-Najafabadi M, Brunskill NJ, Goodall AH, Bevington A. Hyperphosphatemia, phosphoprotein phosphatases, and microparticle release in vascular endothelial cells. (2015) *Journal of American Society of Nephrology* **26(9):** 2152–2162.

Adams RH, Alitalo K. Molecular regulation of angiogenesis and lymphangiogenesis. (2007) *Nature Reviews Molecular Cell Biology* **8(6):** 464–478.

Aird WC. Phenotypic heterogeneity of the endothelium. II. Representative vascular beds. (2007) *Circulation Research* **100(2):** 174–190.

Amann K. Media calcification and intima calcification are distinct entities in chronic kidney disease. (2008) *Clinical Journal of the American Society of Nephrology* **3(6):** 1599–1605.

Amgen. A Phase 3 randomized, double-blind, placebo-controlled, multicentre study of AMG 386 with paclitaxel and carboplatin as first-line treatment of subjects with FIGO Stage III–IV epithelial ovarian, primary peritoneal or fallopian tube cancers. In: ClinicalTrials.gov [Internet]. Bethesda (MD): National Library of Medicine (US). 2000–[cited July 2016]. Available from: https://clinicaltrials.gov/ct2/show/NCT01493505 NLM Identifier: NCT01493505.

Anderson HC. Vesicles associated with calcification in the matrix of epiphyseal cartilage. (1969) *Journal of Cell Biology* **41(1):** 59–72.

Anderson HC. Molecular biology of matrix vesicles. (1995) *Clinical Orthopaedics and Related Research* **314:** 266–280.

Aplin AE, Stewart SA, Assoian RK, Julianof RL. Integrin-mediated adhesion regulates ERK nuclear translocation and phosphorylation of Elk-1. (2001) *Journal of Cell Biology* **153(2):** 273–281.

Augustin HG, Koh GY, Thurston G, Alitalo K. Control of vascular morphogenesis and homeostasis through the angiopoietin-Tie system. (2009) *Nature Reviews Molecular Cell Biology* **10(3):** 165–177.

Balderman JA, Lee HY, Mahoney CE, Handy DE, White K, Annis S, Lebeche D, Hajjar RJ, Loscalzo J, Leopold JA. Bone morphogenic protein-2 decreases microRNA-30b and microRNA-30c to promote vascular smooth muscle cell calcification. (2012) *Journal of American Heart Association* **1(6):** e003905.

Belvitch P, Dudek SM. Role of FAK in S1P-regulated endothelial permeability. (2012) *Microvascular Research* **83(1):** 22–30.

Bennett-Richards KJ, Kattenhorn M, Donald AE, Oakley GR, Varghese Z, Bruckdorfer KR, Deanfield JE, Rees L. Oral L-arginine does not improve endothelial dysfunction in children with chronic renal failure. (2002) *Kidney International* **62(4):** 1372–1378.

Block GA, Hulbert-Shearon TE, Levin NW, Port FK. Association of serum phosphorus and calcium x phosphate product with mortality risk in chronic hemodialysis patients: a national study. (1998) *American Journal of Kidney Diseases* **31(4):** 607–617.

Bogdanovic E, Nguyen VP, Dumont DJ. Activation of Tie2 by angiopoietin-1 and angiopoietin-2 results in their release and receptor internalisation. (2006) *Journal of Cell Science* **119(Pt17):** 3551–3560.

Böger RH, Sydow K, Borlak J, Thum T, Lenzen H, Schubery B, Tsikas D, Bode-Böger SM. LDL Cholesterol upregulates synthesis of asymmetrical dimethylarginine in human endothelial cells. (2000) *Circulation Research* **87(2):** 99–105.

Boström K, Watson KE, Horn S, Wortham C, Herman IM, Demer LL. Bone morphogenic protein expression in human atherosclerotic lesions. (1993) *Journal of Clinical Investigation* **91(4):** 1800–1809.

Boulanger CM, Amabile N, Guérin Ap, Pannier B, Leroyer AS, Nguyen C, Mallat Z, Tedgui A, London GM. *In vivo* shear stress determines circulating levels of endothelial microparticles in end-stage renal disease. (2007) *Hypertension* **49(4):** 902–908.

Brindle NPJ, Saharinen P, Alitalo K. Signalling and functions of angiopoietin-1 in vascular protection. (2008) *Circulation Research* **98(8):** 1014–1023.

Brouty-Boye D, Kolonias D, Savaraj N, Lampidis TJ. Alpha-smooth muscle actin expression in cultured cardiac fibroblasts of newborn rat. (1992) *In Vitro Cellular and Developmental Biology* **28(4):** 293–296.

Brkovic A, Pelletier M, Girard D, Sirois MG. Angiopoietin chemotactic activities on neutrophils are regulated by PI-3K activation. (2007) *Journal of Leukocyte Biology* **81(4):** 1093–1101.

Brunet P, Gondouin B, Duval-Sabatier A, Dou L, Cerini C, Dignat-George F, Jourde-Chiche N, Argiles A, Burtey S. Does uremia cause vascular dysfunction? (2011) *Kidney and Blood Pressure Research* **34(4):** 284–290.

Campbell JH, Campbell GR. Smooth muscle phenotype modulation – a personal experience. (2012) *Arteriosclerosis, Thrombosis, and Vascular Biology* **32(8):** 1784–1789.

Cannon RO. Role of nitric oxide in cardiovascular disease: focus on the endothelium. (1998) *Clinical Chemistry* **44(8):** 1809–1819.

Carmeliet P, Jain RK. Molecular mechanisms and clinical applications of angiogenesis. (2011) *Nature* **473(7347):** 298–307.

Chamleu JH, Campbell GR, Burnstock G. Dedifferentiation, redifferentiation, and bundle formation of smooth muscle cells in tissue culture: the influence of cell number and nerve fibres. (1974) *Journal of Embryology and Experimental Morphology* **32(2):** 297–323.

Chamley JD, Gröshel-Stewart U, Campbell GR, Burnstock G. Distinction between smooth muscle, fibroblasts and endothelial cells in culture by the use of fluorescent antibodies against smooth muscle actin. (1977) *Cell and Tissue Research* **177(4):** 445–457.

Chang FC, Lai TS, Chiang CK, Chen YM, Wu MS, Chu TS, Wu KD, Lin SL. Angiopoietin-2 is associated with albuminuria and micro inflammation in chronic kidney disease. (2013) *PLoS One* **8(3):** e54668.

Chang FC, Chiang WC, Tsai MH, Chou YH, Pan SY, Chang YT, Yeh YT, Chen YT, Chiang CK, Chen YM, Chu TS, Wu KD, Lin SL. Angiopoietin-2-induced arterial stiffness in CKD. (2014) *Journal of the American Society of Nephrology* **25(6)**:1198–1209.

Charakida M, Masi S, Lüscher TF, Kastelein JJP, Deanfield JE. Assessment of atherosclerosis: the role of flow-mediated dilatation. (2010) *European Heart Journal* **31(23):** 2854–2861.

Chavers BM, Molony JT, Solid CA, Rheault MN, Collins AJ. One-year mortality rates in US children with end-stage renal disease. (2015) *American Journal of Nephrology* **41(2):** 121–128.

Chen JX, Zeng H, Reese J, Aschner JL, Meyrick B. Overexpression of angiopoietin-2 impairs myocardial angiogenesis and exacerbates cardiac fibrosis in the diabetic *db/db* mouse model. (2011) *American Journal of Physiology Heart and Circulatory Physiology* **302(4):** H1003–H1012.

Chen NX, Duan D, I'Neil KD, Wolisi GO, Koczman JJ, LaClair R, Moe SM. The mechanisms of uremic serum-induced expression of bone matrix proteins in bovine vascular smooth muscle cells. (2006) *Kidney International* **70(6):** 1046–1053.

Christensen B, Kazanecki CC, Petersen TE, Rittling SR, Denhardt DT, Sørensen ES. Cell-type specific post-translational modifications of mouse osteopontin are associated with different adhesive properties. (2007) *Journal of Biological Chemistry* **282(27):** 19463–19472.

Chen YM, Wu KD, Tsai TJ, Hsieh BS. Pentoxifylline inhibits PDGF-induced proliferation of and TGF-β-stimulated collagen synthesis by vascular smooth muscle cells. (1999) *Journal of Molecular and Cellular Cardiology* **31(4):** 773–783.

Clouthier DL, Harris CN, Harris RA, Martin CE, Puri MC, Jones N. Requisite role for Nck adapters in cardiovascular development, endothelial-to-mesenchymal transition and directed cell migration. (2015) *Molecular and Cellular Biology* **35(9):** 1573–1587.

Coffelt SB, Chen YY, Muthana M, Welford AF, Tal AO, Scholz A, Plate KH, Reiss Y, Murdoch C, De Palma M, Lewis DE. Angiopoietin 2 stimulates TIE2-expressing monocytes to suppress T cell activation and to promote regulatory T cell expansion. (2011) *Journal of Immunology* **186(7):** 4183–4190.

Coppolino G, Bolignano D, Camp S, Loddo S, Teti D, Buemi M. Circulating progenitor cells after cold pressor test in hypertensive and uremic patients. (2008) *Hypertension Research* **31(4):** 717–724.

Covic A, Mardare N, Gusbeth-Tatomir P, Brumaru O, Gavrilovici C, Munteanu M, Prisada O, Goldsmith DJA. Increased arterial stiffness in children on haemodialysis. (2006) *Nephrology Dialysis Transplantation* **21(3):** 729–735.

Cranenburg EC, Van Spaendonck-Zwarts KY, Bonafe L, Mittaz Crettol L, Rödiger LA, Dikers FG, Van Essen AJ, Superti-Furga A, Alexandrakis E, Vermeer C, Schurgers LJ, Laverman GD. Circulating matrix-y-carboxyglutamate protein (MGP) species are refractory to vitamin K treatment in a new case of Keutal syndrome. (2011) *Journal of Thrombosis and Haemostasis* **9(6):** 1225–1235.

Culleton BF, Larson MG, Wilson PW, Evans JC, Parfrey PS, Levy D. Cardiovascular disease and mortality in a community-based cohort with mild renal insufficiency. (1999) *Kidney International* **56(6):** 2214–2219.

Dallabrida SM, Ismail NS, Pravda EA, Parodi EM, Dickie R, Durand EM, Lai J, Cassiola F, Rogers RA, Rupnick MA. Integrin binding angiopoietin-1 monomers reduced cardiac hypertrophy. (2008) *The Journal of the Federation of American Societies for Experimental Biology* **22(8):** 3010–3023.

David S, Kümpers P, Hellpap J, Horn R, Leith H, Haller H, Kielstein JT. Angiopoietin-2 and cardiovascular disease in dialysis and kidney transplantation. (2009) *American Journal of Kidney Disease* **53(5):** 770–778.

David S, Kümpers P, Lukasz A, Fliser D, Martens-Lobenhoffer J, Bode-Böger SM, Kliem V, Haller H, Kielstein JT. Circulating angiopoietin-2 levels increase with the progress of chronic kidney disease. (2010) *Nephrology Dialysis Transplantation* **25(8):** 2571–2576.

David S, John SG, Jeffries HJ, Sigrist MK, Kümpers P, Kielstein JT, Haller H, McIntyre CW. Angiopoietin-2 levels predict mortality in CKD patients. (2012) *Nephrology Dialysis Transplantation* **27(5):** 1867–1872.

Davis S, Aldrich TH, Jones PF, Acheson A, Compton DL, Jain V, Ryan TE, Bruno J, Radziejewski C, Maisonpierre PC, Yancopoulos. Isolation of Angiopoietin-1, a ligand for the Tie2 receptor by secretion-trap expression cloning. (1996) *Cell* **87(7):** 1161–1169.

Davis B, Dei Cas A, Long DA, White KE, Hayward A, Ku CH, Woolf AS, Bilous R, Viberti G, Gnudi L. Podocyte-specific expression of angiopoietin-2 causes proteinuria and apoptosis of glomerular endothelia. (2007) *Journal of American Society of Nephrology* **18(8):** 2320–2329.

De Palma M, Venneri MA, Galli R, Sergi LS, Politi LS, Sampaolesi M, Naldini L. Tie2 identifies hematopoietic monocytes required for tumour lineage of proangiogenic vessel formation and a mesenchymal population of pericytes progenitors. (2005) *Cancer Cell* **8(3):** 211–226.

Deanfield JE, Halcox JP, Rabelink TJ. Endothelial function and dysfunction: testing and clinical relevance. (2007) *Circulation* **115(10):** 1285–1295.

Delanaye P, Krzesinski JM, Warling X, Moonen M, Smelten N, Médart L, Pottel H, Cavalier E. Dephosphorylated-uncarboxylated Matrix Gla protein concentration is predictive of vitamin K status and is correlated with vascular calcification in a cohort of hemodialysis patients. (2014) *BMC Nephrology* **15:** 145.

Di Marco GS, Reuter S, Hillebrand U, Amler S, König M, Larger E, Oberleithner H, Brand E, Pavenstädt H, Brand M. The soluble VEGF receptor sFlt1 contributes to endothelial dysfunction in CKD. (2009) *Journal of American Society of Nephrology* **20(10):** 2235–2245.

Dignat-George F, Boulanger CM. The many faces of microparticles. (2011) *Arteriosclerosis, Thrombosis, and Vascular Biology* **31(1):** 27–33.

Doherty MJ, Ashton BA, Walsh S, Beresford JN, Grant ME, Canfield AE. Vascular pericytes express osteogenic potential *in vitro* and *in vivo*. (1998) *Journal of Bone and Mineral Research* **13(5):** 828–838.

Drüeke TM, Massy ZA. Atherosclerosis in CKD: differences from the general population. (2010) *Nature Reviews Nephrology* **6(12):** 723–735.

Duncker DJ, Zhang J, Bache RJ. Coronary pressure-flow relation in left ventricular hypertrophy. (1993) *Circulation Research* **72(3):** 579–587.

Dunne JV, Keen KJ, Van Eeden SF. Circulating angiopoietin and Tie-2 levels in systemic sclerosis. (2013) *Rheumatology International* **33(2):** 475–484.

Dupont JJ, Farquhar WB, Townsend R, Edwards DG. Ascorbic acid or L-arginine improves subcutaneous microvascular function in chronic kidney disease. (2011) *Journal of Applied Physiology* **111(6):** 1561–1567.

Dursun I, Poyrazoglu HM, Gunduz Z, Ulger H, Yykylmaz A, Dusunsel R, Patyroglu T, Gurgoze M. The relationship between circulating endothelial microparticles and arterial stiffness and atherosclerosis in children with chronic kidney disease. (2009) *Nephrology Dialysis Transplantation* **24(8):** 2511–2518.

Etoh T, Inoue H, Tanaka S, Barnard GF, Kitano S, Mori M. Angiopoietin-2 is related to tumour angiogenesis in gastric carcinoma: possible *in vivo* regulation via induction of proteases. (2001) *Cancer Research* **61(5):** 2145–2153.

Felcht M, Luck R, Schering A, Seidel P, Srivastava K, Hu J, Bartol A, Kienast Y, Vettel C, Loos EK, Kutschera S, Bartlels S, Appak S, Besemfelder E, Terhardt D, Chavakis E, Wieland T, Klein C, Thomas M, Uemura A, Goerdt S, Augustin HG. Angiopoeitin-2 differentially regulates angiogenesis through TIE2 and integrin signalling. (2012) *Journal of Clinical Investigation* **122(6):** 1991–2005.

Fiedler U, Krissl T, Koidl S, Weiss C, Koblizek T, Deutsch U, Martiny-Baron G, Marmé D, Augustin HG. Angiopoietin-1 and Angiopoietin-2 share the same binding domains in the Tie-2 receptor involving the first Ig-like loop and the epidermal growth factor-like repeats. (2002) *The Journal of Biological Chemistry* **278(3):** 1721–1727.

Fiedler U, Reiss Y, Scharpfenecker M, Grunow V, Koidl S, Thurston G, Gale NW, Witzenrath M, Rosseau S, Suttorp N, Sobke N, Herrmann M, Preissner KT, Vajkoczy P, Augustin HG. Angiopoietin-2 sensitises endothelial cells to TNF-alpha and has a crucial role in the induction of inflammation. (2006) *Nature Medicine* **12(2):** 235–239.

Fiedler U, Scharpfenecker M, Koidl S, Hegen A, Grunow V, Schmidt JM, Kriz W, Thurston G, Augustin HG. The Tie-2 ligand angiopoietin-2 is stored in and rapidly released upon stimulation from endothelial cell Weibel-Palade bodies. (2004) *Blood* **103(11):** 4150–4156.

Fitch RM, Vergona R, Sullivan ME, Wang Y. Nitric oxide synthase inhibition increases aortic stiffness measured by pulse wave velocity in rats. (2001) *Cardiovascular Research* **51(2):** 351–358.

Fitts MK, Pike DB, Anderson K, Shiu YT. Hemodynamic shear stress and endothelial dysfunction in haemodialysis access. (2014) *Open Urology and Nephrology Journal* **7(Suppl 1M5):** 33–44.

Flammer AJ, Anderson T, Celermajer DS, Creager MA, Deanfield J, Ganz P, Hamburg N, Lüscher TF, Shechter M, Taddei S, Vita JA, Lerman A. The assessment of endothelial function – from research into clinical practice. (2012) *Circulation* **126(6):** 753–767.

Fliser D. Perspectives in renal disease progression: the endothelium as a treatment target in chronic kidney disease. (2010) *Journal of Nephrology* **23(4):** 369–376.

Foley RN, Parfrey PS, Sarnak MJ. Clinical epidemiology of cardiovascular disease in chronic renal disease. (1998) *American Journal of Kidney Diseases* **32(5 Suppl. 3):** S112–119.

Foster MC, Hwang SJ, Massaro JM, Jacques PF, Fox CS, Chu AY. Lifestyle factors and indices of kidney function in the Framingham Heart study. (2015) *American Journal of Nephrology* **41(0):** 267–274.

Fruchart JC, Nierman MC, Stroes ESG, Kastelein JJP, Duriez P. Atherosclerosis: evolving vascular biology and clinical implications. (2004) *Circulation* **109(23 Suppl.):** III–15-III–19.

Gansevoort RT, Correa-Rotter R, Hemmelgarn BR, Jafar TH, Heerspink HJL, Mann JF, Matsushita K, Wen CP. Chronic kidney disease and cardiovascular risk: epidemiology, mechanisms, and prevention. (2013) *The Lancet* **382(9889):** 339–352.

Giachelli CM, Bae N, Almeida M, Denhardt DT, Alpers CE, Schwartz SM. Osteopontin is elevated during neointima formation in rat arteries and is a novel component of human atherosclerotic plaques. (1993) *Journal of Clinical Investigation* **92(4):** 1686–1696.

Giachelli CM. Mechanisms of vascular calcification in uremia. (2004) *Seminars in Nephrology* **24(5):** 401–402.

Gnudi L, Benedetti S, Woolf AS, Long DA. Vascular growth factors play critical roles in kidney glomeruli. (2015) *Clinical Science* **129(12):** 1225–1236.

Goodman WG, Goldin J, Kuizon B, Yoon C, Gales B, Sider D, Wang Y, Chung J, Emerick A, Greaser L, Elashoff RM, Sulusky IB. Coronary-artery calcification in young adults with end-stage renal disease who are undergoing dialysis. (2000) *New England Journal of Medicine* **342 (20):** 1478–1483.

Grahammer F, Schell C, Huber TB. The podocyte slit diaphragm – from a thin grey line to a complex signalling hub. (2013) *Nature Reviews Nephrology* **9:** 589–598.

Grenga I, Kwilas AR, Donahue RN, Farscaci B, Hodge JW. Inhibition of the angiopoietin/Tie2 axis induces immunogenic modulation, which sensitised human tumor cells to immune attack. (2015) *Journal for Immunotherapy of Cancer* **3:** 52.

Hakanpaa L, Sipila T, Leppanen VM, Gautam P, Nurmi H, Jacquemet G, Eklund L, Vaska J, Alitalo K, Saharinen P. Endothelial destabilisation by angiopoietin-2 via integrin β1 activation. (2015) *Nature Communications* **6:** 5962.

Haberichter SL, Merricks EP, Fahs SA, Chrisopherson PA, Nichols TC, Montgomery RR. Re-establishment of VWF-dependent Weibel-Palade bodies in VWD endothelial cells. (2005) *Blood* **105(1):** 145–152.

Haffner D, Hocher B, Müller D, Simon K, König K, Richter CM, Eggert B, Schwarz J, Godes M, Nissel R, Querfeld U. Systemic cardiovascular disease in uremic rats induced by 1,25(OH)2D3. (2005) *Journal of Hypertension* **23(5):** 1067–1075.

Hammes HP, Lin J, Wagner P, Feng Y, vom Hagen F, Krzizok T, Renner O, Breier G, Brownlee M, Deutsch U. Angiopoietin-2 causes pericyte dropout in the normal retina. (2004) *Diabetes* **53(4):** 1104–1110.

Haydar AA, Covic A, Colhoun H, Rubens M, Goldsmith DJA. Coronary artery calcification and aortic pulse wave velocity in chronic kidney disease patients. (2004) *Kidney International* **65(5):** 1790–1794.

Heiss A, DuChesne A, Denecke B, Grötzinger J, Yamamoto K, Renné T, Jahnen-Dechent W. Structural basis of calcification inhibition by alpha 2-HS glycoprotein/fetuin-A formation of colloidal calciprotein particles. (2003) *Journal of Biological Chemistry* **278(15):** 13333–13341.

Henley C, Colloton M, Cattley RC, Shatzen E, Towler DA, Lacey D, Martin D. 1,25-Dihydroxyvitamin D_3 but not cinacalcet HCl (Sensipar®/Mimpara®) treatment mediates aortic calcification in a rat model of secondary hyperparathyroidism. (2005) *Nephrology Dialysis Transplantation* **20(7):** 1370–1377.

Heydarkhan-Hagvall S, Helenius G, Johansson BR, Li JY, Mattsson E, Risberg B. Co-culture of endothelial cells and smooth muscle cells affects gene expression of angiogenic factors. (2003) *Journal of Cellular Biochemistry* **89(6):**1250–1259.

Hirota S, Imakita M, Kohri K, Ito A, Morii E, Adachi S, Kim HM, Kitamura Y, Yutani C, Nomura S. Expression of osteopontin messenger RNA by macrophages in atherosclerotic plaques: a possible association with calcification. (1993) *American Journal of Pathology* **143(4):** 1003–1008.

Hoffman U, Fischereder M, Marx M, Schweda F, Lang B, Straub RH, Krämer BK. Induction of cytokines and adhesion molecules in stable haemodialysis patients: is there an effect of membrane material? (2003) *American Journal of Nephrology* **23 (6):** 442–447.

Hu B, Cheng SY. Angiopoietin-2: development of inhibitors for cancer therapy. (2009) *Current Oncology Reports* **11(2):** 111–116.

Huang H, Bhat A, Woodnutt G, Lappe R. Targeting the Angpt2-Tie2 pathway in malignancy. (2010) *Nature Reviews Cancer* **10(8):** 575–585.

Huang JL, Woolf AS, Kolatsi-Joannou M, Baluk P, Sandford RN, Peters DJM, McDonald DM, Price KL, Winyard PJD, Long DA. Vascular endothelial growth factor C for polycystic kidney disease. (2016) *Journal of American Society of Nephrology* **27(1):** 69–77.

Huang Y, Li J, Karpatkin S. Identification of a family of alternatively spliced mRNA species of angiopoietin-1. (2000) *Blood* **95(6):** 1993–1999.

Hughes DP, Marron MB, Brindle NPJ. The anti-inflammatory endothelial tyrosine kinase Tie2 interacts with a novel nuclear factor-κB inhibitor ABIN-2. (2003) *Circulation Research* **92(6):** 630–636.

Ikeda T, Shirasawa T, Esaki Y, Yoshiki S, Hirokawa K. Osteopontin mRNA is expressed by smooth muscle-derived foam cells in human atherosclerotic lesions of the aorta. (1993) *Journal of Clinical Investigation* **92(6):** 2814–2820.

Iurlaro M, Scatena M, Zhu W, Fogel E, Weiting SL, Nicosia RF. Rat aorta-derived mural precursor cells express Tie2 receptor and respond directly to stimulation by the angiopoietins. (2003) *Journal of Cell Science* **116(Pt 17):** 3635–3643.

Ix JH, Shlipak MG, Sarnak MJ, Beck GJ, Greene T, Wang X, Kusek JW, Collins AJ, Levey AS, Menon V. Fetuin-A is not associated with mortality in chronic kidney disease. (2007) *Kidney International* **72(11):** 1394–1399.

Jie KE, Lilien MR, Goossens MHJ, Westerweel PE, Ing MK, Verhaar MC. Reduced endothelial progenitor cells in children with hemodialysis but not predialysis chronic kidney disease. (2010) *Paediatrics* **126(4):** e990-e993.

Johnson DW, Dent H, Hawley CM, McDonald SP, Rosman JB, Brown FG, Bannister K, Wiggens KJ. Association of dialysis modality and cardiovascular mortality in incident dialysis patients. (2009) *Clinical Journal of the American Society of Nephrology* **4(10):** 1620–1628.

Jones N, Iljin K, Dumont DJ, Alitalo K. Tie receptors: new modulators of angiogenic and lymphangiogenic responses. (2001) *Nature Reviews Molecular Cell Biology* **2(4):** 257–267.

Jourde-Chiche N, Dou L, Cerini C, Dignat-George F, Brunet P. Vascular incompetence in dialysis patients – protein bound uremic toxins and endothelial dysfunction. (2011) *Seminars in Dialysis* **24 (3):** 327–337.

Jourde-Chiche N, Dou L, Sabatier F, Calaf R, Cerini C, Robert S, Camoin-Jau, L, Argiles A, Dignat-George F, Brunet P. Levels of circulating endothelial progenitor cells are related to uremic toxins and vascular injury in haemodialysis patients. (2009) *Journal of Thrombosis and Haemostasis* **7(9):** 1576–1584.

Juno S, McKee MD, Murry CE, Shioi A, Nishizawa Y, Mori K, Mori H, Giachelli CM. Phosphate regulation of vascular smooth muscle cell calcification. (2000) *Circulation* **87(7):** e10–e17.

Kapustin A, Chatou ML, Drozdov I, Zheng Y, Davidson SM, Soong D, Furmanik M, Sanchis P, De Rosales RT, Alverez-Hernandez D, Shroff R, Yin X, Muller K, Skepper JN, Mar M, Reutelingsperger CP, Chester A, Berazzo S, Schurgers LK, Shanahan CM. Vascular smooth muscle cell calcification is mediated by regulated exosome secretion. (2015) *Circulation Research* **116(8):** 1312–1323.

Kapustin A, Davies JD, Reynolds JL, McNair R, Jones GT, Sidibe A, Schurgers LJ, Skepper JN, Proudfoot D, Mayr M, Shanahan CM. Calcium regulates key components of vascular smooth muscle cell-derived matrix vesicles to enhance calcification. (2011) *Circulation Research* **109(1):** e1–e12.

Kari JA, Donald AE, Vallance DT, Bruckdorfer KR, Leone A, Mullen MJ, Bunce T, Dorado B, Deanfield JE, Rees L. Physiology and biochemistry of endothelial function in children with chronic renal failure. (1997) *Kidney International* **52(2):** 468–472.

Karohl C, Gascón LD, Raggi P. Non-invasive imaging for assessment of calcification in chronic kidney disease. (2011) *Nature Reviews Nephrology* **7(10):** 567–577.

Katsumata K, Kusano K, Hirata M, Tsunemi K, Nagano N, Burke SK, Fukushima N. Sevelamer hydrochloride prevents ectopic calcification and renal osteodystrophy in chronic renal failure rats. (2003) *Kidney International* **64(2):** 441–450.

Kawata T, Nagano N, Obi M, Miyata S, Koyama C, Kobayashi N, Wakita S, Wada M. Cinacalcet suppresses calcification of the aorta and heart in uremic rats. (2008) *Kidney International* **74(10):** 1270–1277.

Keller G, Zimmer G, Mall G, Ritz E, Amann K. Nephron number in patients with primary hypertension. (2003) *New England Journal of Medicine* **348(2):** 101–108.

Kerr M, Bray B, Medcalf J, O'Donoghue DJ, Matthews B. Estimating the financial cost of chronic kidney disease to the NHS in England. (2012) *Nephrology Dialysis Transplantation* **27(Suppl 3):** iii73–80.

Kestenbaum B. Phosphate metabolism in the setting of chronic kidney disease: significance and recommendations for treatment. (2007) *Seminars in Dialysis* **20(4):** 286–294.

Ketteler M, Bongartz P, Westenfeld R, Wildberger JE, Mahnken AH, Böhm R, Metzger T, Wanner C, Jahnen-Dechent W, Floege J. Association of low fetuin-A (AHSG) concentrations in serum with cardiovascular mortality in patients on dialysis: a cross-sectional study. (2003) *The Lancet* **361(9360):** 827–833.

Kidney Disease: Improving Global Outcomes (KDIGO) CKD Work Group (2013) KDIGO 2012 clinical practice guidelines for the evaluation and management of chronic kidney disease. *Kidney International* **(Suppl 3):** 1–150.

Kielstein JT, Böger RH, Bode-Böger SM, Schäffer J, Barbey M, Kock KM, Frölich JC. Asymmetric dimethylarginine plasma concentrations differ in patients with end-stage renal disease. (1999) *Journal of American Society of Nephrology* **10(3):** 594–600.

Kim I, Kim J, Ryu YS, Jung SH, Nah JJ, Koh GY. Characterisation and expression of a novel alternatively spliced human angiopoietin-2. (2000) *Journal of Biological Chemistry* **275(24):** 18550–18556.

Kim I, Kim JH, Moon SO, Kwak HJ, Kim NG, Koh GY. Angiopoietin-2 at high concentration can enhance endothelial cell survival through the phosphatidylinositol 3'-kinase/Akt signal transduction pathway. (2000) *Oncogene* **19(39):** 4549–4552.

Kisanuki YY, Hammer RE, Miyazaki J, Williams SC, Richardson JA, Yanagisawa M. Tie2-Cre transgenic mice: a new model for endothelial cell-lineage analysis *in vivo*. (2001) *Developmental Biology* **230(2):** 230–242.

Koblizek T, Weiss C, Yancopoulos GD, Deutsch U, Risau W. Angiopoietin-1 induces sprouting angiogenesis *in vitro*. (1998) *Current Biology* **8(9):** 529–532.

Korhonen EA, Lampinen A, Giri H, Anisimov A, Kim M, Allen B, Fang S, D'Amico G, Sipilä TJ, Lohela M, Strandin T, Vaheri A, Ylä-Herttuala S, Koh GY, McDonald DM, Alitalo K, Saharinen P. Tie1 controls angiopoietin function in vascular remodelling and inflammation. (2016) *The Journal of Clinical Investigation* **126(9):** 3495–3510.

Krenning G, Dankers PY, Drouven JW, Waanders F, Franssen CF, van Luyn MJ, Harmsen MC, Popa ER. Endothelial progenitor cell dysfunction in patients with progressive chronic kidney disease. (2009) *American Journal of Physiology Renal Physiology* **296(6):** f1314–f1322.

Kümpers P, van Meur M, David S, Molema G, Bijzet J, Lukasz A, Biertz F, Haller H, Zijstra JG. Time-course of angiopoietin-2 release during experimental human endotoxemia and sepsis. (2009) *Critical Care* **13(3):** R64.

Kurts C, Panzer U, Anders H, Rees AJ. The immune system and kidney disease: basic concepts and clinical implications. (2013) *Nature Reviews Immunology* **13(10):** 738–753.

Laouari D, Burtin M, Phelep A, Bienaime F, Noel L, Lee DC, Legendre C, Friendlander G, Pontoglio M, Terzi F. A transcriptional network underlies susceptibility to kidney disease progression. (2012) *European Molecular Biology Organisation Molecular Medicine* **4(8):** 825–839.

Lawrence T. The nuclear factor NF-κB pathway in inflammation. (2009) *Cold Spring Harbour Perspectives in Biology* **1(6):** a001651.

Lee OH, Fueyo J, Xu J, Yung WK, Lemoine MG, Lang FF, Bekele BN, Zhou X, Alonso MA, Aldape KD, Fuller GN, Gomez-Manzano C. Sustained angiopoietin-2 expression disrupts vessel formation and inhibits glioma growth. (2006) *Neoplasia* **8(5):** 419–428.

Lee O, Xu J, Fueyo J, Fuller GN, Aldape KD, Alonso MM, Piao Y, Liu T, Lang FF, Bekele BN, Gomez-Manzano C. Expression of the receptor tyrosine kinase Tie2 in neoplastic glial cells is associated with integrin β1-dependent adhesion to the extracellular matrix. (2006) *Molecular Cancer Research* **4(12):** 915–926.

Lemieux C, Maliba R, Favier J, Theoret JF, Merhi Y, Sirois MG. Angiopoietins can directly activate endothelial cells and neutrophils to promote pro-inflammatory responses. (2005) *Blood* **105(4):** 1523–1530.

Leopold JA. Vascular calcification: an age-old problem of old age. (2013) *Circulation* **137(2):** 2380–2382.

Leopold JA. Vascular calcification: mechanisms of vascular smooth muscle cell calcification. (2015) *Trends in Cardiovascular Medicine* **25(4):** 267–274.

Levin A, Djurdjev O, Barrett B, Burgess E, Carlisle E, Ethier J, Jindal K, Mendelssohn D, Tobe S, Singer J, Thompson C. Cardiovascular disease in patients with chronic kidney disease: getting to the heart of the matter. (2001) *American Journal of Kidney Diseases* **38(6):** 1398–1407.

Li Q, Guo H, Chou DW, Berndt A, Sundberg JP, Uitto J. Mutant *Enpp1^{asj}* mice as a model for generalised arterial calcification of infancy. (2013) *Disease Models and Mechanisms* **6(5):** 1227–1235.

Li X, Yang H, Giachelli CM. BMP-2 promotes phosphate uptake, phenotypic modulation, and calcification of human vascular smooth muscle cells. (2008) *Atherosclerosis* **199(2):** 271–277.

Liao XB, Zhang ZY, Yuan K, Liu Y, Feng X, Cui RR, Hu YR, Yuan ZS, Gu L, Li SJ, Mao DA, Lu Q, Zhou XM, de Jesus Perez VA, Yuan LQ. MiR-133a modulates osteogenic differentiation of vascular smooth muscle cells. (2013) *Endocrinology* **154(9):** 3344–3352.

Limdi NA, Beasley TM, Baird MF, Goldstein JA, McGwin G, Arnett DK, Acton RT, Allon M. Kidney function influences warfarin responsiveness and haemorrhagic complications. (2009) *Journal of American Society of Nephrology* **20(4):** 912–921.

Litwin M, Wüjl E, Jourdan C, Trelewicz J, Niemirska A, Fahr K, Jobs K, Grenda R, Wawer Z, Rajszys P, Tröger J, Mehls O, Schaefer F. Altered morphological properties of large arteries in children with chronic renal failure and after renal transplantation. (2005) *Journal of American Society of Nephrology* **16(5):** 1494–1500.

Litwin M, Wühl E, Jourdan C, Niemirska A, Schenk JP, Jobs K, Grenda R, Wawer ZT, Rajszyz P, Mehls O, Schaefer F. Evolution of large-vessel arteriopathy in paediatric patients with chronic kidney disease. (2008) *Nephrology Dialysis Transplantation* **23(8):** 2552–2557.

Liu Y, Drozdov I, Shroff R, Beltran LE, Shanahan CM. Prelamin A accelerates vascular calcification via activation of the DNA damage response and senescence-associated secretory phenotype in vascular smooth muscle cells. (2013) **112(10):** 99–109.

Locatelli F, Pozzoni P, Tentori F, Del Vecchio L. Epidemiology of cardiovascular risk in patients with chronic kidney disease. (2003) *Nephrology Dialysis Transplantation* **18(Supp 7):** vii2–vii9.

Long DA, Kolatsi-Joannou M, Price KL, Dessapt-Baradez C, Huang JL, Papakrivopoulou E, Hubank M, Korstanje R, Gnudi L, Woolf AS. Albuminuria is associated with too few glomeruli and too much testosterone. (2013) *Kidney International* **83(6):** 1118–1129.

Long DA, Norman JT, Fine LG. Restoring the renal microvasculature to treat chronic kidney disease. (2012) *Nature Reviews Nephrology* **8(4):** 244–250.

Lorell BH, Carabello BA. Left ventricular hypertrophy: pathogenesis, detection, and prognosis. (2000) *Circulation* **102(4):** 470–479.

Luo G, Ducy P, McKee MD, Pinero GJ, Loyer E, Behringer RR, Karsenty G. Spontaneous calcification of arteries and cartilage in mice lacking matrix Gla protein. (1997) *Nature* **386(6620):** 78–81.

Macdonald PR, Progias P, Ciani B, Patel S, Mayer U, Steinmetz MO, Kammerer RA. Structure of the extracellular domain of Tie receptor tyrosine kinases and localization of the angiopoietin-binding epitope. (2006) *Journal of Biological Chemistry* **281(38):** 28408–28414.

Mahmood SS, Levy D, Vasan RS, Wang TJ. The Framingham heart study and the epidemiology of cardiovascular diseases: a historical perspective. (2014) *The Lancet* **383(9921):** 999–1008.

Maisonpierre PC, Suri C, Jones PF, Bartunkova S, Wieland SJ, Radziejewski C, Compton D, McClain J, Aldrich TH, Papadopoulos N, Daly TJ, Davis S, Sato TN, Yancopoulos GD. Angiopoietin-2, a natural antagonist for Tie2 that disrupts *in vivo* angiogenesis. (1997) *Science* **277(5322):** 55–60.

Master Z, Jones N, Tran J, Jones J, Kerbel RS, Dumon DJ. Dok-R plays a pivotal role in angiopoietin-1-dependent cell migration through recruitment and activation of Pak. (2001) *The EMBO Journal* **20(21):** 5919–5928.

Merino A, Portoles J, Selgas R, Ojeda R, Buendia P, Ocana J, Bajo MA, del Peso G, Carracedo J, Ramirez R, Martin-Malo A, Aljima P. Effect of different dialysis modalities on microinflammatory status and endothelial damage. (2010) *Clinical Journal of American Society of Nephrology* **5(2):** 227–234.

Mita AC, Takimoto CH, Mita M, Tolcher A, Sankhala K, Sarantopoulos J, Valdivieso M, Wood L, Rasmussen E, Sun Yu-Nien, Zhong ZD, Bass MB, Le N, LoRosso P. Phase 1 study of AMG 386, a selective angiopoietin 1/2 neutralising peptibody, in combination with chemotherapy in adults with advanced solid tumours. (2010) *Clinical Cancer Research* **16(11):** 3044–3056.

Mitsnefes M. Cardiovascular disease in children with chronic kidney disease. (2012) *Journal of American Society of Nephrology* **23(4):** 578–585.

Mitsnefes MM, Kimball TR, Kartal J, Witt SA, Glascock BJ, Khoury PR, Daniels SR. Progression of left ventricular hypertrophy in children with early chronic kidney disease: 2-year follow-up study. (2006) *The Journal of Paediatrics* **149(5):** 671–675.

Mitsnefes MM, Kimball TR, Witt SA, Glascock BJ, Jhoury PR, Daniels SR. Abnormal carotid artery structure and function in children and adolescents with successful renal transplantation. (2004) *Circulation* **110(1):** 97–101.

Mofarrahi M, Hussain SNA. Expression and functional roles of Angpt2 in skeletal muscles. (2011) *PLoS One*. **6(7):** e22882.

Moe SM, O'Neill KD, Duan D, Ahmed S, Chen NX, Leapman SB, Fineberg N, Kopecky K. Medial artery calcification in ESRD patients is associated with deposition of bone matrix proteins. (2002) *Kidney International* **61(2):** 638–647.

Mohandas R, Segal MS. Endothelial progenitor cells and endothelial vesicles – what is the significance for patients with chronic kidney disease? (2010) *Blood Purification* **29(2):** 188–162.

Monroy MA, Fang J, Li S, Ferrer L, Birkenbach MP, Lee IJ, Wang H, Yang XF, Choi ET. Chronic kidney disease alters vascular smooth muscle cell phenotype. (2015) *Frontiers in Bioscience* **20:**784–795.

Moody WE, Edwards NS, Madhani M, Chue CD, Steeds RP, Ferro CJ, Townend JN. Endothelial dysfunction and cardiovascular disease in early stage kidney chronic kidney disease: cause or association? (2012) *Atherosclerosis* **223(1):** 86–94.

Munroe PB, Olgunturk RO, Fryns JP, Van Maldergem L, Ziereisen F, Yuksel B, Gardiner RM, Chung E. Mutations in the gene encoding the human matrix Gla protein cause Keutel syndrome. (1999) *Nature Genetics* **21(1):** 142–144.

Murphy SW, Foley RN, Parfrey PS. Screening and treatment for cardiovascular disease in patients with chronic renal disease. (1998) *American Journal of Kidney Diseases* **32(5):** S184–S199.

Murshed M, Schinke T, McKee MD, Karsenty G. Extracellular matrix mineralisation is regulated locally; different roles of two Gla-containing proteins. (2004) *Journal of Cell Biology* **165(5):** 625–630.

National Institute for Clinical Excellence. Chronic kidney disease: early identification and management of chronic kidney disease in adults in primary and secondary care. (2014) **NICE Guideline (182)**.

National Kidney Foundation. KDOQI Clinical Practice Guideline for Diabetes and CKD: 2012 update. (2012) *American Journal of Kidney Disease* **60(5):** 850–886.

Neven E, D'Haese PC. Vascular calcification in chronic renal failure: what have we learned from animal studies? (2011) *Circulation Research* **108(2):** 249–264.

New SE, Goettsch C, Aikawa M, Marchini JF, Shibasaki M, Yabusaki K, Libby P, Shanahan CM, Croce K, Aikawa E. Macrophage-derived matrix vesicles: an alternative novel mechanism for microcalcification in atherosclerotic plaques. (2013) *Circulation Research* **113(1):** 72–77.

NHS Blood and Transplant. Organ Donation and Transplantation – *Activity figures for the UK as at 10 April 2015* (Accessed September 2015) https://nhsbtmediaservices.blob.core.windows.net/organ-donation-assets/pdfs/annual_stats.pdf.

Oh J, Wunsch R, Turzer M, Bahner M, Raggi P, Querfeld U, Mehls O, Schaefer F. Advanced coronary and carotid arteriopathy in young adults with childhood-onset chronic renal failure. (2002) *Circulation* **106(1):** 100–105.

Oliner J, Min H, Leal J, Yu D, Rao S, You E, Tang X, Kim H, Meyer S, Han SJ, Hawkins N, Rosenfeld R, Davy E, Graham K, Jacobsen F, Stevenson S, Ho J, Chen Q, Hartmann T, Michaels M, Kelley M, Li L, Sitney K, Martin F, Sun J, Zhang N, Lu J, Estrada J, Kumar R, Coxon A, Kaufman S, Pretorius J, Sully S, Cattley R, Payton M, Coats S, Nguyen L, Desilva B, Ndifor A, Hayward I, Radinsky R, Boone T, Kendall R. Suppression of angiogenesis and tumour growth by selective inhibition of angiopoietin-2. (2004) *Cancer Cell* **6(5):** 507–516.

Owen DRJ, Lindsay AC, Choudhury RP, Fayad ZA. Imaging of atherosclerosis. (2011) *Annual Review of Medicine* **62:** 25–40.

Pai A, Leaf EM, El-Abbadi M, Giacelli CM. Elastin degradation and vascular smooth muscle cell phenotype change precede cell loss and arterial medial calcification in a uremic mouse model of chronic kidney disease. (2011) *American Journal of Pathology* **178(2):**764–773.

Pallone TL, Edwards A, Mattson DL. Renal medullary circulation. (2012) *Comprehensive Physiology* **2(1):** 97-140.

Panizo S, Naves-Díaz M, Carrillo-López N, Martínez-Arias L, Fermández-Martín JL, Ruiz-Torres MP, Cannata-Andia JB, Rodríguez I. MicroRNAs 29b, 133b, and 211 regulate vascular smooth muscle cell calcification mediated by high phosphorus. (2015) *Journal of American Society of Nephrology* **27(3):** 824-834.

Parekh RS, Carroll CE, Wolfe RA, Port FK. Cardiovascular mortality in children and young adults with end-stage kidney disease. (2002) *The Journal of Paediatrics* **141(2):** 191–197.

Patel JI, Hykin PG, Gregor ZJ, Boulton M, Cree IA. Angiopoietin concentrations in diabetic retinopathy. (2004) *British Journal of Ophthalmology* **89(4):** 480–483.

Patel AS, Smith A, Nucera S, Biziato D, Saha P, Attia RQ, Humphries J, Mattock K, Grover SP, Lyons OT, Guidotti LG, Siow R, Ivetic A, Eggington S, Waltham M, Naldini L, De Palma M, Modarai B. TIE2-expressing monocytes/macrophages regulate revascularisation of the ischemic limb. (2013) *EMBO Molecular Medicine* **5(6):** 858–869.

Pivin E, Ponte B, Pruijm M, Ackermann D, Guessous I, Ehret G, Liu YP, Drummen NE, Knapen MH, Pechere-Bertschi A, Paccaud F, Mohaupt M, Vermeer C, Staessen JA, Vogt B, Martin PY, Burnier M, Bochud M. Inactive matrix gla-protein is associated with arterial stiffness in an adult population-based study. (2015) *Hypertension* **66(1):** 86–92.

Potente M, Urbich C, Sasaki K, Hofmann WK, Heeschen C, Aicher A, Kollipara R, DePinho RA, Zeiher AM, Dimmeler S. Involvement of Foxo transcription factors in angiogenesis and postnatal neovascularisation. (2005) *Journal of Clinical Investigation* **115(9):** 2382–2392.

Price PA, Faus SA, Williamson MK. Warfarin causes rapid calcification of the elastic lamellae in rat arteries and heart valves. (1998) *Arteriosclerosis Thrombosis Vascular Biology* **18(9):** 1400–1407.

Price PA, Roublick AM, Williamson MK. Artery calcification in uremic rates ins increased by a low protein diet and prevented by treatment with ibandronate. (2006) *Kidney International* **70(9):** 1577–1583.

Proudfoot D, Skepper JN, Hegyi L, Bennett MR, Shanahan CM, Weissberg PL. Apoptosis regulates human vascular calcification *in vitro*. (2000) *Circulation Research* **87(11):** 1055–1062.

Proudfoot D, Skepper JN, Shanahan CM, Weissberg PL. Calcification of human vascular cells *in vitro* is correlated with high levels of matrix Gla protein and low levels of osteopontin expression. (1998) *Arteriosclerosis Thrombosis and Vascular Biology* **18(3):** 379–388.

Proudfoot D, Shanahan C. Human vascular smooth muscle cell culture. (2012) *Methods in Molecular Biology* **806:** 251–263.

Pruthi R, Hamilton AJ, O'Brien C, Casula A, Braddon F, Inward C, Lewis M, Maxwell H, Stojanovic J, Tse Y, Sinha MD. Demography of the UK paediatric renal replacement therapy population in 2013. (2014) *The UK Renal Registry: The Seventeenth Annual Report* **Chapter 4:** 95–106.

Querfeld U, Anarat A, Bayazit AK, Bakkaloglu AS, Bilginer Y, Caliskan S, Civilibal M, Doyon A, Duzova A, Kracht D, Litwin M, Melk A, Mir S, Sözeri B, Shroff R, Zeller R, Wühl E, Schaefer F; 4C Study Group. The Cardiovascular Comorbidity in Children with Chronic Kidney Disease (4C) study: objectives, design, and methodology. (2010) *Clinical Journal of American Society of Nephrology* **5(9):** 1642–1648.

Ragnauth CD, Warren DT, Liu Y, McNair R, Tajsic T, Figg N, Shroff R, Skepper J, Shanahan CM. Prelamin A acts to accelerate smooth muscle cell senescence and is a novel biomarker of human vascular aging. (2010) *Circulation* **121(20):** 2200–2210.

Reynolds JL, Joannides AJ, Skepper JN, McNair R, Schurgers LJ, Proudfoot D, Jahnen-Dechent W, Weissberg PL, Shanahan CM. Human vascular smooth muscle cells undergo vesicle-mediated calcification in response to changes in extracellular calcium and phosphate concentrations: a potential mechanism for accelerated vascular calcification in ESRD. (2004) *Journal of American Society of Nephrology* **15(11):** 2857–2867.

Reynolds JL, Skepper JN, McNair R, Kasama T, Gupta K, Weissberg PL, Jahnen-Dechent W, Shanahan CM. Multifunctional roles for serum protein fetuin-A in inhibition of human vascular smooth muscle cell calcification. (2005) *Journal of American Society of Nephrology* **16(10):** 2920–2930.

Rodríguez-Ayala E, Yao Q, Holmén C, Lindholm B, Sumitran-Holgersson S, Stenvinkel P. Imbalance between detached circulating endothelial cells and endothelial progenitor cells in chronic kidney disease. (2006) *Blood Purification* **24(2):** 196–202.

Rondaij MG, Bierings R, Kragt A, van Mourik JA, Voorberg J. Dynamics and plasticity of Weibel-Palade bodies in endothelial cells. (2006) *Arteriosclerosis, Thrombosis, and Vascular Biology* **26(5):** 1002–1007.

Ross R. Atherosclerosis – an inflammatory disease. (1999) *The New England Journal of Medicine* **340(2):** 115–126.

Rzucido EM, Martin KA, Powell RJ. Regulation of vascular smooth muscle cell differentiation. (2007) *Journal of Vascular Surgery* **45(6):** A25–A32.

Saaristo A, Karpanen T, Alitalo K. Mechanisms of angiogenesis and their use in the inhibition of tumour growth and metastasis. (2000) *Oncogene* **19(53):** 6122–6129.

Sage AP, Tintut Y, Demer LL. Regulatory mechanisms in vascular calcification. (2010) *Nature Reviews Cardiology* **7(9):** 528–536.

Saharinen P, Alitalo K. The yin, the yang, and the angiopoietin-1. (2011) *Journal of Clinical Investigation* **121(6):** 2157–2159.

Samuel SM, Tonelli MA, Foster BJ, Alexander RT, Nettel-Aguirre A, Soo A, Hemmelgarn BR, Pediatric Renal Outcomes Group. Survival in paediatric dialysis and transplant patients. (2011) *Clinical Journal of American Society of Nephrology* **6(5):** 1094–1099.

Sanz J, Fayad ZA. Imaging of atherosclerotic cardiovascular disease. (2008) *Nature* **451(7181):** 953–957.

Savant S, La Porta S, Budnik A, Busch K, Hu J, Tisch N, Korn C, Valls AF, Benest AV, Terhardt D, Qu X, Adams RH, Baldwin HS, Ruiz de Almodóvar C, Rodewald HR, Augustin HG. The orphan receptor Tie1 controls angiogenesis and vascular remodelling by differentially regulating Tie2 in tip and stalk cells. (2015) *Cell Reports* **12(11):** 1761–1773.

Saygili A, Barutçu O, Cengiz N, Tarhan N, Pourbagher A, Niron E, Saatçi U. Carotid intima media thickness and left ventricle changes in children with end-stage renal disease. (2002) *Transplantation Proceedings* **34(6):** 2073–2075.

Schafer C, Heiss A, Schwarz A, Westenfeld R, Ketteler M, Floege J, Muller-Esterl W, Schinke T, Jahnen-Dechent W. The serum protein alpha 2-Heremans-Schmid glycoprotein/fetuin-A is a systematically acting inhibitor of ectopic calcification. (2003) *Journal of Clinical Investigation* **112(3)** 357–366.

Scharpfenecker M, Fiedler U, Reiss Y, Augustin HG. The Tie-2 ligand Angiopoietin-2 destabilises quiescent endothelium through an internal autocrine loop mechanism. (2005) *Journal of Cell Science* **118(Pt 4):** 771–780.

Schindelin J, Arganda-Carreras I, Frise E. Fiji: an open-source platform for biological-image analysis. (2012) *Nature Methods* **9(7):** 676–682.

Schinke T, Karsenty G. Vascular calcification—a passive process in need of inhibitors. (2000) *Nephrology Dialysis Transplantation* **15(9):** 1272–1274.

Schurgers LJ, Spronk HM, Soute BA, Schiffers PM, DeMey JG, Vermeer C. Regression of warfarin-induced medial elastocalcinosis by high intake of vitamin K in rats. (2007) *Blood* **109(7):** 2823–2831.

Seeger H, Bonani M, Segerer S. The role of lymphatics in renal inflammation. (2012) *Nephrology Dialysis Transplantation* **27(7):** 2634–2641.

Semones M, Feng Y, Johnson N, Adams JL, Winkler J, Hansbury M. Pyridinylimidazole inhibitors of Tie2 kinase. (2007) *Bioorganic and Medicinal Chemistry Letters* **17(17):** 4756–4760.

Sfliligoi C, de Luca A, Cascone I, Sorbello V, Ponzone R, Biglia N, Audero E, Arisio R, Bussolino F, Sismondi P, De Bortoli M. Angiopoietin-2 expression in breast cancer correlates with lymph node invasion and short survival. (2003) *International Journal of Cancer* **103(4):** 466–474.

Shah M, Tsadok MA, Jackevicius CA, Essebag V, Eisenberg MJ, Rahme E, Humpries KH, Tu JV, Behlouli H, Guo H, Pilote L. Warfarin use and the risk for stroke and bleeding in patients with atrial fibrillation undergoing dialysis. (2014) *Circulation* **129(11):** 1196–1203.

Shanahan CM. Mechanisms of vascular calcification in CKD — evidence for premature aging? (2013) *Nature Reviews Nephrology* **9(11):** 661–670.

Shanahan CM, Cary NR, Salisbury JR, Proudfoot D, Weissberg PL, Edmonds ME. Medial localisation of mineralisation-regulating proteins in association with Mönckeberg's sclerosis: evidence for smooth muscle cell-mediated vascular calcification. (1999) *Circulation* **100(21):** 2168–2176.

Shobeiri N, Adams MA, Holden RM. Vascular calcification in animal models of CKD: a review. (2010) *American Journal of Nephrology* **31(6):** 471–481.

Shoshan MC, Linder S. Target specificity and off-target effects as determinants of cancer drugs. (2008) *Expert Opinion on Drug Metabolism & Toxicology* **4(3):** 273–280.

Shroff R. Dysregulated mineral metabolism in children with chronic kidney disease. (2011) *Current Opinion in Nephrology and Hypertension* **20(3):** 233–240.

Shroff C, McNair R, Skepper JN, Figg N, Schurgers LJ, Deanfield J, Rees L, Shanahan CM. Chronic mineral dysregulation promotes vascular smooth muscle cell adaptation and extracellular matrix calcification. (2010) *Journal of American Society of Nephrology* **21(1):** 103–112.

Shroff R, Long DA, Shanahan C. Mechanistic insights into vascular calcification in CKD. (2012) *Journal of the American Society of Nephrology* **24(2):** 179–189.

Shroff RC, McNair R, Figg N, Skepper JN, Schurgers L, Gupta A, Hiorns M, Donald AE, Deanfield J, Rees L, Shanahan CM. Dialysis accelerates medial vascular calcification in part by triggering smooth muscle cell apoptosis. (2008) *Circulation* **118(17):** 1748–1757.

Shroff RC, Price K, Kolatsi-Joannou M, Todd AF, Wells D, Deanfield J, Johnson RJ, Rees L, Woolf AS, Long DA. Circulating Angiopoietin-2 is a marker for early cardiovascular disease in children on chronic dialysis. (2013) *PLoS One* **8(2):** e56273.

Singh H, Tahir TA, Alawo DOA, Issa E, Brindle NPJ. Molecular control of angiopoietin signalling. (2011) *Biochemical Society Transactions* **39(6):** 1592–1596.

Sinnathamby T, Yun J, Clavet-Lanthier ME, Cheong C, Sirois MG. VEGF and angiopoietins promote inflammatory cell recruitment and mature blood vessel formation in murine sponge/Matrigel model. (2015) *Journal of Cellular Biochemistry* **116(1):** 45–57.

Soriano S, Carmona A, Triviño F, Rodriguez M, Alvarez-Benito M, Martín-Malo A, Alvarez-Lara MA, Ramírez R, Aljama P, Carracedo J. Endothelial damage and vascular calcification in patients with chronic kidney disease. (2014) *American Journal of Physiology Renal Physiology* **307(11):** F1302–11.

Speer MY, Chien YC, Quan M, Yang HY, Vali H, McKee MD, Giachelli CM. Smooth muscle cells deficient in osteopontin have enhanced susceptibility to calcification *in vitro*. (2005) *Cardiovascular Research.* **66(2):** 324–333.

Speer MY, Giachelli CM. Regulation of cardiovascular calcification. (2004) *Cardiovascular Pathology* **13(2):** 63–70.

Speer T, Rohrer L, Blyszczuk P, Shroff R, Kuscgnerus K, Kränkel N, Kania G, Zewinger S, Akhmedov A, Shi Y, Martin T, Perisa D, Winnik S, Müller MF, Sester U, Wernicke G, Jung A, Gutteck U, Eriksson U, Geisel J, Deanfield J, von Eckardstein A, Lüscher TF, Flisher D, Bahlmann FH, Landmesser U. Abnormal high-density lipoprotein induces endothelial dysfunction via activation of toll-like receptor-2. (2013) *Immunity* **38(4):** 754–768.

Srinivasan R, Zabuawala T, Huang H, Zhang J, Gulati P, Fernadez S, Karlo JC, Landreth GE, Leone G, Ostrowski MC. *Erk1* and *Erk2* regulate endothelial cell proliferation and migration during mouse embryonic angiogenesis. (2009) *PLOS ONE* **4(12):** e8283.

Steenkamp R, Rao A, Roderick P. Survival and cause of death in UK adult patients on renal replacement therapy in 2013: national and centre-specific analyses. (2014) *The UK Renal Registry: The Seventeenth Annual Report* **Chapter 5:** 107–137.

Stokes JB. Consequences of frequent hemodialysis: comparison to conventional hemodialysis and transplantation. (2011) *Transactions of the American Clinical and Climatological Association* **122:** 124–136.

Stolz DB, Sims-Lucas S. Unwrapping the origins and roles of the renal endothelium. (2015) *Pediatric Nephrology* **30(6):** 865–872.

Takahama M, Tsutsumi M, Tsujiuchi T, Nezu K, Kushibe K, Taniguchi S, Kotake Y, Konishi Y. Enhanced expression of Tie2, its ligand angiopoietin-1, vascular endothelial growth factor, and CD31 in human non-small cell lung carcinomas. (1999) *Clinical Cancer Research* **5(9):** 2506–2510.

Tanaka S, Mori M, Sakamoto Y, Makuuchi M, Sugimachi K, Wands JR. Biologic significance of angiopoietin-2 expression in human hepatocellular carcinoma. (1999) *Journal of Clinical Investigation* **103(3):** 341–345.

Tantisattamo E, Han KH, O'Neill WC. Increased vascular calcification in patients receiving warfarin. (2015) *Arteriosclerosis, Thrombosis, and Vascular Biology*. **35(1):** 237–42.

Thamratnopkoon S, Susantitaphong P, Tumkosit M, Katavetin P, Tiranathanagul K, Praditpornsilpa K, Eiam-Ong S. Correlations of plasma desphosphorylated uncarboxylated matrix Gla protein with vascular calcification and vascular stiffness in chronic kidney disease. (2017) *Nephron* **135(3):** 167–172.

Thurston G, Daly C. The complex role of Angiopoietin-2 in the angiopoietin-Tie signalling pathway. *Cold Spring Harbour Perspectives in Medicine* (2012) **2(9):** a006650.

Thurston G, Suri C, Smith K, McClain J, Sato TN, Yancopoulos GD, McDonald DM. Leakage-resistant blood vessels in mice transgenically overexpressing angiopoietin-1. (1999) *Science* **286 (5449):** 2511–2514.

Thurston G, Rudge JS, Ioffe E, Zhou H, Ross L, Croll SD, Glazer N, Holash J, McDonald DM, Yancopoulos GD. Angiopoietin-1 protects the adult vasculature against plasma leakage. (2000) *Nature Medicine* **6(4):** 460–463.

Tian S, Hayes AJ, Metheny-Barlow LJ, Li Y. Stabilisation of breast cancer xenograft neovasculature by angiopoietin-1. (2002) *British Journal of Cancer* **86(4):**645–651.

Tintut Y, Alfonso Z, Saini T, Radcliff K, Watson K, Boström K, Demer LL. Multilineage potential of cells from the artery wall. (2003) *Circulation* **108(20):** 2505–2510.

Tomlinson JA, Caplin B, Boruc O, Bruce-Cobbold C, Cutillas P, Dormann D, Faull P, Grossman RC, Khadayate S, Mas VR, Nitsch DD, Wang Z, Norman JT, Wilcox CS, Wheeler DC, Leiper J. Reduced renal methylarginine metabolism protects against progressive kidney disease. (2015) *Journal of American Society of Nephrology* **26(12):** 3045–3059.

Tsai MC, Chen L, Zhou J, Tang Z, Hsu TF, Wang Y, Shih YT, Peng HH, Wang N, Guan Y, Chien S, Chiu JJ. Sheer stress induces synthetic-to-contractile phenotypic modulation in smooth muscle cells via peroxisome proliferator-activated receptor a/d activations by prostacyclin released by sheared endothelial cells. (2009) *Circulation Research* **105(5):** 471–480.

Tuppurainen L, Sallinen H, Karvonen A, Valkonen E, Laakso H, Liimatainen T, Hytönen E, Hämäläinen K, Kosma VM, Anttila M, Ylä-Herttuala S. Combined gene therapy using AdsVEGFR2 and AdsTie2 with chemotherapy reduces the growth of human ovarian cancer and formation of ascites in mice. (2017) *International Journal of Gynaecological Cancer* **27(5):** 879–886.

Urbich C, Heeschen C, Aicher A, Dernback E, Zeiher AM, Dimmeler S. Relevance of monocytic features for neovascularisation capacity of circulating endothelial progenitor cells. (2003) *Circulation* **108(2):** 2511–2516.

Valentijn KM, Sadler JE, Valentijn JA, Voorberg J, Eikenboom J. Functional architecture of Weibel-Palade bodies. (2011) *Blood* **117(19):** 5033–5043.

Valenzuela DM, Griffiths JA, Rojas J, Aldrich TH, Jones PF, Zhou H, McClain J, Copeland NG, Gilbert DJ, Jenkins NA, Huang T, Papadopoulos N, Maisonpierre PC, Davis S, Yancopoulos GD. Angiopoietins 3 and 4: diverging gene counterparts in mice and humans. (1999) *Proceedings of the National Academy of Science* **96(5):** 1904–1909.

van Summeren MJH, Hameleers JM, Schurgers LJ Hoeks AP, Uiterwaal CS, Krüger T, Vermeer C, Kuis W, Lilien MR. Circulating calcification inhibitors and vascular properties in children after renal transplantation (2008) *Pediatric Nephrology* **23(6):** 985–993.

Venneri MA, De Palma M, Ponzoni M, Pucci F, Scielzo C, Zonari E, Mazzieri R, Doglinion C, Naldini L. Identification of proangiogenic TIE2-expressing monocytes (TEMs) in human peripheral blood and cancer. (2007) *Blood* **109(12):** 5276–6285.

Wada T, McKee MD, Steitz S, Giachelli CM. Calcification of vascular smooth muscle cell cultures: inhibition by osteopontin. (1999) *Circulation* **84(2):** 166–178.

Wadei HM, Textor SC. The role of the kidney in regulating arterial blood pressure. (2012) *Nature Reviews Nephrology* **8(10):** 602–609.

Walker F, Kato A, Gonex L, Hibbs ML, Pouliot N, Levitzki A, Burgess AW. Activation of the Ras/mitogen-activated protein kinase pathway by kinase-defective epidermal growth factor receptors results in cell survival but not proliferation. (1998) *Molecular and Cellular Biology* **18(12):** 7192–7204.

Wallin R, Cain D, Sane DC. Matrix Gla protein synthesis and gamma-carboxylation in the aortic vessel wall and proliferating vascular smooth muscle cells. (1999) *Thrombosis and Haemostasis* **82(6):** 1764–1767.

Wang W, Ha CH, Jhun BS, Wong C, Jain MK, Jin ZG. Fluid shear stress stimulates phosphorylation-dependent nuclear export of HDAC5 and mediates expression of KLF2 and eNOS. (2010) *Blood* **115(14):** 2971-2979.

Weber C, Noels H. Atherosclerosis: current pathogenesis and therapeutic options. (2011) *Nature Medicine* **17(11):** 1410–1422.

Weber CC, Cai H, Ehrbar M, Kubota H, Martiny-Baron G, Weber W, Djonov V, Weber E, Mallik AS, Fussenegger M, Frei K, Hubbell JA, Zisch AH. Effects of protein and gene transfer of the angiopoietin-1 fibrinogen-like receptor binding domain on endothelial and vessel organisation. (2005) *The Journal of Biological Chemistry* **280(23):** 22445–22453.

Welford AF, Biziato D, Coffelt SB, Nucera S, Fisher M, Pucci F, Di Serio C, Naldini L, De Palma M, Tozer GM, Lewis CE. Tie2-expressing macrophages limit the therapeutic efficiency of the vascular-disrupting agent combretastatin A4 phosphate in mice. (2011) *The Journal of Clinical Investigation* **121(5):** 1969–1973.

Westenfeld R, Schäfer C, Krüger T, Haarmann C, Schurgers LJ, Reutelingsperger C, Ivanovski O, Drueke T, Massy ZA, Ketteler M, Floege J, Jahnen-Dechent W. Fetuin-A protects against atherosclerotic calcification in CKD. (2009) *Journal of American Society of Nephrology* **20(6):** 1264–1274.

Wilson AC, Urbina E, Witt SA, Glascock BJ, Kimball TR, Mitsnefes M. Flow-mediated vasodilation of the brachial artery in children with chronic kidney disease. (2008) *Pediatric Nephrology* **23(8):** 1297–1302.

Xiao S, Wagner L, Schmidt RJ, Baylis C. Circulating endothelial nitric oxide synthase inhibitory factor in some patients with chronic renal disease. (2001) *Kidney International* **59(4):** 1466–1472.

Woolf AS, Gnudi L, Long DA. Roles of angiopoietins in kidney development and disease. (2009) *Journal of American Society of Nephrology* **20(2):** 239–244.

Wu SS, Lin X, Yuan LQ, Liao EY. The role of epigenetics in arterial calcification. (2015) *Biomed Research International* **Vol 2015**: Article ID 320849.

Yamada S, Tokumoto M, Tsuruya K, Tatsumoto N, Noguchi H, Kitazono T, Ooboshi H. Fetuin-A decrease induced by a low protein diet enhances vascular calcification in uremic rats with hyperphosphataemia. (2015) *American Journal of Physiology Renal Physiology* **309(8):** F744–F754.

Yilmaz MI, Saglam M, Caglar K, Cakir E, Sonmez A, Ozgurtas T, Aydin A, Eyileten T, Ozcan O, Acikel C, Tasar M, Genctoy G, Erbil K, Vural A, Zoccali C. The determinants of endothelial dysfunction in CKD: oxidative stress and asymmetric dimethylarginine. (2006) *American Journal of Kidney Diseases* **47(1):** 42–50.

Yuan HT, Khankin EV, Karumanchi SA, Parikh SM. Angiopoietin 2 is a partial agonist/antagonist of Tie2 signalling in the endothelium. (2009) *Molecular and Cellular Biology* **29(8):** 2011–2022.

Yun JH, Park SW, Kim JH, Park YJ, Cho CH, Kim JH. Angiopoietin-2 induces astrocyte apoptosis via αvβ5-integrin signalling in diabetic retinopathy. (2016) *Cell Death and Disease* **7(2):** e2101.

Zebboudj AF, Imura M, Boström K. Matrix Gla protein, a regulatory protein for bone morphogenic protein-2. (2002) *Journal of Biological Chemistry* **277(6):** 4388–4394.

Zhang SH, Reddick RL, Piedrahita JA, Maeda N. Spontaneous hypercholesterolemia and arterial lesions in mice lacking apolipoprotein E. (1992) *Science* **258(5081):** 468–71.

Zhang H, Bradley A. Mice deficient for BMP2 are nonviable and have defects in amnion/chorion and cardiac development. (1996) *Development* **122(10):** 2977–2986.

Appendix

Funding Sources

Funding for this project was awarded by Kids Kidney Research (£92,201) to Drs Lesley Rees, David A Long, and Rukshana Shroff.

Further funding for consumables was awarded by the National Institute of Health Research/ Biomedical Research Council/ Great Ormond Street Hospital Charity as part of the Doctoral support fund (£4500). This funding was awarded based on the translational merit of this project and supported further investigation into pathway inhibition – namely siRNA transfection and chemical inhibition of Tie2.

Travel bursaries were awarded by the Institute of Child Health (£250), the UCL School of Life and Medical Sciences (£250), and The Physiological Society (£500) to attend and present an oral presentation at the American Society of Nephrology 'Kidney Week' in November 2014.

Scholarships were awarded from the Canadian Council of Marine Carriers ($2500) and the Washington Marine Group ($1000) to help with maintenance over the final year.

This project has provided the preliminary data to obtain funding from Kidney Research UK (£191,801). This funding has been awarded to Dr David A Long, Dr Rukshana Shroff, and Professor Catherine Shanahan to fund a post-doctoral researcher.

Oral Presentations

Todd AF, Price K, Joannou MK, Rees L, Long DA, Shroff RC. Angiopoietin-2 accelerates vascular calcification in children with chronic kidney disease undergoing dialysis. European Renal Association/Dialysis and Transplantation Association Congress, London May 2015.

Todd AF, Price K, Joannou MK, Rees L, Shroff RC, Long DA. Angiopoietin-2 accelerates vascular calcification in children with chronic kidney disease undergoing dialysis. American Society of Nephrology 'Kidney Week', Philadelphia November 2014.

Todd AF, Price K, Joannou MK, Rees L, Shroff RC, Long DA. Angiopoietin-2 accelerates vascular calcification in children with chronic kidney disease undergoing dialysis. European Nephrogenesis Workshop, Manchester July 2014.

Poster Presentations

Todd AF, Price KL, Kolatsi-Joannou M, Rees L, Shroff RC, Long DA. Angiopoietin-2 accelerates vascular calcification in children with chronic kidney disease, The Physiological Society 'Physiology 2014', London July 2014.

Todd AF, Price K, Kolatsi-Joannou M, Woolf AS, Rees L, Shroff RC, Long DA. Angiopoietin-2 is a marker and mediator of cardiovascular disease in children with severe chronic kidney disease. British Transplantation Society and Renal Association Annual Congress, Bournemouth March 2013.

Publications

Shroff RC, Price KL, Kolatsi-Joannou M, **Todd AF,** Wells D, Deanfield J, Johnson RJ, Rees L, Woolf AS, Long DA. Circulating angiopoietin-2 is a marker for early cardiovascular disease in children on chronic dialysis. (2013): *PLOS ONE* 8(2): e56273.